The PLPAK™

Verification Manuals

Youssef F. Rashed

Ahmed Fady Farid

Ibrahim A. Eldardeer

https://www.plpak.com 2022

Preface

The purpose of this verification manual is to give the user the opportunity to verify the results obtained from different PLPAK packages. The verification examples are ranged from simple and small problems to practical applications. The results are compared to those obtained from analytical methods or from other numerical methods such as the finite element methods. It is the responsibility of the user to verify his own model and to use the listed examples to train on modelling using the PLPAK.

Most of the presented examples are previously published by Prof Rashed and his post-graduate students.

The authors

Youssef F. Rashed
Ahmed Fady Farid
Ibrahim A. Eldardeer

November 2022

Table of Contents

Introduction 1
1. The Single-Floor (Basic) Package 2
Example 1.1 [1] 3
Example 1.2 [1] 8
Example 1.3 [7] 17
Example 1.4 [7] 18
Example 1.5 [7] 20
Example 1.6 [7] 22
Example 1.7 [7] 25
Example 1.8 [9] 31
Example 1.9 [9] 34
Example 1.10 [9] 37
Example 1.11 [10] 41
Example 1.12 [10] 44
Example 1.13 [10] 48
2. The Advanced Single-Floor (Foundation) Package: 60
Example 2.1 [13] 61
Example 2.2 [13] 62
Example 2.3 [13] 63
Example 2.4 [13] 65
Example 2.5 [13] 67
Example 2.6 [13] 69
Example 2.7 [13] 70
Example 2.8 [13] 71
Example 2.9 [13] 72
Example 2.10 [13] 73
Example 2.11 [13] 75
Example 2.12 [25] 76
Example 2.13 [27] 80
Example 2.14 [27] 84
Example 2.15 [27] 86
Example 2.16 [27] 88
3. The Multiple-Floor Package: 95
Example 3.1 [31] 96

Example 3.2 [31] 98
Example 3.3 [31] 102
Example 3.4 [31] 104
Example 3.5 [31] 106
Example 3.6 [31] 109
Example 3.7 [32] 111
Example 3.8 [32] 115
Example 3.9 [32] 117
Example 3.10 [33] 124
Example 3.11 [33] 128
Example 3.12 [33] 133
Example 3.13 136
Example 3.14 138
Example 3.15 139
Example 3.16 141
4. The Design (PLDesign) Tool: 144
Example 4.1 [38] 146
Example 4.2 [38] 149
Example 4.3 [38] 150
5. The Dynamics Tool: 154
Example 5.1 [39] 155
Example 5.2 [41] 157
Example 5.3 [39] 158
Example 5.4 [41] 160
Example 5.5 [43] 162
Example 5.6 [43] 165
Example 5.7 [43] 167
Example 5.8 [43] 168
6. The Post-Tension Tool: 169
Example 6.1 [44] 170
Example 6.2 [44] 172
Example 6.3 [44] 174
Example 6.4 [44] 175
Example 6.5 183
Example 6.6 187
Example 6.7 193

Example 6.8 196
References 199

List of figures:

Figure 1.1: Geometry of the problem analyzed in Example 1.1 and Example 1.2. 4
Figure 1.2: Deflection along x axis at y=0 in Example 1.1. 4
Figure 1.3: Deflection along x axis at y=9 in Example 1.1. 5
Figure 1.4: Bending moment M_{xx} along x axis at y=0 in Example 1.1. 5
Figure 1.5: Bending moment M_{yy} along x axis at y=0 in Example 1.1. 6
Figure 1.6: Bending moment M_{xx} along x axis at y=9 in Example 1.1. 6
Figure 1.7: Bending moment M_{yy} along x axis at y=9 in Example 1.1. 7
Figure 1.8: Deflection distribution along line 1-1 (t=0.4) in Example 1.2. 9
Figure 1.9: Deflection distribution along line 2-2 (t=0.4) in Example 1.2. 10
Figure 1.10: Bending moment diagram along line 1-1 (t=0.4) in Example 1.2. 10
Figure 1.11: Bending moment diagram along line 2-2 (t=0.4) in Example 1.2. 11
Figure 1.12: Deflection distribution along line 1-1 (t=0.1) in Example 1.2. 11
Figure 1.13: Deflection distribution along line 2-2 (t=0.1) in Example 1.2. 12
Figure 1.14: Bending moment diagram along line 1-1 (t=0.1) in Example 1.2. 12
Figure 1.15: Bending moment diagram along line 2-2 (t=0.1) in Example 1.2. 13
Figure 1.16: Deflection distribution along line 1-1 (t=0.05) in Example 1.2. 13
Figure 1.17: Deflection distribution along line 2-2 (t=0.05) in Example 1.2. 14
Figure 1.18: Bending moment diagram along line 1-1 (t=0.05) in Example 1.2. 14
Figure 1.19: Bending moment diagram along line 2-2 (t=0.05) in Example 1.2. 15
Figure 1.20: Changing of column bending moment M_{xx} by increasing Lx (and Ly) for square column dimensions in Example 1.2. 15
Figure 1.21: Changing of column bending moment M_{yy} by increasing Lx (Ly is constant = 0.05 m) for square column dimensions in Example 1.2. 16
Figure 1.22: Changing of column bending moment M_{xx} by increasing Lx (Ly is constant = 0.05 m) for square column dimensions in Example 1.2. 16
Figure 1.23: The beam considered in Example 1.3 with the PLPAK model results. 17
Figure 1.24: The slab with edge beams considered in Example 1.4. 18
Figure 1.25: Slab's deflection along middle axis x in Example 1.4. 19
Figure 1.26: Slab's deflection along x'-axis in Example 1.4. 19
Figure 1.27: Slab's deflection along y-axis in Example 1.4. 19
Figure 1.28: The slab with edge beams and internal beam considered in Example 1.5. 20
Figure 1.29: Slab's deflection along middle axis x in Example 1.5. 21
Figure 1.30: Slab's deflection along x'-axis in Example 1.5. 21
Figure 1.31: Slab's deflection along y-axis in Example 1.5. 21
Figure 1.32: The slab geometry considered in Example 1.6. 22
Figure 1.33: The used boundary element mesh in Example 1.6. 23
Figure 1.34: Sketch showing the slab finite element models considered in Example 1.6. 23

Figure 1.35: Deflection diagram of slab in Example 1.6. 23
Figure 1.36: Bending moment diagram of slab in Example 1.6. 24
Figure 1.37: Torsion moment diagram of slab in Example 1.6. 24
Figure 1.38: Shear force diagram of slab in Example 1.6. 24
Figure 1.39: Structural plan of slab considered in Example 1.7. 25
Figure 1.40: Proposed model deflection contours in Example 1.7..26
Figure 1.41: FEM deflection contours in Example 1.7. 26
Figure 1.42: Bending moment (M_{yy}) along Section 1 in Example 1.7. 27
Figure 1.43: Bending moment (M_{yy}) along Section 2 in Example 1.7. 27
Figure 1.44: Bending moment (M_{xx}) along Section 3 in Example 1.7. 27
Figure 1.45: Proposed model bending moment for B1 in Example 1.7. 28
Figure 1.46: FEM bending moment for B1 in Example 1.7. 28
Figure 1.47: Proposed model shearing force for B1 in Example 1.7. 28
Figure 1.48: FEM shearing force for B1 in Example 1.7. 28
Figure 1.49: Proposed model bending moment for B2 in Example 1.7. 28
Figure 1.50: Proposed model shearing force for B2 in Example 1.7. 29
Figure 1.51: FEM bending moment for B2 in Example 1.7. 29
Figure 1.52: FEM shearing force for B2 in Example 1.7. 29
Figure 1.53: Proposed model bending moment for B3 in Example 1.7. 29
Figure 1.54: FEM bending moment for B3 in Example 1.7. 30
Figure 1.55: Proposed model shearing force for B3 in Example 1.7. 30
Figure 1.56: FEM shearing force for B3 in Example 1.7. 30
Figure 1.57: Layout of the multi thickness cantilever slab in Example 1.8.............................31
Figure 1.58: Stiffness cells with 5×20 discretization in Example 1.8. 32
Figure 1.59: Deflection of the slab along Strip"1" in Example 1.8..32
Figure 1.60: Bending moment of the slab along Strip"1" in Example 1.8. 33
Figure 1.61: Layout of the multi thickness circular slab in Example 1.9.................................34
Figure 1.62: Stiffness cells with 441 discretization in Example 1.9. 35
Figure 1.63: Deflection of the slab along Strip"1" in Example 1.9..35
Figure 1.64: Bending moment of the slab along Strip"1" in Example 1.9. 36
Figure 1.65: Layout of the slab over four columns in Example 1.10. 38
Figure 1.66: Stiffness cells with 15×15 divisions discretization in Example 1.10. 38
Figure 1.67: Deflection of the slab along Strip"1" in Example 1.10. 39
Figure 1.68: Bending moment of the slab along Strip"1" in Example 1.10. 39
Figure 1.69: Deflection of the slab along Strip"2" in Example 1.10. 40
Figure 1.70: Bending moment of the slab Strip"2" in Example 1.10. 40
Figure 1.71: The considered simple raft on non-homogenous soil in Example 1.11. 41
Figure 1.72: Comparison between PLPAK results and results of [11] along section 1–1 for the simple raft (raft thickness equal to 0.6 m) in Example 1.11. 42
Figure 1.73: Comparison between PLPAK results and results of [11] along section 2–2 for the simple raft (raft thickness equal to 0.6 m) in Example 1.11. 42
Figure 1.74: Comparison between PLPAK results and results of [11] along section 1–1 for the simple raft (raft thickness equal to 1.5 m) in Example 1.11. 43

Figure 1.75: Comparison between PLPAK results and results of [11] along section 2–2 for the simple raft (raft thickness equal to 1.5 m) in Example 1.11. 43
Figure 1.76: Soil spring forces obtained from the finite element analysis for one quarter of the simple raft problem in Example 1.12...45
Figure 1.77: One quarter of the simple raft problem in Example 1.12 showing: First value: denotes the soil cell reaction of the present boundary element analysis, and (Second value): denotes the equivalent finite element value..............................45
Figure 1.78: Detail showing corner, internal and edge spring groups for determining the equivalent finite element value for soil reaction in Example 1.12. 46
Figure 1.79: Comparison between PLPAK deflection and results of the finite element method along lines A and B for the simple raft problem (raft thickness equal to 0.6 m) in Example 1.12...46
Figure 1.80: Comparison between PLPAK bending moments and results of the finite element method along lines A and B for the simple raft problem (raft thickness equal to 0.6 m) in Example 1.12. 47
Figure 1.81: Comparison between PLPAK shear forces and results of the finite element method along lines A and B for the simple raft problem (raft thickness equal to 0.6 m) in Example 1.12. 47
Figure 1.82: Geometry of the considered practical raft problem in Example 1.13................50
Figure 1.83: Different boundary element meshes for the considered practical raft problem in Example 1.13...50
Figure 1.84: Different soil cell meshes for the considered practical raft problem in Example 1.13. 51
Figure 1.85: Different finite element meshes for the considered practical raft problem in Example 1.13...51
Figure 1.86: Comparison of the deflection results along axis B–B for the considered practical raft problem in Example 1.13. 52
Figure 1.87: Comparison of the bending moment results along axis B–B for the considered practical raft problem in Example 1.13...52
Figure 1.88: Comparison of the shear force results along axis B–B for the considered practical raft problem in Example 1.13. 53
Figure 1.89: Comparison of the deflection results along axis C–C for the considered practical raft problem in Example 1.13. 53
Figure 1.90: Comparison of the bending moment results along axis C–C for the considered practical raft problem in Example 1.13...54
Figure 1.91: Comparison of the shear force results along axis C–C for the considered practical raft problem in Example 1.13. 54
Figure 1.92: Comparison of the deflection results along axis 3–3 for the considered practical raft problem in Example 1.13. 55
Figure 1.93: Comparison of the bending moment results along axis 3–3 for the considered practical raft problem in Example 1.13...55
Figure 1.94: Comparison of the shear force results along axis 3–3 for the considered practical raft problem in Example 1.13. 56

Figure 1.95: Comparison of the deflection results along axis 6–6 for the considered practical raft problem in Example 1.13. 56
Figure 1.96: Comparison of the bending moment results along axis 6–6 for the considered practical raft problem in Example 1.13...57
Figure 1.97: Comparison of the shear force results along axis 6–6 for the considered practical raft problem in Example 1.13. 57
Figure 1.98: Comparison of the deflection results along axis 10–10 for the considered practical raft problem in Example 1.13. 58
Figure 1.99: Comparison of the bending moment results along axis 10–10 for the considered practical raft problem in Example 1.13...58
Figure 1.100: Comparison of the shear force results along axis 10–10 for the considered practical raft problem in Example 1.13...59
Figure 2.1: Displacement distribution for a centrally concentrated loaded square plate in Example 2.1...61
Figure 2.2: Displacement distribution for a uniformly distributed loaded square plate in Example 2.2...62
Figure 2.3: Displacement distribution for a centrally patch loaded square plate with c/B=0.25 in Example 2.3...63
Figure 2.4: Displacement distribution for a centrally patch loaded square plate with c/B=0.50 in Example 2.3...64
Figure 2.5: Displacement distribution for a centrally patch loaded square plate with c/B=0.75 in Example 2.3...64
Figure 2.6: Displacement distribution for a side-long patch loaded square plate with c/B=0.25 in Example 2.4...65
Figure 2.7: Displacement distribution for a side-long patch loaded square plate with c/B=0.50 in Example 2.4...66
Figure 2.8: Displacement distribution for a side-long patch loaded square plate with c/B=0.75 in Example 2.4...66
Figure 2.9: Displacement distribution for a circular plate under uniform load in Example 2.5. 68
Figure 2.10: Displacement distribution for a rectangular plate under uniform load at A, B, C and D in Example 2.6. 69
Figure 2.11: Displacement distribution for a square plate under four concentrated loads along the strip A–A in Example 2.7..70
Figure 2.12: Four-layered elastic half space in Example 2.10..74
Figure 2.13: Trapezoidal plate layout in Example 2.11...75
Figure 2.14: Practical raft layout in Example 2.12. 77
Figure 2.15: Displacement distribution for a practical raft along the strip 1-1 in Example 2.12. 78
Figure 2.16: Bending moment distribution for a practical raft along the strip 1-1 in Example 2.12. 78
Figure 2.17: Displacement distribution for a practical raft along the strip 2-2 in Example 2.12. 79

Figure 2.18: Bending moment distribution for a practical raft along the strip 2-2 in Example 2.12. 79
Figure 2.19: Pile cap geometry presented in Example 2.13. 80
Figure 2.20: Deflection along centerline strip for case t = 0.079 m in Example 2.13. 81
Figure 2.21: Bending moments along centerline strip for case t = 0.079 m in Example 2.13. 81
Figure 2.22: Deflection along centerline strip for case t = 0.37 m in Example 2.13. 82
Figure 2.23: Bending moments along centerline strip for case t = 0.37 m in Example 2.13...82
Figure 2.24: Deflection along centerline strip for case t = 0.79 m in Example 2.13. 83
Figure 2.25: Bending moments along centerline strip for case t = 0.79 m in Example 2.13...83
Figure 2.26: Piled raft geometry presented in Example 2.14. 84
Figure 2.27: Settlement along centerline strip in Example 2.14. 85
Figure 2.28: Bending moments along centerline strip in Example 2.14. 85
Figure 2.29: Four cases of piles configurations and raft geometry in Example 2.15. 87
Figure 2.30: Practical piled raft foundation geometry in Example 2.16. 89
Figure 2.31: Columns and wall loads ID in Example 2.16. 89
Figure 2.32: BEM model of practical piled raft foundation in Example 2.16. 91
Figure 2.33: Sample pile forces in Example 2.16. 91
Figure 2.34: Pile forces distribution in Example 2.16. (a) Without considering interaction effects. (b) With considering interaction effects 92
Figure 2.35: Deflection values along the horizontal strip 1 in Example 2.16. 93
Figure 2.36: Bending moment values along the horizontal strip 1 in Example 2.16. 93
Figure 3.1: Example 3.1 structural drawing. 96
Figure 3.2: Example 3.1 BEM model. 96
Figure 3.3: Example 3.1 FEM model. 97
Figure 3.4: Example 3.1 lateral drift results. 97
Figure 3.5: Example 3.2 structural drawing. 98
Figure 3.6: Example 3.2 BEM model. 99
Figure 3.7: Example 3.2 FEM model. 99
Figure 3.8: Example 3.2 FEM deflection results. 100
Figure 3.9: Example 3.2 BEM deflection results. 100
Figure 3.10: Example 3.2 lateral drift results. 101
Figure 3.11: Example 3.2 beam bending moment results. 101
Figure 3.12: Example 3.3 structural drawing. 102
Figure 3.13: Example 3.3 BEM model. 102
Figure 3.14: Example 3.3 FEM model. 103
Figure 3.15: Example 3.3 lateral drift comparison. 103
Figure 3.16: Example 3.4 structural drawing. 104
Figure 3.17: Example 3.4 BEM model. 104
Figure 3.18: Example 3.4 FEM model. 105
Figure 3.19: Example 3.4 lateral drift comparison. 105
Figure 3.20: Example 3.5 BEM model. 106
Figure 3.21: Example 3.5 FEM model. 107
Figure 3.22: Example 3.5 lateral drift results. 107
Figure 3.23: Example 3.5 Bending moment results. 108

Figure 3.24: Example 3.5 BEM deflection results. 108
Figure 3.25: Example 3.5 FEM deflection results. 108
Figure 3.26: Example 3.6 BEM model. 109
Figure 3.27: Example 3.6 FEM model. 110
Figure 3.28: Example 3.6 lateral drift comparisons. 110
Figure 3.29: Dimensions considered for the slab in Example 3.7. 112
Figure 3.30: Boundary element model (model 1) in Example 3.7. 112
Figure 3.31: Solid element column model with slab plate bending finite element method (model 2) in Example 3.7. 112
Figure 3.32: Frame element column model with slab plate bending finite element model (model 3) in Example 3.7. 112
Figure 3.33: Bending moment Mxx contour in model 1 in Example 3.7. 113
Figure 3.34: Bending moment Mxx contour map in the finite element model 2 in Example 3.7. 113
Figure 3.35: Bending moment Mxx contour map in the finite element model 3 in Example 3.7. 113
Figure 3.36: Comparison of bending moment M_{xx} for the considered three models in Example 3.7. 114
Figure 3.37: Comparison of bending moment M_{xx} for the considered two models in Example 3.7. 114
Figure 3.38: Drift in x axis in Example 3.8. 115
Figure 3.39: Drift in Y axes in Example 3.8. 116
Figure 3.40: Rotation about Z axes in Example 3.8. 116
Figure 3.41: Dimensions of the Practical Building in Example 3.9. 117
Figure 3.42: The used boundary element model in Example 3.9. 118
Figure 3.43: The finite element mesh used in Example 3.9. 118
Figure 3.44: The multi-storey finite element model in Example 3.9. 119
Figure 3.45: Slabs deflection U_Z _BEM_Model (1) in Example 3.9. 119
Figure 3.46: Slabs deflection U_Z- FEM-Model (2) in Example 3.9. 120
Figure 3.47: Strip guide in Example 3.9. 120
Figure 3.48: Comparison of deflection U_Z diagram between two models strip 1 in Example 3.9. 121
Figure 3.49: Comparison of deflection U_Z diagram between two models strip 2 in Example 3.9. 121
Figure 3.50: Comparison of deflection U_Z diagram between two models strip 3 in Example 3.9. 122
Figure 3.51: Comparison of deflection U_Z diagram between two models strip 4 in Example 3.9. 122
Figure 3.52: Comparison of deflection U_Z diagram between two models strip 5 in Example 3.9. 123
Figure 3.53: Comparison of lateral drifts in X direction in Example 3.9. 123
Figure 3.54: Example 3.10 structural Plan. 125
Figure 3.55: Example 3.10 BEM model. 125
Figure 3.56: Example 3.10 single story FEM model. 125

Figure 3.57: Example 3.10 multi-story FEM model. 125
Figure 3.58: Example 3.10 bending moment M_{xx} for the FEM model due to gravity load 1 t/m^2. 126
Figure 3.59: Example 3.10 bending moment M_{xx} for the BEM model due to gravity load 1 t/m^2. 126
Figure 3.60: Direction, magnitude, and location of the applied lateral load in Example 3.10. 126
Figure 3.61: Example 3.10 bending moment M_{xx} for the FEM due to 100 t in x-direction. .. 126
Figure 3.62: Example 3.10 bending moment M_{xx} for the BEM due to 100 t in x-direction... 126
Figure 3.63: Example 3.10 multi-story FEM solid & plate model. 127
Figure 3.64: Example 3.10 multi-story FEM all solid model. 127
Figure 3.65: Example 3.10 U_x values along the building elevation. 127
Figure 3.66: Example 3.11 structural Plan. 128
Figure 3.67: Example 3.11 BEM model. 128
Figure 3.68: Example 3.11 single story FEM model. 129
Figure 3.69: Example 3.11 multi-story FEM model. 129
Figure 3.70: Example 3.11 bending moment M_{xx} for the FEM due to gravity load 1 t/m^2. .. 129
Figure 3.71: Example 3.11 bending moment M_{xx} for the BEM mode 1 due to gravity load 1 t/m^2. 129
Figure 3.72: Example 3.11 bending moment M_{xx} for the BEM mode 2 due to gravity load 1 t/m^2. 129
Figure 3.73: Example 3.11 beams bending moment in FEM due to gravity load 1 t/m^2. 130
Figure 3.74: Example 3.11 beams bending moment in BEM mode 1 due to gravity load 1 t/m^2. 130
Figure 3.75: Example 3.11 beams bending moment in BEM mode 2 due to gravity load 1 t/m^2. 130
Figure 3.76: Example 3.11 beams shearing force in FEM due to gravity load 1 t/m^2. 130
Figure 3.77: Example 3.11 beams shearing force in BEM mode 1 due to gravity load 1 t/m^2. 131
Figure 3.78: Example 3.11 beams shearing force in BEM mode 2 due to gravity load 1 t/m^2. 131
Figure 3.79: Example 3.11 beams Torsional moment in FEM due to gravity load 1 t/m^2..... 131
Figure 3.80: Example 3.11 beams Torsional moment in BEM mode 1 due to gravity load 1 t/m^2. 131
Figure 3.81: Example 3.11 beams Torsional moment in BEM mode 2 due to gravity load 1 t/m^2. 132
Figure 3.82: Direction, magnitude, and location of the applied lateral load in Example 3.11. 132
Figure 3.83: Example 3.11 U_x values along the building elevation. 132
Figure 3.84: Example 3.12 structural Plan. 133
Figure 3.85: Example 3.12 BEM model. 133
Figure 3.86: Example 3.12 single story FEM model. 134
Figure 3.87: Example 3.12 multi-story FEM model. 134
Figure 3.88: Example 3.12 bending moment M_{xx} for the FEM due to gravity load 1 t/m^2. .. 134

Figure 3.89: Example 3.12 bending moment M_{xx} for BEM mode 1 due to gravity load 1 t/m^2. 134
Figure 3.90: Example 3.12 bending moment M_{xx} for BEM mode 2 due to gravity load 1 t/m^2. 134
Figure 3.91: Direction, magnitude, and location of the applied lateral load in Example 3.12. 135
Figure 3.92: Example 3.12 U_x values along the building elevation. 135
Figure 3.93: Dimensions of the considered slab in Example 3.13. 137
Figure 3.94: Comparison of deflection contour maps between model 1 and model 3 (warping is ignored) in Example 3.13. 137
Figure 3.95: Comparison of deflection contour maps between model 2 and model 4 (warping is considered) in Example 3.13. 137
Figure 3.96: Dimensions of slab and core considered in Example 3.14. 138
Figure 3.97: Rotation results at different story level in Example 3.14. 138
Figure 3.98: Bi-moment results at different story level in Example 3.14. 138
Figure 3.99: Dimensions of the considered slab in Example 3.15. 139
Figure 3.100: The considered boundary element discretization of the slab in Example 3.15. 139
Figure 3.101: Displacement (meters) in x-direction in Example 3.15. 140
Figure 3.102: Distribution of the angle of twist along the shear wall building in Example 3.15. 140
Figure 3.103: Distribution of total torque in the central core in Example 3.15. 140
Figure 3.104: Distribution of bi-moment along the central core in Example 3.15. 140
Figure 3.105: Plan of the typical floor in the building in Example 3.16. 142
Figure 3.106: Boundary element model in Example 3.16. 142
Figure 3.107: Finite element model in Example 3.16. 142
Figure 3.108: Shows the relation between the drift corresponding to the maximum value of theta and the number of floors in Example 3.16. 143
Figure 3.109: Shows the relation between the maximum value of theta and the number of stories in Example 3.16.. It shows also the code limit value (0.3). 143
Figure 4.1: High-rise building structural drawing in Example 4.1. 146
Figure 4.2: BIM of the high-rise building in the preprocessing stage in Example 4.1. 147
Figure 4.3: 3D model building in the preprocessing stage in Example 4.1. 147
Figure 4.4: BIM-BEM model view of the high-rise building in Example 4.1. 148
Figure 4.5: Pile reactions captured from the postprocessor GUI in Example 4.2. 149
Figure 4.6: Piled raft strips and local contour results captured from the postprocessor GUI in Example 4.2. 149
Figure 4.7: BIM-BEM model view of the building floor in Example 4.3. 150
Figure 4.8: Example 4.3 slab design using method III. 150
Figure 4.9: Example 4.3 Slab design using method IV. 151
Figure 4.10: Example 4.3 BIM beam detailing. 151
Figure 4.11: Example 4.3 sample design calculation note. 152
Figure 4.12: Example 4.3 design summary spreadsheet. 152
Figure 4.13: Example 4.3 slab and beam detail drawing. 153

Figure 5.1: Slab, boundary element model and finite element model of Example 5.1. 155
Figure 5.2: Time History for Topmost "x" Displacement for Example 5.2 (m). 157
Figure 5.3: Time History for Base Shear for Example 5.2 (Tons). 157
Figure 5.4: Slab, boundary element model and finite element model of Example 5.3. 158
Figure 5.5: Elcentro-EW acceleration time history in G units...160
Figure 5.6: Time History for Topmost (x) Displacement for Example 5.4 (m). 161
Figure 5.7: Time History for Topmost (x) Displacement for Example 5.4 (m). 161
Figure 5.8: BEM slab model of Example 5.5. 162
Figure 5.9: Slab plan of Example 5.5. 162
Figure 5.10: Top Displacement time history with damping in Example 5.5. 163
Figure 5.11: Top Displacement time history with no damping in Example 5.5. 163
Figure 5.12: Base Shear time history in Example 5.5...163
Figure 5.13: Maximum inter story drift in Example 5.5. 164
Figure 5.14: Slab plan of Example 5.6. 165
Figure 5.15: Top Displacement time history of Example 5.6. 166
Figure 5.16: Slab model in Example 5.7. 167
Figure 5.17: Top Displacement time history in Example 5.7. 167
Figure 5.18: Slab model in Example 5.8. 168
Figure 5.19: Top Displacement time history in Example 5.8. 168
Figure 6.1: The simply supported slab considered in Example 6.1. 170
Figure 6.2: Boundary element and cable internal cells for the simply supported slab considered in Example 6.1. 171
Figure 6.3: Deflection and bending moment distribution under the slab own weight along the slab center line in the simply supported slab considered in Example 6.1. 171
Figure 6.4: Deflection and bending moment distributions under the slab own weight plus the balancing force prestressing cable along the slab center line in the simply supported slab considered in Example 6.1. 173
Figure 6.5: The practical slab geometry and section locations in Example 6.4 (dimensions are in mm). 176
Figure 6.6: Cables layout in the X-direction in Example 6.4. 176
Figure 6.7: Cables layout in the Y-direction in Example 6.4. 176
Figure 6.8: The boundary element model with cable cells and support cells in Example 6.4. 177
Figure 6.9: The finite element model in Example 6.4. 177
Figure 6.10: Example 6.4 bending moment along section A (m.t). 177
Figure 6.11: Example 6.4 deflection along section A (m). 177
Figure 6.12: Example 6.4 bending moment along section B (m.t). 178
Figure 6.13: Example 6.4 deflection along section B (m). 178
Figure 6.14: Example 6.4 bending moment along section C (m.t). 178
Figure 6.15: Example 6.4 deflection along section C (m). 178
Figure 6.16: Example 6.4 bending moment along section D (m.t). 178
Figure 6.17: Example 6.4 deflection along section D (m). 179
Figure 6.18: Example 6.4 bending moment along section E (m.t)..179
Figure 6.19: Example 6.4 deflection along section E (m)...179

Figure 6.20: Example 6.4 bending moment along section F (m.t)..179
Figure 6.21: Example 6.4 deflection along section F (m)..180
Figure 6.22: Example 6.4 bending moment along section G (m.t).......................................180
Figure 6.23: Example 6.4 deflection along section G (m)..180
Figure 6.24: Example 6.4 contour map for bending moment Mxx in the finite element model (m.t)..181
Figure 6.25: Example 6.4 contour map for bending moment Mxx in the boundary element model (m.t). 181
Figure 6.26: Example 6.4 contour map for bending moment Myy in the finite element model (m.t)..181
Figure 6.27: Example 6.4 contour map for bending moment Myy in the boundary element model (m.t). 182
Figure 6.28: Example 6.4 contour map for vertical deflection Uz in the finite element model (m)...182
Figure 6.29: Example 6.4 contour map for vertical deflection Uz in the boundary element model (m)...182
Figure 6.30: The structural system of post-tensioned garage floor in Example 6.5.............184
Figure 6.31: Layout of cables for the garage floor in Example 6.5.......................................184
Figure 6.32: The PLGen model of the garage floor in Example 6.5. 184
Figure 6.33: The used finite element mesh in the analysis in Example 6.5..........................184
Figure 6.34: The PLView of the garage floor in Example 6.5 showing the numerical boundary element model before and after cable updating. 185
Figure 6.35: Results for deflections in Example 6.5 (Left: the proposed PLPAK-PTPAK, right: the finite element results). 185
Figure 6.36: Results for moment in x-direction in Example 6.5 (Left: the proposed PLPAK-PTPAK, right: the finite element results). 186
Figure 6.37: Results for moment in y-direction in Example 6.5 (Left: the proposed PLPAK-PTPAK, right: the finite element results). 186
Figure 6.38: Structural System of the office building in Example 6.6..................................188
Figure 6.39: Cables in the X-direction for the office building in Example 6.6. 188
Figure 6.40: Cables in the Y-direction for the office building in Example 6.6. 189
Figure 6.41: The PLGen model of the office building in Example 6.6..................................189
Figure 6.42: The PLView of the office building in Example 6.6 showing the boundary elements and the cable loading cells...190
Figure 6.43: The used finite element divisions of the office building in Example 6.6 with cables 190
Figure 6.44: Results for moment in x-direction in Example 6.6 (Left: The finite element results, right: the proposed PLPAK-PTPAK). 191
Figure 6.45: Results for deflection in Example 6.6 (Left: The finite element result, right: the proposed PLPAK-PTPAK). 191
Figure 6.46: Example 6.6 moments in the x-direction along section A-A. 192
Figure 6.47: Example 6.6 deflections along for section A-A...192
Figure 6.48: Example 6.7 slab model. 193
Figure 6.49: Example 6.7 PLPAK bending moment contour...194

Figure 6.50: Example 6.7 FEM bending moment contour. 194
Figure 6.51: Example 6.7 PLPAK design strips. 194
Figure 6.52: Example 6.7 FEM design strips. 194
Figure 6.53: Example 6.7 PLPAK design strips stresses. 195
Figure 6.54: Example 6.7 FEM design strips stresses. 195
Figure 6.55: Example 6.8 PLPAK slab model. 196
Figure 6.56: Example 6.8 FEM slab model. 196
Figure 6.57: Example 6.8 PLPAK bending moment contour. 197
Figure 6.58: Example 6.8 FEM bending moment contour. 197
Figure 6.59: Example 6.8 design strips. 197
Figure 6.60: Example 6.8 PLPAK design strips stresses. 198
Figure 6.61: Example 6.8 PLPAK bending moment for strip passing throw the drop. 198
Figure 6.62: Example 6.8 FEM design strips stresses. 198

List of tables

Table 1.1: Column models, dimensions and loads used in the simple raft in Example 1.11. 41
Table 1.2: Column models, dimensions and loads used in the practical raft in Example 1.13. 49
Table 2.1: Displacement of a circular plate under uniform load in Example 2.5. 67
Table 2.2: Displacement at the center of a square plate under uniform load on an elastic half space in Example 2.8. 71
Table 2.3: Displacement at the center, mid-edge and corner of a square plate on an elastic half space in Example 2.9. 72
Table 2.4: Displacement at the center and mid-edge of a square plate on a multi-layered elastic half space in Example 2.10. 73
Table 2.5: Displacement at different points on a trapezoidal plate on an elastic half space in Example 2.11. 75
Table 2.6: Column models, dimensions and loads used in the practical raft in Example 2.12. 76
Table 2.7: Number of DOFs before and after condensation process. 80
Table 2.8: Number of DOFs before and after condensation process in Example 2.14. 84
Table 2.9: Maximum settlement value (m) for different piles pattern in Example 2.15. 86
Table 2.10: Number of DOFs before and after condensation process in Example 2.15. 86
Table 2.11: Columns, walls and cores loads in Example 2.16. 90
Table 2.12: Number of DOFs before and after condensation process in Example 2.16. 90
Table 2.13: Shearing force distribution over considered four regions in Example 2.16. 94
Table 4.1: Verification Criteria for Example 4.1-Example 4.3. 145
Table 4.2: Performance Evaluation for Example 4.1-Example 4.3. 145
Table 5.1: Natural periods "Example 5.1 A". 156
Table 5.2: Natural periods "Example 5.1 B". 156
Table 5.3: Natural periods "Example 5.3" 159
Table 5.4: Material properties for Example 5.5. 162

Table 5.5: Time period of the models (Example 5.5)...164
Table 5.6: Time period of the models of Example 5.6...166
Table 6.1: Comparison of central deflection against analytical values (m) in Example 6.2. .172
Table 6.2: Comparison of fixed end moments against analytical values (m.t) in Example 6.3. 174
Table 6.3: A comparison between the present BEM and FEM results in Example 6.4. 175
Table 6.4: Capacity and elapsed time comparison in Example 6.6. 187
Table 6.5: PLPAK and FEM design strips bending moments in Example 6.7.........................193
Table 6.6: PLPAK and FEM design strips stresses in Example 6.7...193
Table 6.7: PLPAK and FEM design strips bending moments in Example 6.8.........................196
Table 6.8: PLPAK and FEM design strips stresses in Example 6.8...196

Introduction

The PLPAK is a structural analysis software based on the boundary element method. It consists of three packages and four tools. The three packages are the Single-Floor (Basic) Package, the Advanced Single-Floor (Foundation) Package, and the Multiple-Floor (Fixed-Base) Package. While the four tools are the Design (PLDesign) Tool, the Post-Tension Tool, the Dynamics Tool, and the 3D Viewer (OpenGL) Tool.

The main purpose of this manual is to verify the results of these packages and tools by comparing these results by either an analytical solution or by other available software that uses the finite element method.

1. The Single-Floor (Basic) Package

This package is used to model and carry out structural analysis of single floor slab over columns, walls, beams, and cores. No internal discretization is required since the core solver is based on boundary element method.

Example 1.1 [1]

Purpose : Compare the results of the PLPAK against those of the BEM using the thin plate theory of [2].

Description : In this example the plate in Figure 1.1 is considered with $L_1 = 12.5$ and $L_2 = 10$. The column dimensions are chosen to be 1×1 to match the dimensions considered in [2]. The following properties are used: $E = 480000, v = 0.35$ and the thickness of the slab was 0.5. The column length was 10 and stopped at the plate (i.e. B(y)=0). It has to be noted that units in [2] are not defined. Herein it is assumed that the given values have consistent units. In [2], three models were considered. In model 1, the internal patches were assumed totally rigid. In model 2, the patches were assumed also rigid but by modelling them as holes inside the slab domain and place 4 boundary elements to surround each hole with clamped boundary conditions. In model 3, both the plate and the supporting columns are modelled using the formulation presented in [2], which employs the thin plate theory. Each side are modelled using six second-order boundary elements. In the PLPAK analysis, two models are considered. The first model is employing the present formulation considering the column actual stiffness (to be compared to model 3 in [2]), and the second model is based on modelling the column as rigid patches (to be compared to model 1 and model 2 in [2]). Four quadratic boundary elements were used on each side of the plate.

Results : Figure 1.2-Figure 1.7 demonstrate the deflections and bending moments M_{xx} and M_{yy} at y=0 and y=9. It can be seen that the present formulation results are in good agreement with those of [2]. The following notes could be concluded from these figures:

1- The results presented in [2] were plotted at (y=0) or near the column edges (y=9), i.e. away from the column's centres (column are located at y=9.5 to y=10.5). This is mainly due to the formulation presented in [2] is not capable to compute values over columns due to the singularity of the model used in [2].
2- In [2] special second order boundary elements were used to model the problem. This is mainly due to the used free-edge boundary conditions. Such a case could be easily solved using the traditional quadratic elements with high accuracy when employing the shear-deformable plate-bending theory as demonstrated in the present model.
3- Several values of the Mxx are not zero at the free edge in the results of [2]. Whereas they are absolutely zero in the present formulation. On the other hand, values of Myy are overshooting, which is not the case in the present formulation.
4- Always values of bending moments obtained from FEM (obtained from [2]) and BEM (results of the present formulation) are closer than those for the deflections. This is due to the use of different plate-bending theories as mentioned in [3], [4].

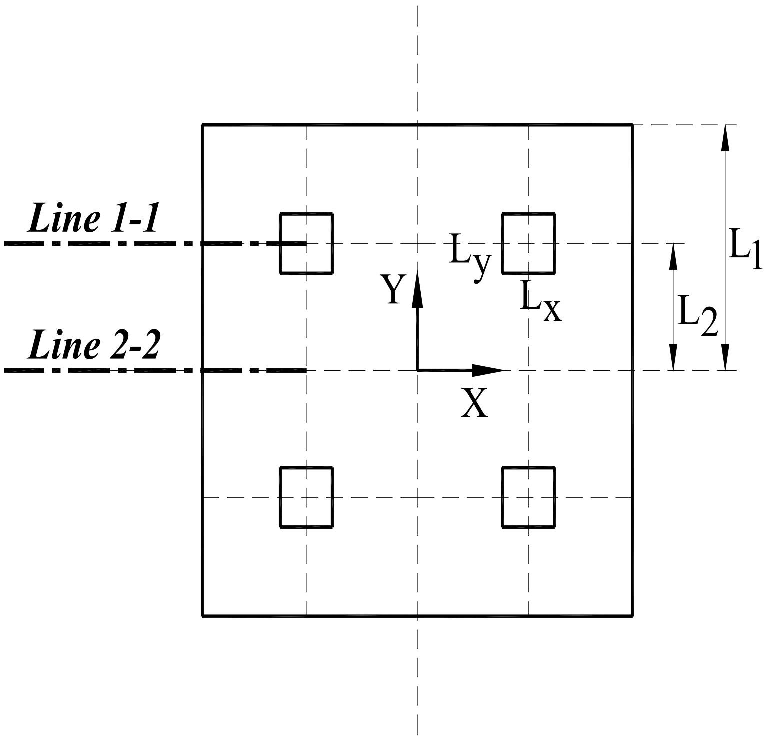

Figure 1.1: Geometry of the problem analyzed in Example 1.1 and Example 1.2.

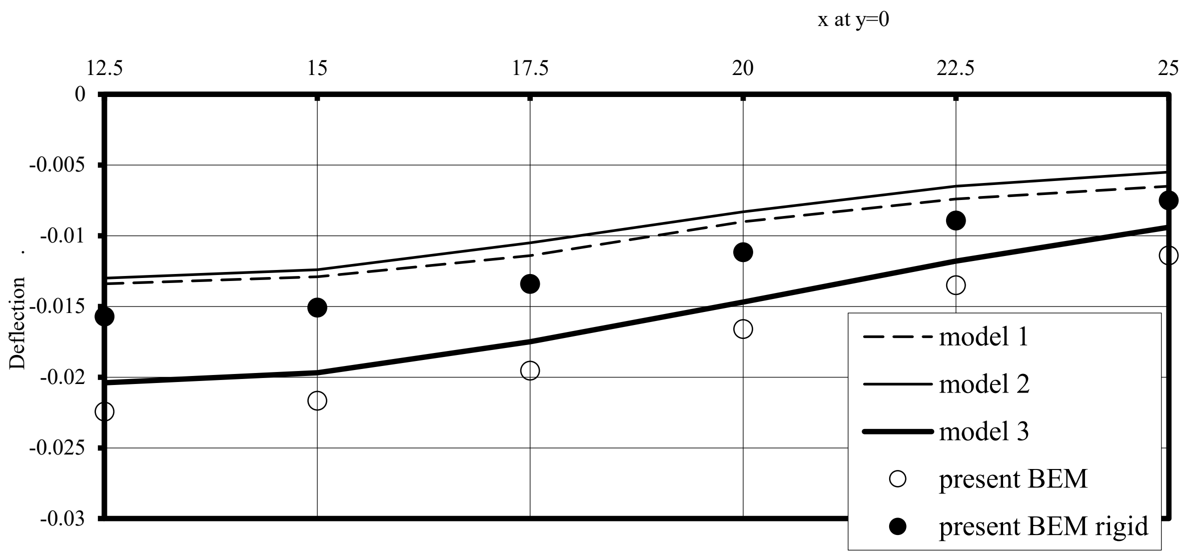

Figure 1.2: Deflection along x axis at y=0 in Example 1.1.

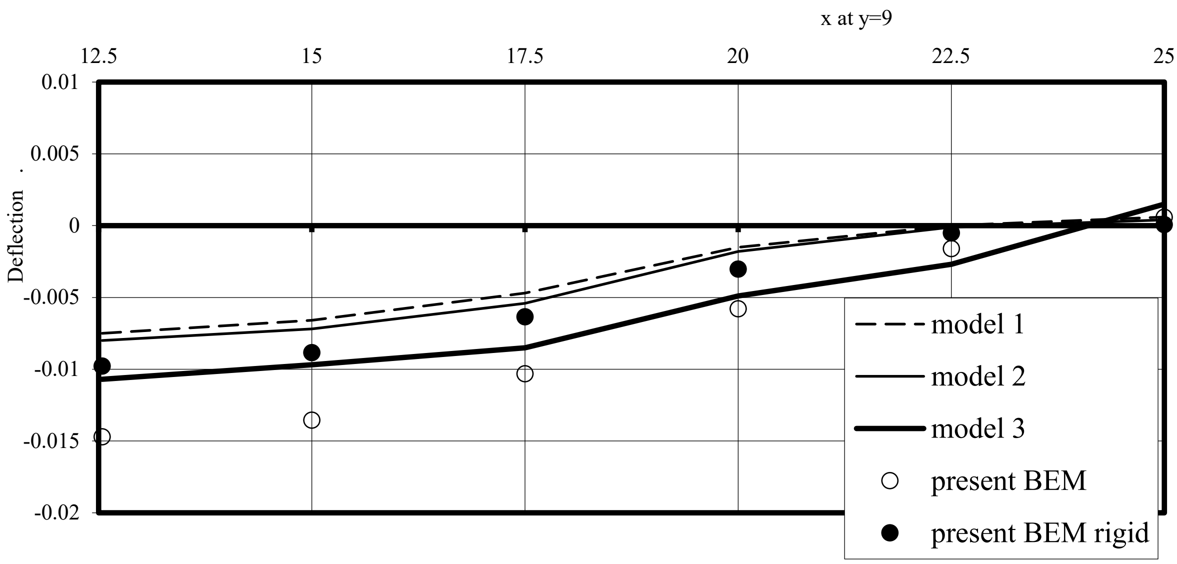

Figure 1.3: Deflection along x axis at y=9 in Example 1.1.

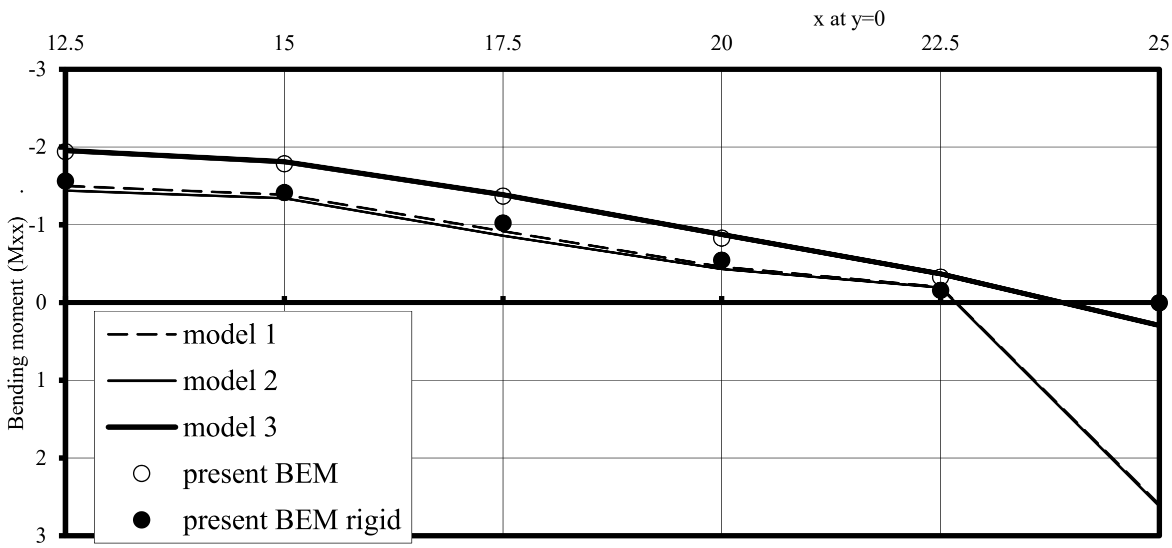

Figure 1.4: Bending moment M_{xx} along x axis at y=0 in Example 1.1.

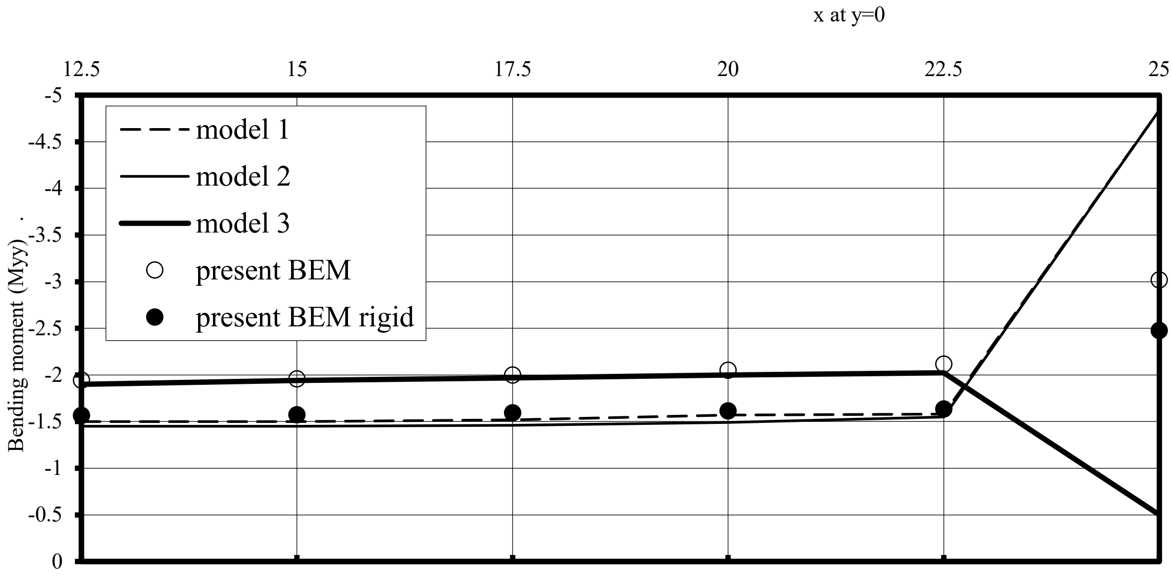

Figure 1.5: Bending moment M_{yy} along x axis at y=0 in Example 1.1.

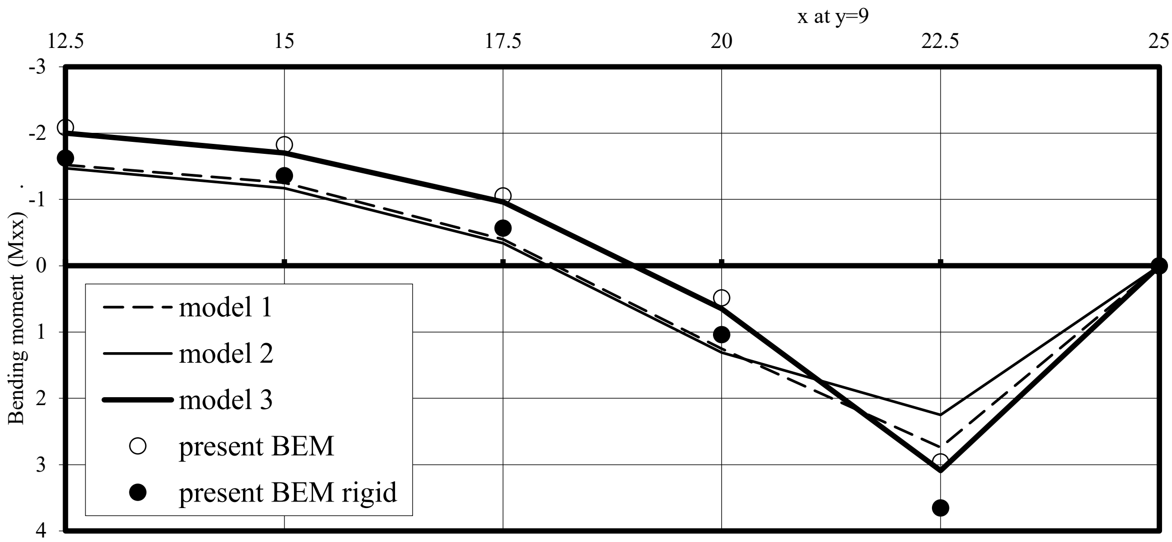

Figure 1.6: Bending moment M_{xx} along x axis at y=9 in Example 1.1.

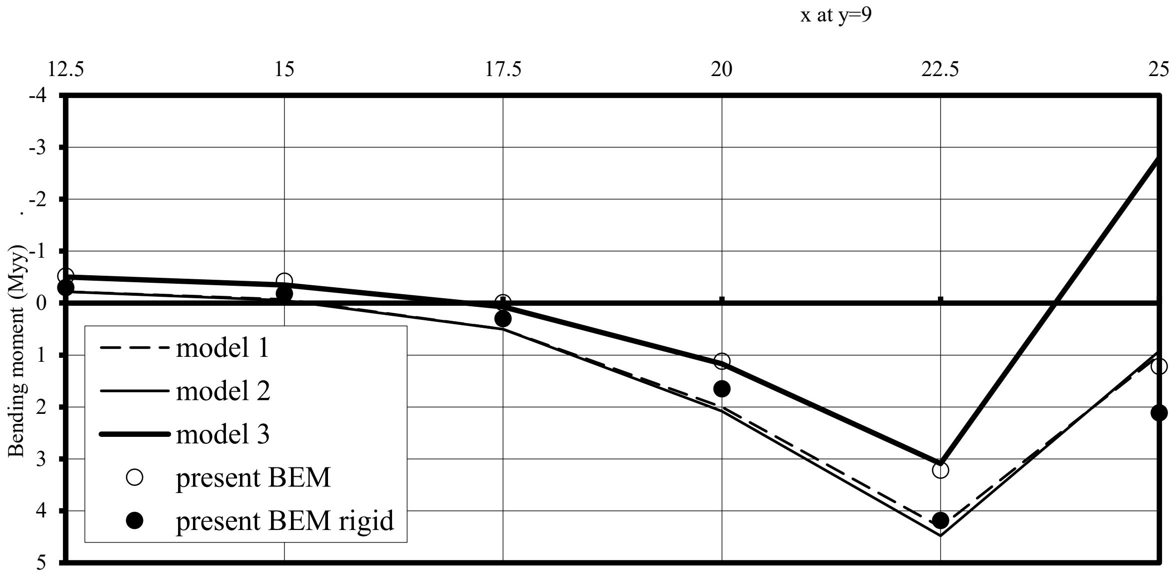

Figure 1.7: Bending moment M_{yy} along x axis at y=9 in Example 1.1.

Example 1.2 [1]

Purpose : Comparison between the results obtained from the PLPAK against results of the finite element method.

Description : The example will focus on both the field deflections and bending moments in the slab as well as the moment transferred from the slab to the column, which is usually not considered. The same slab shown in Figure 1.1 is reconsidered in this example with $L_1 = 4\,m$ and $L_2 = 3\,m$. The slab is discretized using 16×16 finite elements (4-noded rectangular elements are used) and 3×3 boundary elements (quadratic elements). Both BEM and FEM use the shear-deformable plate-bending theory.

In order to show the effect of the column cross-section geometry on the transferred moment from slab to the column, the following two analyses are carried out:

1- Using square columns $(L_x = L_y)$ and varying L_x from 0.05 to $2\,m$.

2- Using rectangular columns by fixing $L_y = 0.05\,m$, and varying $L_x = 0.05$ to $2\,m$.

Results : Figure 1.8-Figure 1.19 demonstrate values of the deflections and bending moments along line 1-1 (at $y = 2$) and line 2-2 (at $y = 0$) respectively for the cases $L_x = L_y = 0.4, 0.1, 0.05\,m$. It can be seen that:

1- As more as the size of the column dimensions decreases both results of FEM and BEM became very close. This is mainly due to modelling the columns in both methods are similar: In the FEM, each column is represented using frame element connected to the slab at single node and in the BEM the connection between the column and the slab is represented using very small cell ($0.05 \times 0.05\,m$).

2- Peak values over the columns in the finite element analysis are mainly due to the use of fine discretization in the FEM analysis. Unlike to the popular belief, such values do not affect the positive filed moment, which confirms the conclusion of [5]. It has to be noted that such peaks do not appear in the present BEM analysis, when the real cross section of the column is taken into account.

For the square columns, Figure 1.20 demonstrates values of bending moments carried by each column against L_x. Results are plotted from both the FEM and the present BEM solutions. It can be seen that after a certain value of the column width (0.8 m), the value of the transferred moment obtained from the FEM became constant (i.e., the FEM does not feel any changes in column geometry); whereas, in the BEM analysis, the value of such moment is decreased until it reached zero when the column width $L_x = 2\,m$. This is true as in this case the problem can be considered as one-dimensional compression problem with no bending moments.

For the rectangular columns, Figure 1.21-Figure 1.22 demonstrates the change of the column moment M_{yy} and M_{xx} by changing L_x. The following notes could be drawn from such figures:

1- A good agreement between the FEM and the BEM results for the bending moment M_{yy}, which is the bending moment in the direction of the column short dimension. As in both FEM and BEM models the column connection to slab is modelled using either single node in FEM or very small length ($L_y = 0.05\ m$) in BEM.

In the column long direction, as the length L_x increases the column stiffness increases and can attract more bending moment. This is true, until columns became enough long in a certain direction and in this case the slab behaves as one-way slab that carries the load in the short direction; hence the value of the bending moment decreases. It can be seen such point could not be observed in the FEM. This conclusion confirms the experimental results presented in [6].

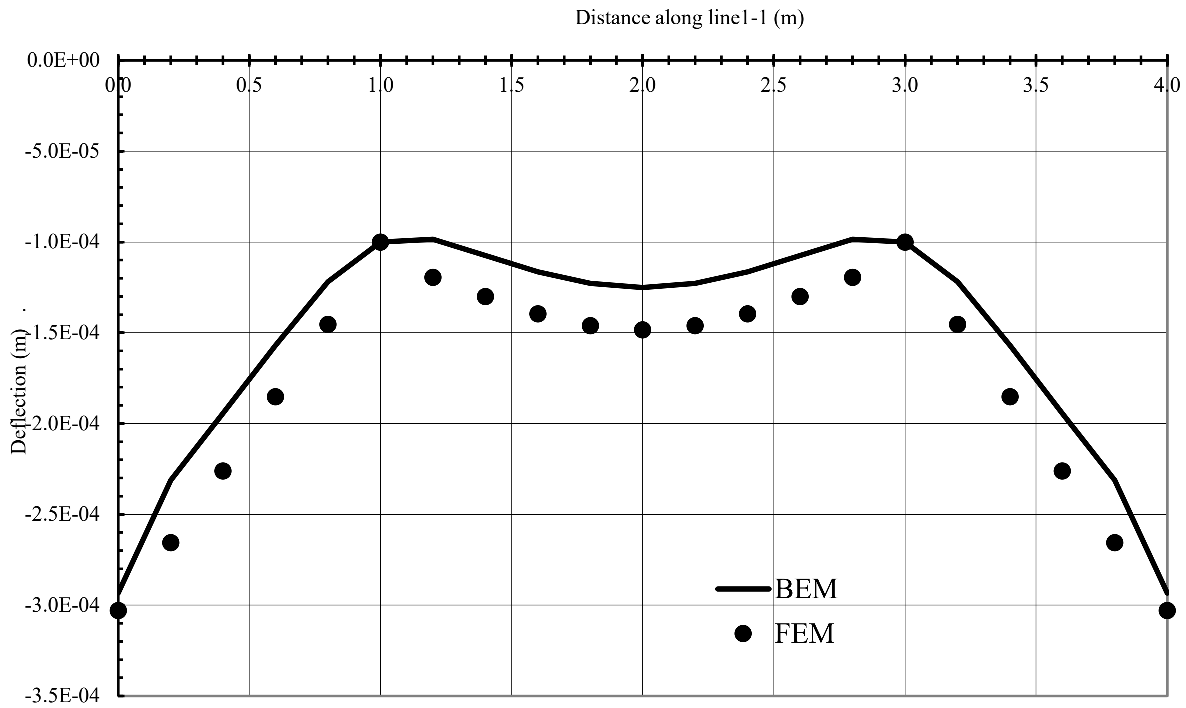

Figure 1.8: Deflection distribution along line 1-1 (t=0.4) in Example 1.2.

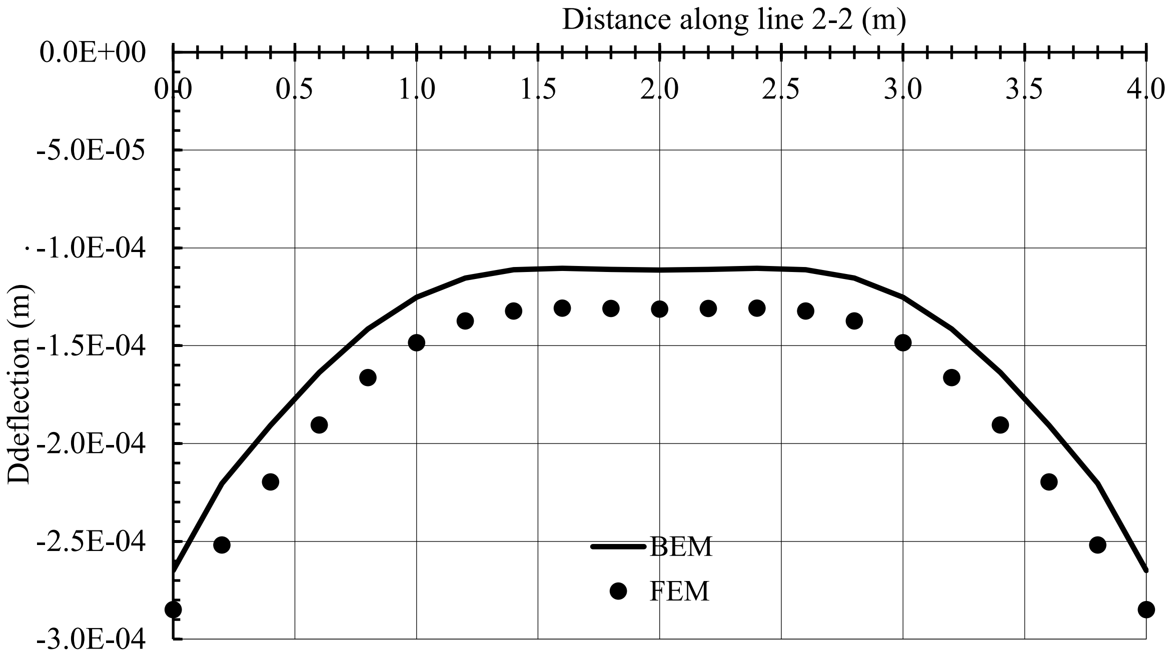

Figure 1.9: Deflection distribution along line 2-2 (t=0.4) in Example 1.2.

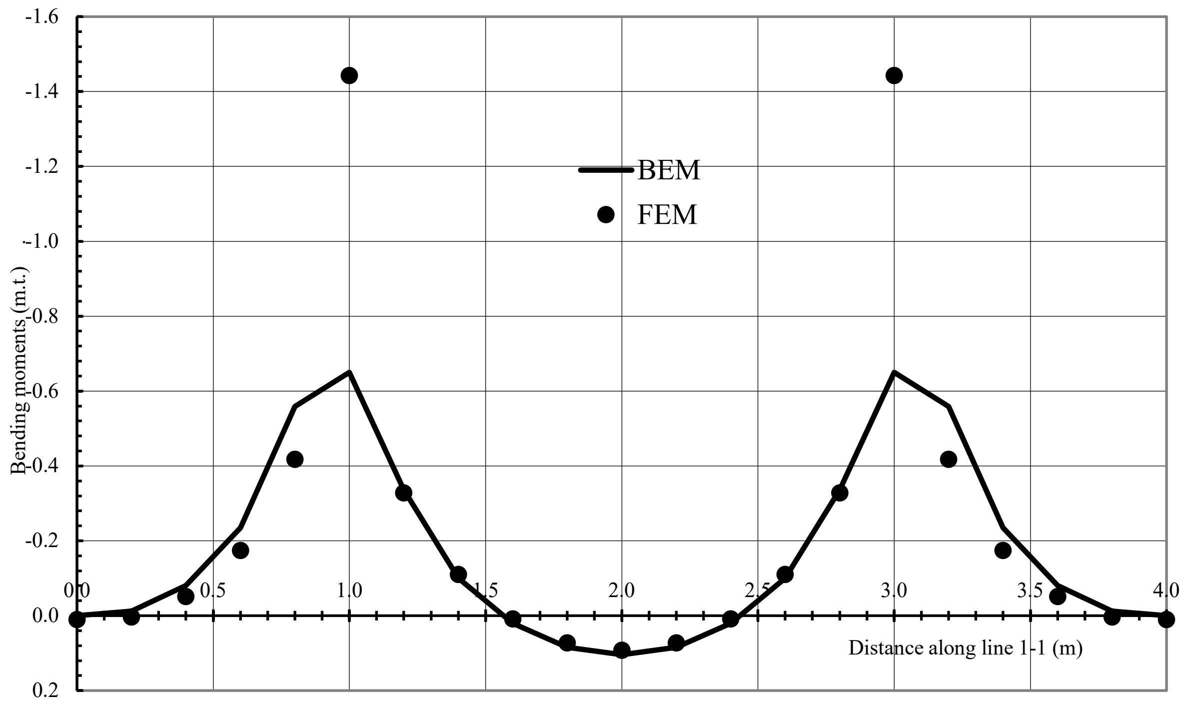

Figure 1.10: Bending moment diagram along line 1-1 (t=0.4) in Example 1.2.

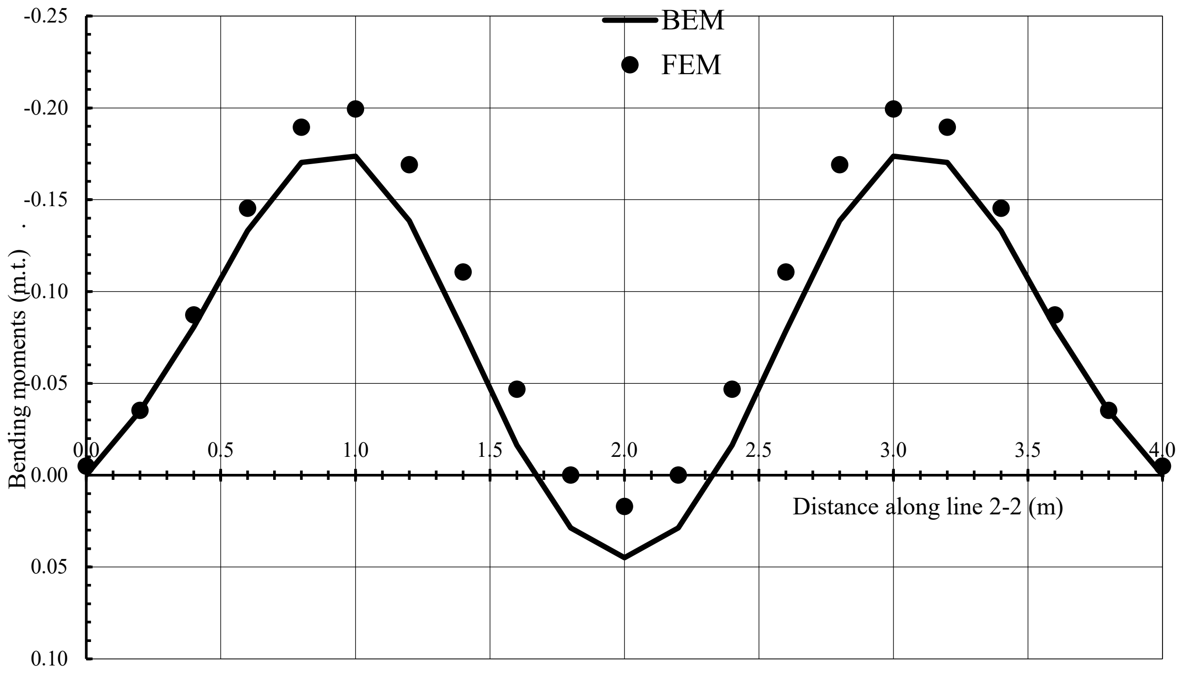

Figure 1.11: Bending moment diagram along line 2-2 (t=0.4) in Example 1.2.

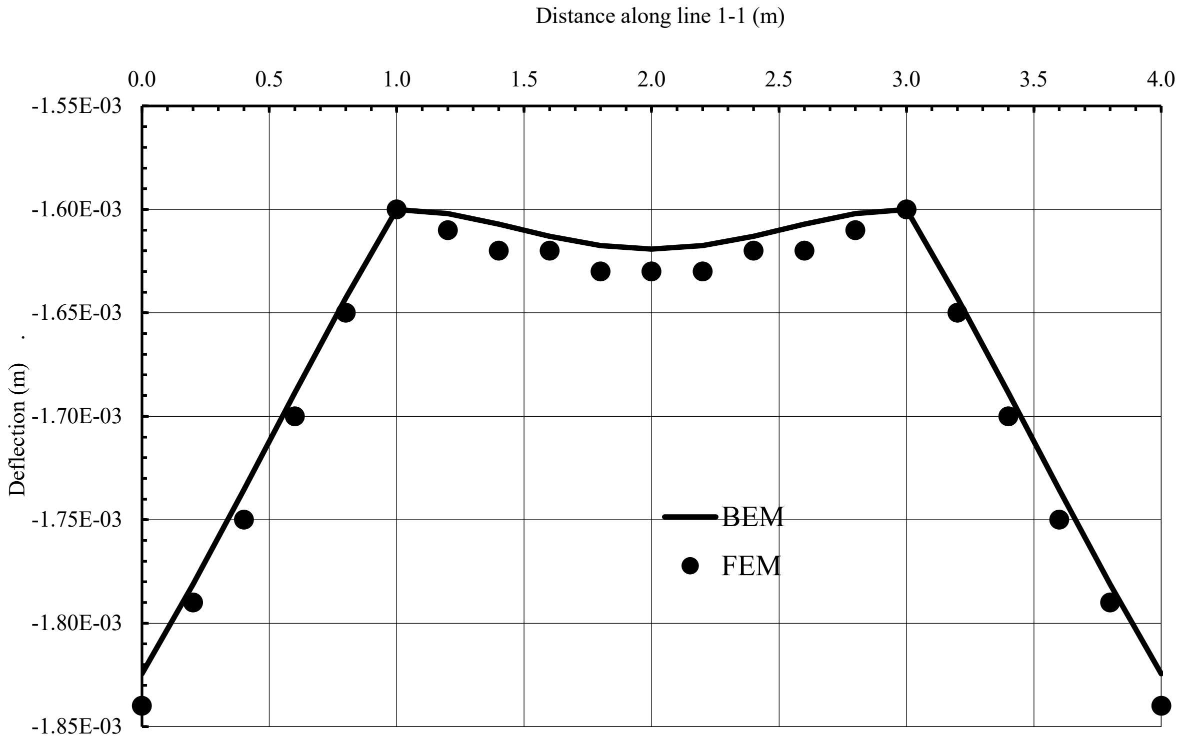

Figure 1.12: Deflection distribution along line 1-1 (t=0.1) in Example 1.2.

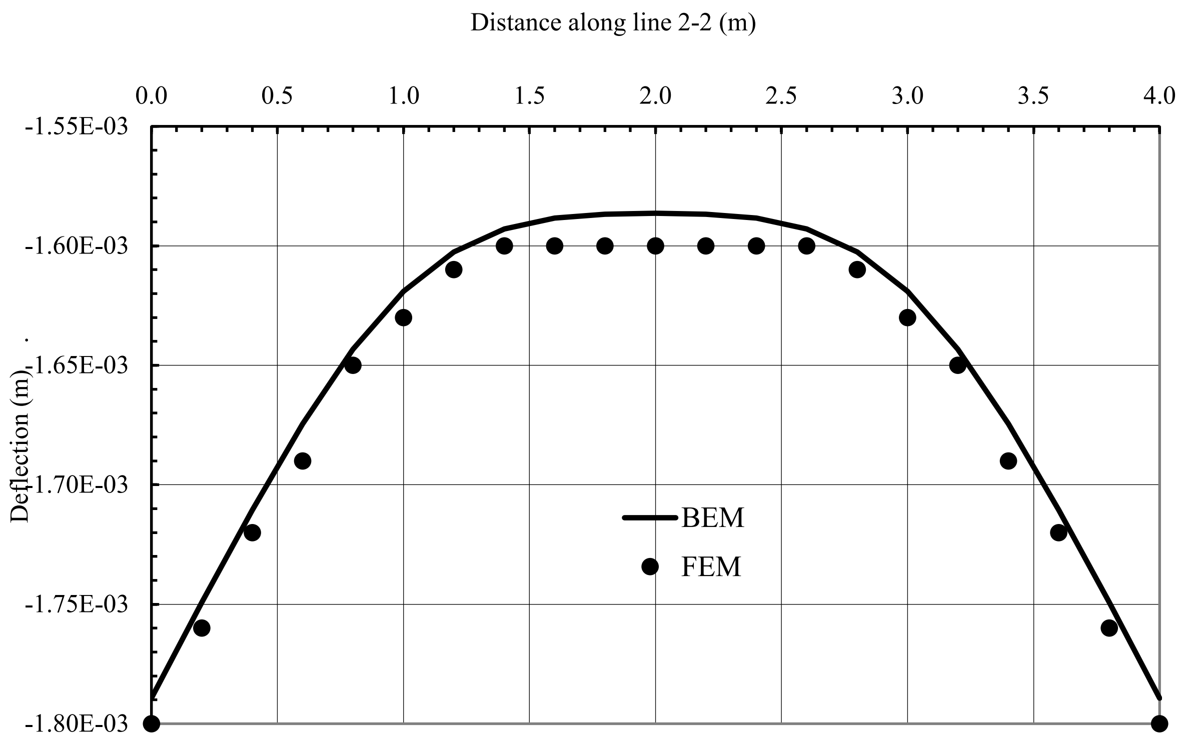

Figure 1.13: Deflection distribution along line 2-2 (t=0.1) in Example 1.2.

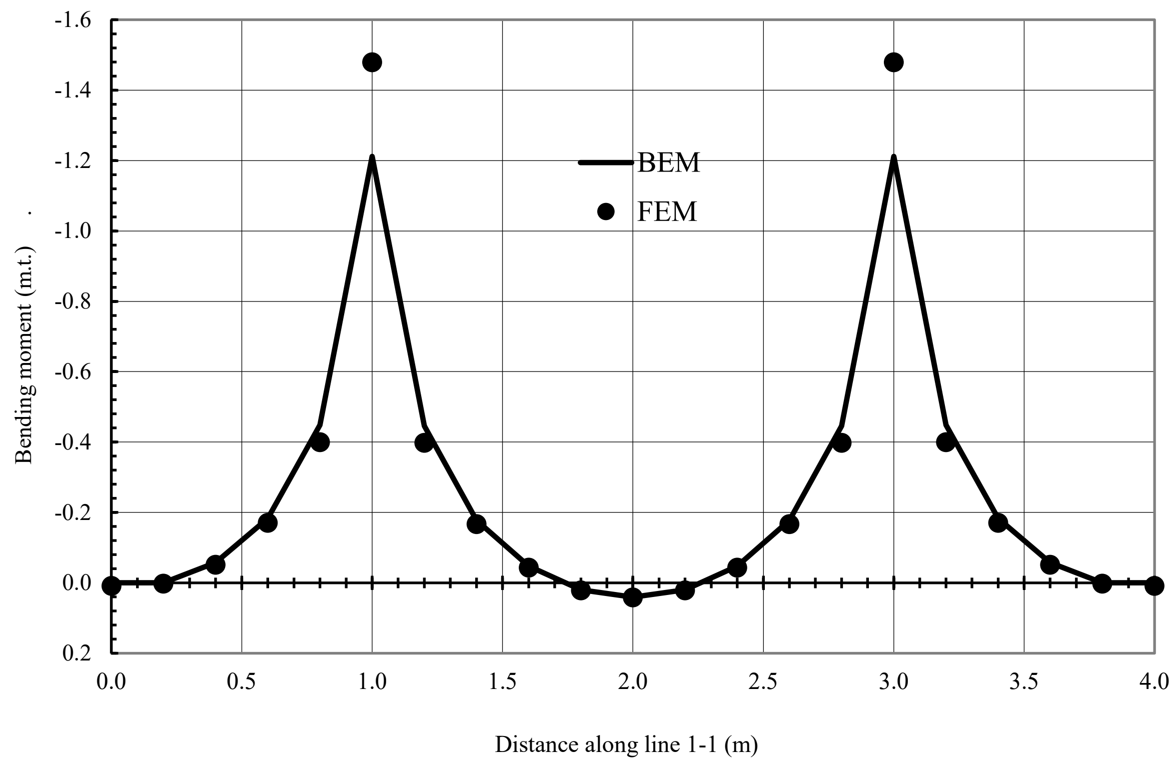

Figure 1.14: Bending moment diagram along line 1-1 (t=0.1) in Example 1.2.

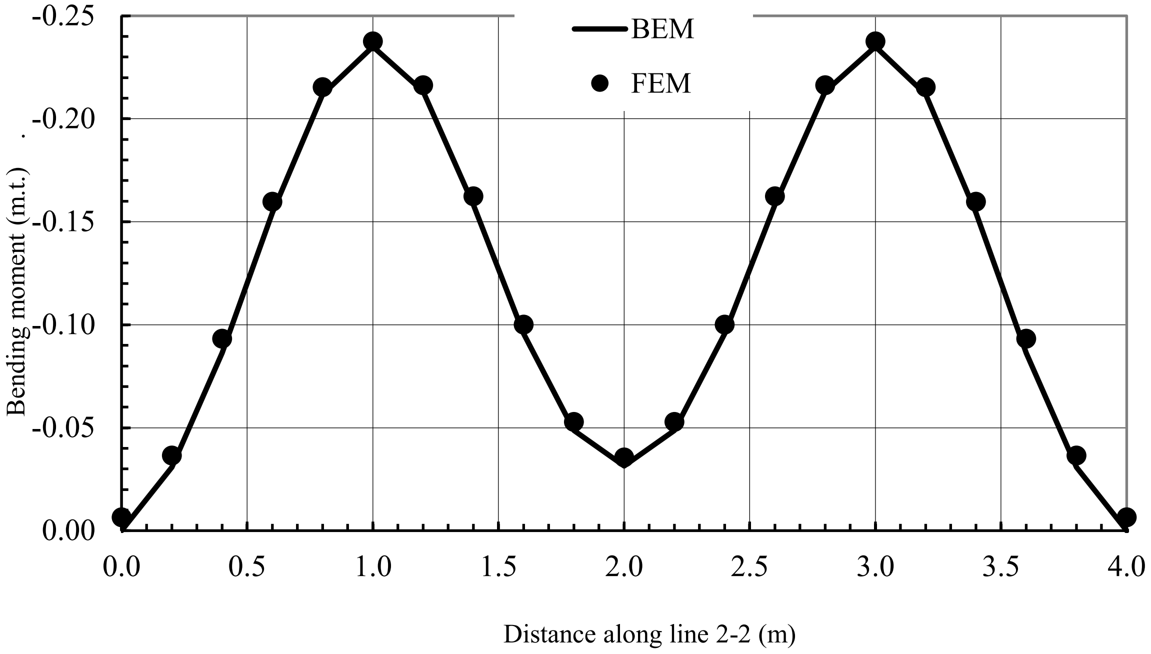

Figure 1.15: Bending moment diagram along line 2-2 (t=0.1) in Example 1.2.

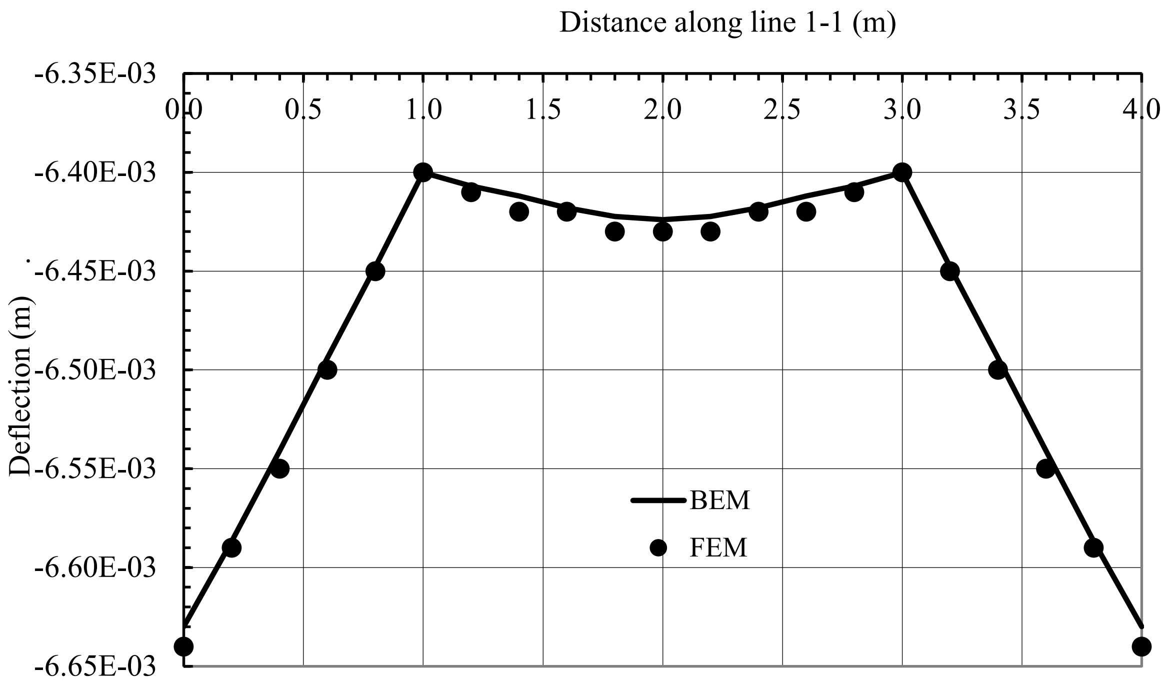

Figure 1.16: Deflection distribution along line 1-1 (t=0.05) in Example 1.2.

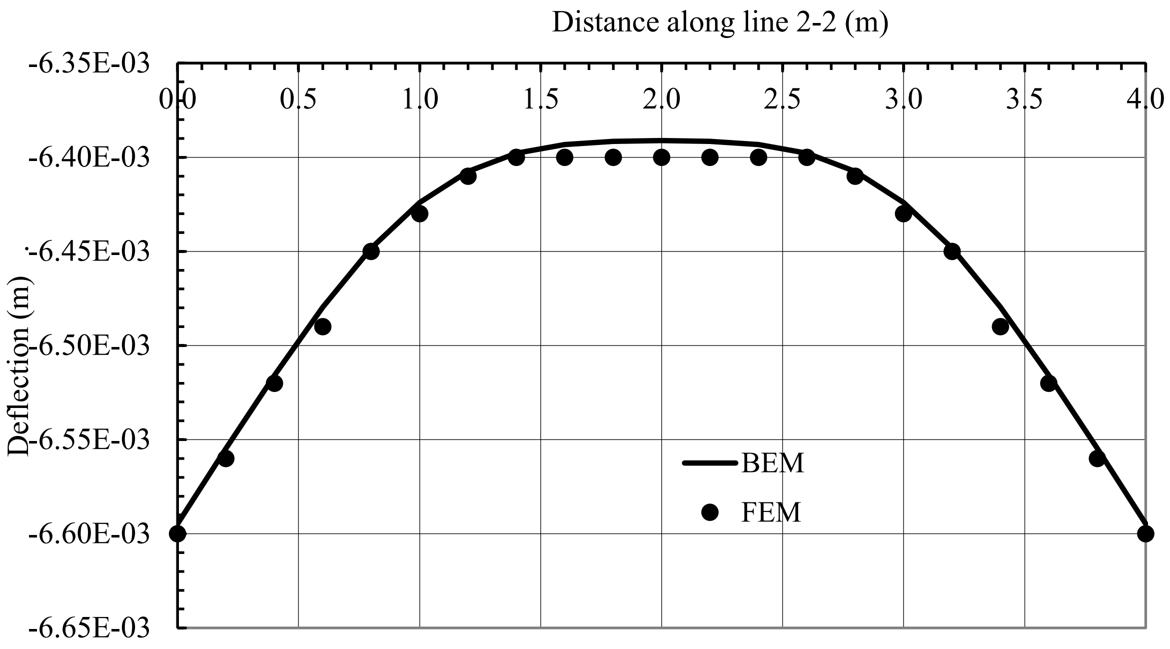

Figure 1.17: Deflection distribution along line 2-2 (t=0.05) in Example 1.2.

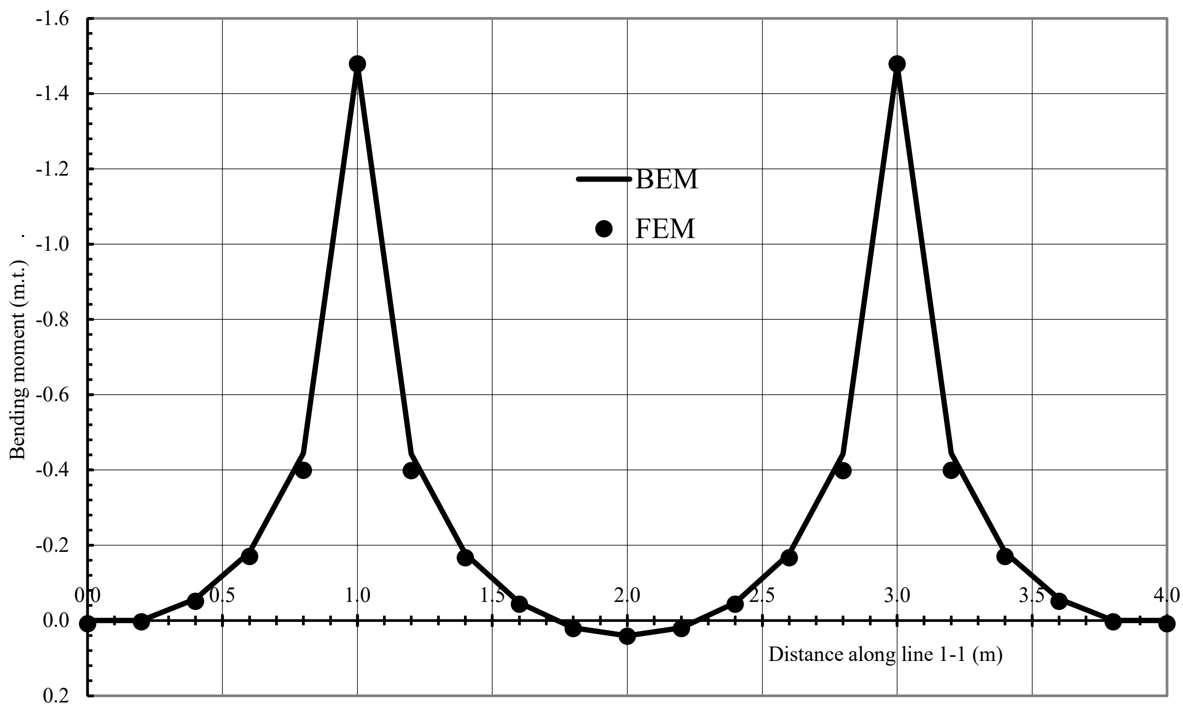

Figure 1.18: Bending moment diagram along line 1-1 (t=0.05) in Example 1.2.

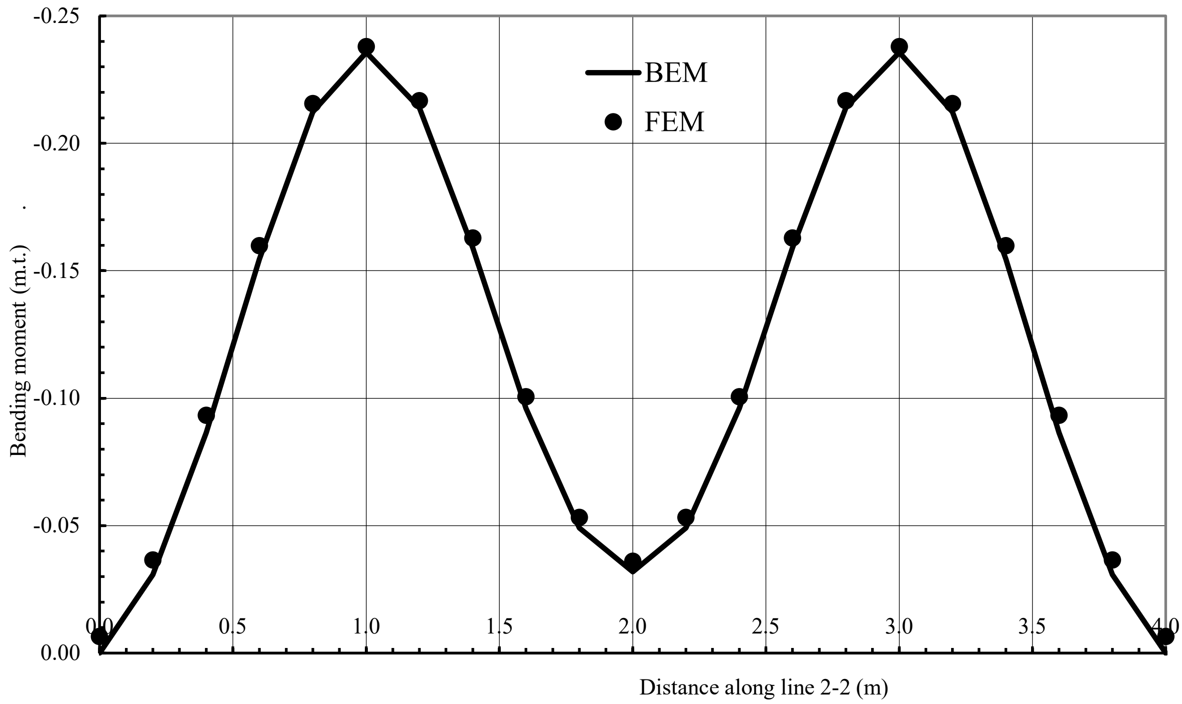

Figure 1.19: Bending moment diagram along line 2-2 (t=0.05) in Example 1.2.

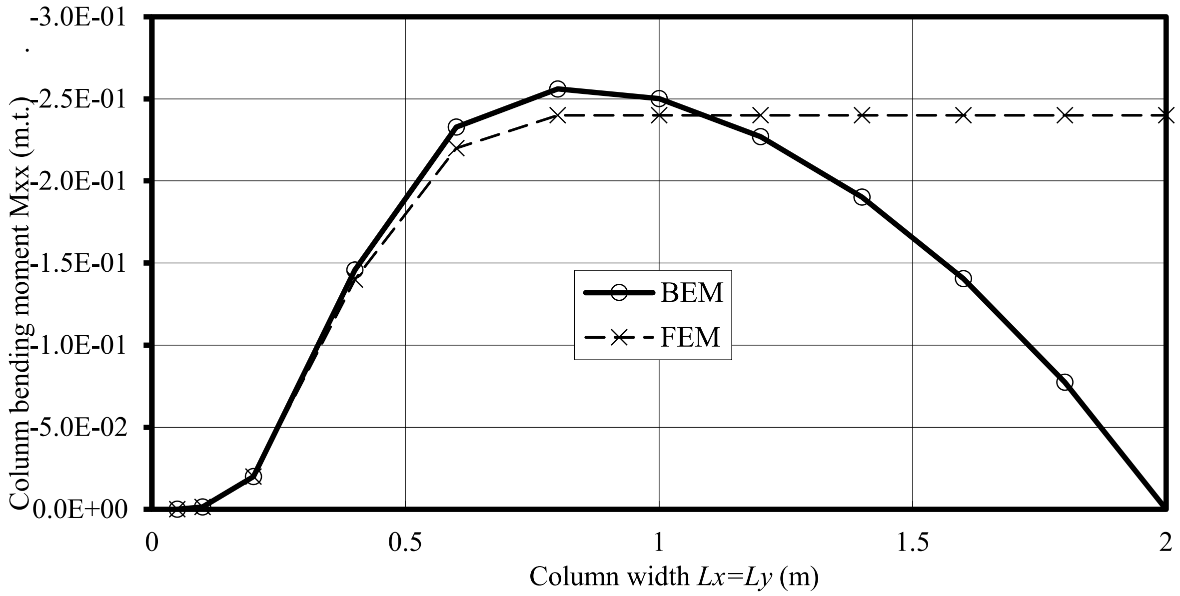

Figure 1.20: Changing of column bending moment M_{xx} by increasing Lx (and Ly) for square column dimensions in Example 1.2.

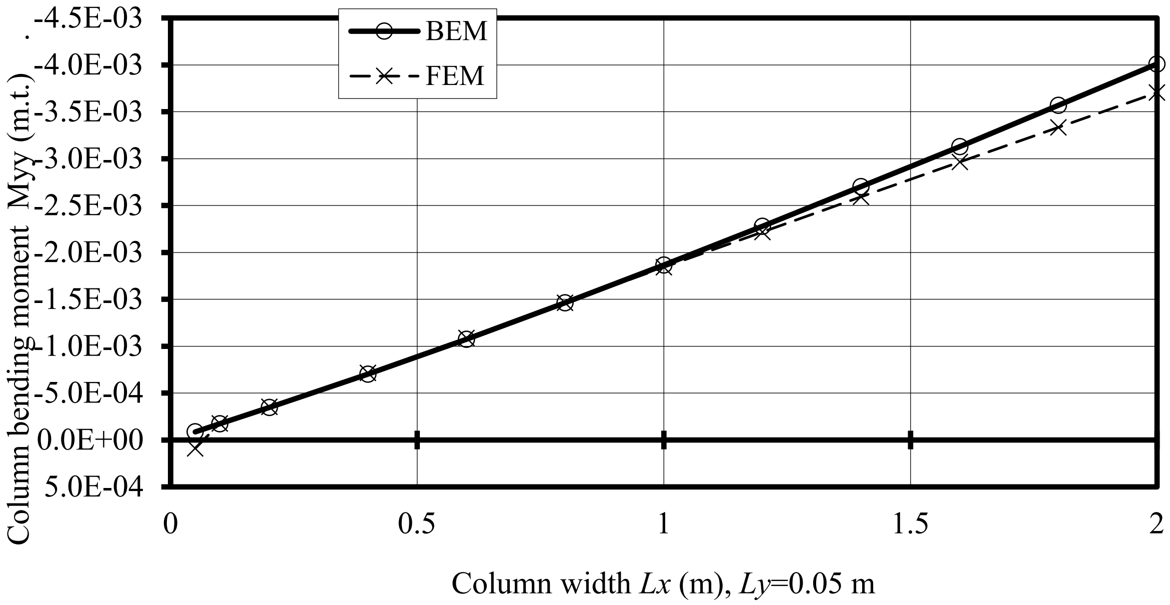

Figure 1.21: Changing of column bending moment M_{yy} by increasing Lx (Ly is constant = 0.05 m) for square column dimensions in Example 1.2.

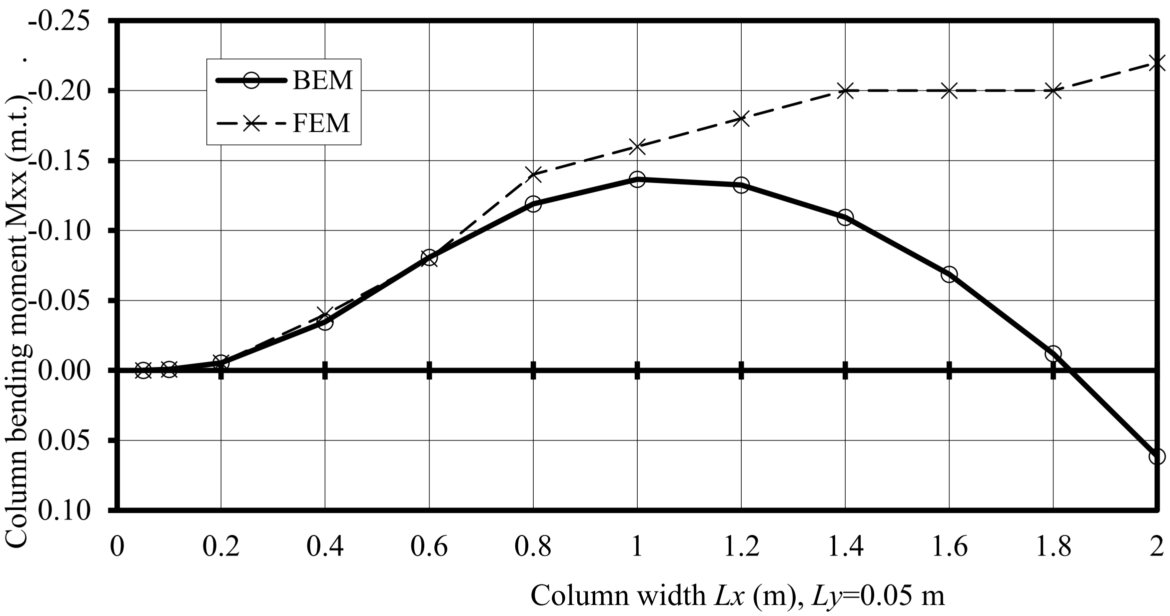

Figure 1.22: Changing of column bending moment M_{xx} by increasing Lx (Ly is constant = 0.05 m) for square column dimensions in Example 1.2.

Example 1.3 [7]

Purpose : Verify that the PLPAK area modelling can really model the actual structure. This is done by modelling a beam and comparing the results against the analytical solution.

Description : The beam shown in Figure 1.23 is of $0.50 \times 0.25\ m^2$ cross section is carrying a slab of $2.00 \times 0.25\ m^2$ (thickness $0.10\ m$) and supported on two eccentric columns $(0.25 \times 0.10\ m^2)$ cross section. The beam is loaded by central cell $(0.25 \times 0.10\ m2)$ loading of $1000\ kN$. The boundary element model used is 4 elements along the slab long side and 2 for the short side. The beam is divided into 20 cells. It should be noted that additional boundary elements are not necessary to improve the result accuracy. Simple manual calculations to obtain the value of the bending moment and torsion moment as follows:

Torsion moment = column reaction $(500\ kN) \times (0.125 - 0.05)m = 37.5\ kN.m$

This moment will be carried by the slab ($J = 6.234 \times 10^{-5}\ m^4$) and the beam ($J = 1.787 \times 10^{-3}\ m^4$) according to their torsional stiffness.

Results : Therefore, the analytical torsional moment for beam is $36.2356\ kN.m$. Figure 1.23 demonstrates the torsional moment distribution for this beam which is $35.1\ kN.m$, i.e., 3% difference from the analytical value. Similarly analytical bending moment can be computed as $425\ kN.m$ and the portion that carried by the beam (according to the moment of inertia ratio) is $421.6\ kN.m$. The obtained value from the present boundary element model is $419\ kN.m$, i.e., 0.6% difference from the analytical value. This demonstrates the strength of the PLPAK in modelling real area connection between slab-beam floor and column.

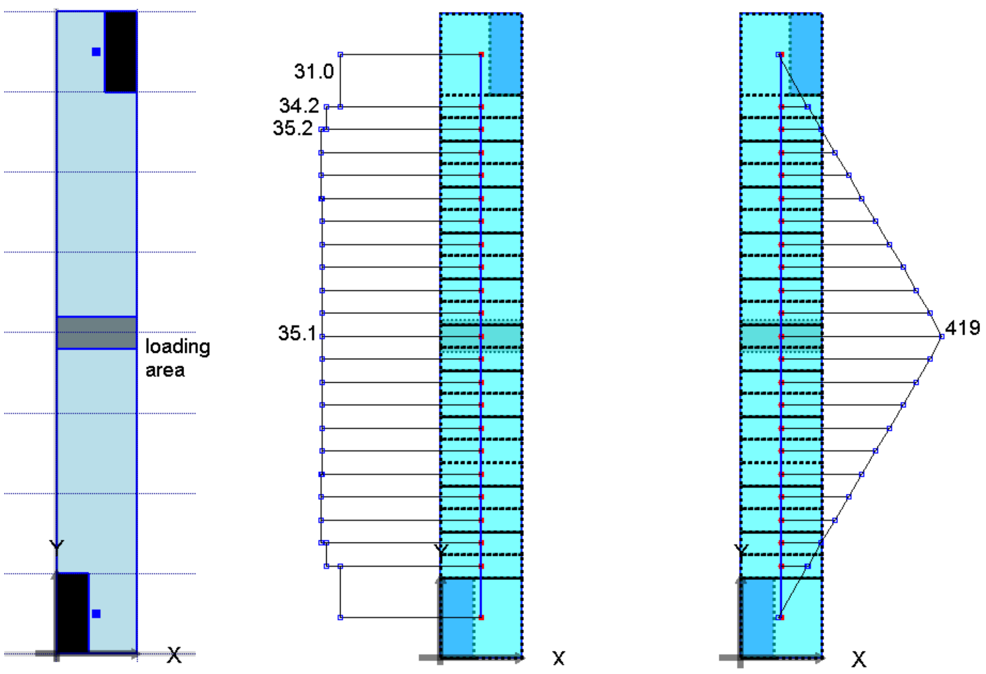

a) The b) Torsional moment C) Bending moment

Figure 1.23: The beam considered in Example 1.3 with the PLPAK model results.

Example 1.4 [7]

Purpose : Compare the PLPAK's results with other boundary element formulation and with the finite element.

Description : The other boundary element formulation is the one proposed by [8]. For finite element models, ANSYS (version 14) is used where shell elements (shell143) have been discretized to $5 \times 5\ cm^2$ to model both beams and slabs (the same element and discretization are used by [8]). The slab shown in Figure 1.24 is considered. Slab's thickness is $8\ cm$. Four external beams are provided on slab's edges, beams' thickness is $25\ cm$. The external beams' edges are pinned. Modulus of elasticity and Poisson's ratio are equal to $25 \times 106\ kN/m^2$ and 0.25 respectively. A distributed load of $20\ kN/m^2$ is applied on the whole surface of slab and beams. The same problem was analyzed by [8] using his proposed formulation and using finite element method (ANSYS).

Results : Figure 1.25-Figure 1.27 show the deflection computed along axes x, x' and y, respectively. These results conclude that the PLPAK results agree with [8] results and the FEM; which verify the PLPAK's results.

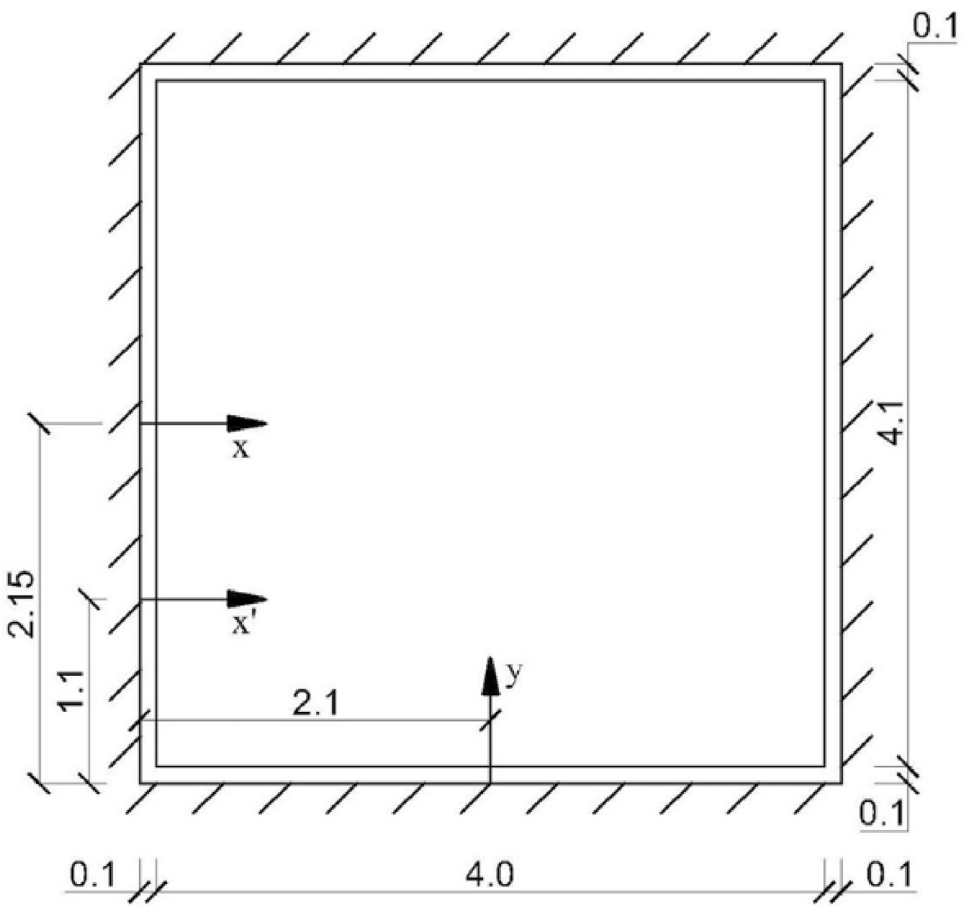

Figure 1.24: The slab with edge beams considered in Example 1.4.

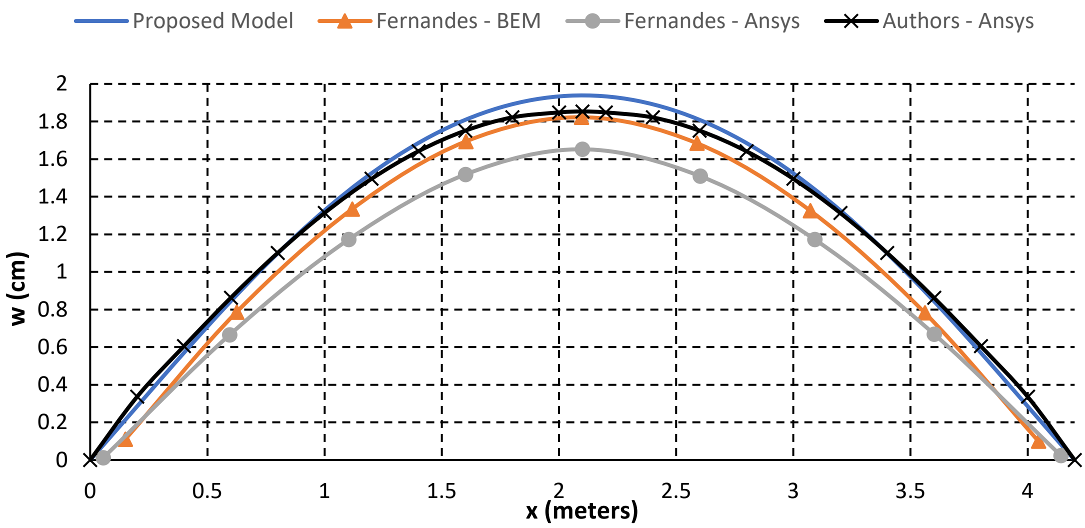

Figure 1.25: Slab's deflection along middle axis x in Example 1.4.

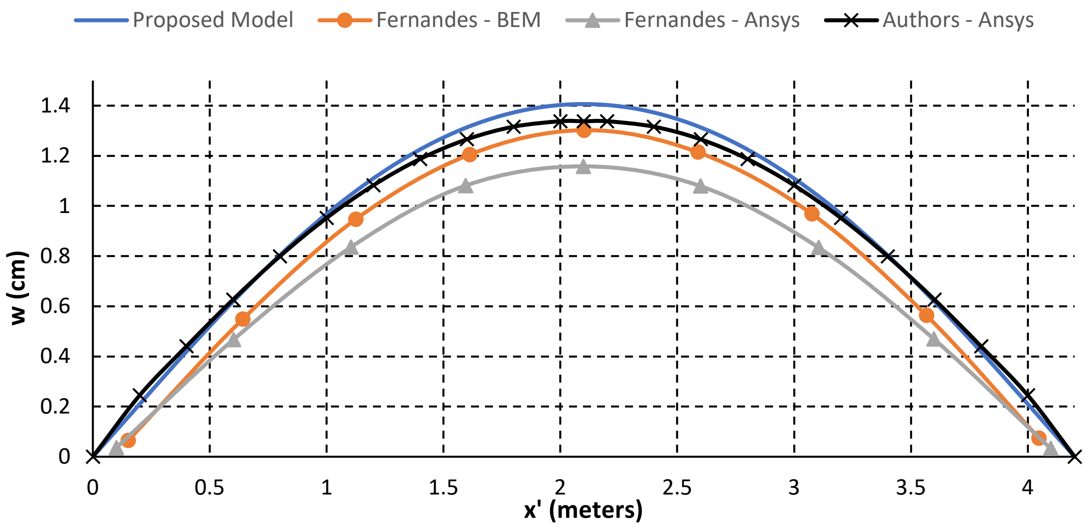

Figure 1.26: Slab's deflection along x'-axis in Example 1.4.

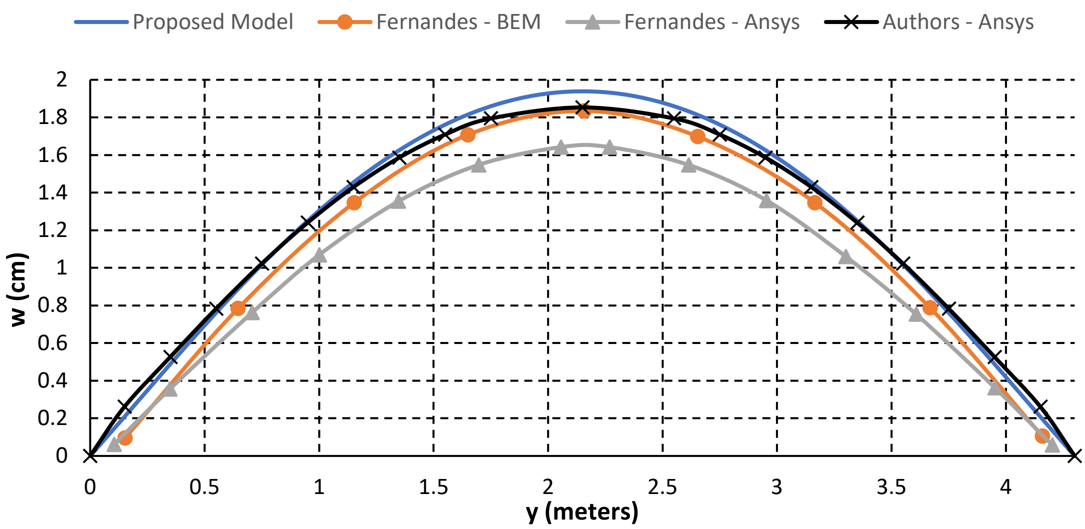

Figure 1.27: Slab's deflection along y-axis in Example 1.4.

Example 1.5 [7]

Purpose	:	Compare the PLPAK's results with other boundary element formulation and with the finite element.
Description	:	Slab in Example 1.4 is reconsidered here by adding an internal beam as shown in Figure 1.28. All data in Example 1.4 is the same in this example.
Results	:	Figure 1.29-Figure 1.31 show the deflection computed along axes x, x' and y respectively. These results conclude that the PLPAK results agree with [8] results and the FEM; which verify the PLPAK's results.

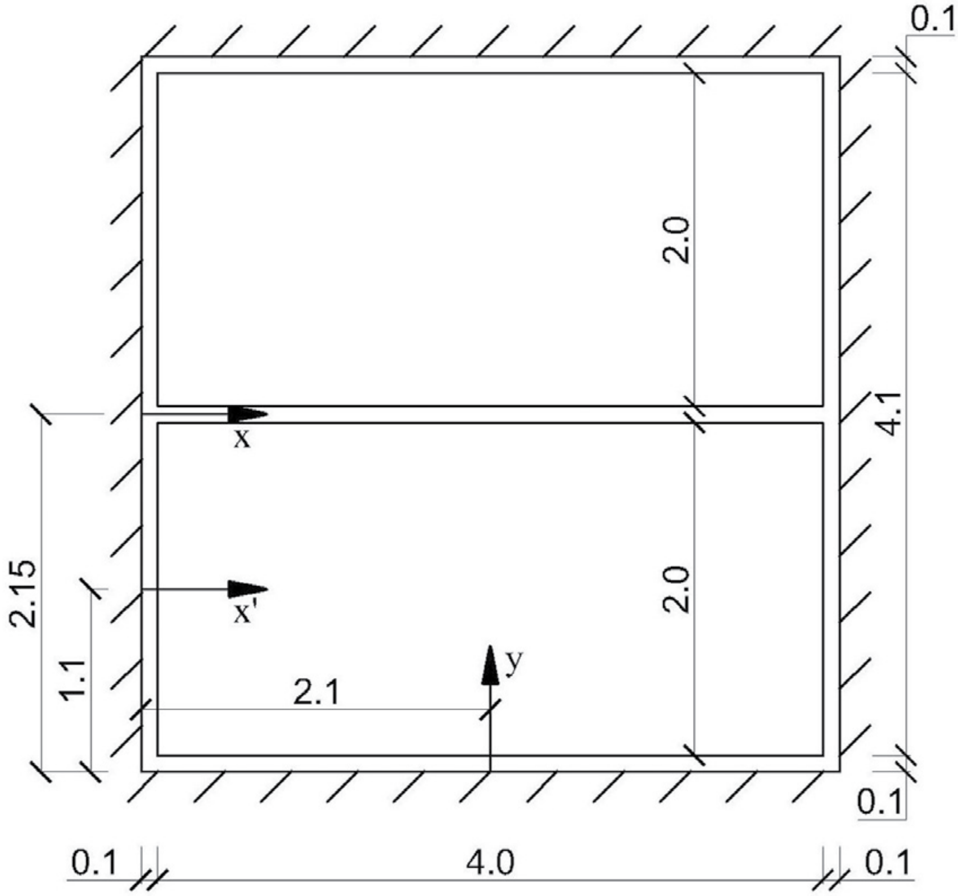

Figure 1.28: The slab with edge beams and internal beam considered in Example 1.5.

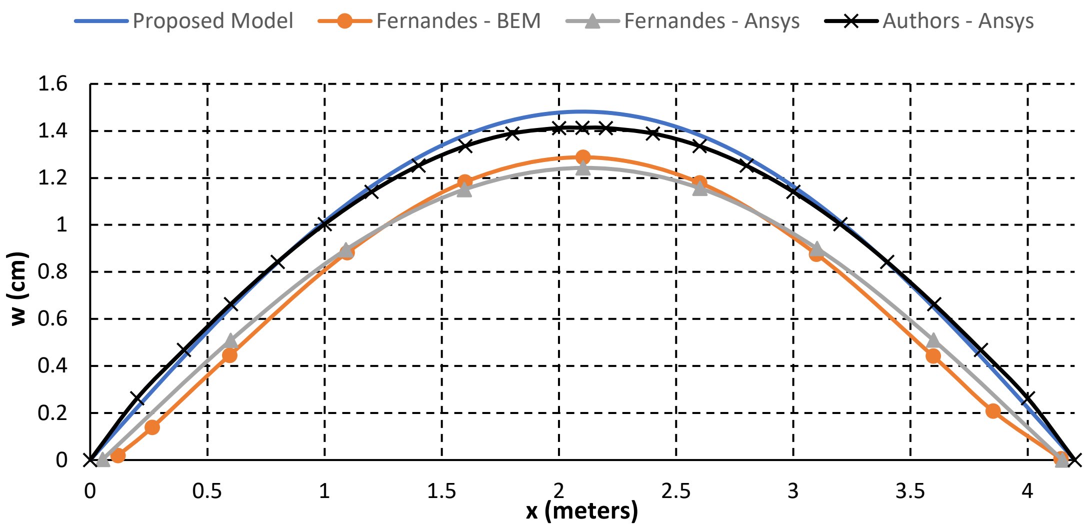

Figure 1.29: Slab's deflection along middle axis x in Example 1.5.

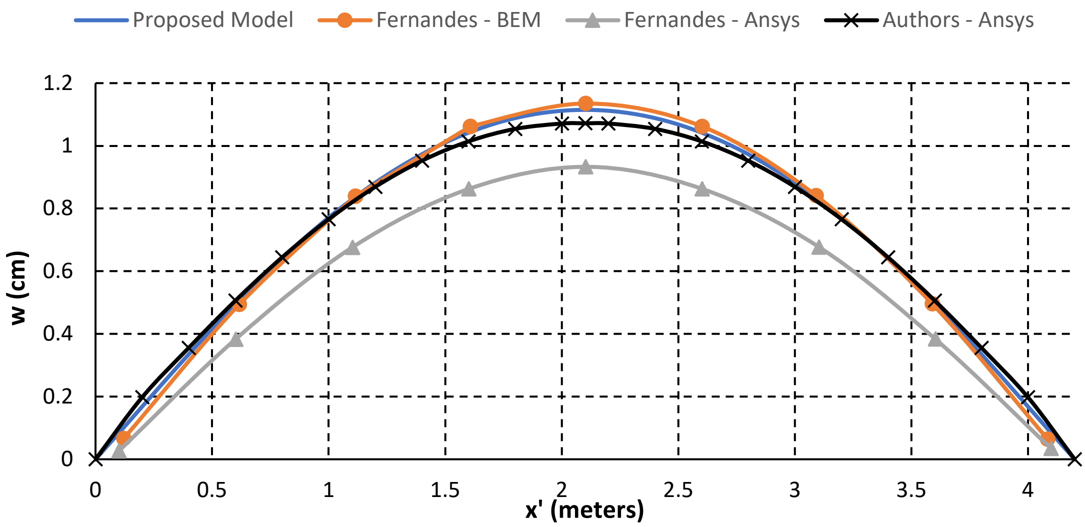

Figure 1.30: Slab's deflection along x'-axis in Example 1.5.

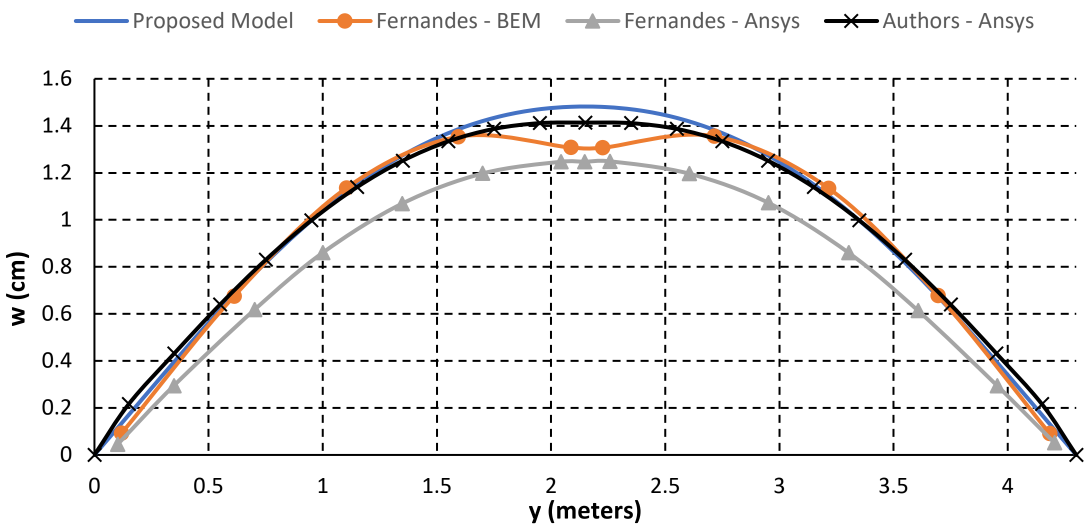

Figure 1.31: Slab's deflection along y-axis in Example 1.5.

Example 1.6 [7]

Purpose : Demonstrate the ability of the PLPAK to solve practical applications by analyzing more complicated slab-beam floors and comparing results with the finite element.

Description : The $6 \times 4\, m$ slab shown in Figure 1.32 is considered. The slab has thickness of $0.2\, m$ and rested on four columns ($0.5 \times 0.5\, m^2$ in cross section) and two beams AB and CD of cross section of $0.25 \times 0.50\, m^2$. The used modulus of elasticity is $2{,}210{,}000\, kN/m^2$ and Poisson's ratio is 0.2. The slab is loaded by uniform loading of $1000\, kN/m^2$. Figure 1.33 demonstrates the used boundary element model, where four quadratic elements are used per side and columns are represented using its actual cross section. Each beam is modelled using 23 cells as shown in Figure 1.33. The finite element models are modelled using CSI SAP2000 (version 16). Two finite element meshes are considered. The first mesh (FEM model 1, 3200 four-node plate bending elements) considers the beams are linked from the column centres as the actual geometry; whereas the second model (FEM model 2, 1600 four-node plate bending elements) considers that the columns are moved to the slab corners hence beams are located along the slab diagonals. It should be noted that FEM model 2 does not represent the actual geometry, however it is commonly used daily in engineering practice.

Results : Figure 1.35-Figure 1.38 demonstrate the deflection, bending moment, torsional moment and shear forces along the x-axis which is located along the beam AB centre as shown in Figure 1.32. Results of the PLPAK BEM model are in a good agreement against those obtained from the finite element results.

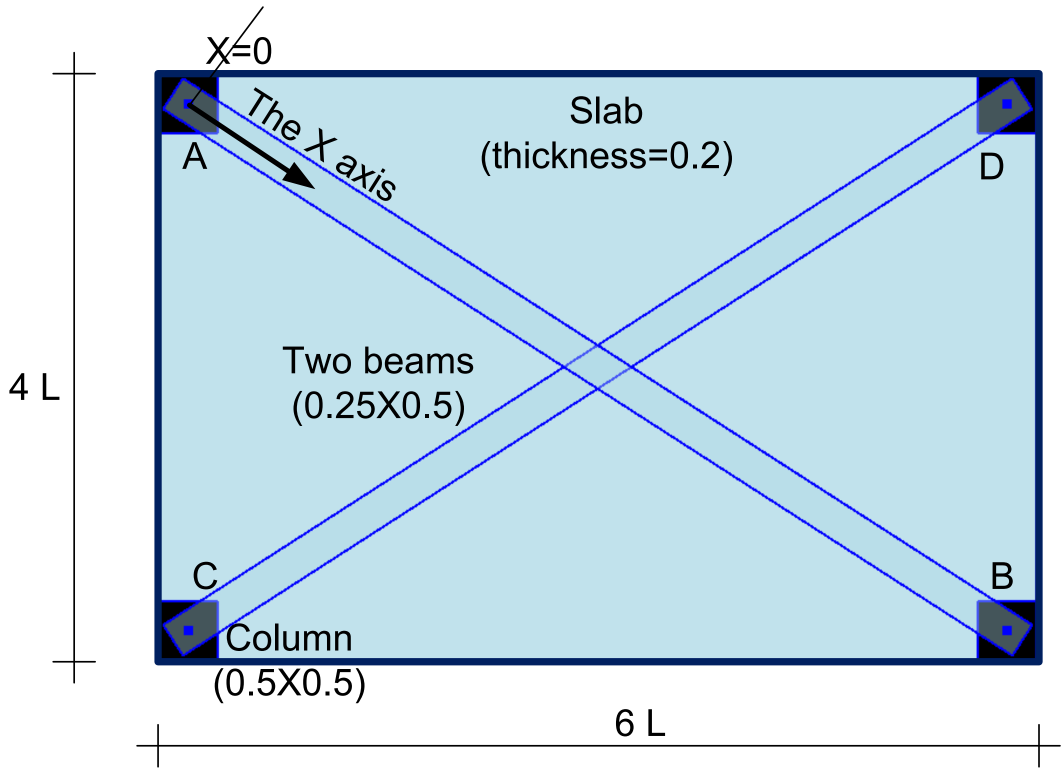

Figure 1.32: The slab geometry considered in Example 1.6.

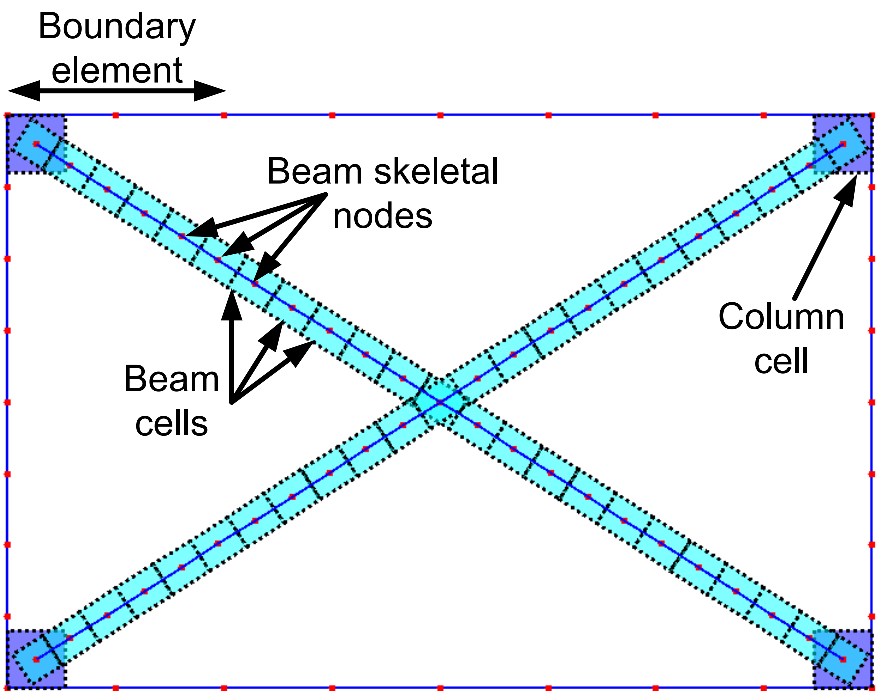

Figure 1.33: The used boundary element mesh in Example 1.6.

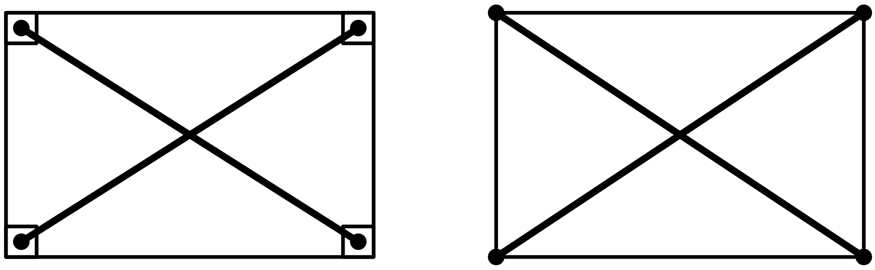

Figure 1.34: Sketch showing the slab finite element models considered in Example 1.6.

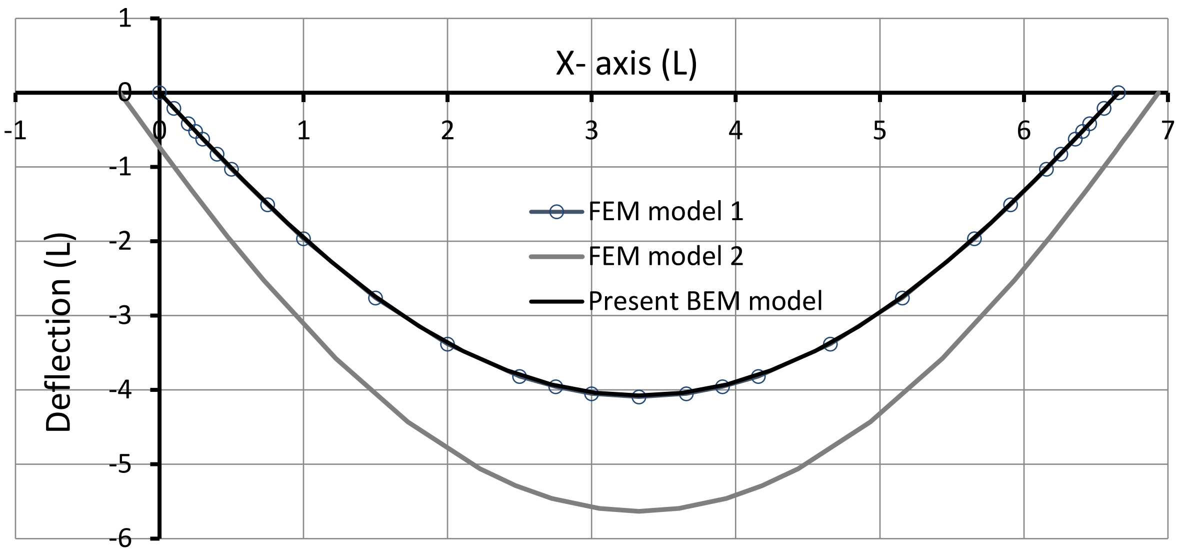

Figure 1.35: Deflection diagram of slab in Example 1.6.

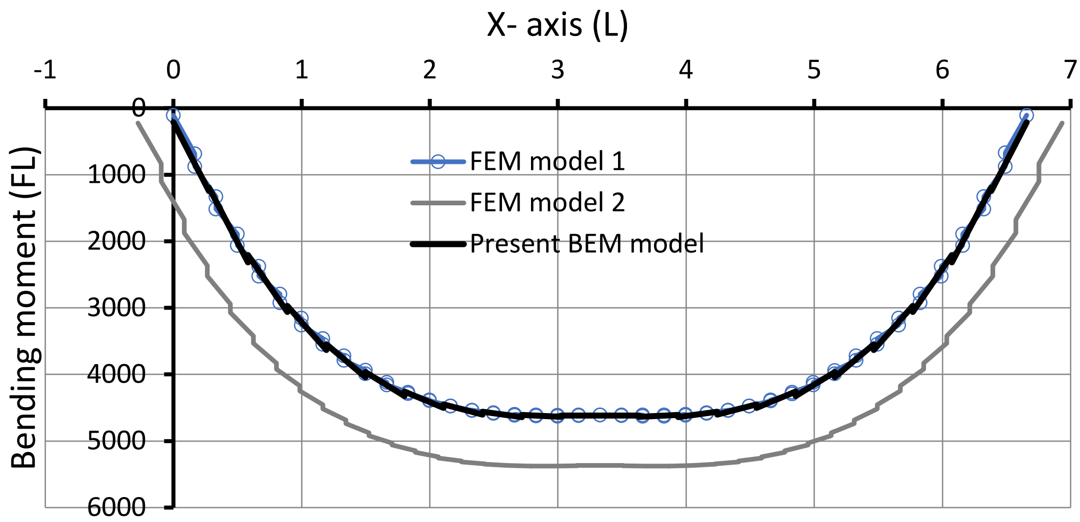

Figure 1.36: Bending moment diagram of slab in Example 1.6.

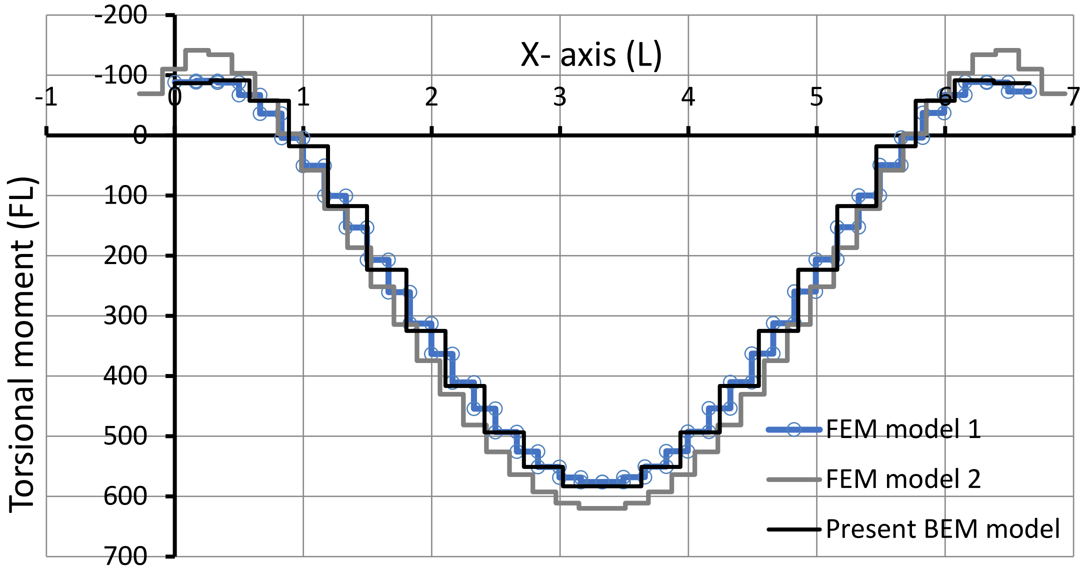

Figure 1.37: Torsion moment diagram of slab in Example 1.6.

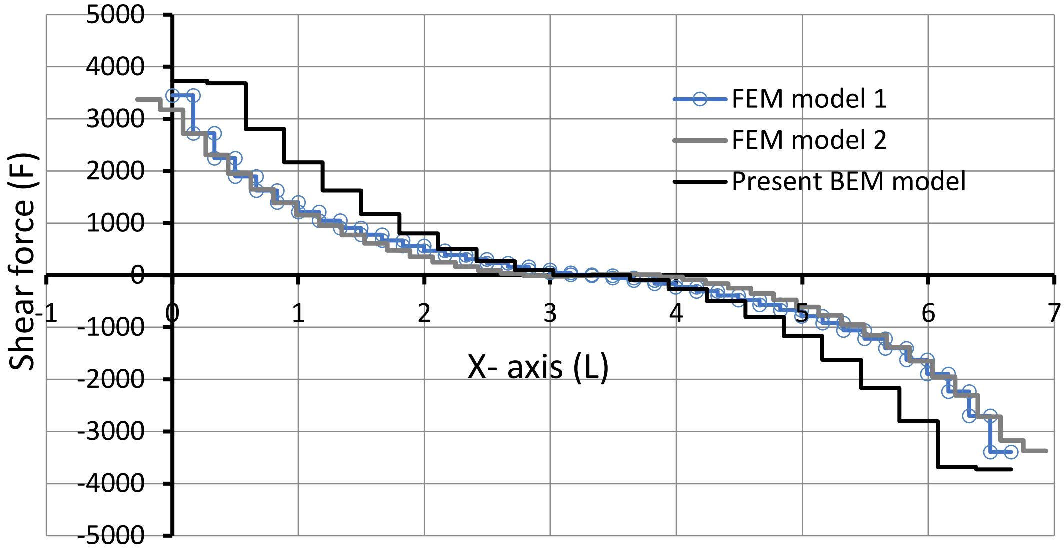

Figure 1.38: Shear force diagram of slab in Example 1.6.

Example 1.7 [7]

Purpose : Demonstrate the ability of the PLPAK to solve practical applications by analyzing real building's slab and comparing results with the finite element.

Description : The real building's slab shown in Figure 1.39 is considered. Slab's thickness is $0.2\ m$. Beams' dimensions are shown in Figure 1.39. Columns' height is $3\ m$. Modulus of elasticity and Poisson ratio are equal to $2{,}210{,}000\ kPa$ and 0.3, respectively. The considered slab was analyzed under distributed vertical load of $10\ kN/m^2$ using both the PLPAK for the BEM model and the CSI ETABS (version 16) for the FEM model. Columns and beams in the FEM are modelled using frame element, as used commonly in engineering practice.

Results : Figure 1.40 and Figure 1.41 show the contour map of deflection for both models. Figure 1.42 and Figure 1.43 show the slab's bending moment (M_{yy}) along Sections 1 and 2, respectively. Figure 1.44 shows the slab's bending moment (M_{xx}) along Section 3. Figure 1.45-Figure 1.56 show the bending moment and shearing force diagrams along beams $B1$, $B2$ and $B3$, as shown in Figure 1.39. Results of the PLPAK are of good agreement with those obtained from FEM.

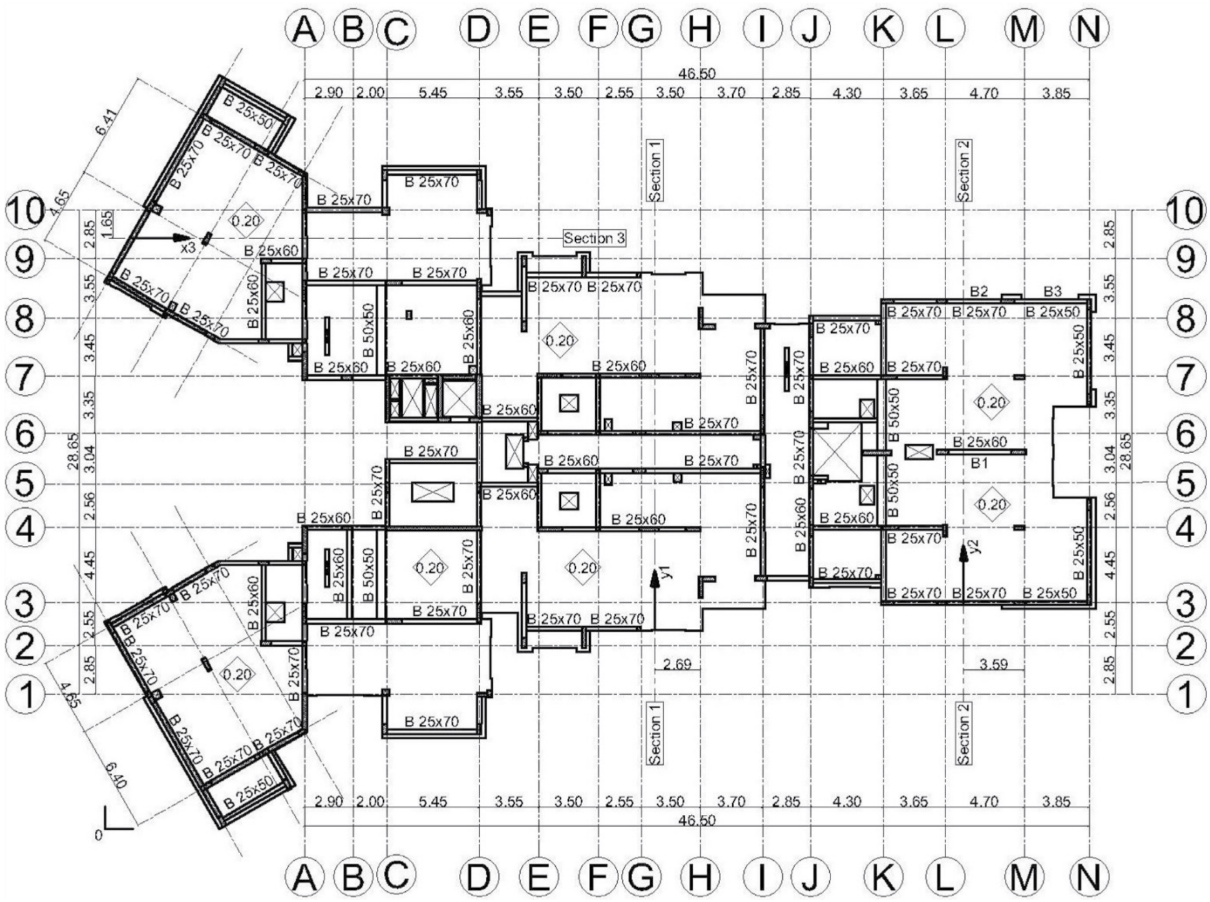

Figure 1.39: Structural plan of slab considered in Example 1.7.

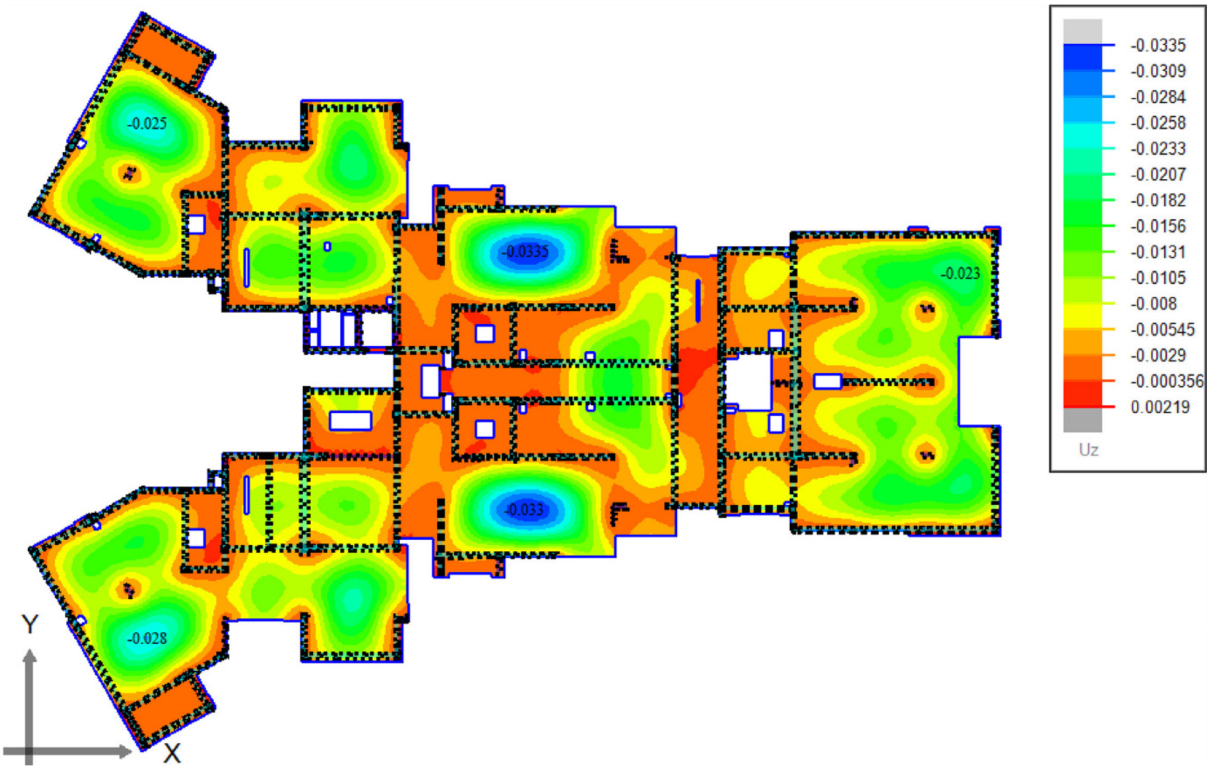

Figure 1.40: Proposed model deflection contours in Example 1.7.

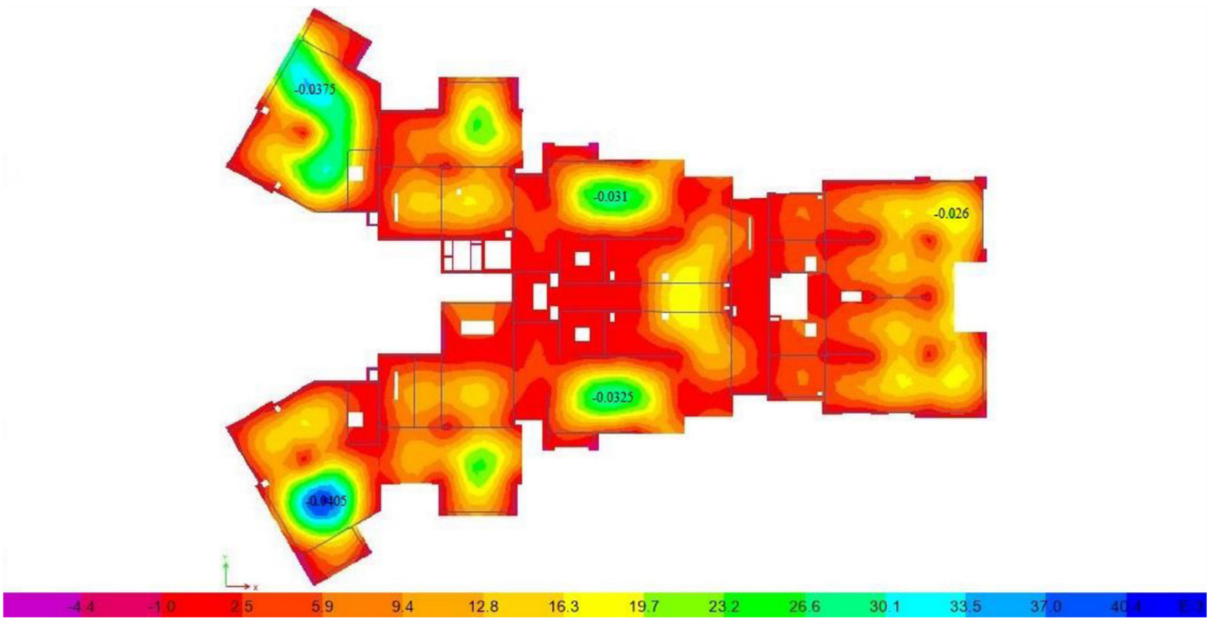

Figure 1.41: FEM deflection contours in Example 1.7.

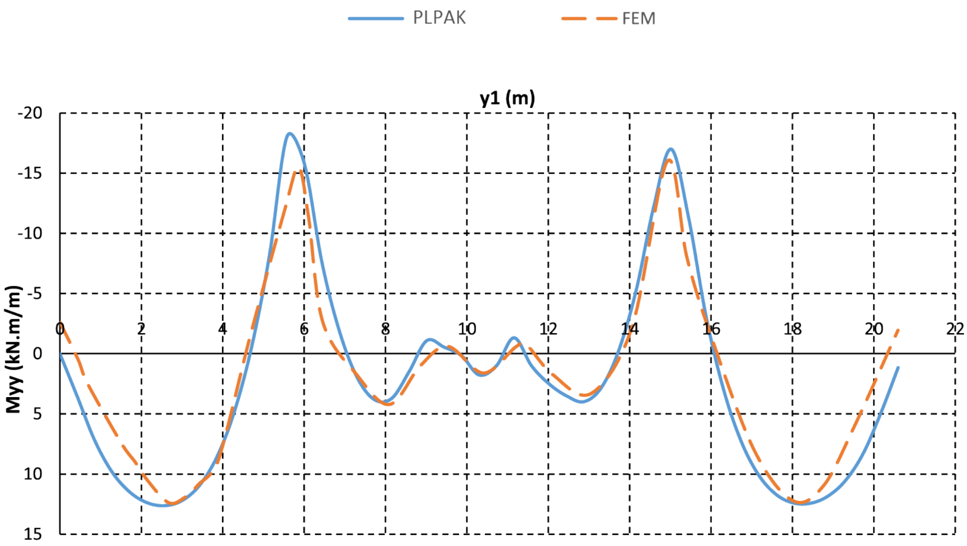

Figure 1.42: Bending moment (M_{yy}) along Section 1 in Example 1.7.

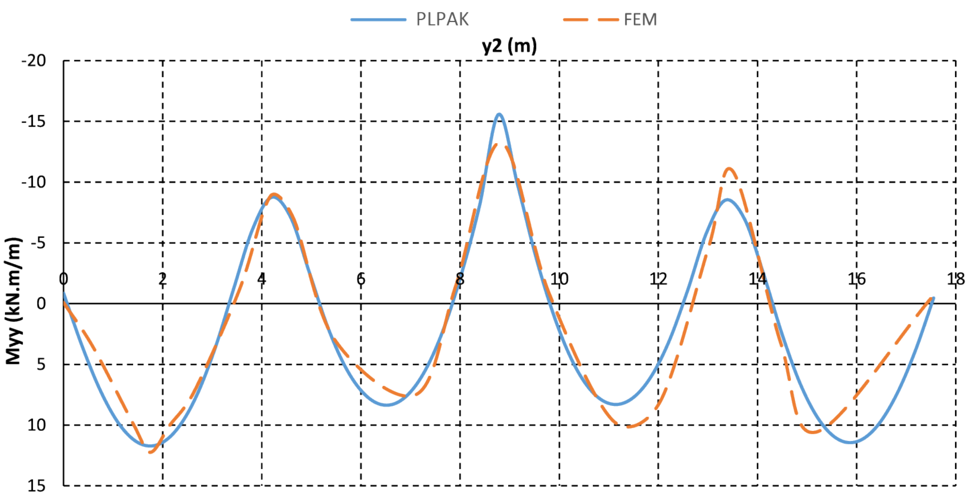

Figure 1.43: Bending moment (M_{yy}) along Section 2 in Example 1.7.

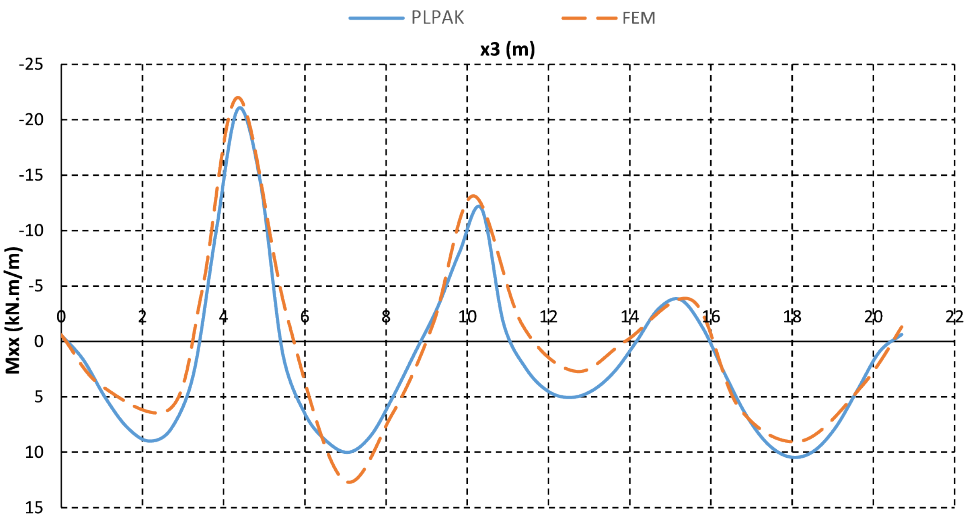

Figure 1.44: Bending moment (M_{xx}) along Section 3 in Example 1.7.

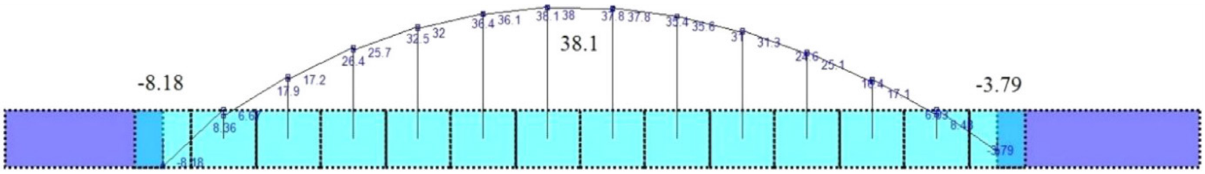

Figure 1.45: Proposed model bending moment for B1 in Example 1.7.

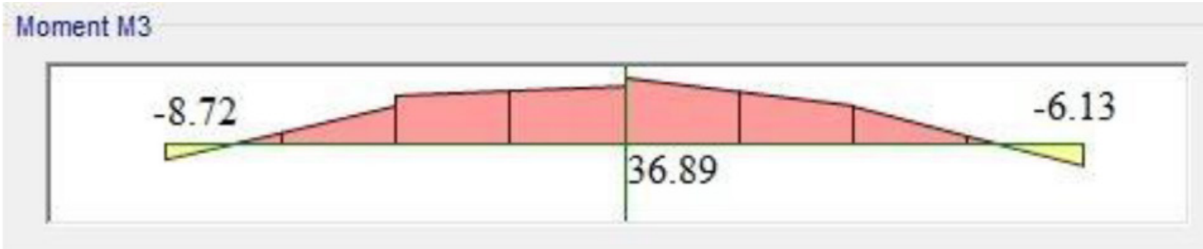

Figure 1.46: FEM bending moment for B1 in Example 1.7.

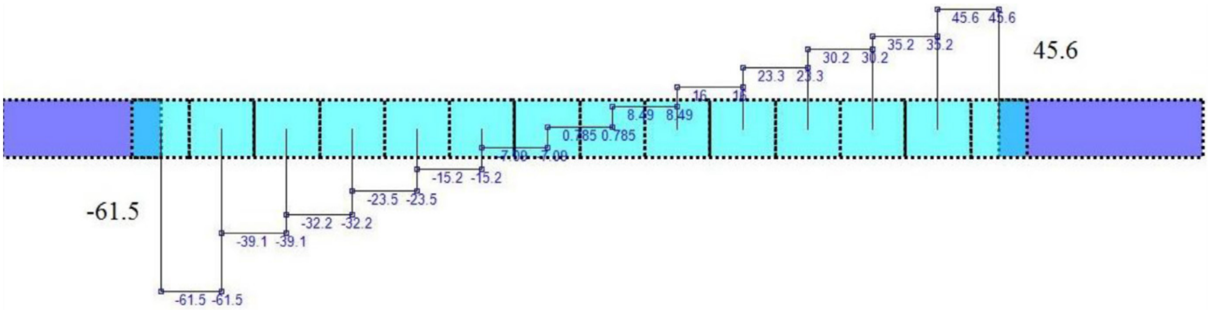

Figure 1.47: Proposed model shearing force for B1 in Example 1.7.

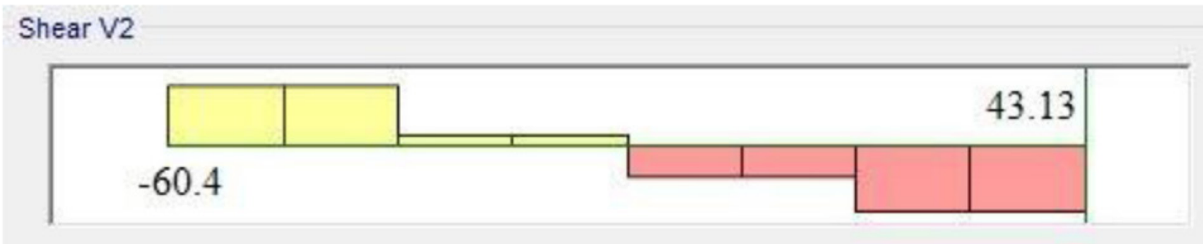

Figure 1.48: FEM shearing force for B1 in Example 1.7.

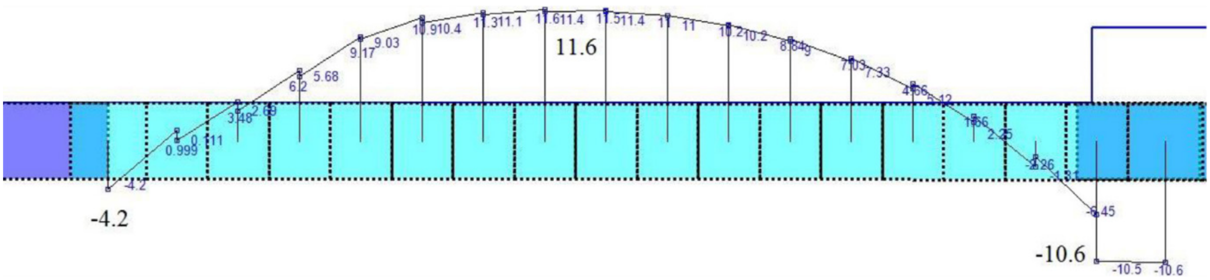

Figure 1.49: Proposed model bending moment for B2 in Example 1.7.

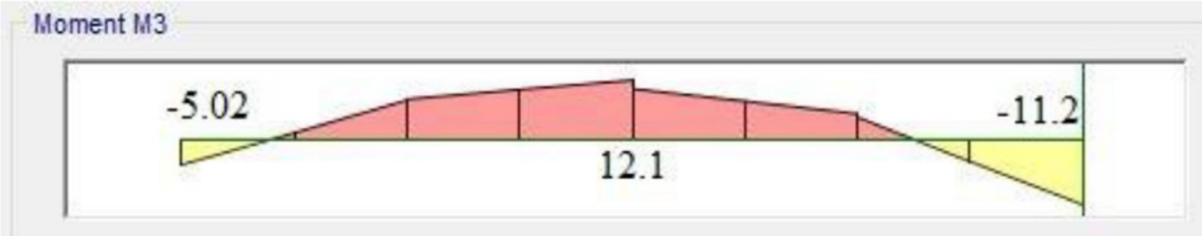

Figure 1.51: FEM bending moment for B2 in Example 1.7.

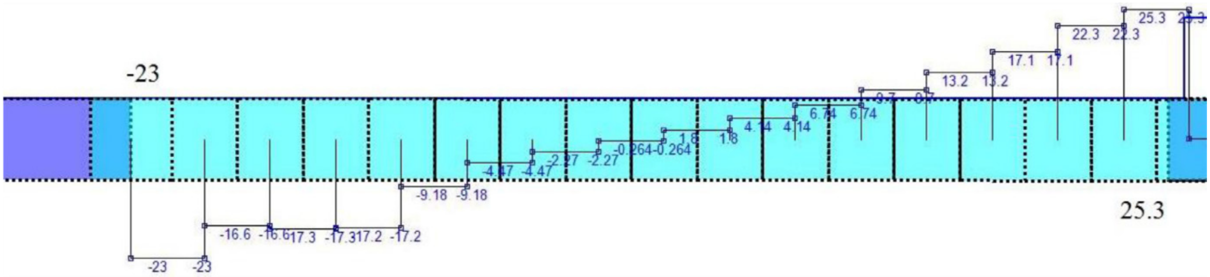

Figure 1.50: Proposed model shearing force for B2 in Example 1.7.

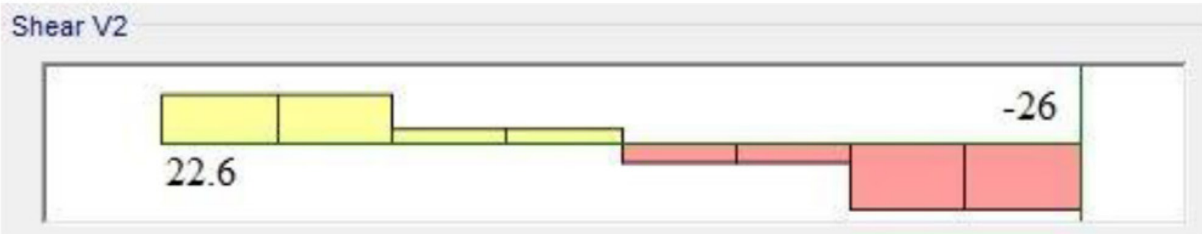

Figure 1.52: FEM shearing force for B2 in Example 1.7.

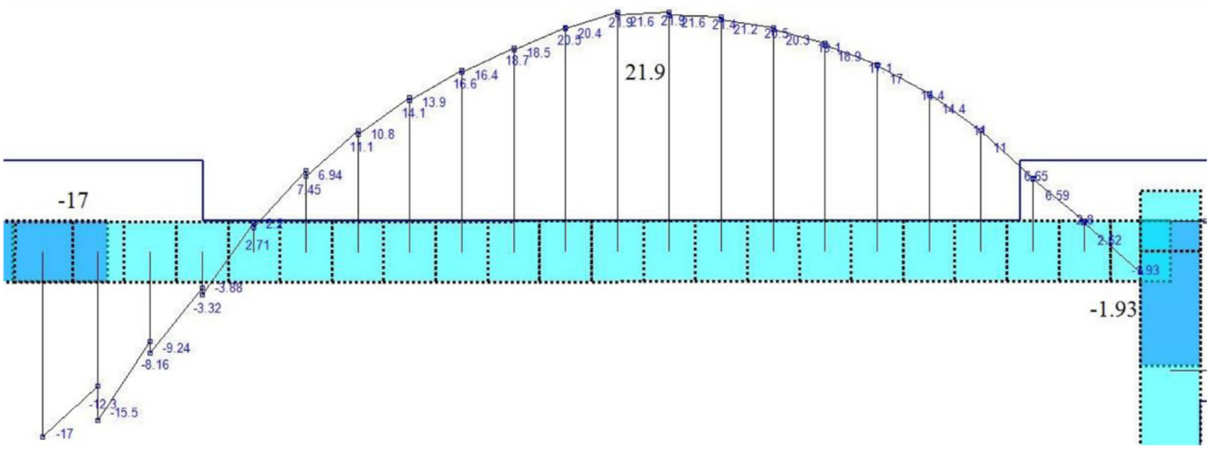

Figure 1.53: Proposed model bending moment for B3 in Example 1.7.

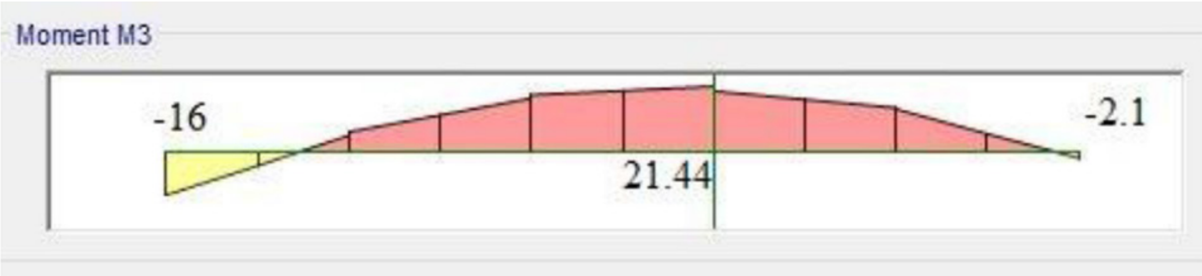

Figure 1.54: FEM bending moment for B3 in Example 1.7.

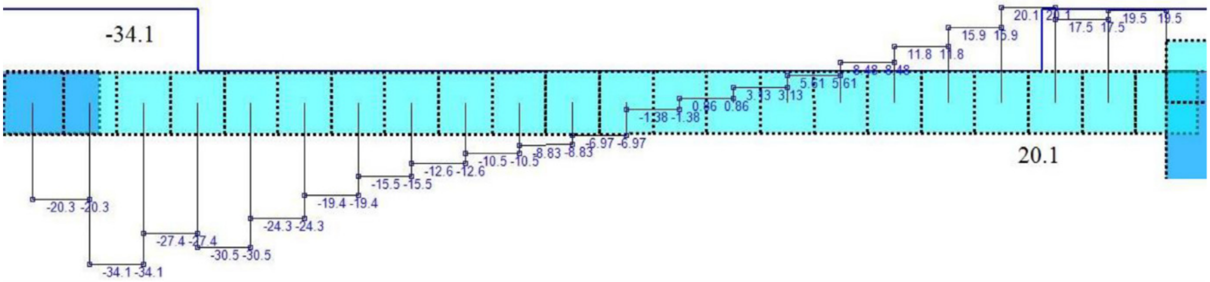

Figure 1.55: Proposed model shearing force for B3 in Example 1.7.

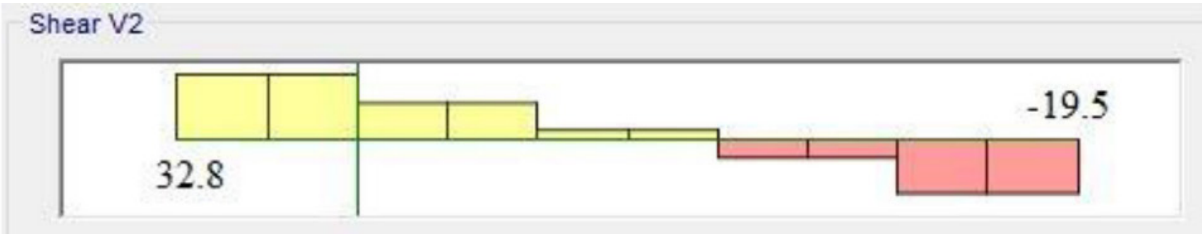

Figure 1.56: FEM shearing force for B3 in Example 1.7.

Example 1.8 [9]

Purpose : Comparing results of multi-thickness cantilever slab against the analytical solution.

Description : The cantilever slab demonstrated in Figure 1.57 has a multi-thickness of 0.25m/0.5 m. The slab is loaded by a uniform distributed load of 1 t/m2 acting downward. The properties of the used material are: $E = 100000\ t/m^2, \nu = 0$. The analysis using the PLPAK is carried out by considering a single slab of thickness 0.25 m and having additional 0.25 m as drop or stiffness cell. Two cell divisions are considered (5×20 and 5×25, as demonstrated in Figure 1.58). The boundary is divided into 40 quadratic boundary elements. The results of these two discretization are compared against the analytical solution in [9].

Results : Figure 1.59 and Figure 1.60 demonstrate the deflection and the bending moment of the considered cantilever along x-direction. The results demonstrate excellent agreement between the present solution and the analytical solution.

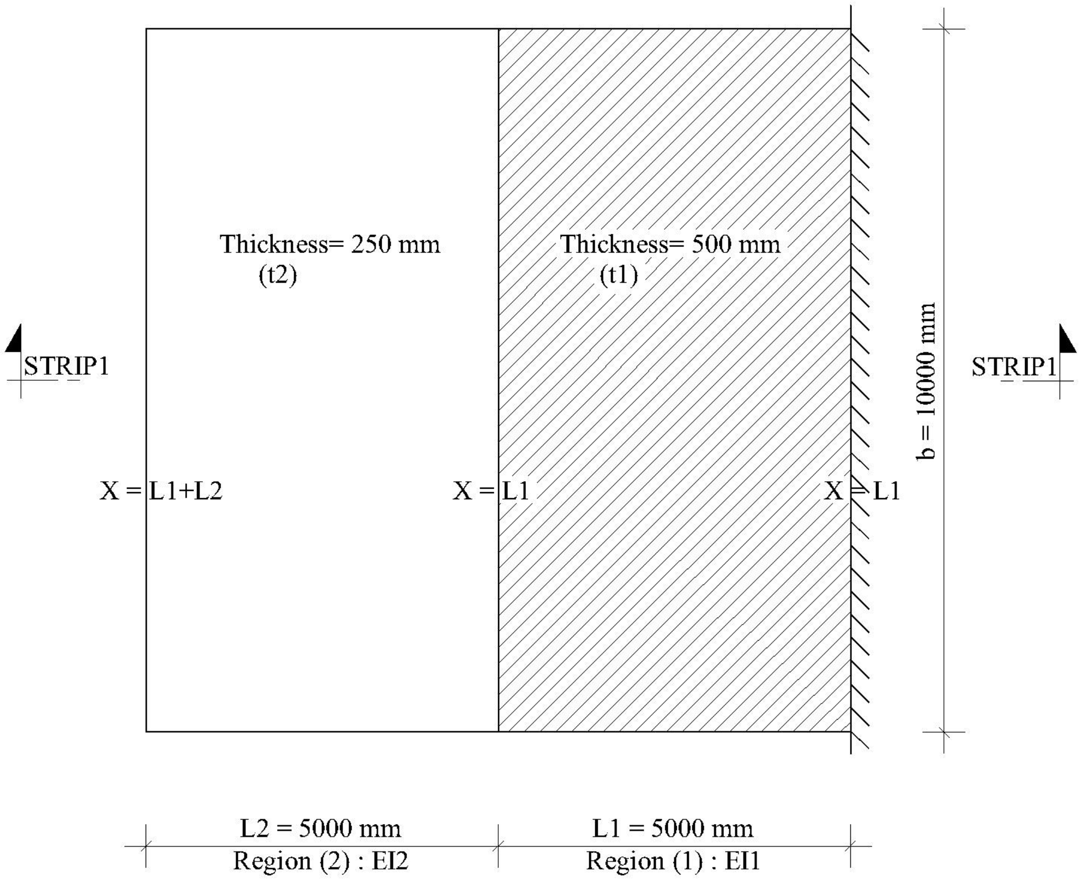

Figure 1.57: Layout of the multi thickness cantilever slab in Example 1.8.

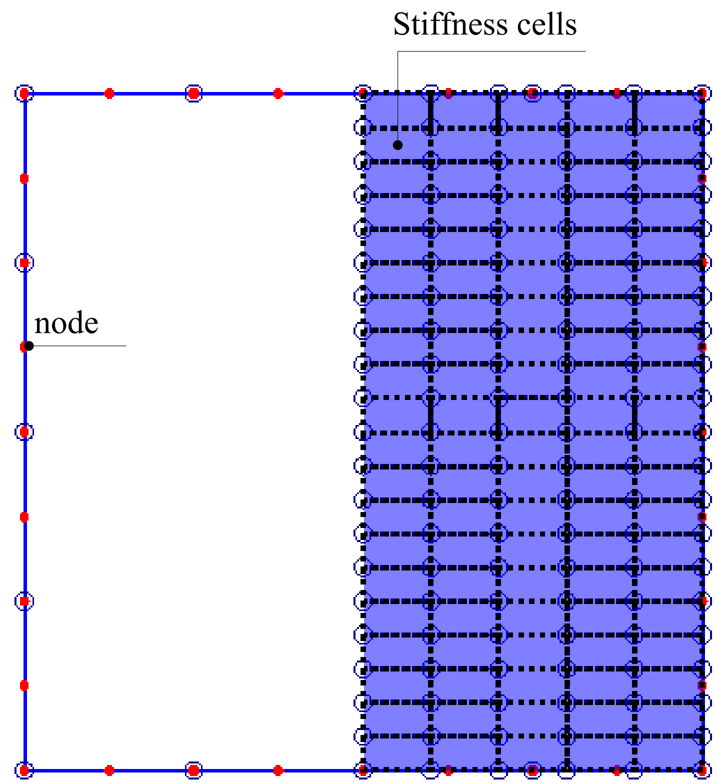

Figure 1.58: Stiffness cells with 5×20 discretization in Example 1.8.

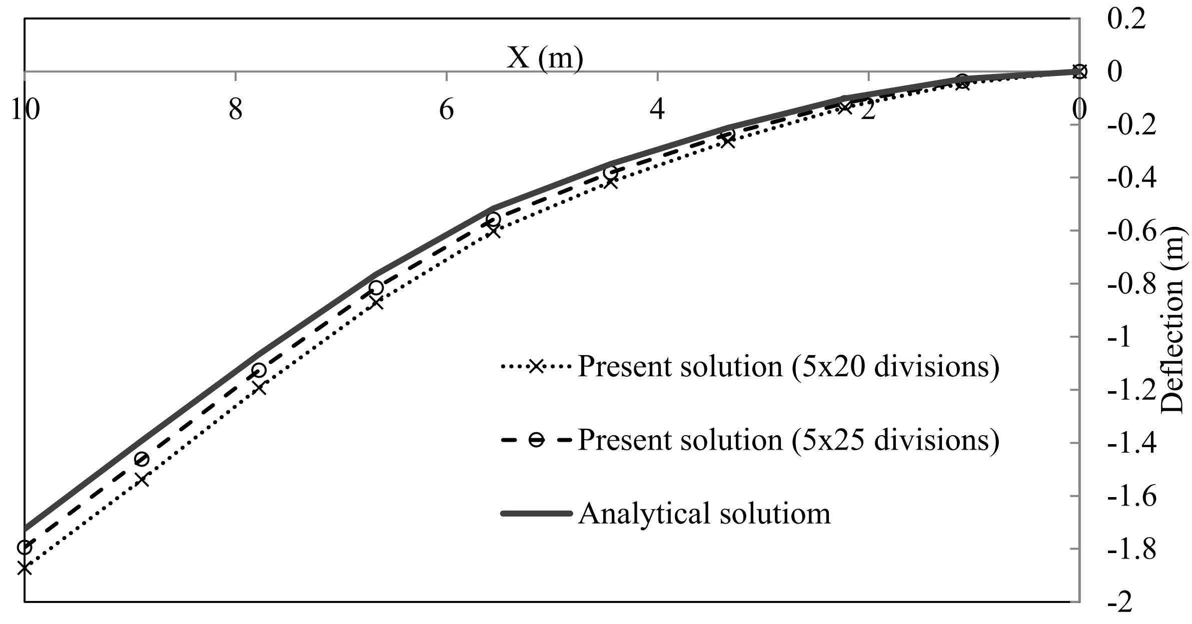

Figure 1.59: Deflection of the slab along Strip"1" in Example 1.8.

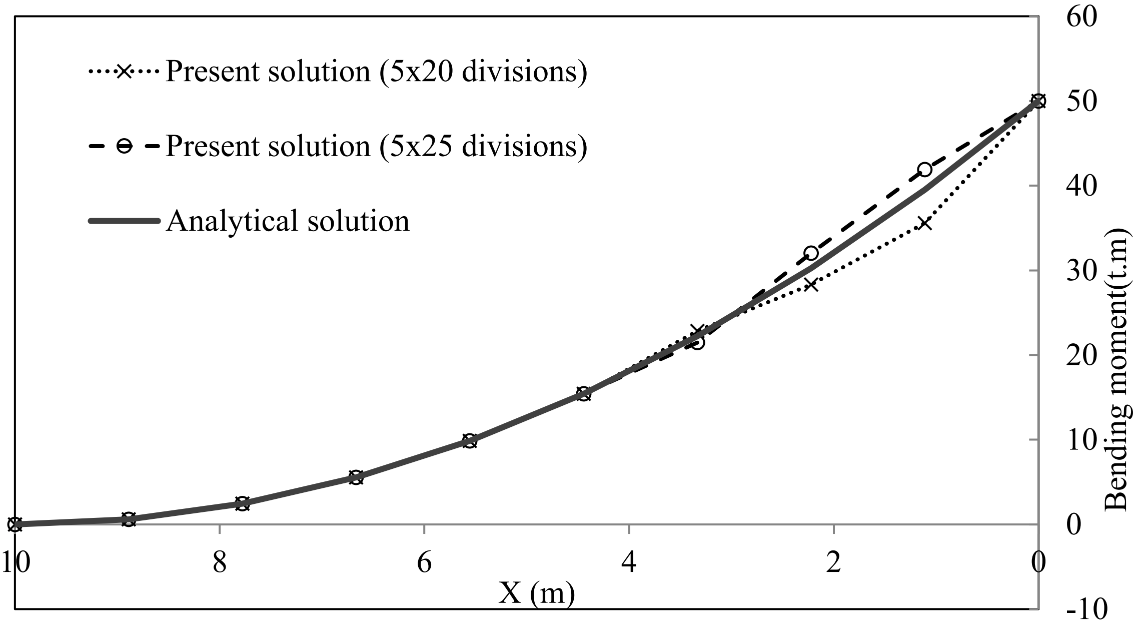

Figure 1.60: Bending moment of the slab along Strip"1" in Example 1.8.

Example 1.9 [9]

Purpose : Comparing results of multi-thickness circular slab against the analytical solution.

Description : In this example a multi-thickness slab of 0.25m/0.5 m is considered (see Figure 1.61). The slab is simply supported from the outer perimeter and is under domain loading of $1\ t/m^2$ acting downward. The properties of the used material are: $E = 300000\ t/m^2$, $\nu = 2.5$. Three internal cell meshing are employed using the PLPAK to discretize the additional thickness into stiffness cells (256, 441 and 676 stiffness cells, see Figure 1.62). The boundary is divided into 40 quadratic boundary elements. The results of these models are compared to those obtained from the analytical solutions in [9].

Results : Figure 1.63 and Figure 1.64 demonstrates the deflection and the bending moment of the slab for the previously considered models. It can be seen that results are in excellent agreement with the analytical values.

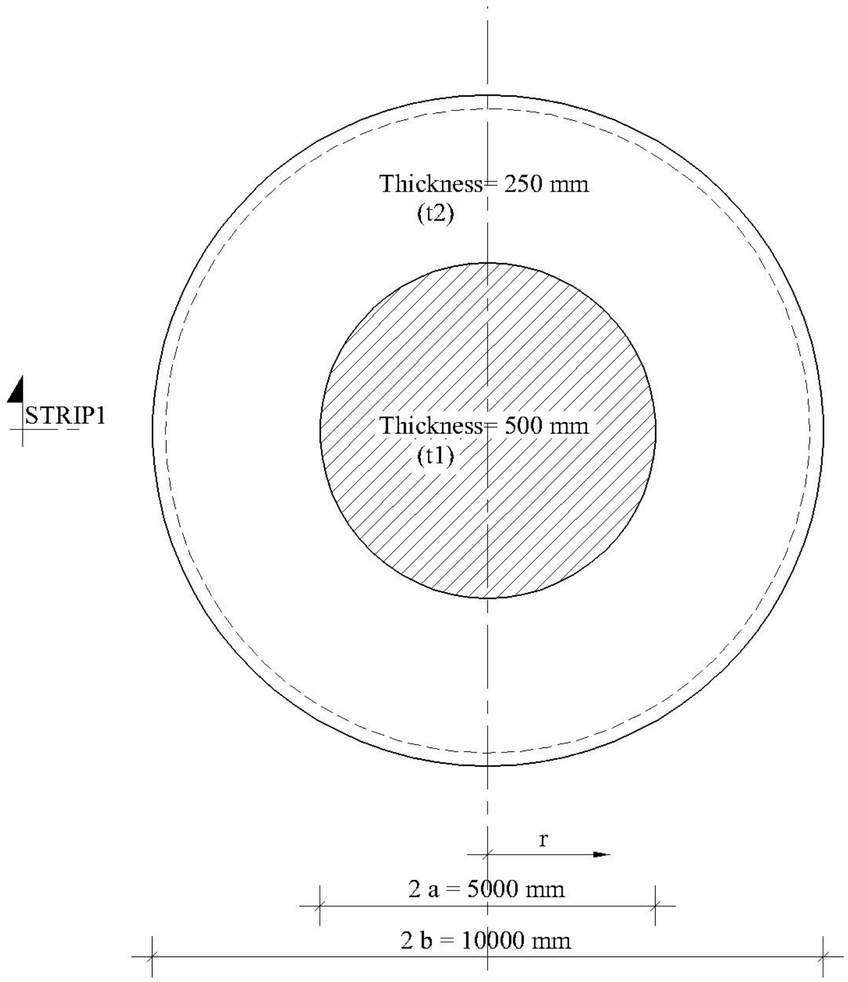

Figure 1.61: Layout of the multi thickness circular slab in Example 1.9.

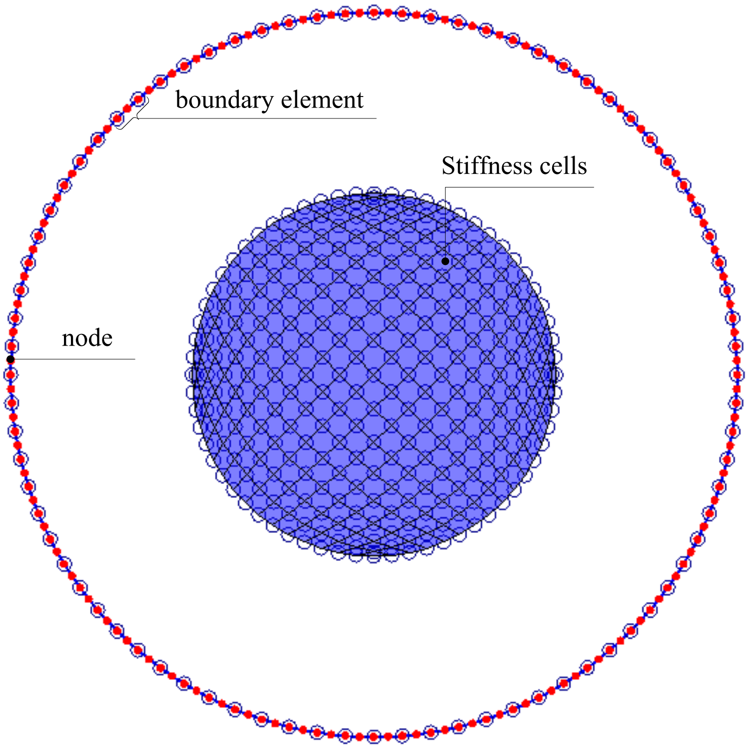

Figure 1.62: Stiffness cells with 441 discretization in Example 1.9.

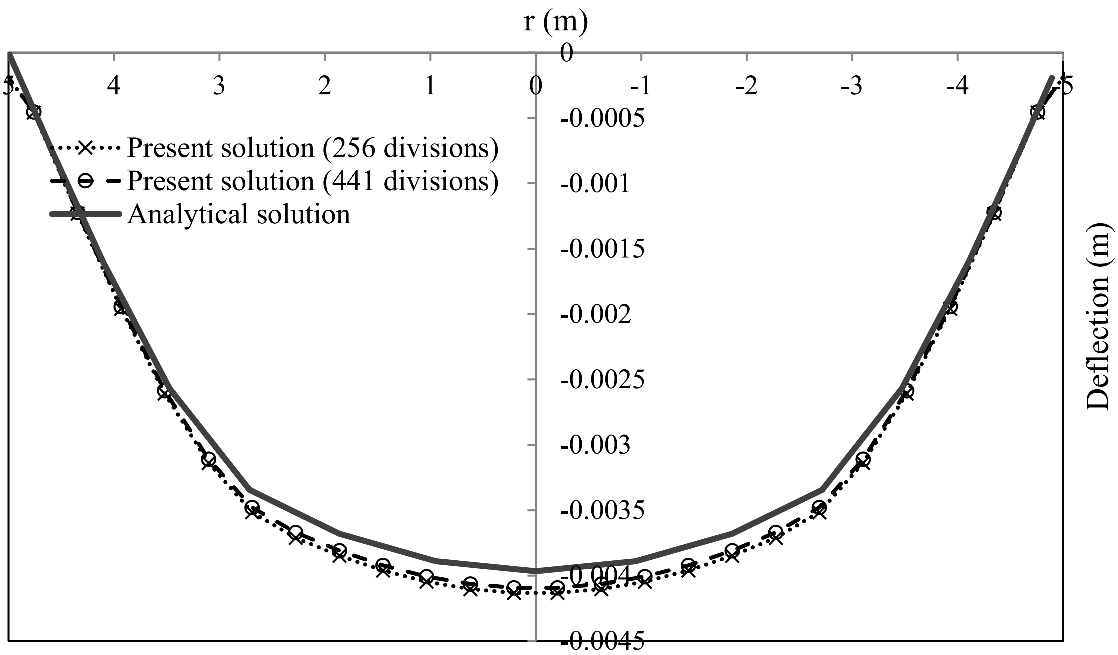

Figure 1.63: Deflection of the slab along Strip"1" in Example 1.9.

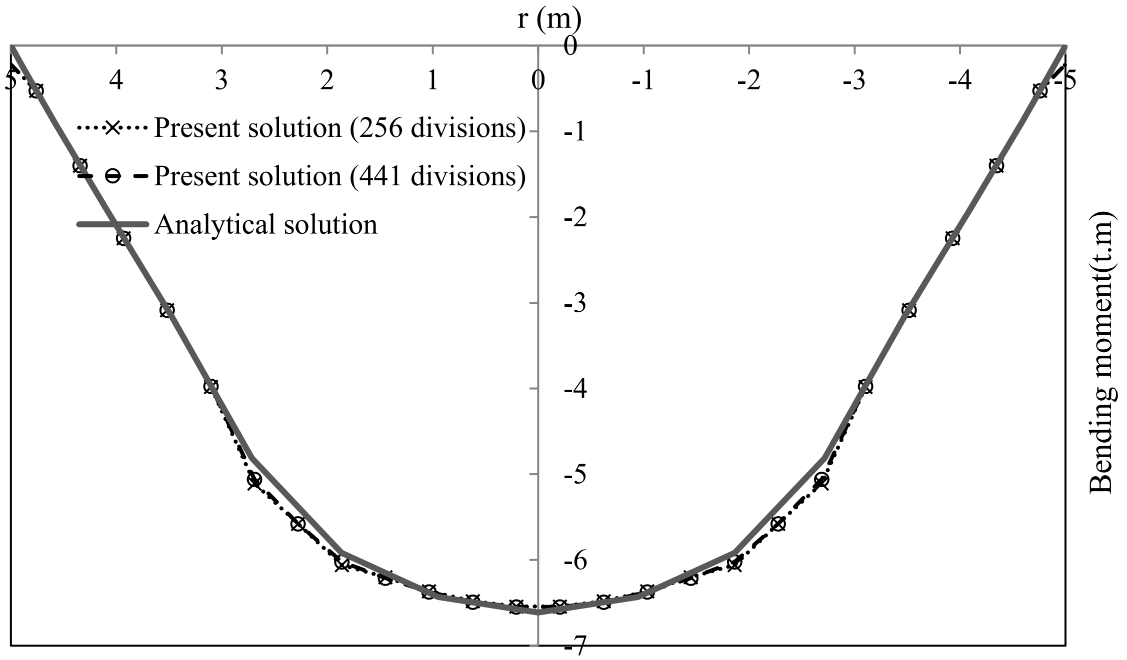

Figure 1.64: Bending moment of the slab along Strip"1" in Example 1.9.

Example 1.10 [9]

Purpose : Compare results of slab over four columns by modelling half of the slab's thickness as a drop, against the finite element and another boundary element model.

Description : In this example the slab demonstrated in Figure 1.65 has a thickness 0.4 m. This slab is supported on four square columns of 0.5×0.5 m in dimensions and 3 m in height above together with another 3 m below the slab. The slab is loaded by its own weight. The used material properties are: $E = 3000000\ t/m^2$, $\nu = 0.2$ and $\gamma = 2.5\ t/m^3$.

Six numerical models are considered. The first model is based on the traditional boundary element solution [3] with 16 quadratic boundary elements considering a slab thickness of 0.4 m. Three other models are employed using the PLPAK considering the slab thickness to be 0.2 m with additional thickness of 0.2 m as drop panel. Different drop divisions (12×12, 15×15, 20×20, see Figure 1.66) are considered in the following three models. The last two models are based on the finite element method by dividing the slab into 12×16 of four noded shell elements. With two different approaches for modeling columns, one where Columns are modeled as frame element connected to the slab in one node representing the center of the column and the other where columns are modeled as solid element connected to the slab in the exact area of the column.

Results : The results are demonstrated along two strips one along the center line of the slab and the other along a line passing by the face of the columns (see Figure 1.65). Figure 1.67 and Figure 1.69 demonstrate the deflection of the slabs for the previously considered models. The results indicates that with more drop discretization, the more the solution tend to be closer to the solution of the traditional B.E.M. and with slight difference with the result of the finite element due to column geometry approximation in finite elements. Figure 1.68 and Figure 1.70 demonstrates the bending moment of the slab. The results indicates that the result from different discretization coincide with the result of both the boundary elements and the finite elements results.

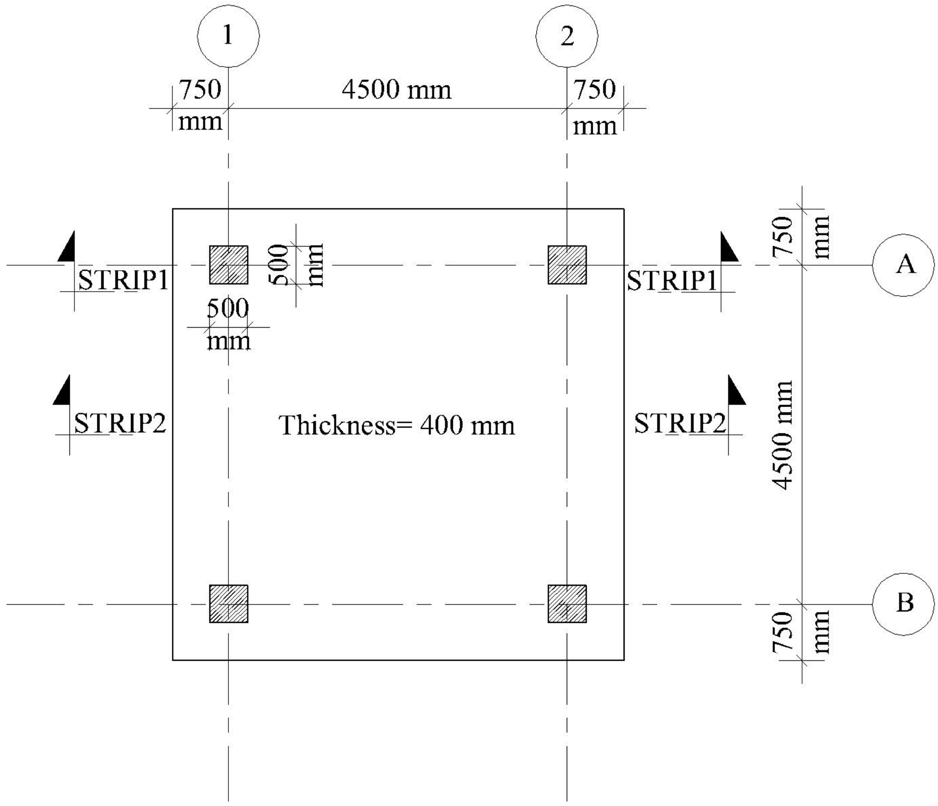

Figure 1.65: Layout of the slab over four columns in Example 1.10.

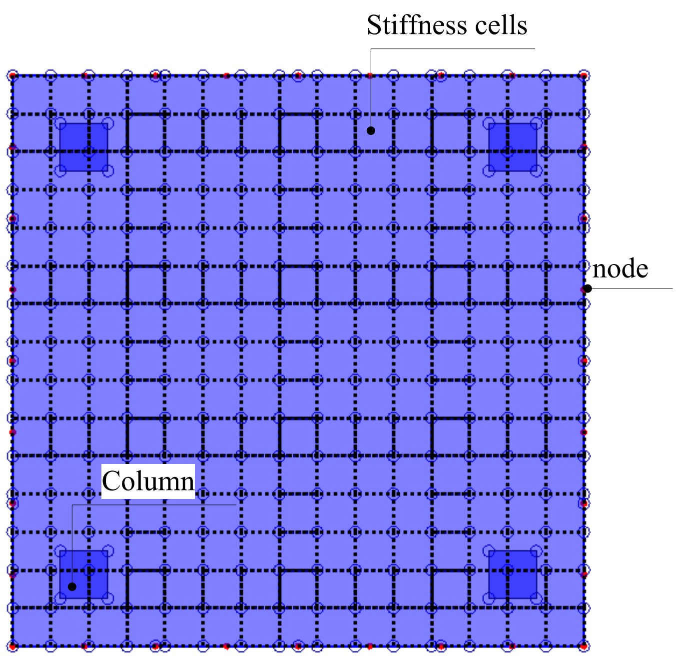

Figure 1.66: Stiffness cells with 15×15 divisions discretization in Example 1.10.

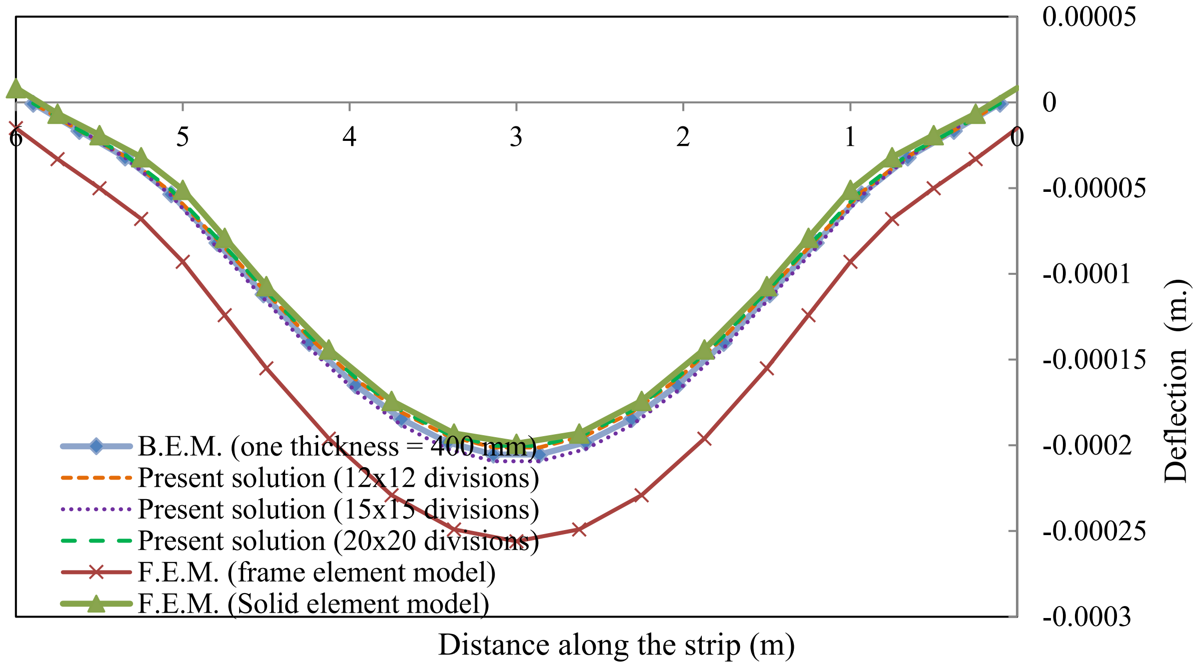

Figure 1.67: Deflection of the slab along Strip"1" in Example 1.10.

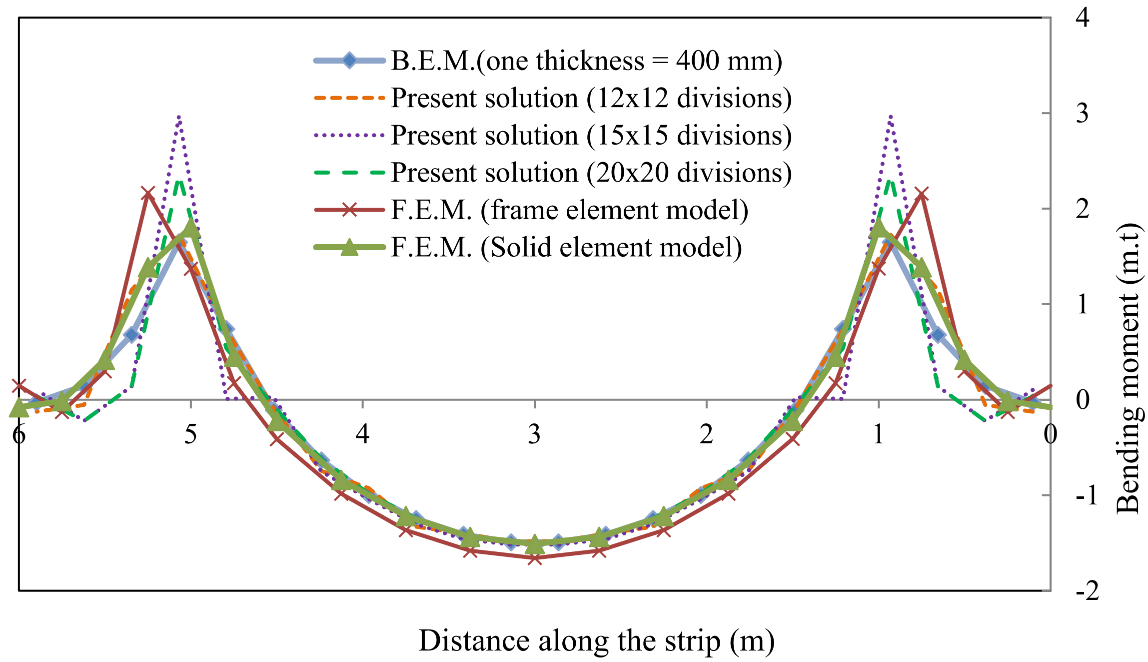

Figure 1.68: Bending moment of the slab along Strip"1" in Example 1.10.

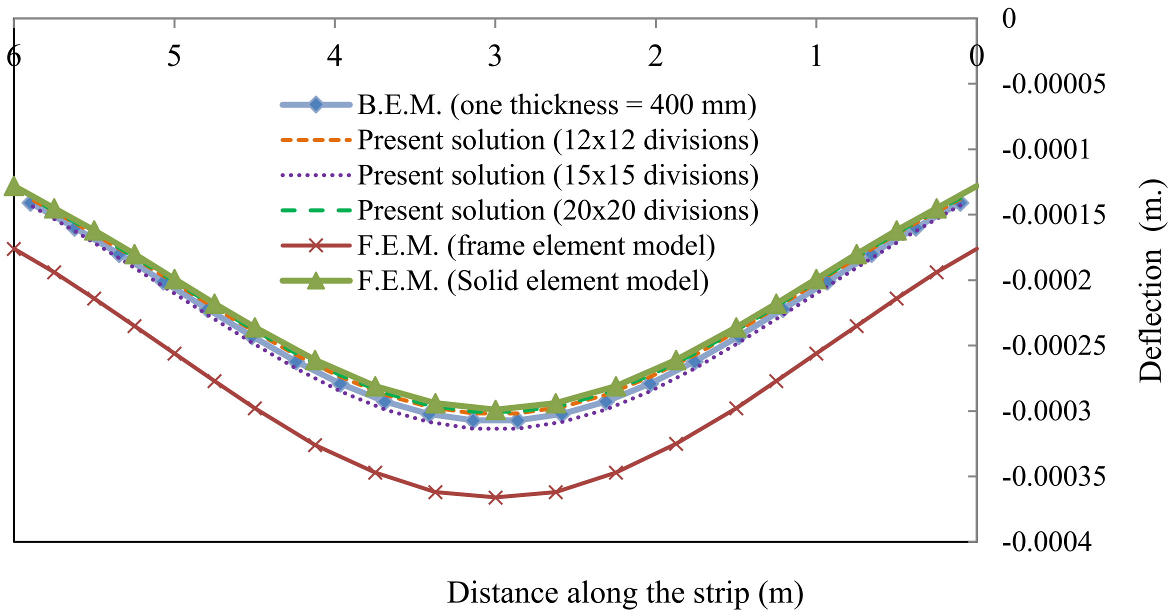

Figure 1.69: Deflection of the slab along Strip"2" in Example 1.10.

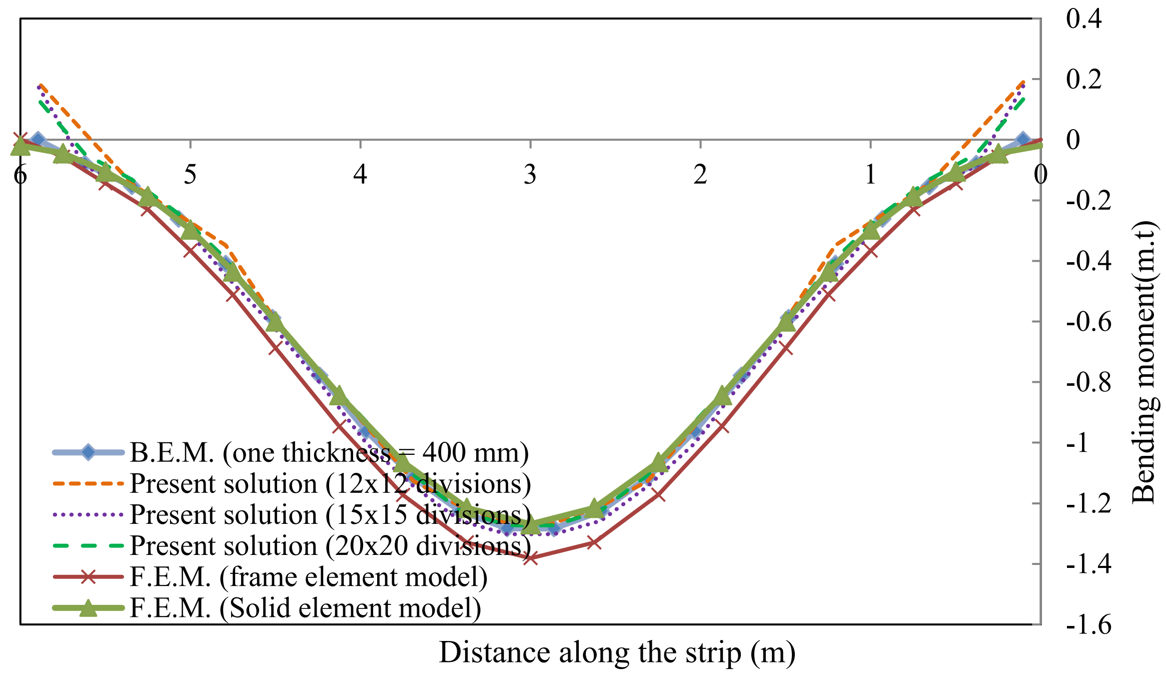

Figure 1.70: Bending moment of the slab Strip"2" in Example 1.10.

Example 1.11 [10]

Purpose : Compare the results of a simple raft on non-homogeneous soil against BEM analysis using thin plate and domain elements for the soil done by El-Mohr in [11].

Description : The $10 \times 10\ m$ raft shown in Figure 1.71 is considered (and considered previously in [11]). The raft modulus of elasticity is taken: $2 \times 10^6\ t/m^2$ and Poisson's ratio equal to 0.2. The column models, loads and dimensions are given in Table 1.1. The raft thickness is taken 0.6 and 1.5 m to allow comparison against results of [11]. The raft own weight is ignored. The values of the sub grade reactions are given as follows:
Case of having homogenous soil: $K = 40{,}000\ t/m^3$, and
Case of having non-homogenous soil: $K = 40{,}000\ t/m^3$ underneath the raft except the bottom $3\ m$ horizontal strip, which has modulus of sub grade reaction equal to $K' = 5{,}000\ t/m^3$.
In [11] the plate is divided into 4 higher order boundary elements and 5×5 domain cells. Herein, the plate is discretized into 10 elements along each side. The soil is represented by 10×10 cells.

Results : Figure 1.72-Figure 1.75 demonstrates comparison of the bending moment M_{yy} for Sections 1 and 2 (see Figure 1.71) when the raft thickness is 0.6 and 1.5 m, respectively. It can be seen that the PLPAK results are in good agreements with results of [11]. Few differences between the model results are found in Figure 1.72 and Figure 1.73. This could be due to the few number of elements used in [11] and the ignorance of the shear deformation in [11].

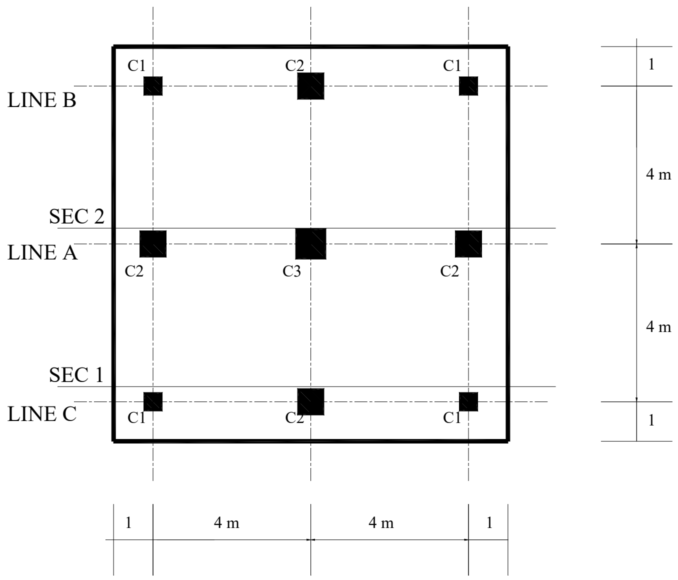

Figure 1.71: The considered simple raft on non-homogenous soil in Example 1.11.

Table 1.1: Column models, dimensions and loads used in the simple raft in Example 1.11.

Column model	Dimensions (cm)	Load (ton)
C1	40×40	80
C2	60×60	150
C3	70×70	250

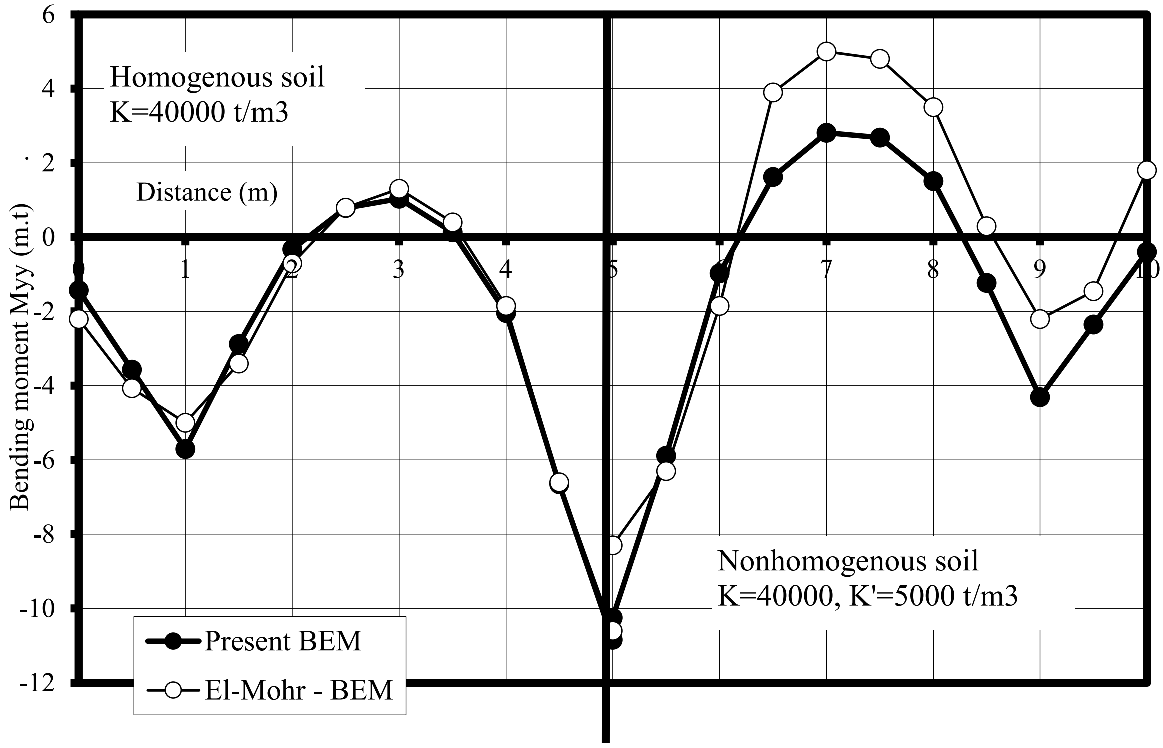

Figure 1.72: Comparison between PLPAK results and results of [11] *along section 1–1 for the simple raft (raft thickness equal to 0.6 m) in Example 1.11.*

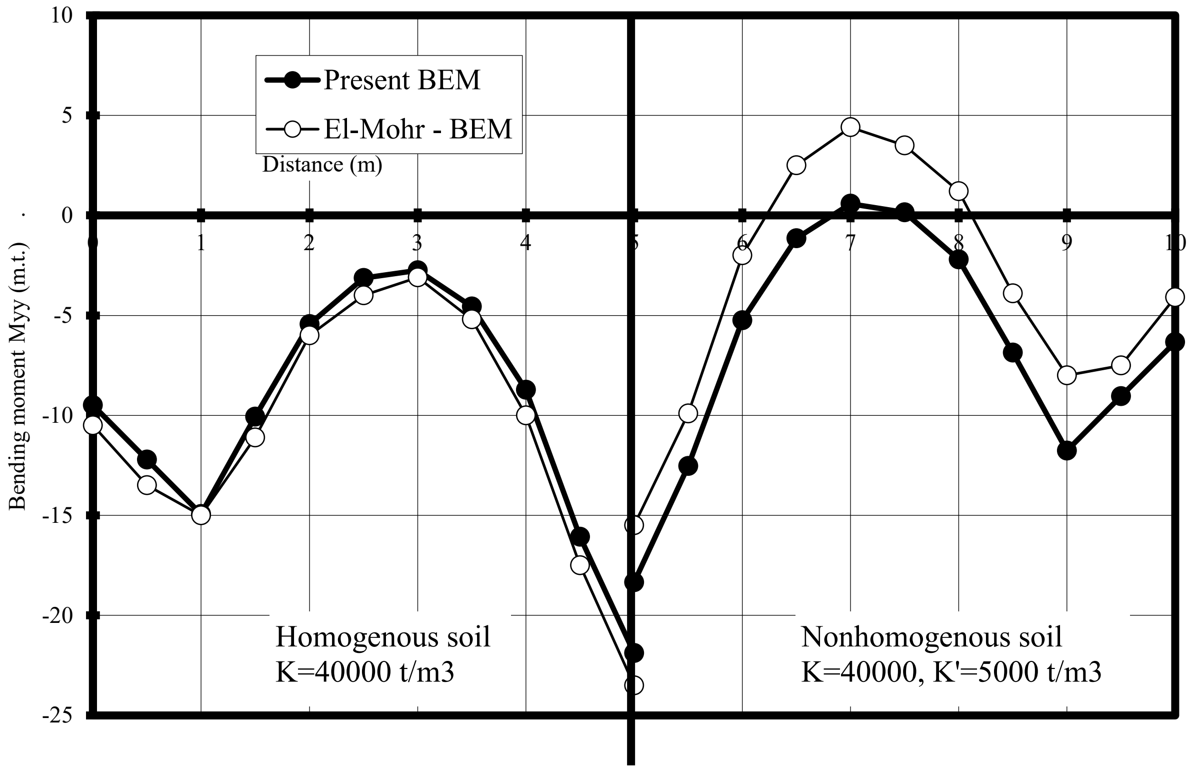

Figure 1.73: Comparison between PLPAK results and results of [11] *along section 2–2 for the simple raft (raft thickness equal to 0.6 m) in Example 1.11.*

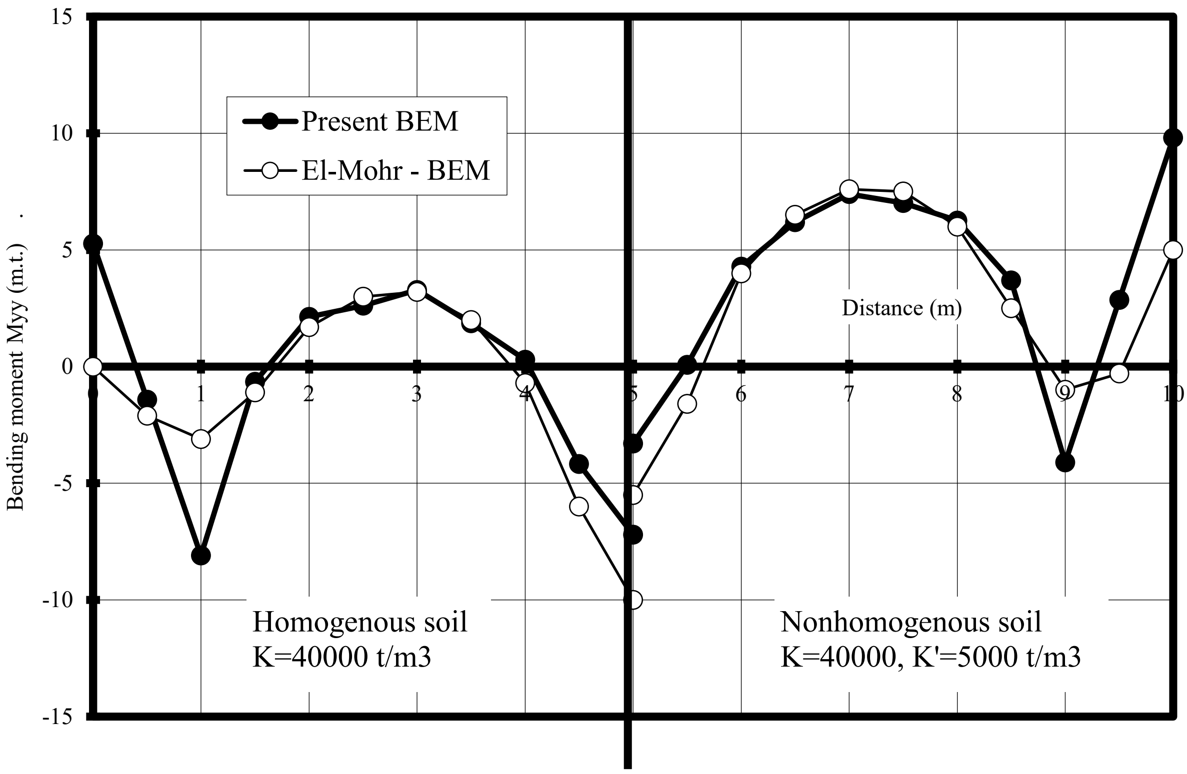

Figure 1.74: Comparison between PLPAK results and results of [11] *along section 1–1 for the simple raft (raft thickness equal to 1.5 m) in Example 1.11.*

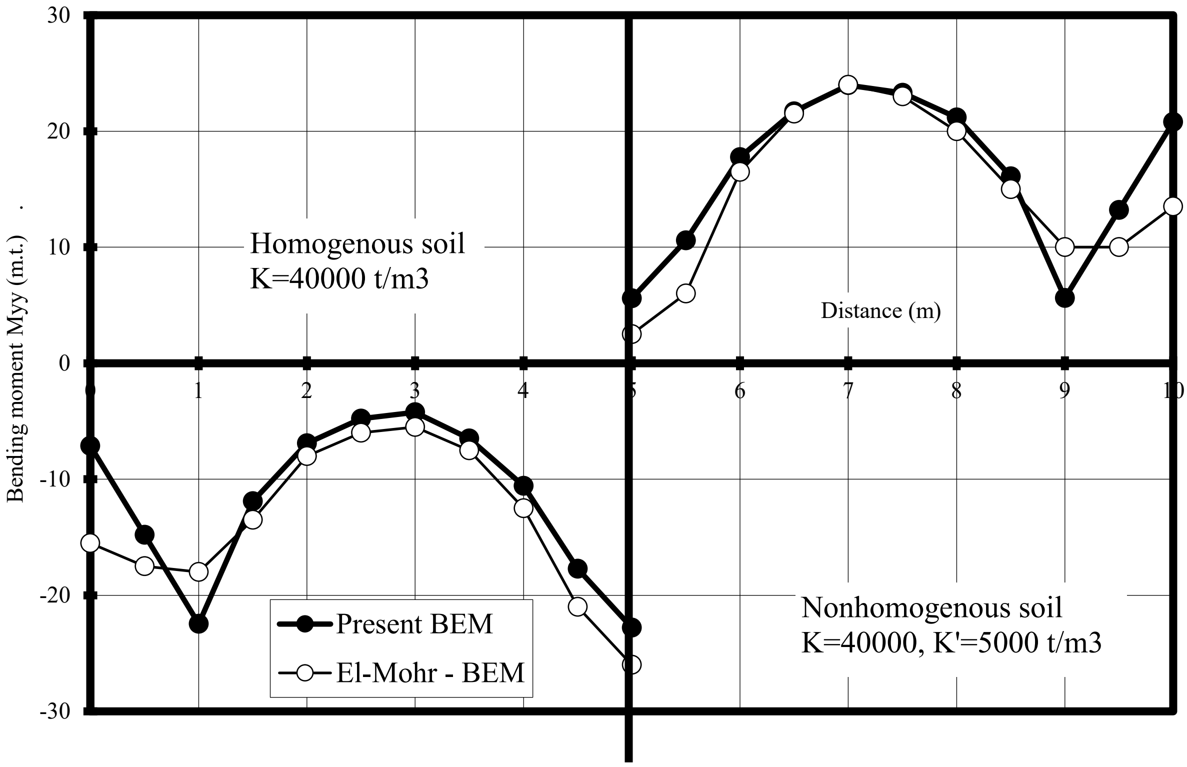

Figure 1.75: Comparison between PLPAK results and results of [11] *along section 2–2 for the simple raft (raft thickness equal to 1.5 m) in Example 1.11.*

Example 1.12 [10]

Purpose : Compare the results of a simple raft on non-homogeneous soil against finite element method based on the shear-deformable plate bending theory and discrete springs for the soil.

Description : The $10 \times 10\ m$ raft shown in Figure 1.71 is considered. The raft modulus of elasticity is taken: $2 \times 10^6\ t/m^2$ and Poisson's ratio equal to 0.2. The column models, loads and dimensions are given in Table 1.1. The raft thickness is taken 0.6 m and the own weight of the raft and the weight of the soil above the raft is considered to be $6\ t/m^2$. The same boundary element mesh in Example 1.11 was used herein. In the finite element analysis the plate is divided into 20×20 elements, and the soil is represented using discrete springs. The value of the sub grade reaction for the soil is taken $K = 5{,}000\ t/m^3$ under the raft except for weak horizontal strip of width $2\ m$ having $K = 1{,}000\ t/m^3$ around line A–A.

Results : Figure 1.76 demonstrates the spring reactions in the finite element analysis for one quarter of the raft. Figure 1.77 demonstrates the soil cell reactions obtained from the PLPAK. In order to compare both results, each group of nine springs in the finite element results that corresponds to a single cell in the boundary element analysis is replaced by equivalent reaction R_e value according to the equations in (Ref. EABE rafts) (consider Figure 1.78). The values of the equivalent reactions R_e are shown also in Figure 1.77 in parenthesis for the sake of comparison. It can be seen from Figure 1.77 that values of soil reaction obtained from the finite element method in the weak strip is higher that values obtained from the PLPAK results. This is mainly due to the finite element discretization increases the flexibility of the raft and hence increases the deflection at the weak strip and consequently increases the foundation reaction. In order to demonstrate this behaviour, the deflection, bending moment and shear force distributions are plotted along line A–A (at the weak strip) and along line B–B (away from the weak strip) in Figure 1.79-Figure 1.81 respectively. It can be seen from Figure 1.79 that the finite element deflection along line A is higher than that obtained from the boundary element results. Figure 1.79-Figure 1.81, in general, demonstrate that the obtained results from the PLPAK are in good agreement with those obtained from finite element models.

2.76	2.64	2.33	2.00	1.78	1.70	1.78	1.95	2.13	2.26	1.18
5.72	5.40	4.72	4.07	3.64	3.52	3.69	4.08	4.47	4.68	2.41
5.82	5.45	4.72	4.10	3.70	3.59	3.77	4.19	4.60	4.77	2.43
5.52	5.25	4.67	4.13	3.78	3.69	3.84	4.19	4.54	4.74	2.43
5.24	5.08	4.69	4.28	3.99	3.90	4.01	4.27	4.55	4.79	2.48
5.40	5.28	5.00	4.66	4.41	4.33	4.42	4.64	4.91	5.16	2.69
6.09	5.97	5.69	5.36	5.12	5.04	5.14	5.37	5.67	5.96	3.11
7.28	7.14	6.77	6.36	6.06	5.99	6.14	6.45	6.82	7.17	3.74
5.31	5.17	4.84	4.48	4.26	4.22	4.36	4.64	4.93	5.17	2.70
2.09	2.01	1.83	1.67	1.58	1.57	1.64	1.77	1.91	1.98	1.02
2.25	2.13	1.92	1.74	1.64	1.68	1.71	1.87	2.02	2.09	1.07

Figure 1.76: Soil spring forces obtained from the finite element analysis for one quarter of the simple raft problem in Example 1.12

18.43 (21.17)	16.67 (16.46)	16.00 (14.33)	16.67 (16.25)	17.53 (18.58)
20.17 (20.73)	18.79 (16.32)	18.21 (15.11)	18.87 (16.84)	19.70 (18.96)
22.03 (21.43)	21.21 (19.06)	20.81 (18.03)	21.31 (18.97)	22.18 (21.03)
25.54 (25.22)	24.59 (22.17)	24.20 (21.44)	24.91 (22.96)	26.05 (25.44)
5.89 (11.20)	5.53 (9.65)	5.43 (9.10)	5.69 (10.06)	5.99 (11.21)

Figure 1.77: One quarter of the simple raft problem in Example 1.12 showing: First value: denotes the soil cell reaction of the present boundary element analysis, and (Second value): denotes the equivalent finite element value.

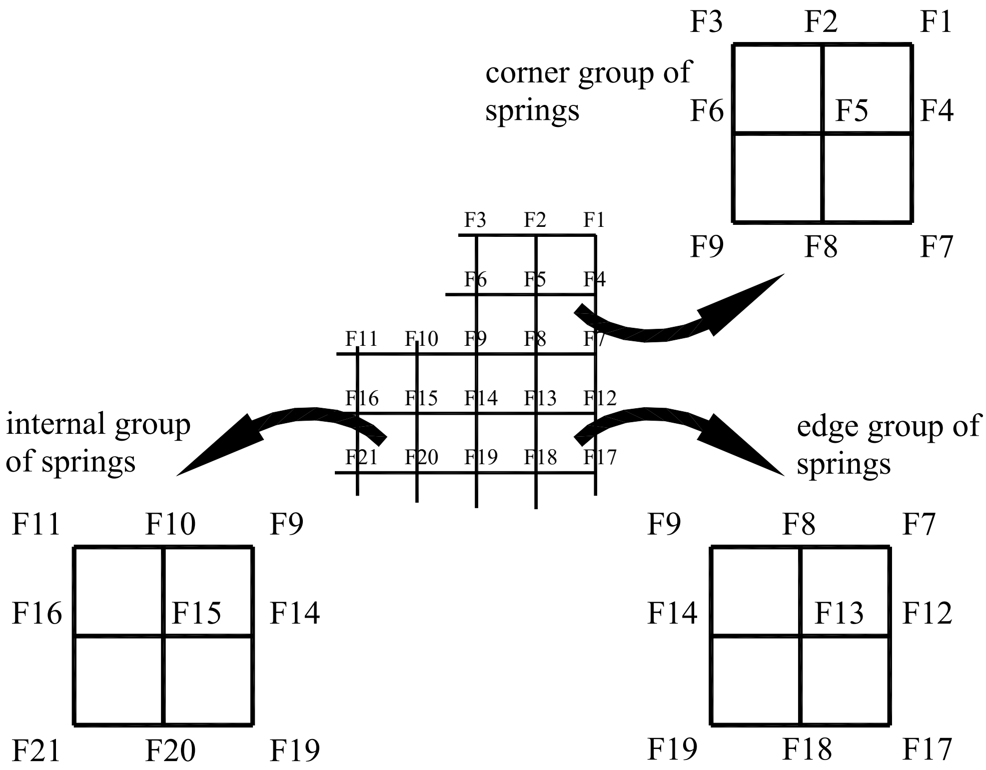

Figure 1.78: Detail showing corner, internal and edge spring groups for determining the equivalent finite element value for soil reaction in Example 1.12.

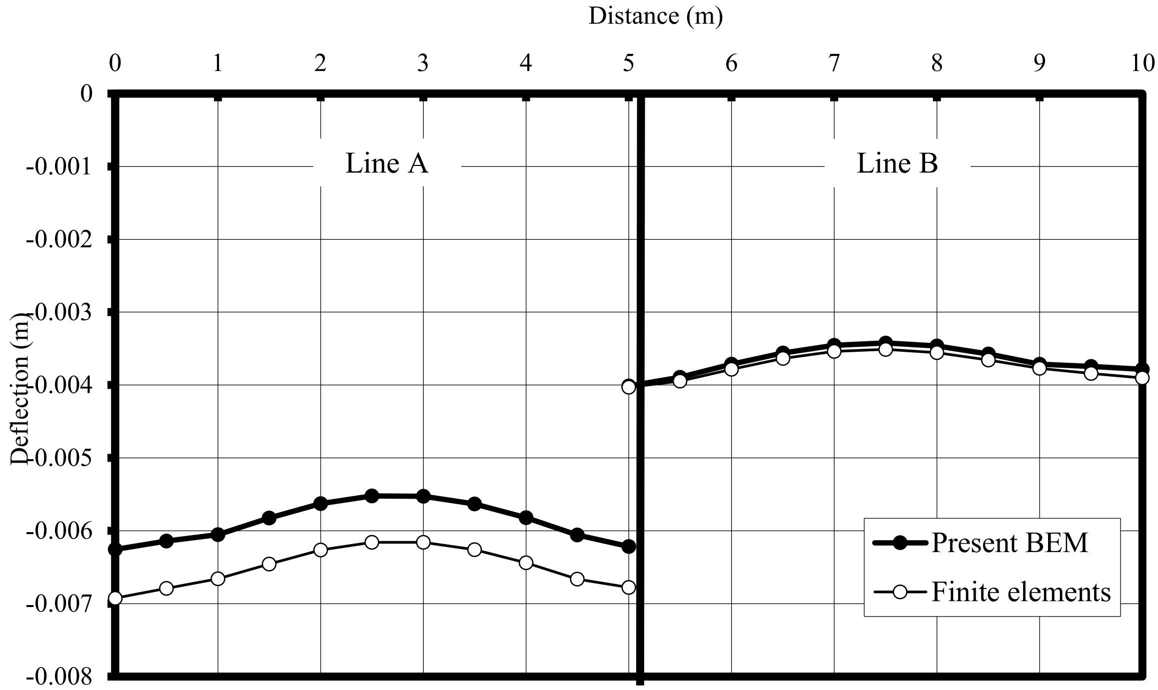

Figure 1.79: Comparison between PLPAK deflection and results of the finite element method along lines A and B for the simple raft problem (raft thickness equal to 0.6 m) in Example 1.12.

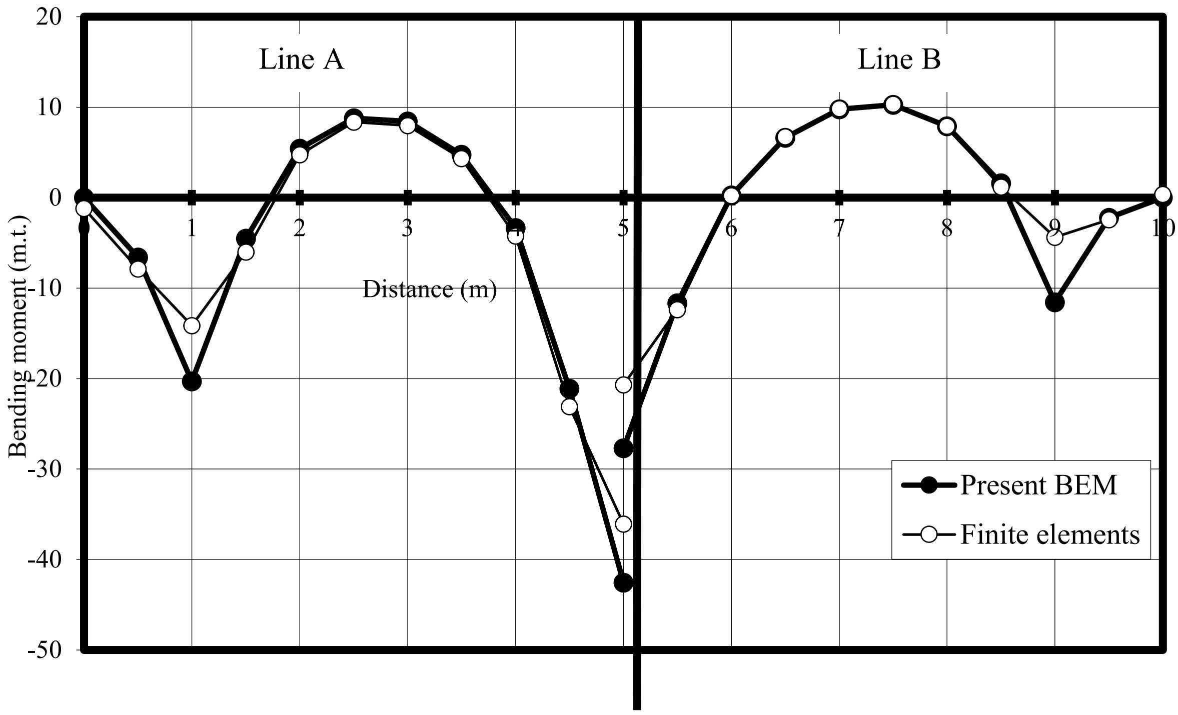

Figure 1.80: Comparison between PLPAK bending moments and results of the finite element method along lines A and B for the simple raft problem (raft thickness equal to 0.6 m) in Example 1.12.

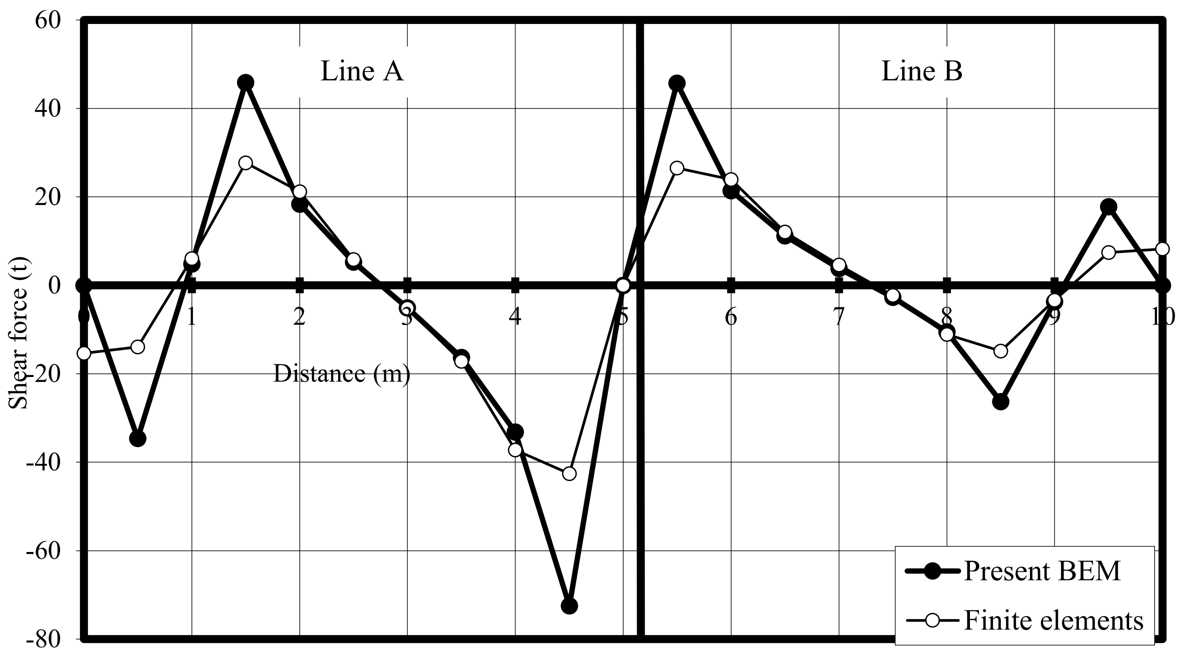

Figure 1.81: Comparison between PLPAK shear forces and results of the finite element method along lines A and B for the simple raft problem (raft thickness equal to 0.6 m) in Example 1.12.

Example 1.13 [10]

Purpose : Compare the results of a practical building raft foundation against the finite element analysis.

Description : The raft foundation shown in Figure 1.82 is considered. The raft supports 37 columns (Table 1.2 shows column cross sectional dimensions and loads) and has $0.7\ m$ thickness. The following properties of reinforced concrete are used: $E = 2 \times 10^6\ t/m^2$ and $v = 0.2$. The considered raft own weight is $-1.75\ t/m^2$. The soil underneath the raft has modulus of sub-grade reaction of $1{,}100\ t/m^3$. The considered raft is analysed several times as follows:

The first analysis is carried out using the present BEM formulation, where the following schemes of mesh combinations are tested:

Scheme 1: has the following discretization, BEM mesh 1 (44 boundary elements, see Figure 1.83(a)) together with Cell mesh 1 (74 soil cells, see Figure 1.84(a)).

Scheme 2: has the following discretization, BEM mesh 1 together with Cell mesh 2 (252 soil cells, see Figure 1.84(b)).

Scheme 3: has the following discretization, BEM mesh 2 (82 boundary elements, see Figure 1.83(b)) together with Cell mesh 1.

Scheme 4: has the following discretization, BEM mesh 2 together with Cell mesh 2.

Scheme 5: has the following discretization, BEM mesh 2 together with Cell mesh 3 (the same as Scheme 1 having 74 soil cells but with no continuity at cell corners, see Figure 1.84(c)). The purpose of this scheme is to demonstrate that there is no need to ensure continuity at corners of cells.

It was found that the result of Scheme 1 is very accurate and all of these tests give nearly identical results. Therefore, herein in this example, the result of Scheme 1 will be shown later on the plots, and will be referred to as 'Present BEM'. In order to compare the obtained results, two finite element analyses are carried out. The first analysis is carried out where the raft plate is modelled using the shear-deformable plate-bending model and the soil is considered as discrete springs. Two finite element meshes are set up (see Figure 1.85). The first mesh has 736 elements (in the plots, this mesh will be referred to as 'FEM model 1'). The second mesh has 2944 elements (in the plots, this mesh will be referred to as 'FEM model 2'). The second finite element model, on the other hand, has the same finite element discretization as that of 'FEM model 1', whereas the soil is modelled using continuous area spring and is directly incorporated into the finite element stiffness matrix. This model will be referred to as 'FEM model 3' in the plots.

In order to study the bending moment and shear behaviour in the vicinity of columns, the same problem is modelled using the formulation presented by author in [12]. In this model (which will be referred to as 'BEM model 2' in the plots) the same boundary element mesh of BEM mesh 1 is used; but in this case with full discontinuous elements to avoid inter-element singularity appeared in the formulation of [12].

Results : Figure 1.86-Figure 1.100 demonstrate values of deflections, bending moments and shear forces along axes B–B, C–C, 3–3, 6–6 and 10–10 respectively.

It can be seen that the PLPAK results are in good agreement with other finite element models. The following notes can be observed:

1. As finer as the finite element mesh, as more deflection obtained as discretization increases flexibility of the structure.
2. The PLPAK results are more accurate w.r.t. FEM model 3. This is mainly due to both models treat the soil in similar and more realistic representation.
3. The BEM results for the deflections are usually less than those of the finite element results. This is due to the consideration of the plate as continuum body in the BEM with no discretization flexibility.
4. Consequently, values of the bending moments and shear forces in the PLPAK BEM model is larger than those obtained from the FEM; especially in the vicinity of columns.

The results of the formulation presented by author in [12] are plotted together with formerly obtained results in Figure 1.86-Figure 1.100. It can be seen that the PLPAK BEM model results are very accurate compared to the results of the BEM model 2, as both models treats the plate as continuum and the foundation as continuous springs. This confirms the accuracy and the more realistic modelling of the developed formulation.

Table 1.2: Column models, dimensions and loads used in the practical raft in Example 1.13.

Column model	Dimensions (cm)	Load (ton)
c1	20×25	80
c2	25×30	120
c3	25×40	170
c4	25×50	210
c5	25×55	230
c6	30×60	310
c7	30×80	410

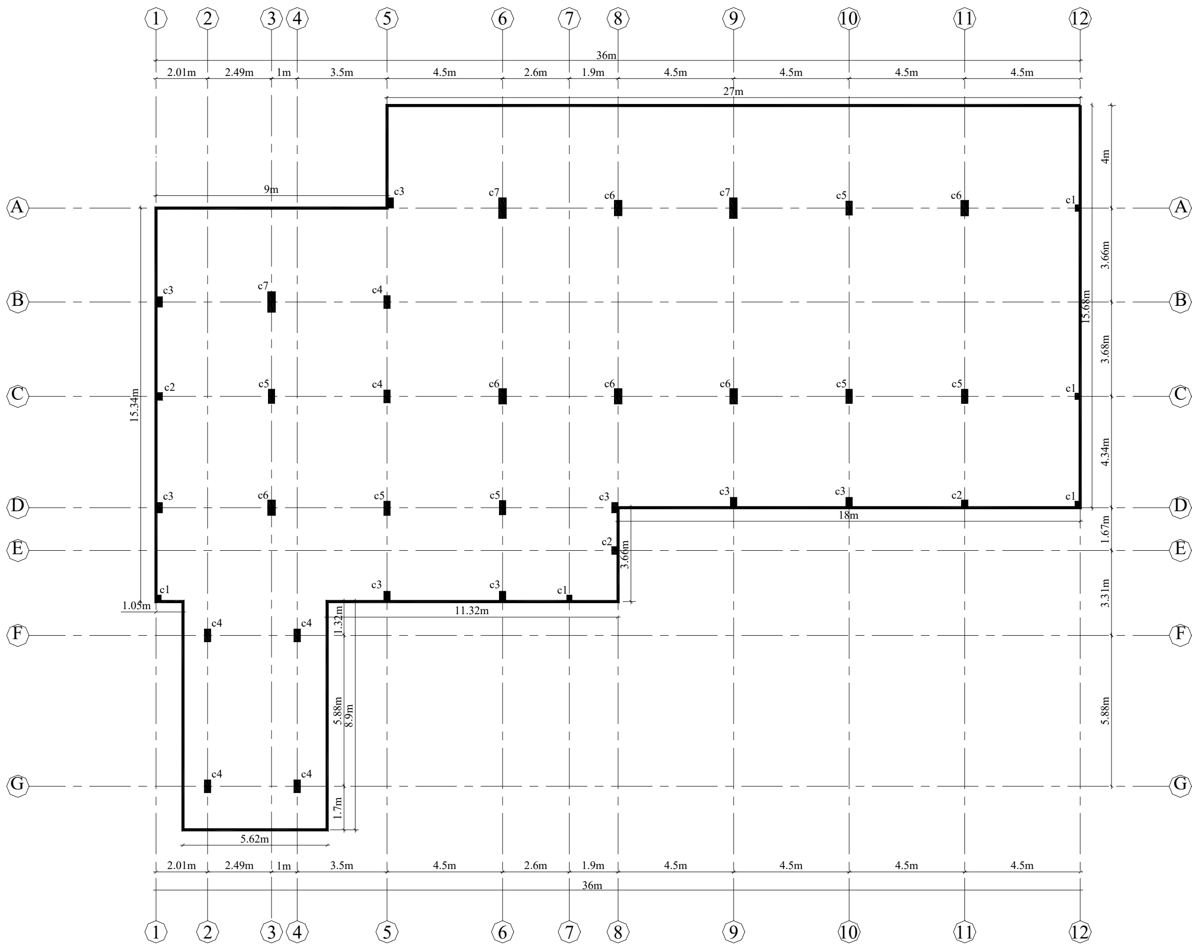

Figure 1.82: Geometry of the considered practical raft problem in Example 1.13.

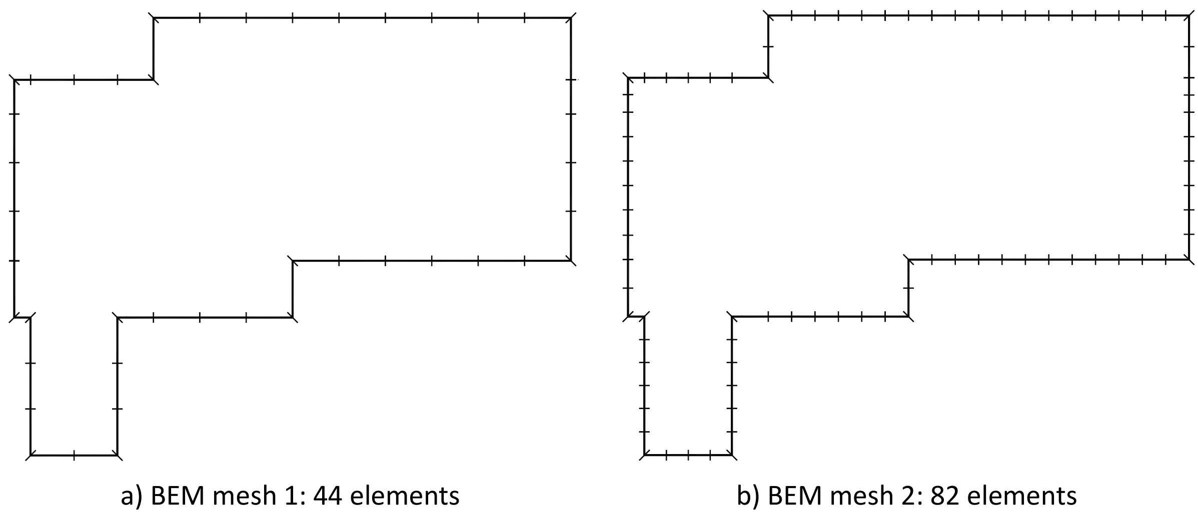

Figure 1.83: Different boundary element meshes for the considered practical raft problem in Example 1.13.

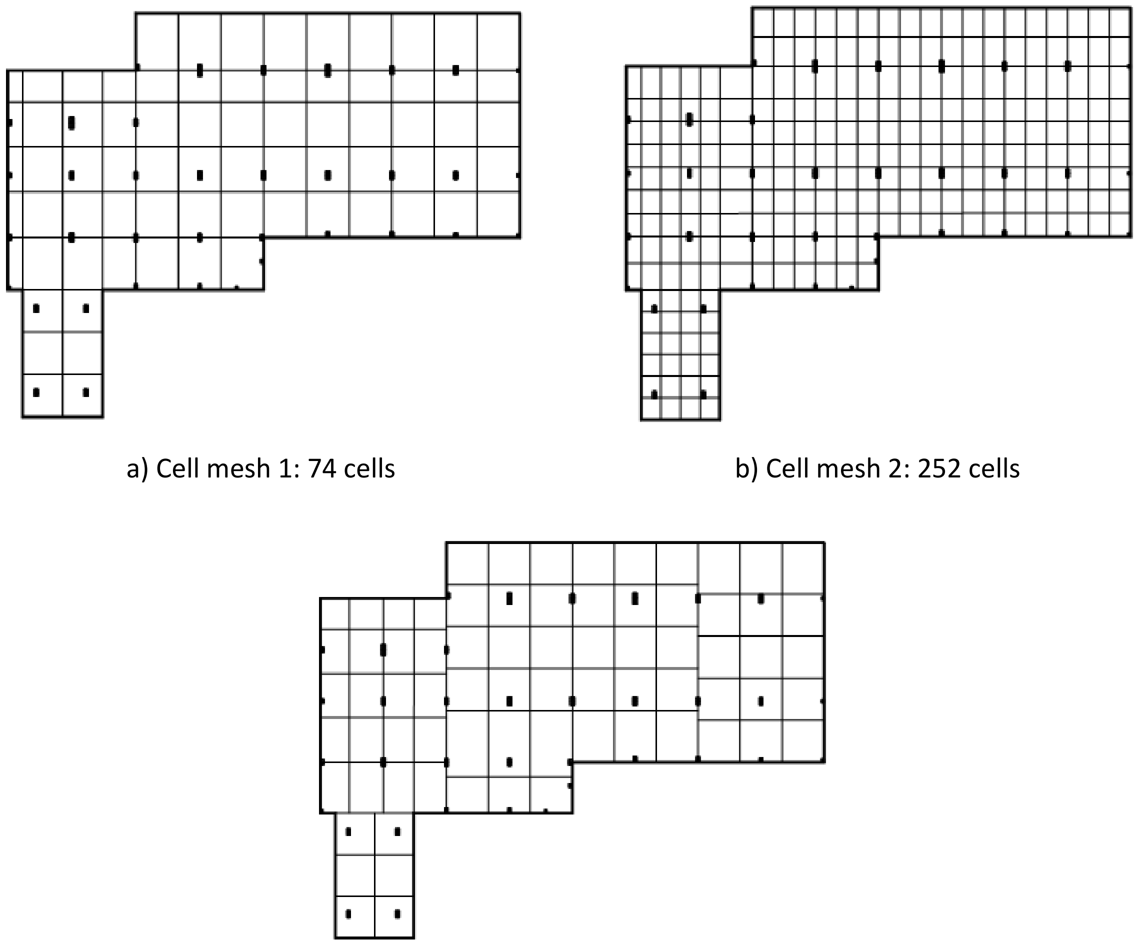

a) Cell mesh 1: 74 cells

b) Cell mesh 2: 252 cells

c) Cell mesh 3: 74 cells

Figure 1.84: Different soil cell meshes for the considered practical raft problem in Example 1.13.

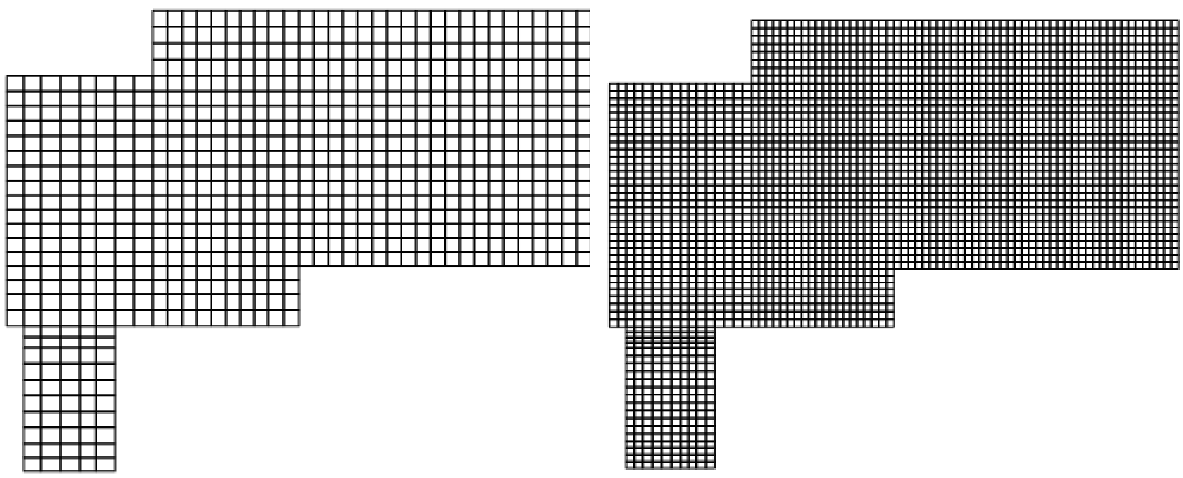

a) Finite element mesh 1: 736 elements

b) Finite element mesh 2: 2944 elements

Figure 1.85: Different finite element meshes for the considered practical raft problem in Example 1.13.

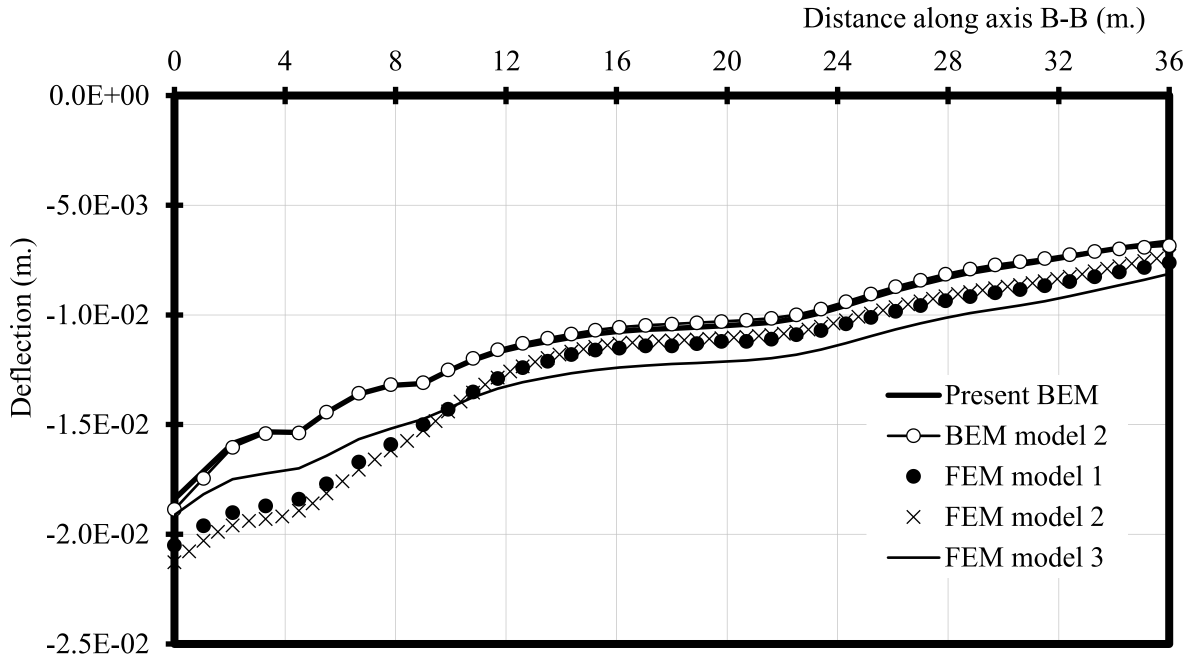

Figure 1.86: Comparison of the deflection results along axis B–B for the considered practical raft problem in Example 1.13.

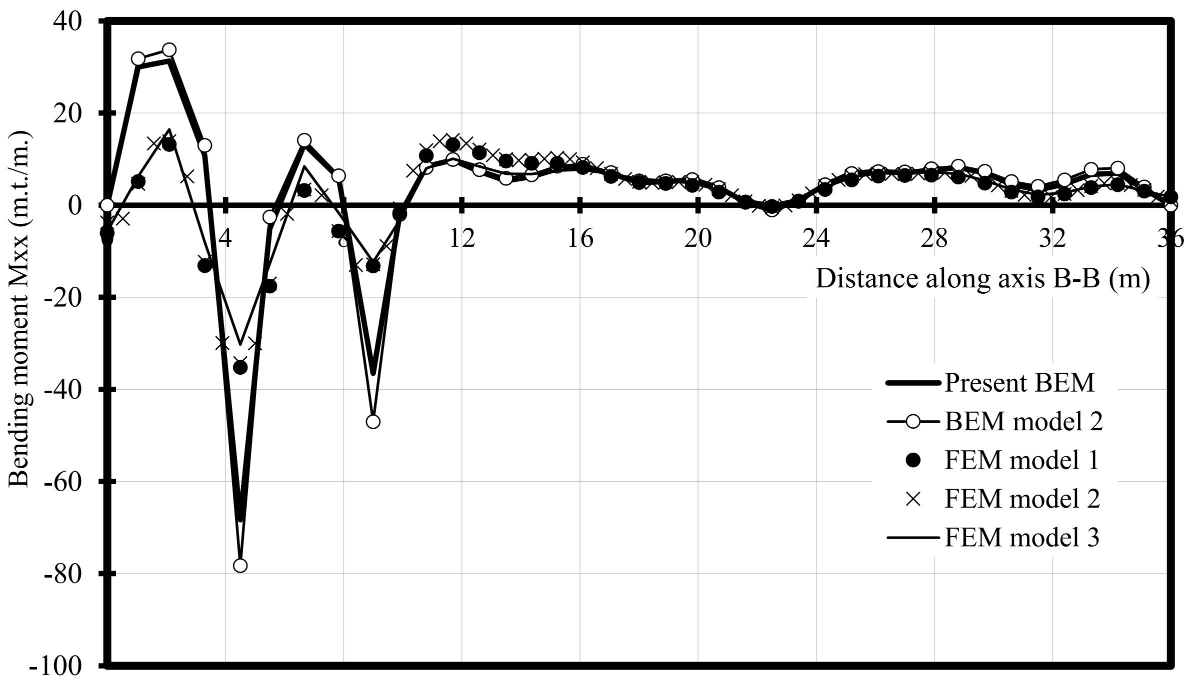

Figure 1.87: Comparison of the bending moment results along axis B–B for the considered practical raft problem in Example 1.13.

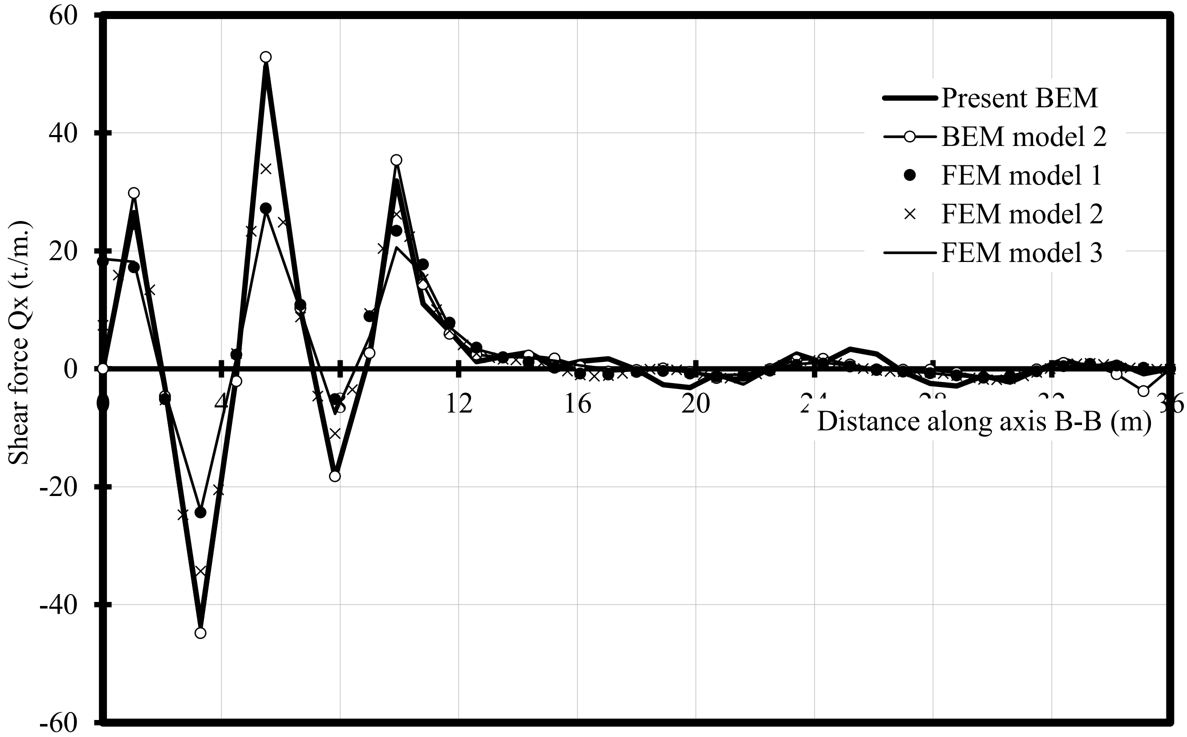

Figure 1.88: Comparison of the shear force results along axis B–B for the considered practical raft problem in Example 1.13.

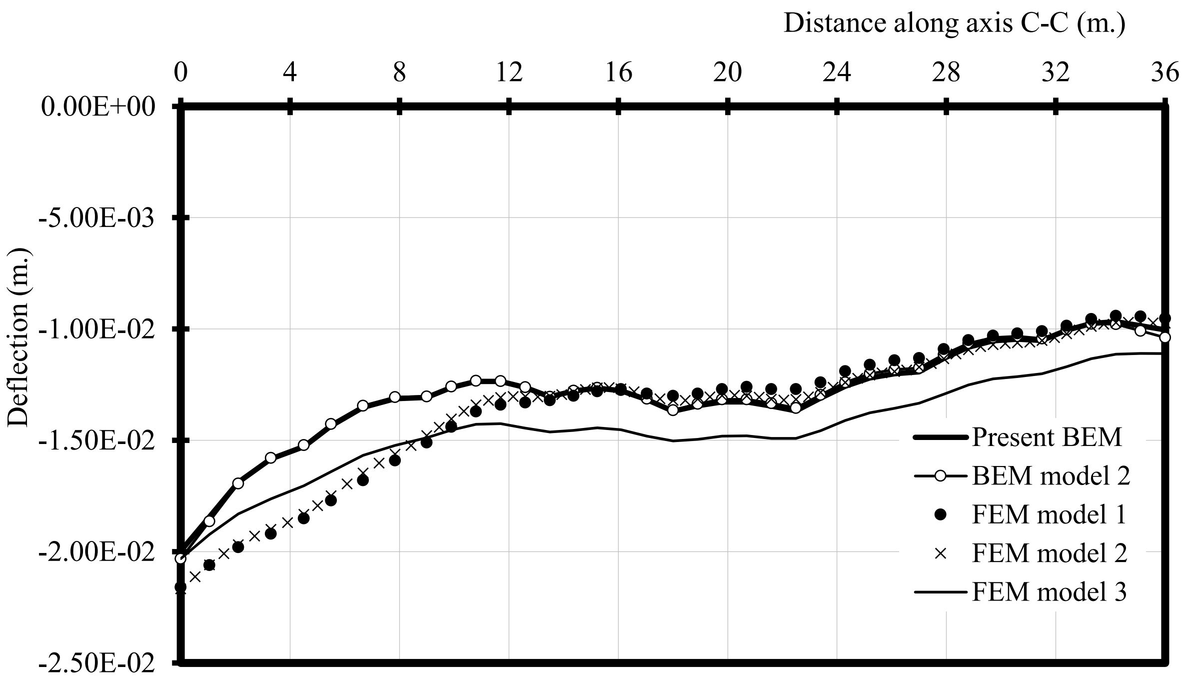

Figure 1.89: Comparison of the deflection results along axis C–C for the considered practical raft problem in Example 1.13.

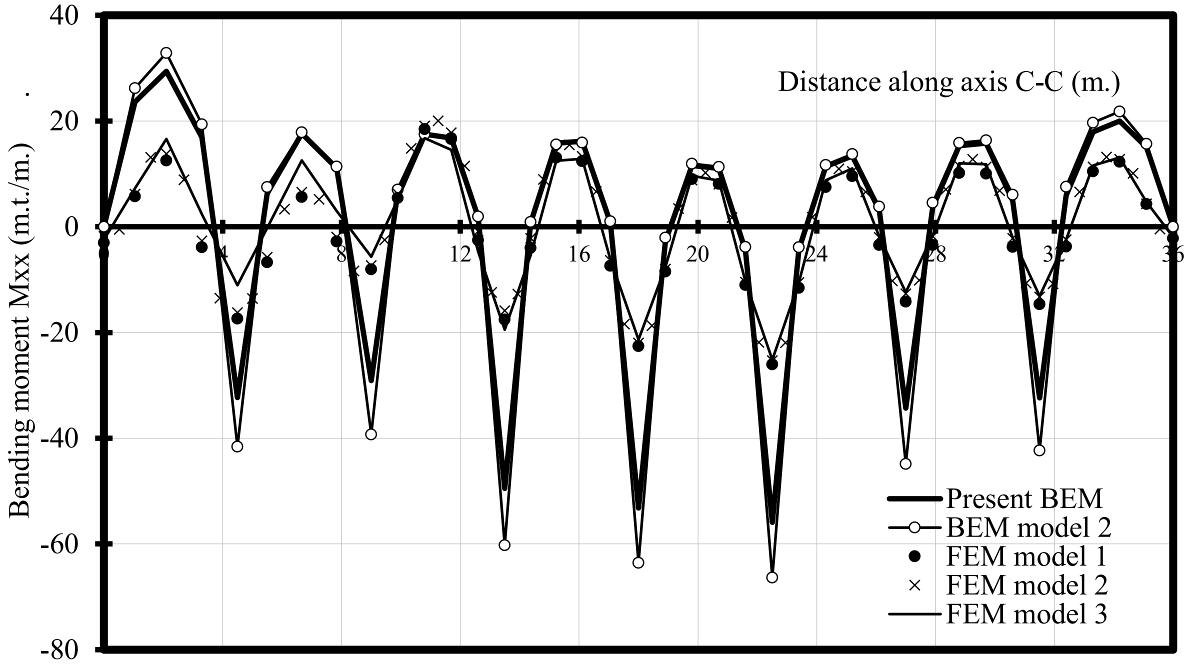

Figure 1.90: Comparison of the bending moment results along axis C–C for the considered practical raft problem in Example 1.13.

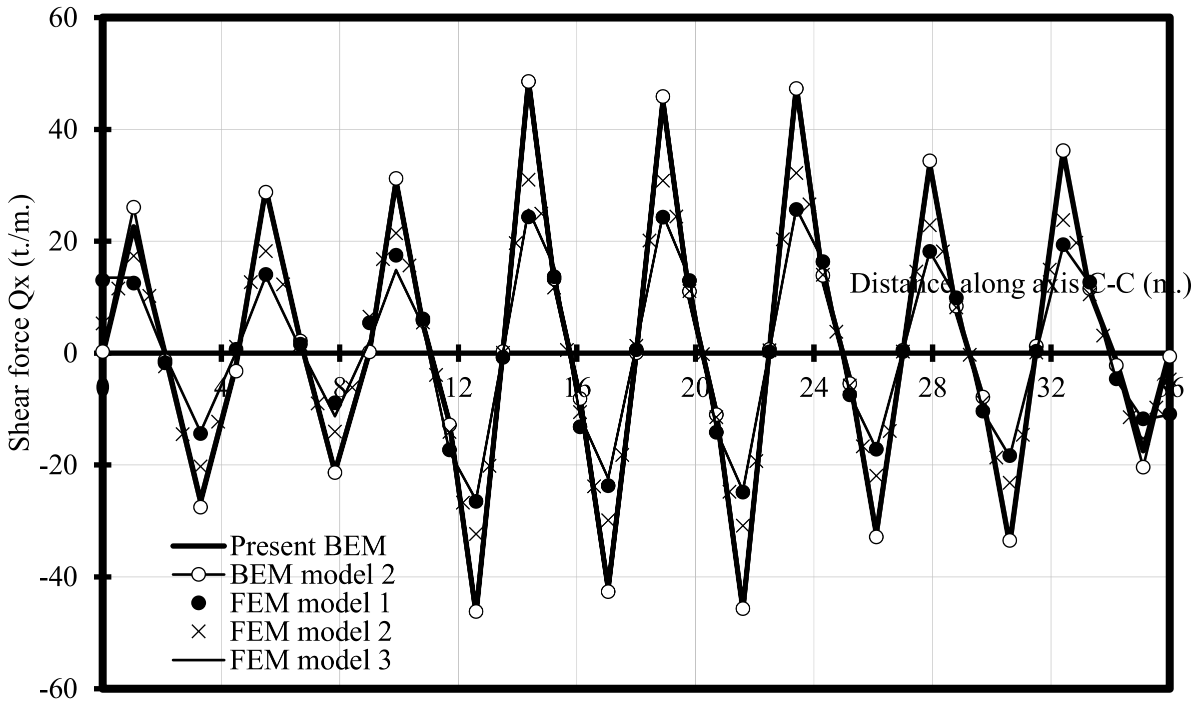

Figure 1.91: Comparison of the shear force results along axis C–C for the considered practical raft problem in Example 1.13.

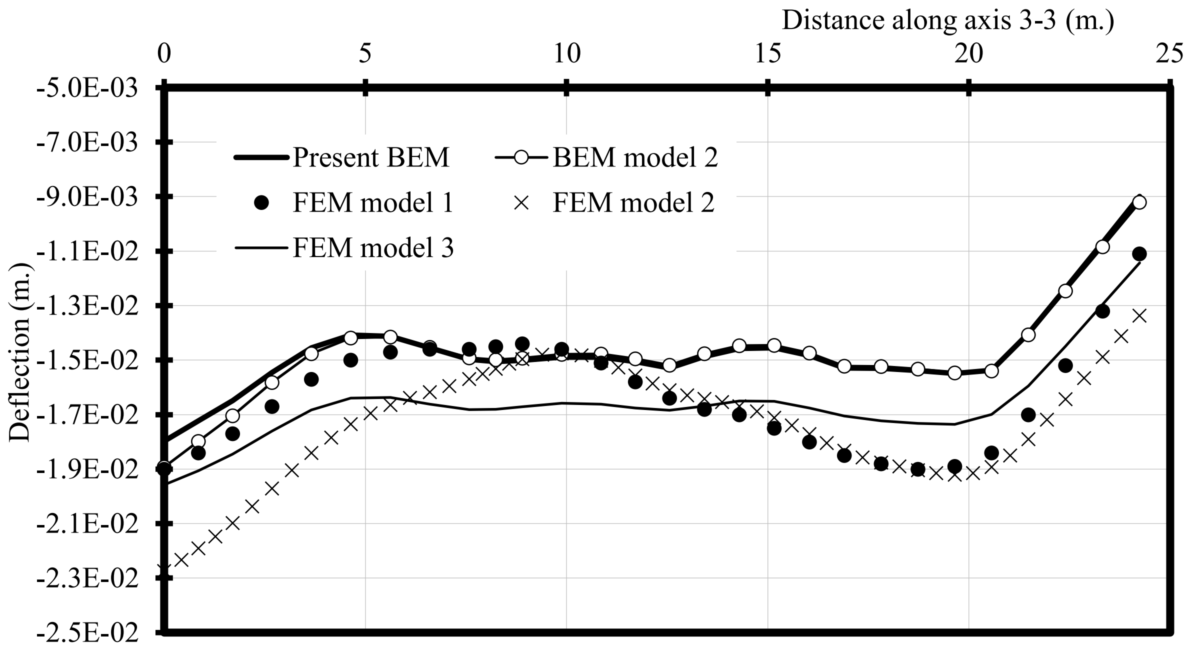

Figure 1.92: Comparison of the deflection results along axis 3–3 for the considered practical raft problem in Example 1.13.

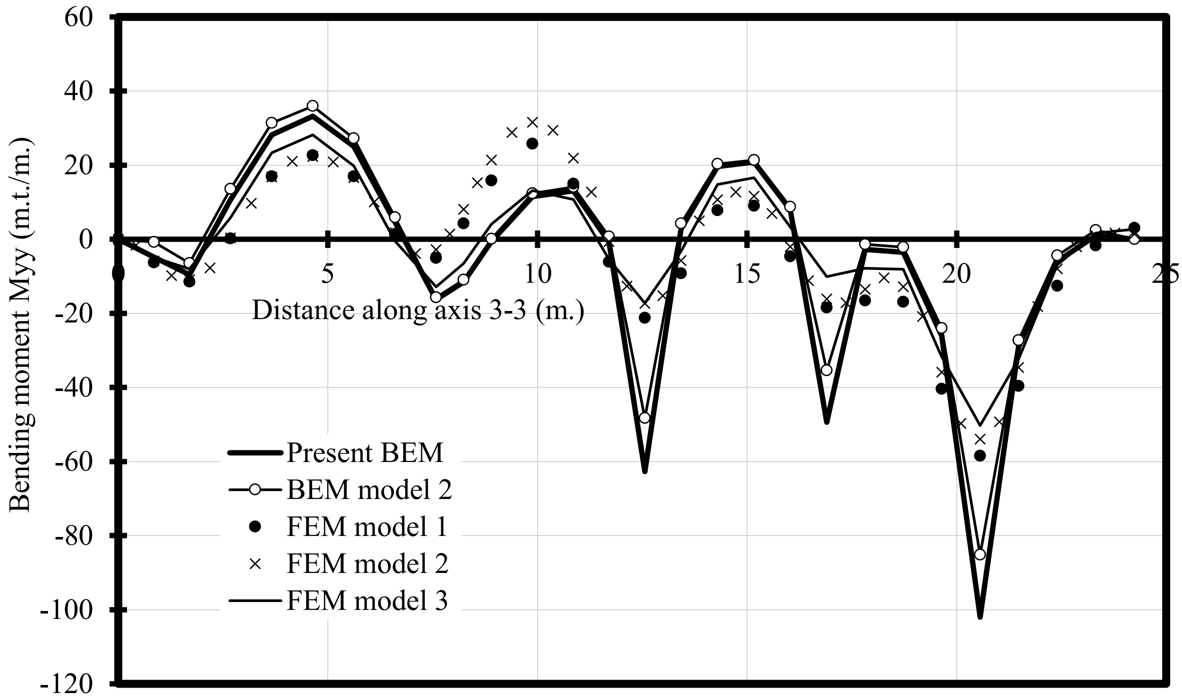

Figure 1.93: Comparison of the bending moment results along axis 3–3 for the considered practical raft problem in Example 1.13.

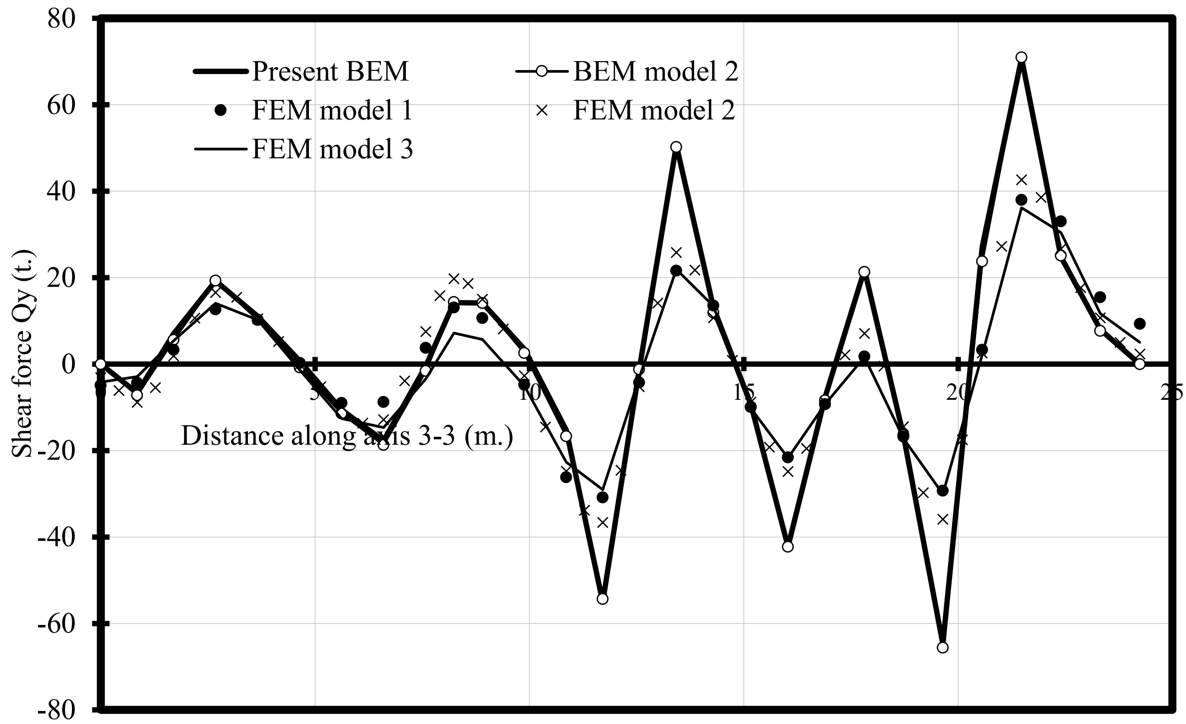

Figure 1.94: Comparison of the shear force results along axis 3–3 for the considered practical raft problem in Example 1.13.

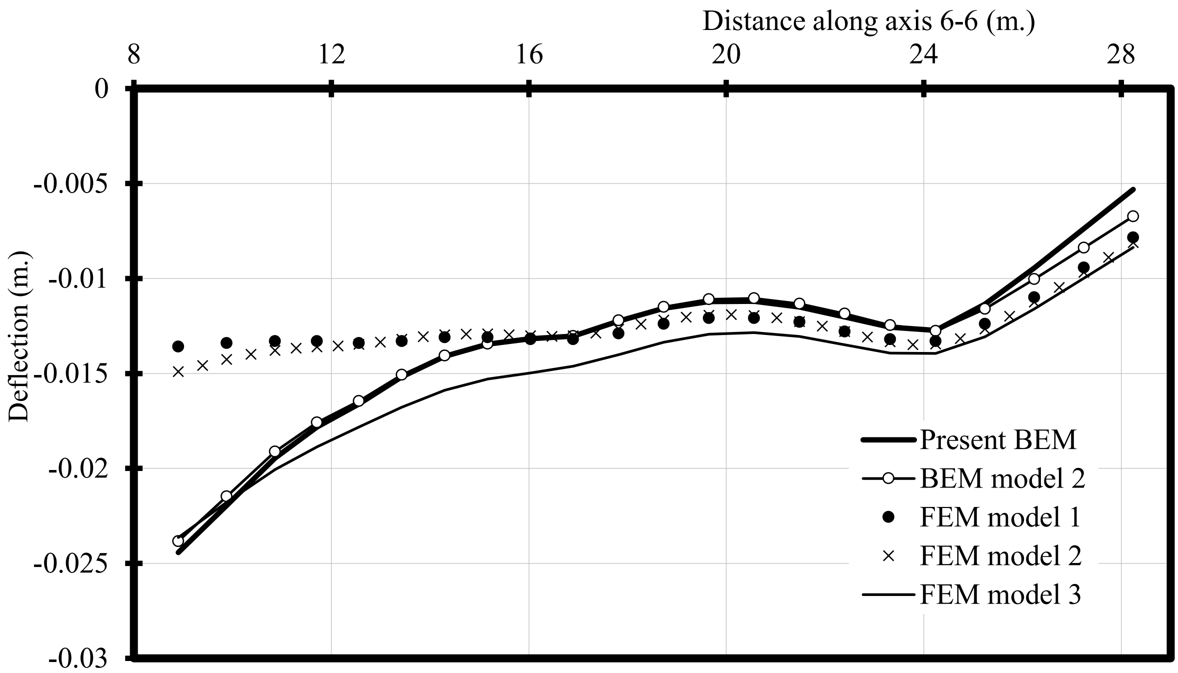

Figure 1.95: Comparison of the deflection results along axis 6–6 for the considered practical raft problem in Example 1.13.

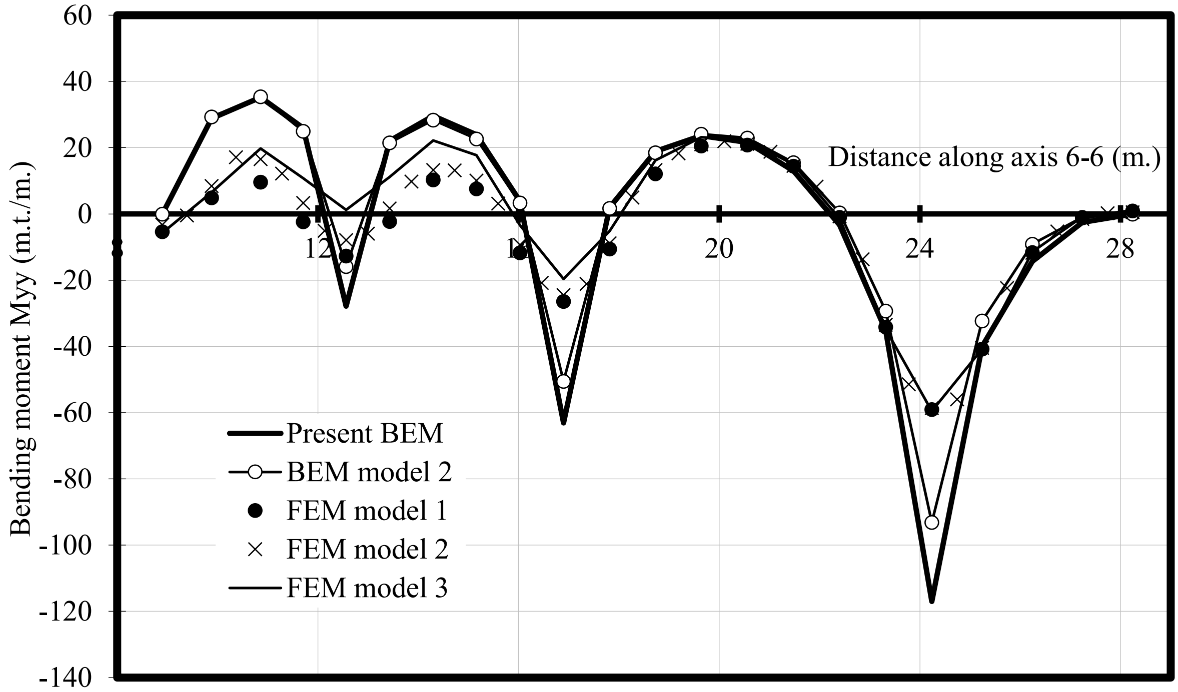

Figure 1.96: Comparison of the bending moment results along axis 6–6 for the considered practical raft problem in Example 1.13.

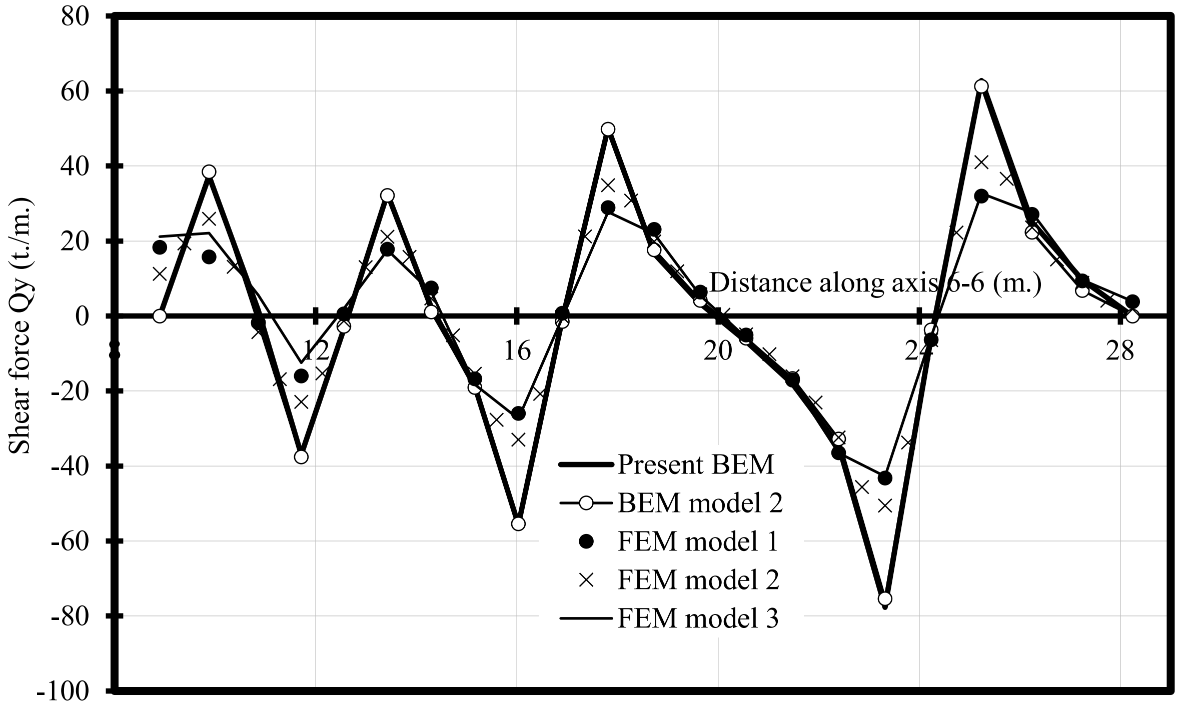

Figure 1.97: Comparison of the shear force results along axis 6–6 for the considered practical raft problem in Example 1.13.

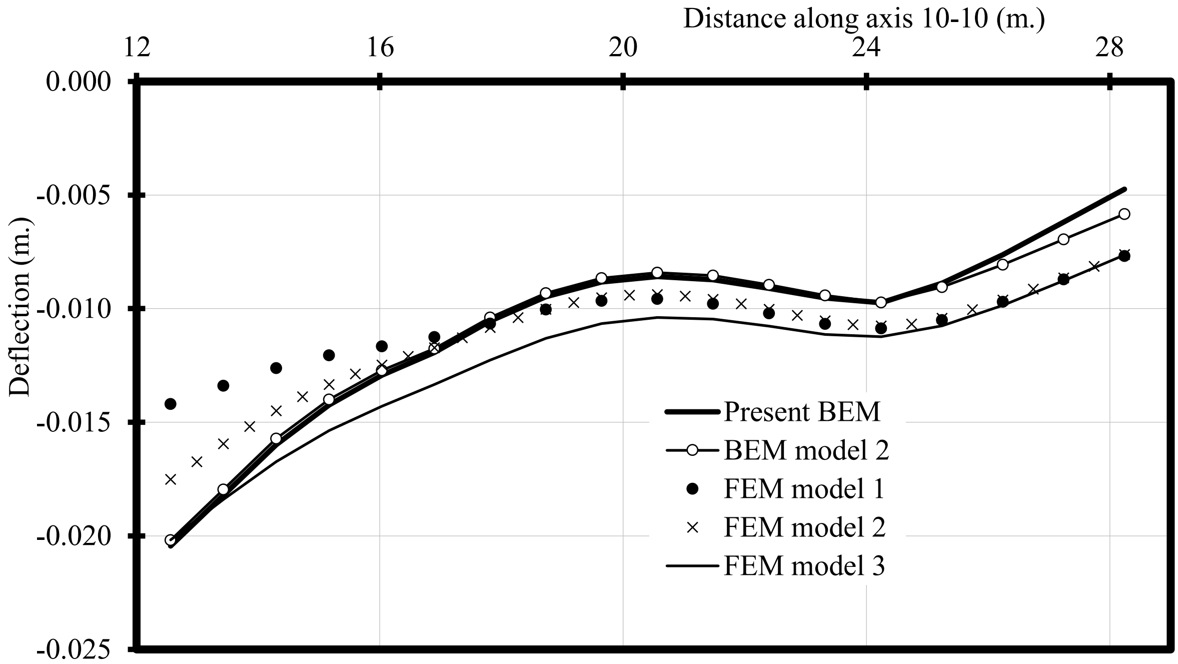

Figure 1.98: Comparison of the deflection results along axis 10–10 for the considered practical raft problem in Example 1.13.

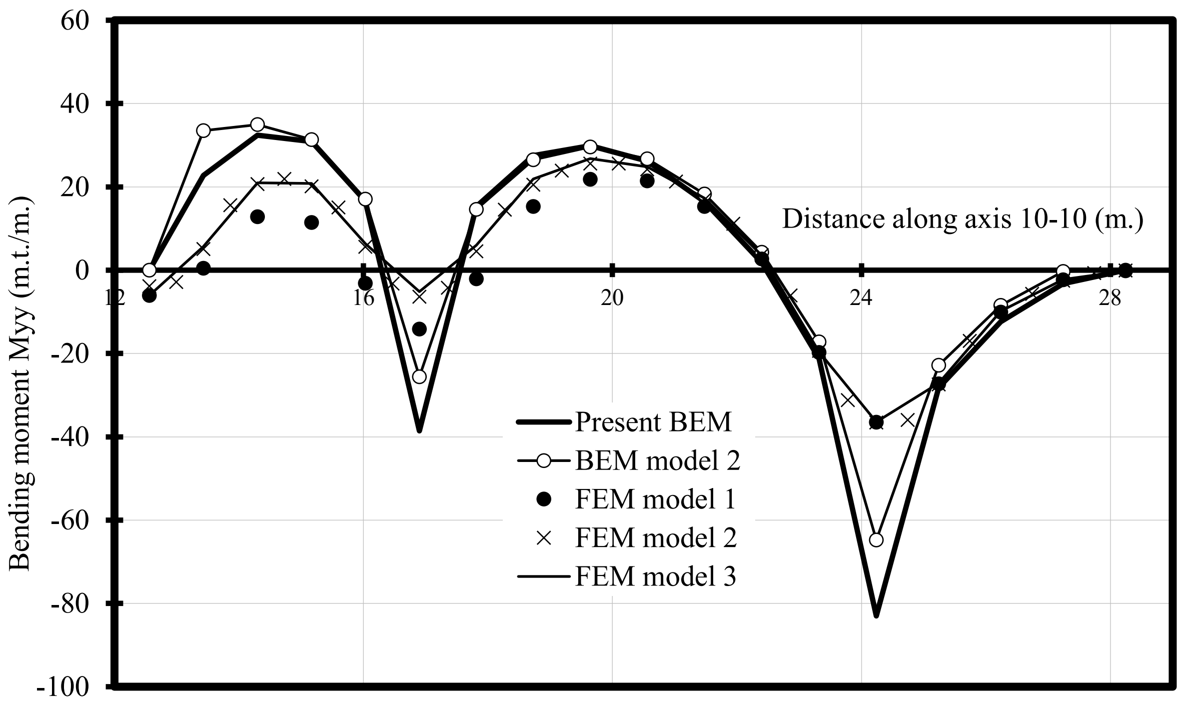

Figure 1.99: Comparison of the bending moment results along axis 10–10 for the considered practical raft problem in Example 1.13.

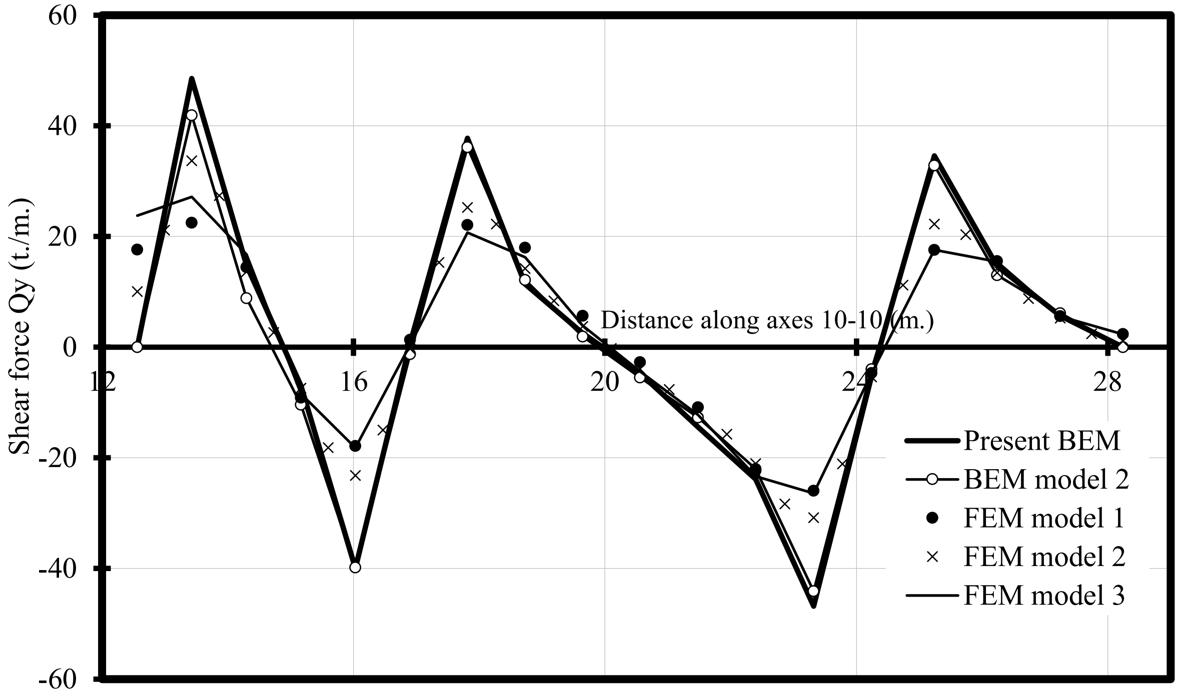

Figure 1.100: Comparison of the shear force results along axis 10–10 for the considered practical raft problem in Example 1.13.

2. The Advanced Single-Floor (Foundation) Package:

This package inherits all features in the "Single-Floor (Basic) Package" in addition to advanced modelling features of soil and piles. Therefore, it is used in advanced foundation (rafts and piled rafts) analysis and modelling.

In this package:

- Soil can be modelled as Winkler continuous area springs or as elastic half space (Soil-soil interaction) for raft foundation analysis.
- The pile-pile or the pile-soil-pile interactions can be also taken into consideration in modeling piled rafts.
- As a BIM centered package, the model can be exported from Autodesk Revit.

As a boundary element-based package:

- No internal discretization is required, which allows analysis of huge applications.
- Micro piles modelling is allowed.

The package supports real geometry modelling for foundation slab with different thicknesses, piles (as real circular elements), beams, and loading areas (columns, walls, cores).

Example 2.1 [13]

Purpose : Comparing the displacement results of a plate under central concentrated load obtained from the PLPAK models against those obtained from Ritz method presented in [14], which considers results based on both the Mindlin plate theory (MPT) and the classical thin plate theory (CPT).

Description : A square plate of uniform thickness h, width B, modulus of elasticity E_r and Poisson's ratio v_r, and resting on an elastic half space of modulus of elasticity E_s and Poisson's ratio v_s with infinite depth is subjected to a central concentrated load P. Figure 2.1 demonstrates the displacement parameters, $Iw = E_s wB/[P(1-{v_s}^2)]$, along the centerline of the plate with the following parameters: $h/B = 0.133$, $v_r = 0.15$, $k_{rs} = 0.126$, (where k_{rs} is the plate-soil stiffness ratio used by [15] and the $k_{rs} = 4E_r(1-{v_s}^2)h^3/3E_s(1-{v_r}^2)B^3$) and $v_s = 0.15$. It has to be noted that, in the PLPAK, the soil is divided into 81 stiffness cells.

Results : It can be seen that all results are in excellent agreements. The difference between the PLPAK models and the Ritz-MPT model compared to the Ritz-CPT model demonstrates the effect of the plate shear deformation.

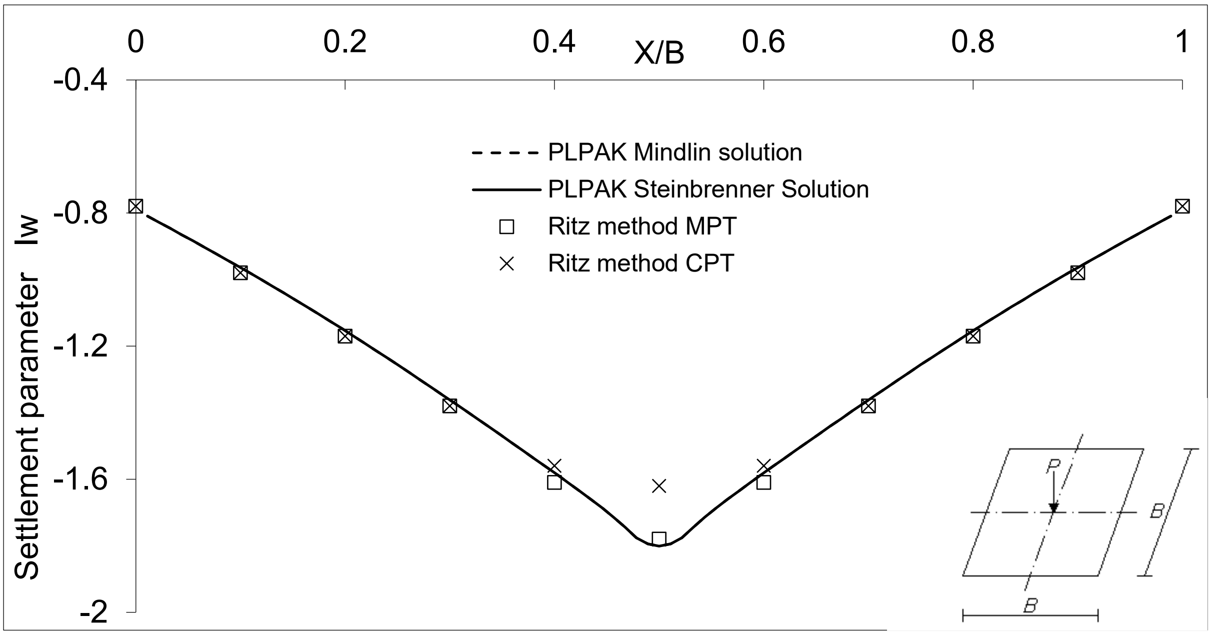

Figure 2.1: Displacement distribution for a centrally concentrated loaded square plate in Example 2.1.

Example 2.2 [13]

Purpose : Comparing the displacement results of a Plate under uniformly distributed load obtained from the PLPAK models against those obtained from Ritz method presented in [14], which considers results based on both the Mindlin plate theory (MPT) and the classical thin plate theory (CPT).

Description : A square plate of uniform thickness h, width B, modulus of elasticity E_r and Poisson's ratio v_r, and resting on an elastic half space of modulus of elasticity E_s and Poisson's ratio v_s with infinite depth is subjected to a uniformly distributed load p_r. Figure 2.2 demonstrates the variations of the displacement parameter, $Iw = E_s w/[p_r B(1 - v_s{}^2)]$, along the centerline of the plate for various k_{rs}
(where k_{rs} is the plate-soil stiffness ratio used by [15] and the $k_{rs} = 4E_r(1 - v_s{}^2)h^3/3E_s(1 - v_r{}^2)B^3)$ values and $h/B = 0.15$. In the PLPAK models, the soil is divided into 961 stiffness cells.

Results : It can be seen that all results are in excellent agreements.

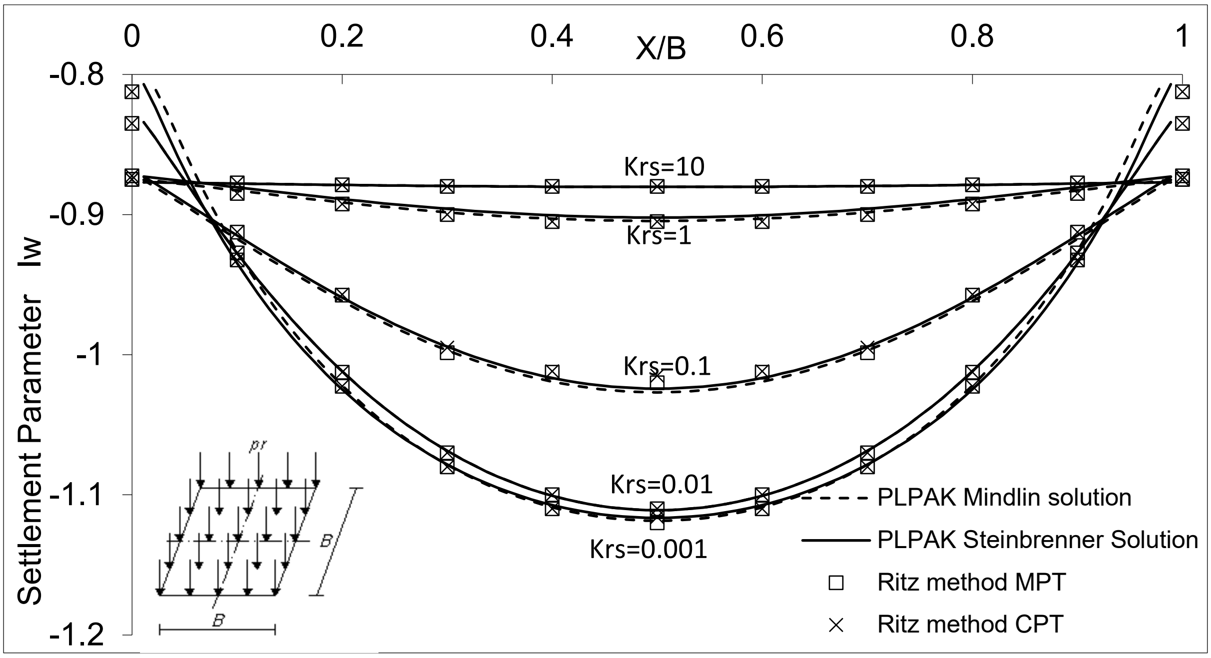

Figure 2.2: Displacement distribution for a uniformly distributed loaded square plate in Example 2.2.

Example 2.3 [13]

Purpose : Comparing the displacement results of a plate under central square patch load obtained from the PLPAK models against those obtained from Ritz method presented in [14], which considers results based on both the Mindlin plate theory (MPT) and the classical thin plate theory (CPT).

Description : A square plate of uniform thickness h, width B, modulus of elasticity E_r and Poisson's ratio v_r, and resting on an elastic half space of modulus of elasticity E_s and Poisson's ratio v_s with infinite depth is subjected to a central square patch load. The size of the central patch load is defined by the parameter C/B. Figure 2.3–Figure 2.5 demonstrate the variations of the displacement parameter, $Iw = E_s w/[p_r B(1 - v_s{}^2)]$, along the plate centerline for various k_{rs} values (where k_{rs} is the plate-soil stiffness ratio used by [15] and the $k_{rs} = 4E_r(1 - v_s{}^2)h^3/3E_s(1 - v_r{}^2)B^3)$ and for $C/B = 0.25$, 0.50 and 0.75, respectively where the value of the plate constant h/B is 0.15. In the PLPAK models, the soil is divided into 81 stiffness cells.

Results : It can be seen that all results are in good agreement. A very small value of C/B is equivalent to concentrated load, whereas, a large value of C/B can be regarded as a uniformly distributed load. The effect of the plate shear deformation is obvious in the Ritz-MPT model and in the PLPAK models rather than the Ritz-CPT model for low values of k_{rs}.

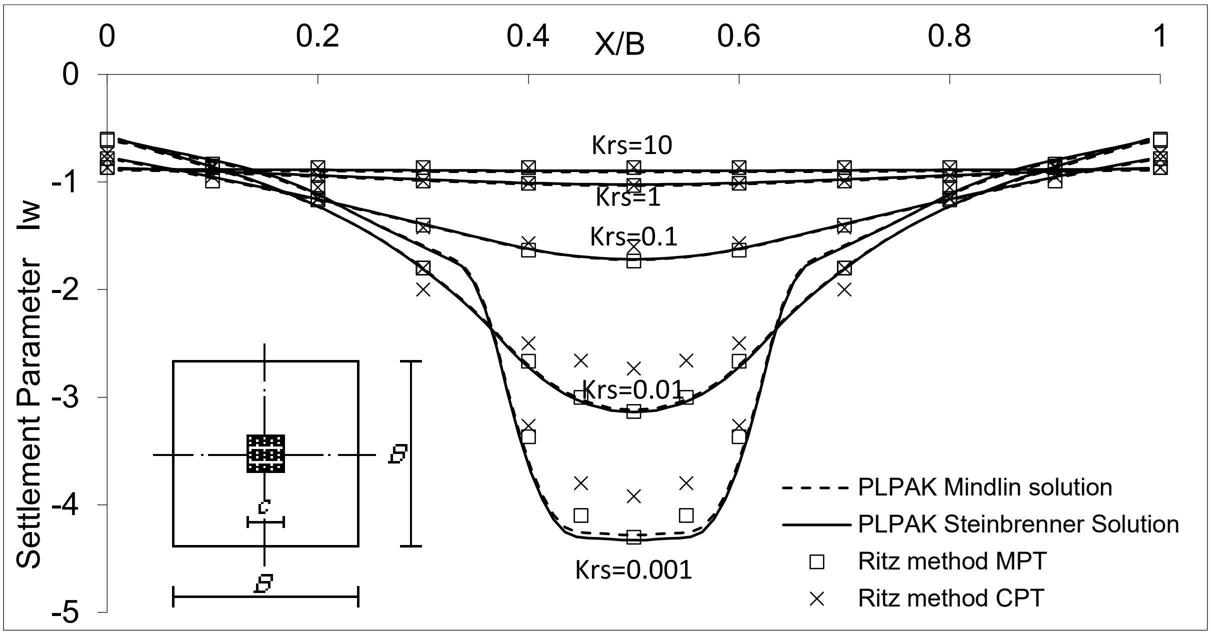

Figure 2.3: Displacement distribution for a centrally patch loaded square plate with c/B=0.25 in Example 2.3.

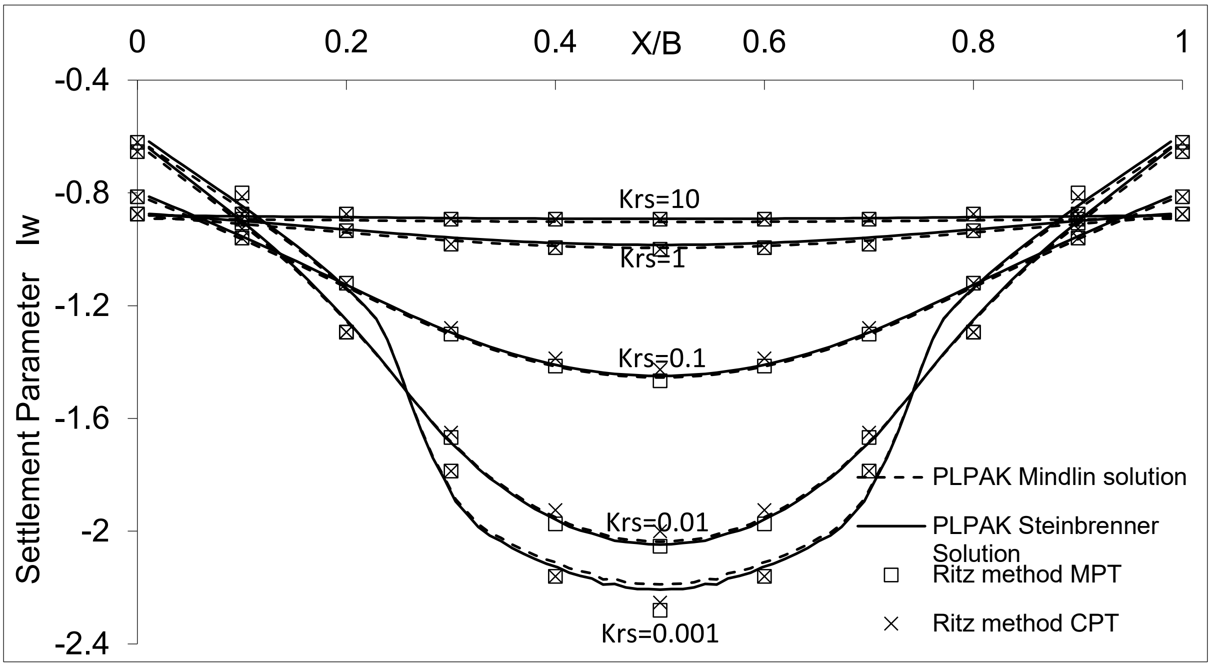

Figure 2.4: Displacement distribution for a centrally patch loaded square plate with c/B=0.50 in Example 2.3.

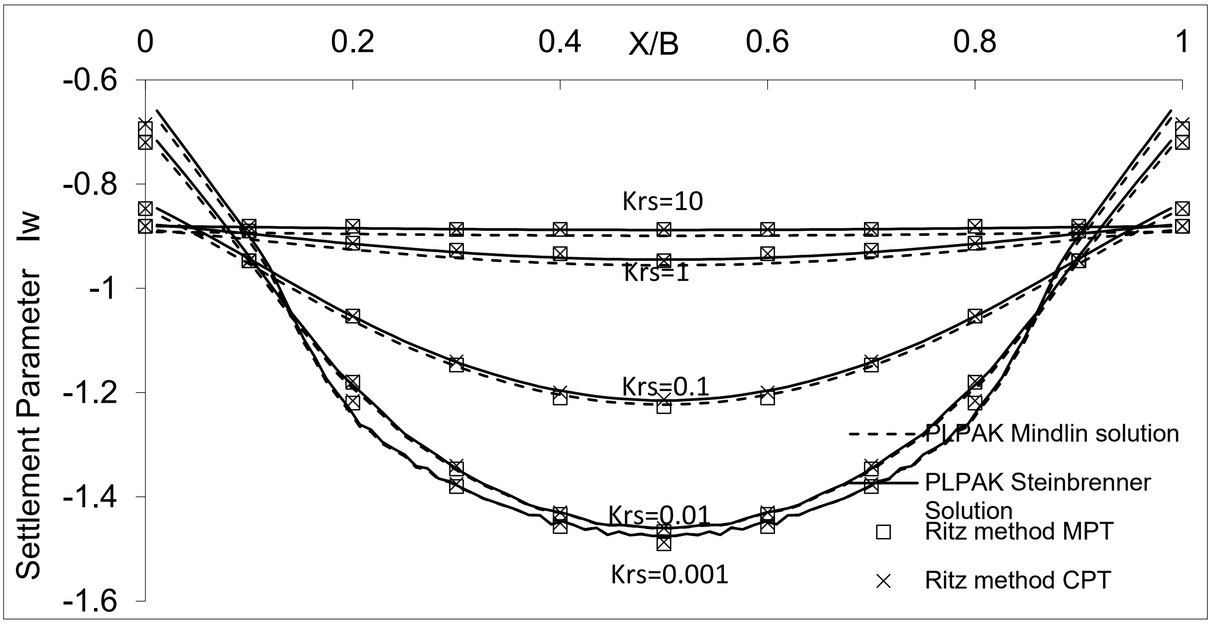

Figure 2.5: Displacement distribution for a centrally patch loaded square plate with c/B=0.75 in Example 2.3.

Example 2.4 [13]

Purpose : Comparing the displacement results of a plate under side-long rectangular patch load obtained from the PLPAK models against those obtained from Ritz method presented in [14], which considers results based on both the Mindlin plate theory (MPT) and the classical thin plate theory (CPT).

Description : A square plate of uniform thickness h, width B, modulus of elasticity E_r and Poisson's ratio v_r, and resting on an elastic half space of modulus of elasticity E_s and Poisson's ratio v_s with infinite depth is subjected to a side-long rectangular patch load. The size of the side-long patch load is defined by the parameter C/B. Figure 2.6–Figure 2.8 demonstrate the variations of the displacement parameter, $Iw = E_s w/[p_r B(1 - {v_s}^2)]$, along the plate centerline for various values k_{rs} (where k_{rs} is the plate-soil stiffness ratio used by [15] and the $k_{rs} = 4E_r(1 - {v_s}^2)h^3/3E_s(1 - {v_r}^2)B^3$) and for $C/B = 0.25$, 0.50 and 0.75, respectively where the value of the plate constant h/B is 0.15. It has to be noted that, in the PLPAK models, the soil is divided into 961 stiffness cells.

Results : It can be seen that, all results are in good agreement.

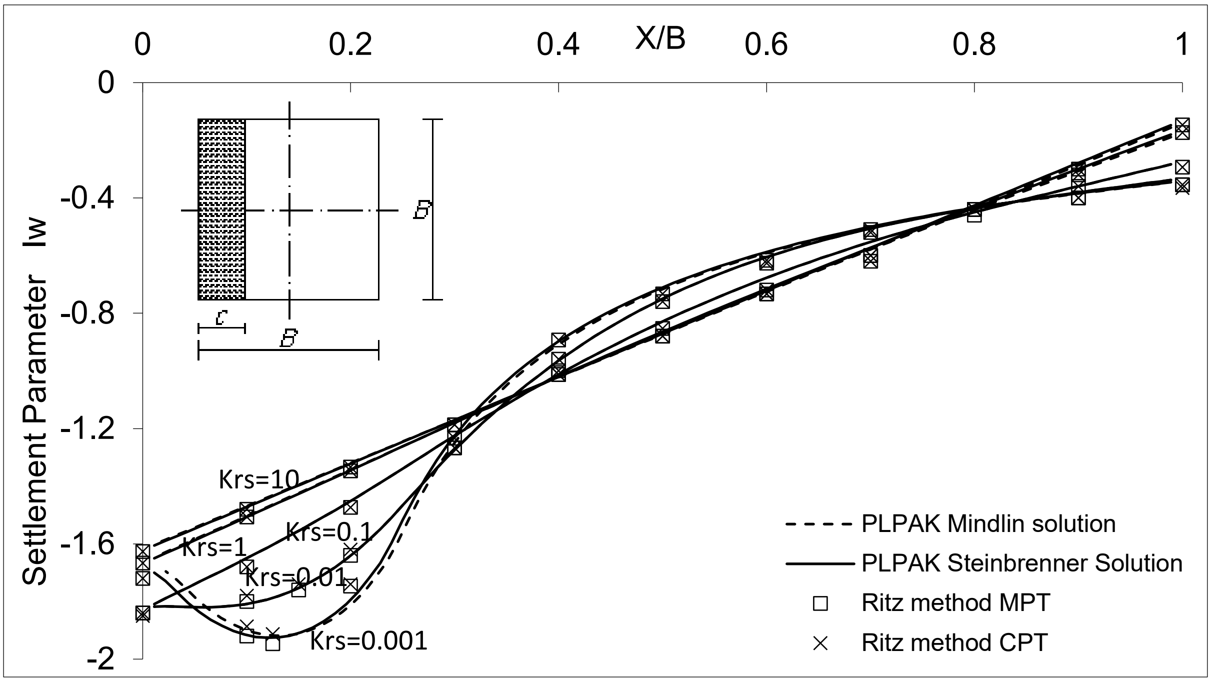

Figure 2.6: Displacement distribution for a side-long patch loaded square plate with c/B=0.25 in Example 2.4.

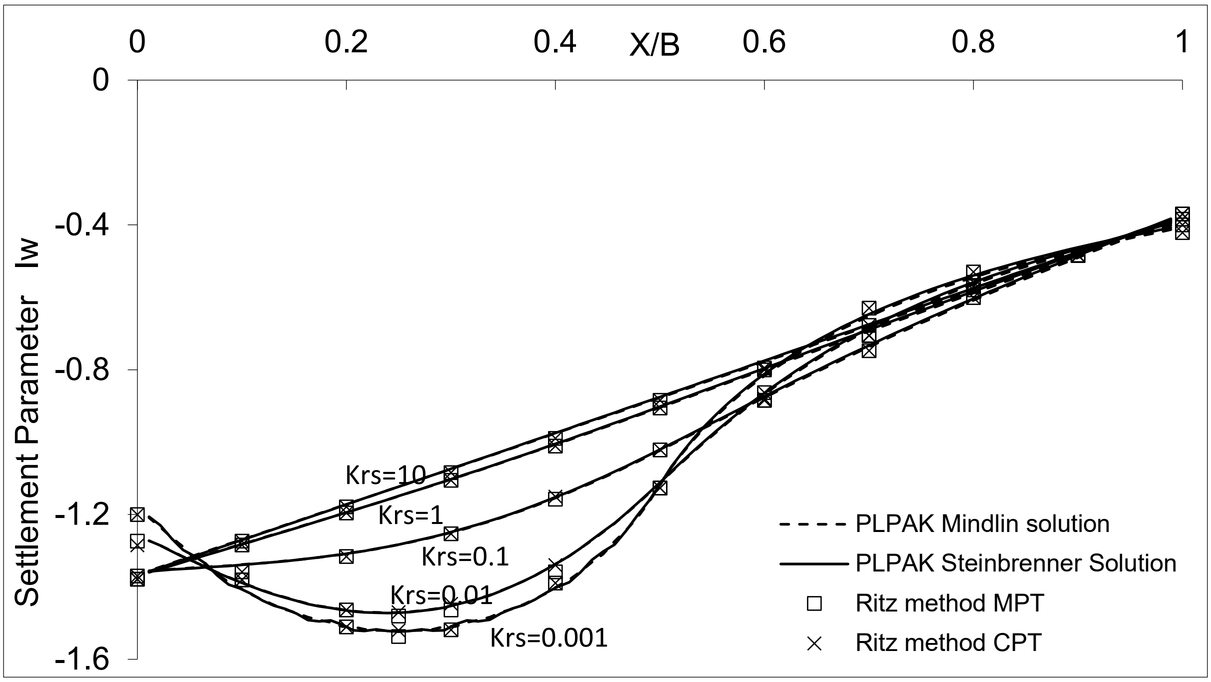

Figure 2.7: Displacement distribution for a side-long patch loaded square plate with c/B=0.50 in Example 2.4.

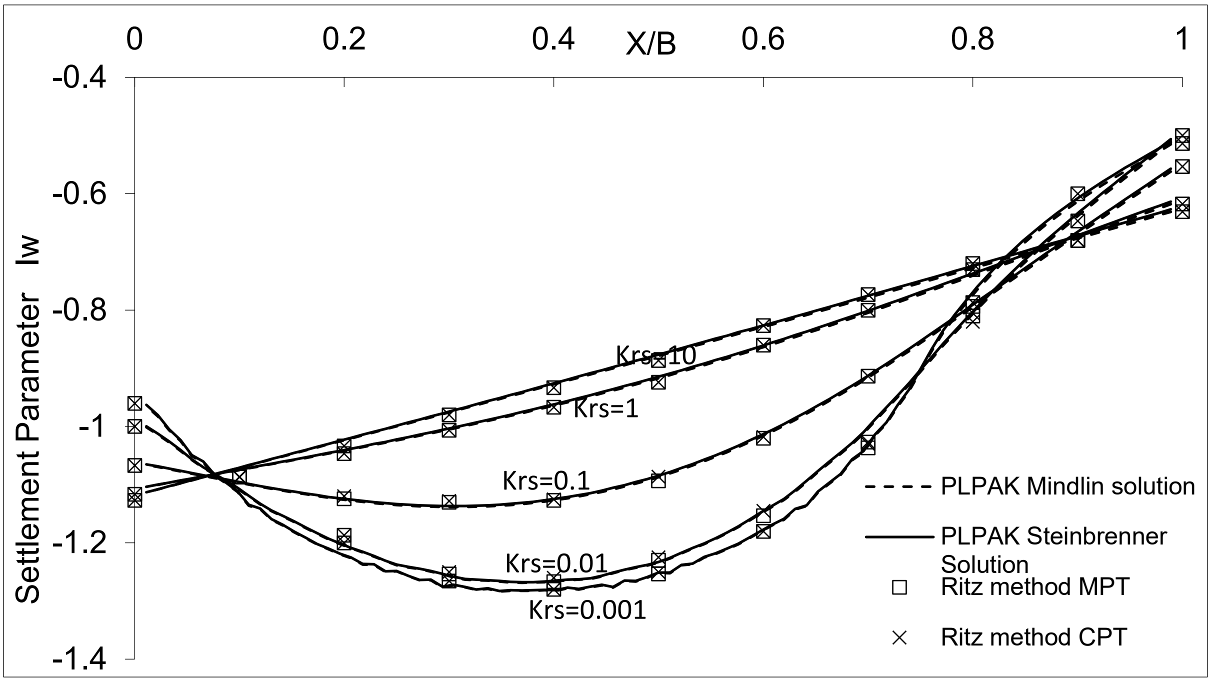

Figure 2.8: Displacement distribution for a side-long patch loaded square plate with c/B=0.75 in Example 2.4.

Example 2.5 [13]

Purpose : Comparing the displacement results of a thin plate on Boussinesq half space obtained from the PLPAK models against to those obtained from the analysis of the formulation of [16].

Description : A circular plate with free edge boundary condition and subjected to a uniform load p is considered. The plate has a uniform thickness h, radius a, modulus of elasticity E_r, Poisson's ratio v_r, and resting on an infinite elastic half space of modulus of elasticity E_s and Poisson's ratio v_s. The plate-soil stiffness ratio used in this comparison is $k_r = E_r(1-{v_s}^2)h^3/E_s(1-{v_r}^2)a^3$. The values: $h = 0.1\,m$, $a = 1\,m$, $Es = 21\,MPa$, $v_r \times v_s = 0.2$ are used in the comparison. In the PLPAK models, the soil is modeled using three meshes. The numbers of stiffness cells used are 97, 177, and 277 for meshes 1, 2 and 3 respectively. Twenty-eight internal points are used to calculate results along the plate centerline.

Results : Figure 2.9 demonstrates the displacement results of the present models using both of Mindlin and Steinbrenner solutions based on mesh 2. These results are compared to those of [16] together with previous predictions of hybrid finite-surface element scheme by [17]. Table 2.1 demonstrates the displacement results for the above-mentioned numerical models and the analytical theoretical predictions for plates with negligible rigidity $(K_r = 0)$ and another time with infinite rigidity $(K_r = \infty)$ analyzed by [18]. It has to be noted that, the computed displacement is divided by the quantity $W_o = pa(1-{v_s}^2)/E_s$ to allow dimensionless comparisons. It can be seen that all results are in good agreement. The PLPAK models are a bit closer to results given by [17], which confirms the accuracy and the validity of the PLPAK.

Table 2.1: Displacement of a circular plate under uniform load in Example 2.5.

Solution	$W(0)/W(o)$				$W(a)/W(o)$			
	$K_r = 0$	$K_r = 0.1$	$K_r = 1$	$K_r = \infty$	$K_r = 0$	$K_r = 0.1$	$K_r = 1$	$K_r = \infty$
[16]		1.972	1.663			1.309	1.408	
BEM mesh 1 [16]		1.969	1.677			1.331	1.432	
BEM mesh 2 [16]		1.964	1.68			1.329	1.439	
BEM mesh 3 [17]		1.96	1.685			1.363	1.465	
Timoshenko and [18]	2			1.57	1.273			1.57
Present Mindlin solution mesh 1	1.967	1.942	1.708	1.577	0.783	1.4	1.519	1.578
Present Mindlin solution mesh 2	1.977	1.944	1.712	1.583	1.228	1.411	1.528	1.585
Present Mindlin solution mesh 3	1.983	1.943	1.719	1.597	1.338	1.425	1.543	1.6
Present Steinbrenner solution mesh 1	1.984	1.959	1.72	1.588	0.79	1.409	1.531	1.59
Present Steinbrenner solution mesh 2	1.99	1.956	1.721	1.593	1.233	1.419	1.537	1.595
Present Steinbrenner solution mesh 3	1.994	1.953	1.726	1.605	1.343	1.431	1.551	1.607

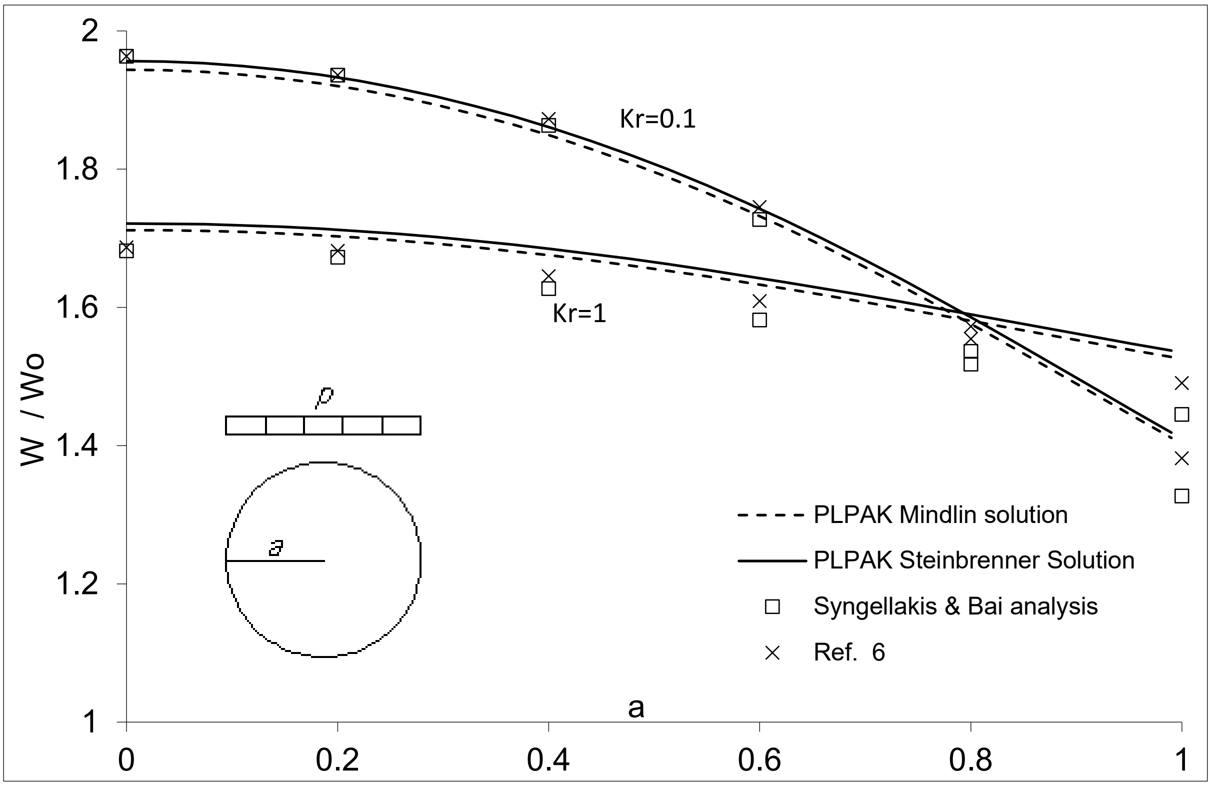

Figure 2.9: Displacement distribution for a circular plate under uniform load in Example 2.5.

Example 2.6 [13]

Purpose : Comparing the displacement results of a rectangular plate under uniform load on infinite single-layered elastic half space obtained from the PLPAK against to those obtained from the analysis of the finite layer formulation of [19].

Description : A rectangular plate of thickness h, width B, length L, modulus of elasticity E_r and Poisson's ratio v_r, and resting on an elastic half space of modulus of elasticity E_s and Poisson's ratio v_s with infinite depth is subjected to a uniform load of intensity p_r. The plate-soil stiffness ratio used in the comparison is $k_{rs} = 4E_r(1-{v_s}^2)h^3/3E_s(1-{v_r}^2)B^3$. In the PLPAK models, the soil is divided into 496 stiffness cells. Figure 2.10 demonstrates the variations of the displacement parameter, $Iw = E_s w/[p_r B(1-{v_s}^2)]$, at points A, B, C and D (See Figure 2.10) in the plate for various k_{rs} values.

Results : The displacement results obtained from the PLPAK models using both Mindlin and Steinbrenner solutions are compared to those results obtained from [19] as well as results analysis of [15]. It can be seen that all results are in good agreement.

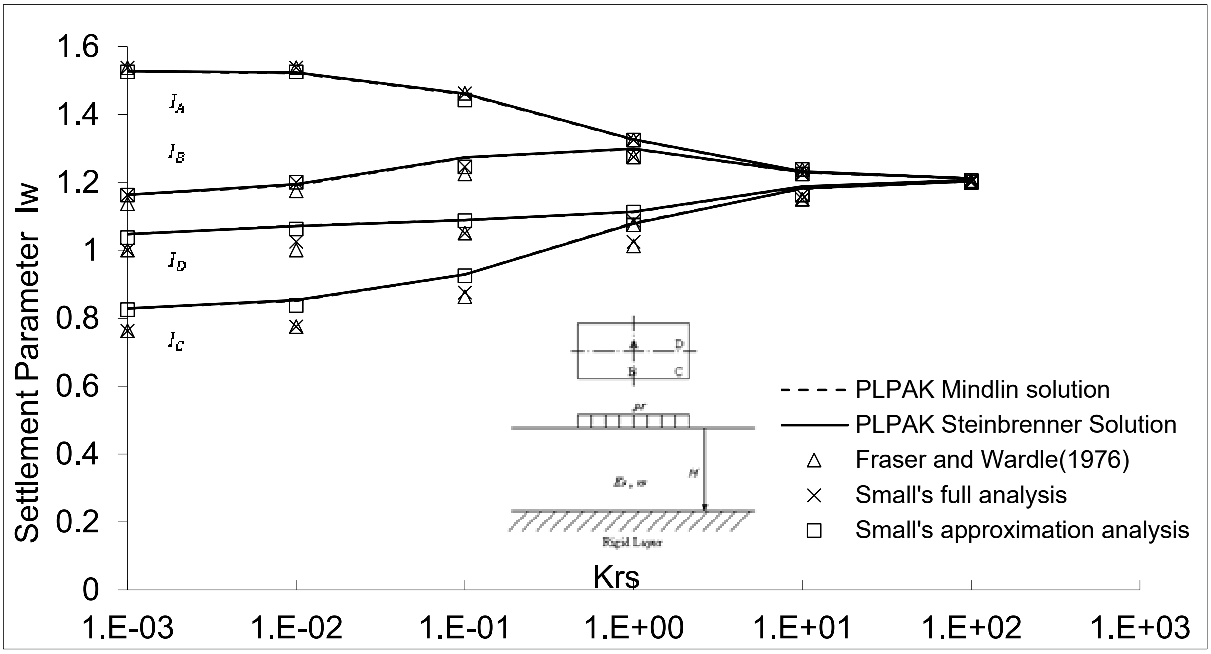

Figure 2.10: Displacement distribution for a rectangular plate under uniform load at A, B, C and D in Example 2.6.

Example 2.7 [13]

Purpose : Comparing the displacement results of a square plate under four concentrated loads on two-layered elastic half space obtained from the PLPAK against to those obtained from the analysis of the finite layer formulation of [19].

Description : A square plate of thickness $h = 0.4$, width $B = 12\ m$, modulus of elasticity $E_r = 3000$ and Poisson's ratio $v_r = 0.2$. The plate is resting on a two-layered elastic half space and has a rigid end layer. The elastic parameters of each layer from the upper layer down to the lower one above the rigid layer are as follow:

Modulus of elasticity $E_{s1} = 1\ MPa$, Poisson's ratio $v_{s1} = 0.3$ and thickness $H_1 = 4\ m$.

Modulus of elasticity $E_{s2} = 5\ MPa$, Poisson's ratio $v_{s2} = 0.3$ and thickness $H_2 = 6\ m$.

The plate is loaded by four concentrated loads (two P_1 loads at the right and two P_2 loads at the left). Each load is located at a distance $B/4$ in both direction of X and Y from the nearest corner as demonstrated in Figure 2.11. In the present model, the soil is divided into 441 stiffness cells. Fifty-five internal points are used to calculate results along the column strip which includes both loads P_1 and P_2.

Results : Figure 2.11 demonstrates the effect of the load ratio P_2/P_1 on the non-dimensional displacement parameter $I = 4wD_r/P_1B^2$ along the strip $A–A$ (see Figure 2.11), where w is the vertical displacement of the plate and $D_r = E_rh^3/[12(1 - v_r{}^2)]$ is the flexure rigidity of the plate. It can be seen from Figure 2.11 that, the results of Steinbrenner solution in the PLPAK model are in a good agreement with those of [19].

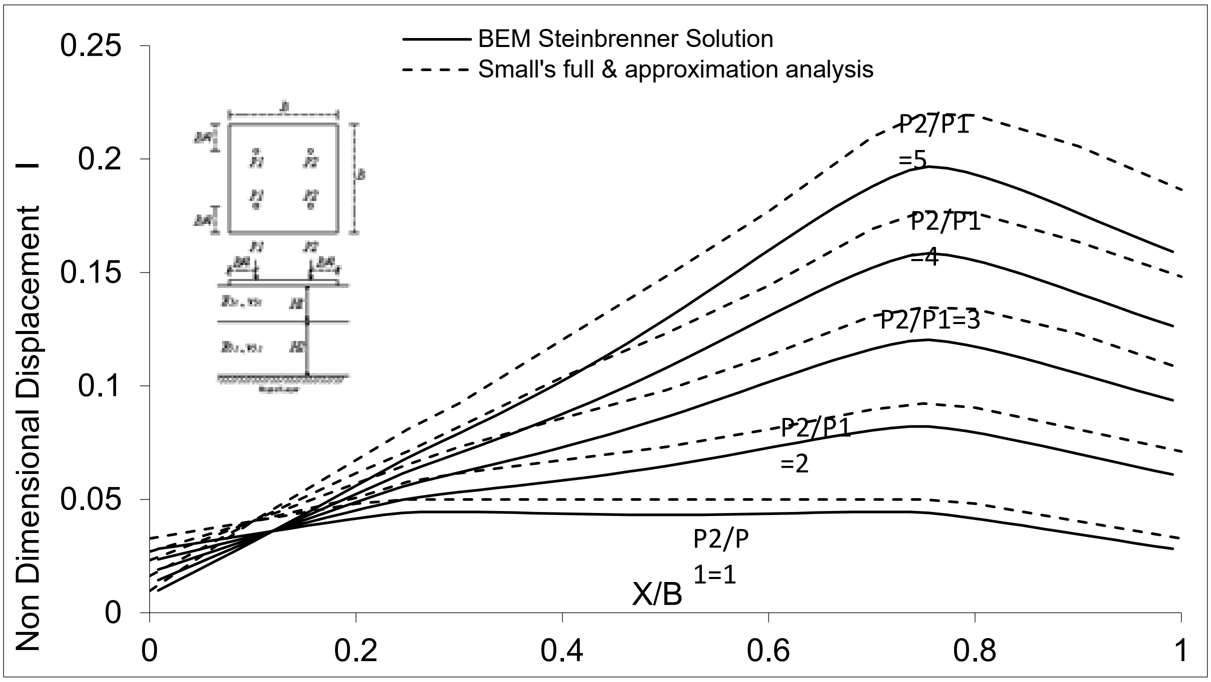

Figure 2.11: Displacement distribution for a square plate under four concentrated loads along the strip A–A in Example 2.7.

Example 2.8 [13]

Purpose : Comparing the displacement results of a square plate under a uniform load and resting on infinite single-layered elastic half space obtained from the PLPAK models using both Mindlin and Steinbrenner solutions to those obtained from the analysis of several referenced work including [20], the spline method [21], the displacement method [21] and the FEM for plate on half space [22].

Description : The plate demonstrated in this example is subjected to a uniform load of intensity $p_r = 0.98\ MPa$ and has thickness $h = 0.2\ m$ and length $L = 4\ m$. Modulus of elasticity is $E_r = 0.343 \times 10^5\ MPa$ and Poisson's ratio is $v_r = 0.167$. The plate is resting on an elastic half space having modulus of elasticity $E_s = 0.343 \times 10^3\ MPa$ and Poisson's ratio $v_s = 0.4$ with infinite depth. In the PLPAK models, the soil is presented with 3 meshes. In meshes 1, 2 and 3, the soil is divided into 4×4, 6×6 and 8×8 stiffness cells respectively.

Results : Table 2.2 demonstrates the computed displacements at the center point of the plate. It can be seen that all results are in good agreement.

Table 2.2: Displacement at the center of a square plate under uniform load on an elastic half space in Example 2.8.

	Spline method [21]	Displacement method [21]	FEM for plate on half space [22]	[20]	PLPAK Mindlin solution	PLPAK Steinbrenner solution
Mesh (4×4)	0.01054	0.01054	0.01068	0.01045	0.01066	0.01085
Mesh (6×6)	0.01059	0.01059	0.01063	0.01052	0.01062	0.01074
Mesh (8×8)	0.01062	0.01062	0.01061	0.0106	0.01065	0.01075

Example 2.9 [13]

Purpose : Comparing the displacement results of a square plate under uniform load and resting on finite single-layered elastic half space obtained from the PLPAK models using both Mindlin and Steinbrenner solutions to those obtained from the analysis of [20] and the equivalent method presented in [15].

Description : The plate demonstrated in this example is a square plate subjected to a uniform load of intensity $p_r = 0.1\ MPa$ and has thickness $h = 0.5\ m$ and length $L = 10\ m$. Modulus of elasticity is $E_r = 0.15 \times 10^5\ MPa$ and Poisson's ratio is $v_r = 0.2$. It is resting on a one-layered elastic half space of modulus of elasticity $E_s = 0.832 \times 10^2\ MPa$ and Poisson's ratio $v_s = 0.3$ and it has a rigid end layer at depth $H = 40\ m$. In the PLPAK models, the soil is divided into 64 stiffness cells. Table 2.3 demonstrates the computed displacements at the center, mid-edge and corner points of the plate.

Results : It can be seen from Table 2.3 that, the results of the PLPAK models are a bit closer to results given by the equivalent method [15], which confirms the accuracy and the validity of the PLPAK.

Table 2.3: Displacement at the center, mid-edge and corner of a square plate on an elastic half space in Example 2.9.

	Equivalent method [15]	[20]	PLPAK Mindlin solution	PLPAK Steinbrenner solution
Center point	0.0107	0.0129	0.0103	0.0104
Mid-edge point	0.0078	0.095	0.0083	0.0082
Corner point	-	0.0663	0.0066	0.0062

Example 2.10 [13]

Purpose : Comparing the displacement results of a square plate under a uniform load and resting on multi-layered elastic half space obtained from the PLPAK models using both Mindlin and Steinbrenner solutions to those obtained from the analysis of [20] and both of the equivalent method in [15] and the numerical method in [23].

Description : The plate demonstrated in this example is the same plate demonstrated in Example 2.9. It is resting on four-layered elastic half space, and it has a rigid end layer, (see Figure 2.12). The elastic parameters for each layer starting from the upper layer down to the lower one above the rigid end layer are given as follow:

Modulus of elasticity $E_{s1} = 100\ MPa$, Poisson's ratio $v_{s1} = 0.3$ and thickness $H_1 = 10\ m$.

Modulus of elasticity $E_{s2} = 80\ MPa$, Poisson's ratio $v_{s2} = 0.3$ and thickness $H_2 = 10\ m$.

Modulus of elasticity $E_{s3} = 60\ MPa$, Poisson's ratio $v_{s3} = 0.3$ and thickness $H_3 = 10\ m$.

Modulus of elasticity $E_{s4} = 100\ MPa$, Poisson's ratio $v_{s4} = 0.3$ and thickness $H_4 = 10\ m$.

It has to be noted that, the equivalent layer (according to [24]) to these layers gives $E_s = 0.832 \times 10^2\ MPa$ and $v_s = 0.3$, which are similar values to those used in Example 2.9. In the PLPAK models, the soil is divided into 64 stiffness cells.

Results : Table 2.4 demonstrates the computed displacements at the center and mid-edge points of the plate. It can be seen that all results are in good agreement. The PLPAK results in the current example are a bit less than those obtained from the equivalent layer in Example 2.9 because of the presence of a strong top soil layer. This could be overcome by considering more refined layering system.

Table 2.4: Displacement at the center and mid-edge of a square plate on a multi-layered elastic half space in Example 2.10.

	Equivalent method [15]	Numerical method[23]	[20]	PLPAK Mindlin solution	PLPAK Steinbrenner solution
Center point	0.0107	0.0114	0.012	0.0094	0.0097
Mid-edge point	0.0078	0.087	0.0089	0.0076	0.0077

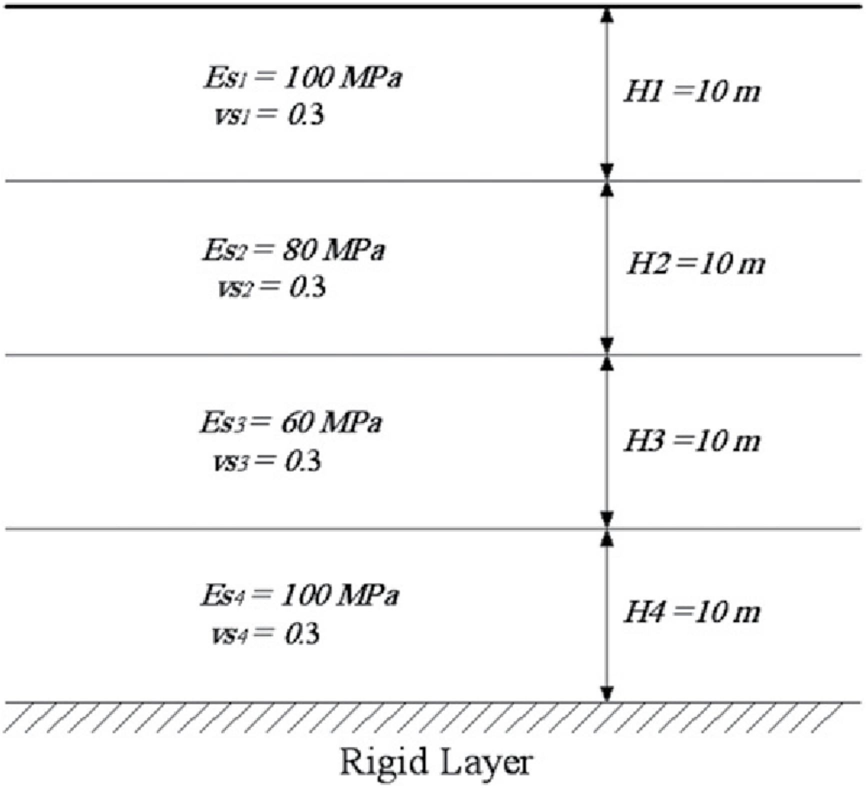

Figure 2.12: Four-layered elastic half space in Example 2.10.

Example 2.11 [13]

Purpose : Comparing the displacement results of a trapezoidal plate under uniform load and resting on finite single-layered elastic half space obtained from the PLPAK models using both Mindlin and Steinbrenner solutions to those obtained from the analysis of [20].

Description : The trapezoidal plate demonstrated in Figure 2.13 is considered in this example. The plate is subjected to a uniform load of intensity $p_r = 1\ MPa$ and has thickness $h = 2\ m$, modulus of elasticity is $E_r = 0.26 \times 10^5\ MPa$ and Poisson's ratio is $v_r = 0.167$. The plate is resting on a single-layered elastic half space with modulus of elasticity $E_s = 0.26 \times 10^3\ MPa$ and Poisson's ratio $v_s = 0.25$ with a rigid end layer at depth $H = 50\ m$. In the PLPAK models, the soil is divided into 811 stiffness cells.

Results : Table 2.5 demonstrates the computed displacements at the points P1, P2, P3, P4 and P5 (shown in Figure 2.13). It can be seen that all results are in good agreement.

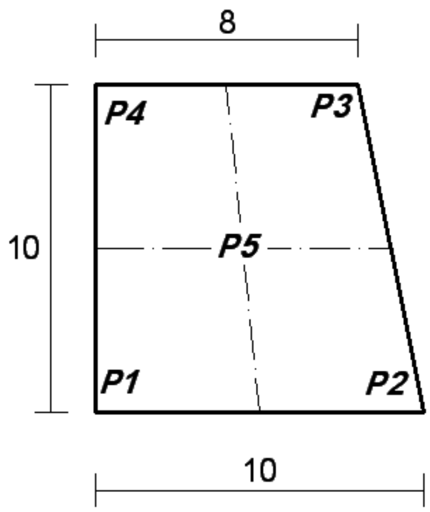

Figure 2.13: Trapezoidal plate layout in Example 2.11.

Table 2.5: Displacement at different points on a trapezoidal plate on an elastic half space in Example 2.11.

	[20]	PLPAK Mindlin solution	PLPAK Steinbrenner solution
Point P1	0.0244	0.026	0.0256
Point P2	0.0254	0.0255	0.025
Point P3	0.022	0.0268	0.0263
Point P4	0.0226	0.0259	0.0255
Point P5	0.026	0.028	0.0276

Example 2.12 [25]

Purpose : Comparing the results of a practical raft to the uncoupled iterative method [26].

Description : Only Mindlin and Steinbrenner results are presented, as Mindlin and Boussinesq solutions give similar results. In the PLPAK models, only two iterations are carried out, as results do not change with additional iterations. Moreover, only two iterations are commonly performed in practice. The raft foundation demonstrated in Figure 2.14 is considered. The raft carries 81 columns (Table 2.6 demonstrates the column cross sectional dimensions and loads) and has 1.4 m thickness. The following properties of reinforced concrete are used: Modulus of elasticity $E_r = 0.22 \times 10^5\ MPa$ and Poisson's ratio is $\upsilon_r = 0.2$. The considered raft own weight is $-0.035\ MPa$. It is resting on an elastic half space of modulus of elasticity $E_s = 50\ MPa$, Poisson's ratio $\upsilon_s = 0.3$ and it has a rigid end layer at depth $H = 30\ m$.

It has to be noted that, in the PLPAK models; the plate is modeled using 16 quadratic boundary elements, the number of used Gauss points is 10 for numerical integration purposes, and the soil is divided into 35×38 stiffness cells.

Results : Figure 2.15-Figure 2.18 demonstrates values of deflections and bending moment along axes 1-1 and 2-2 respectively. It can be seen that all results are in good agreements.

Table 2.6: Column models, dimensions and loads used in the practical raft in Example 2.12.

Column Model	Dimensions (cm)	Load (ton)
U1	90x30	200
U2	110x30	280
U3	120x35	350
U4	130x35	430
U5	140x40	475
U6	120x50	545
U7	150x50	520
U8	105x50	500
U9	100x40	350
U10	65x70	375
W1	385x25	270
W2	265x25	380
W3	340x25	955
W4	270x25	195
W5	490x35	845
W6	330x25	470
Core	see plan	2125

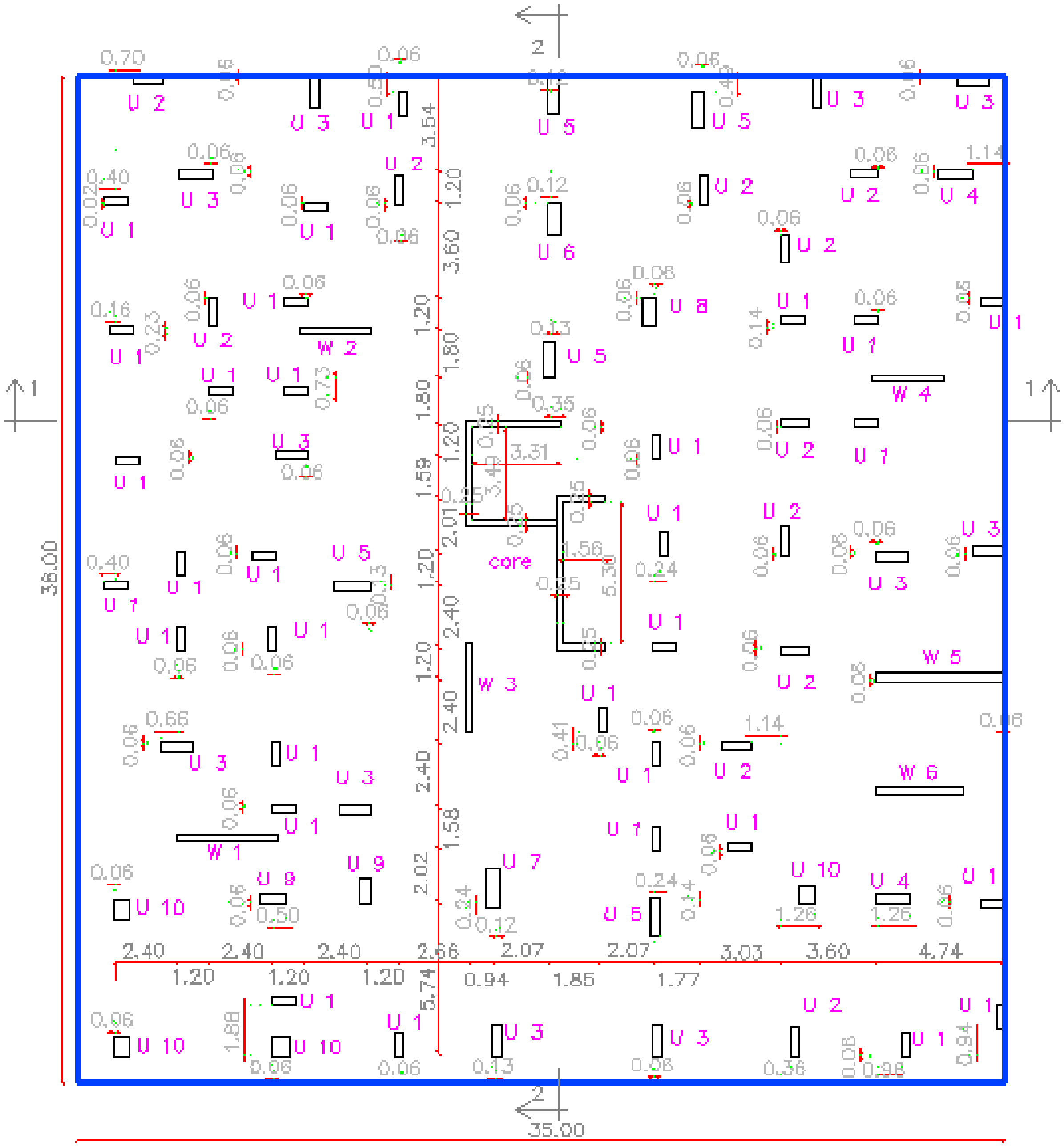

Figure 2.14: Practical raft layout in Example 2.12.

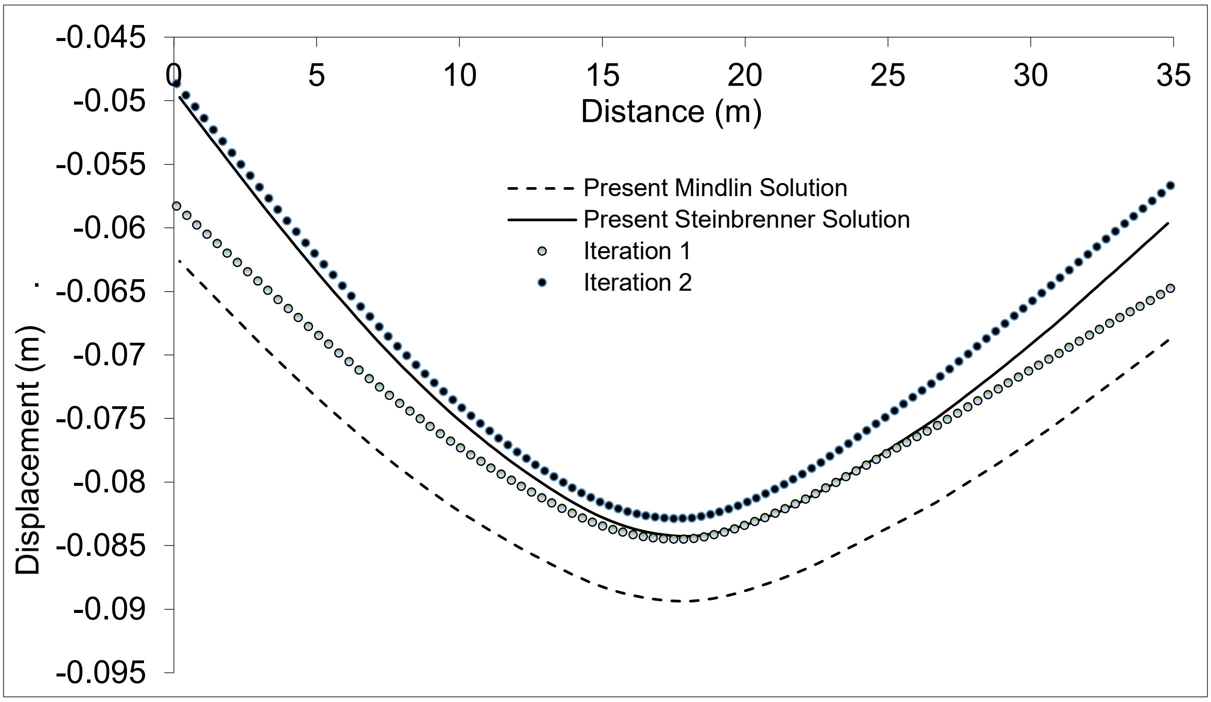

Figure 2.15: Displacement distribution for a practical raft along the strip 1-1 in Example 2.12.

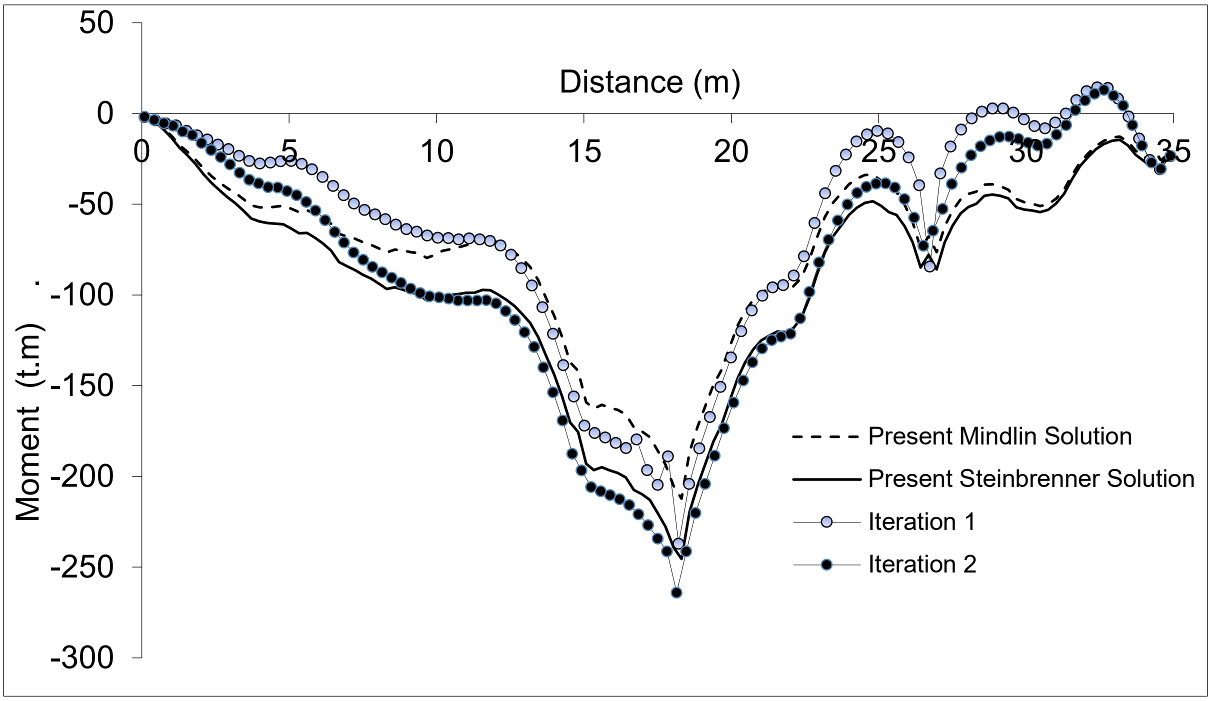

Figure 2.16: Bending moment distribution for a practical raft along the strip 1-1 in Example 2.12.

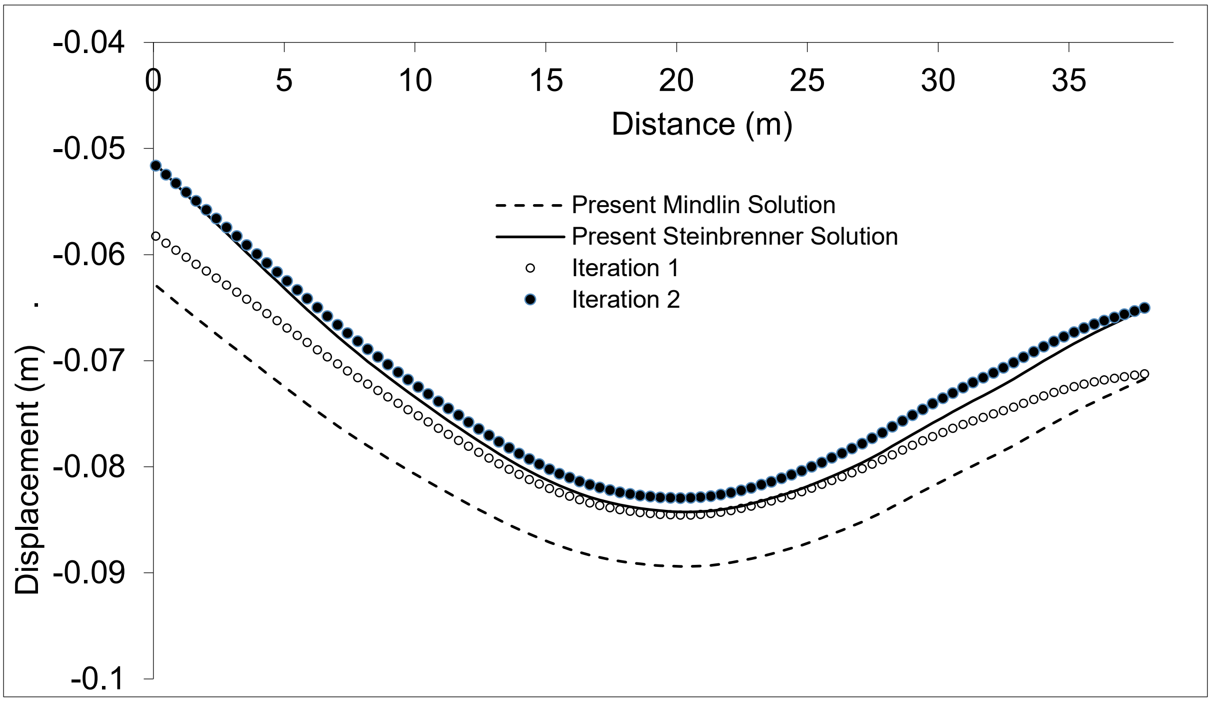

Figure 2.17: Displacement distribution for a practical raft along the strip 2-2 in Example 2.12.

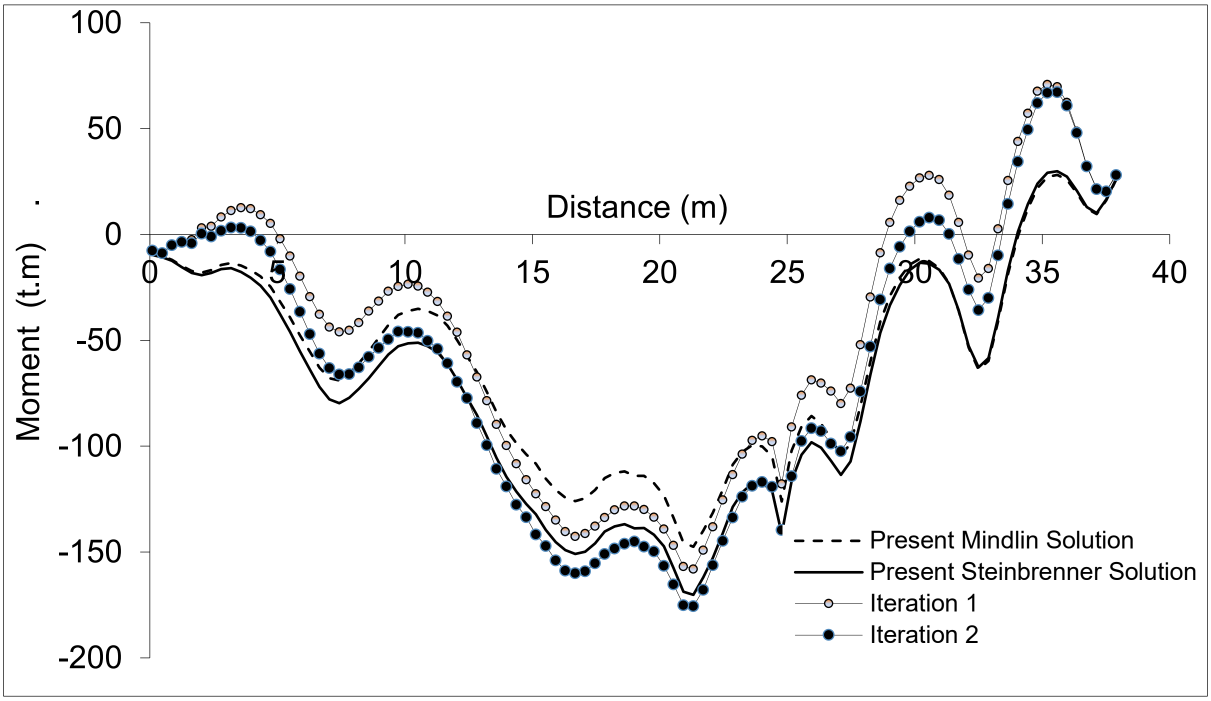

Figure 2.18: Bending moment distribution for a practical raft along the strip 2-2 in Example 2.12.

Example 2.13 [27]

Purpose : Comparing the results of a plie cap supported on four piles with another boundary element model by Mendonça and de Paiva in [28].

Description : The pile cap supported on four piles and shown in Figure 2.19 is considered. The pile diameter is 0.5 m; length is 25 m. Soil modulus of elasticity is 2000 kN/m^2, and Poisson's ratio is 0.5. The pile cap is loaded by uniform load (g) and is modeled with three different thicknesses (0.079, 0.37, 0.79 m) to allow comparison to result of [28]. The soil is divided into 25 × 3 rectangular elements. Piles are divided into 50 cylindrical elements and two circular elements for end bearing and coupling DOFs. In [28], the boundary element method is used to model the pile cap as thin plate on elastic foundations and soil under raft is divided into triangular elements.

Results : Results are presented along the centerline strip of pile cap. Figure 2.20-Figure 2.25 present deflection (w) and bending moments (M_{xx}) for the three cap thicknesses. Table 2.7 presents the number of solved DOFs before and after the condensation process. It can be seen from Figure 2.20-Figure 2.25 that results are in good agreement with results of [28].

Table 2.7: Number of DOFs before and after condensation process.

	before condensation process	after condensation process
No. of DOFs	183	79

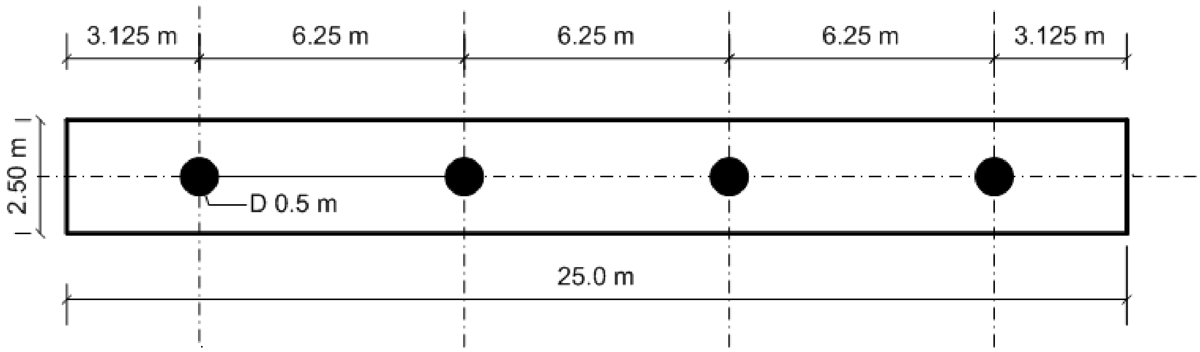

Figure 2.19: Pile cap geometry presented in Example 2.13.

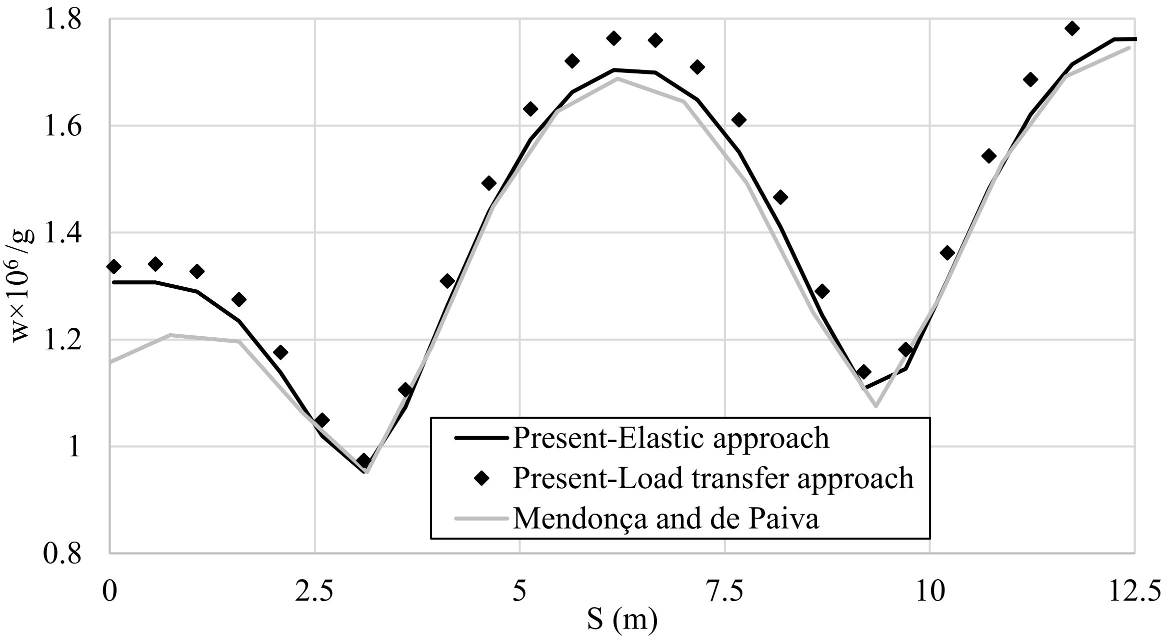

Figure 2.20: Deflection along centerline strip for case t = 0.079 m in Example 2.13.

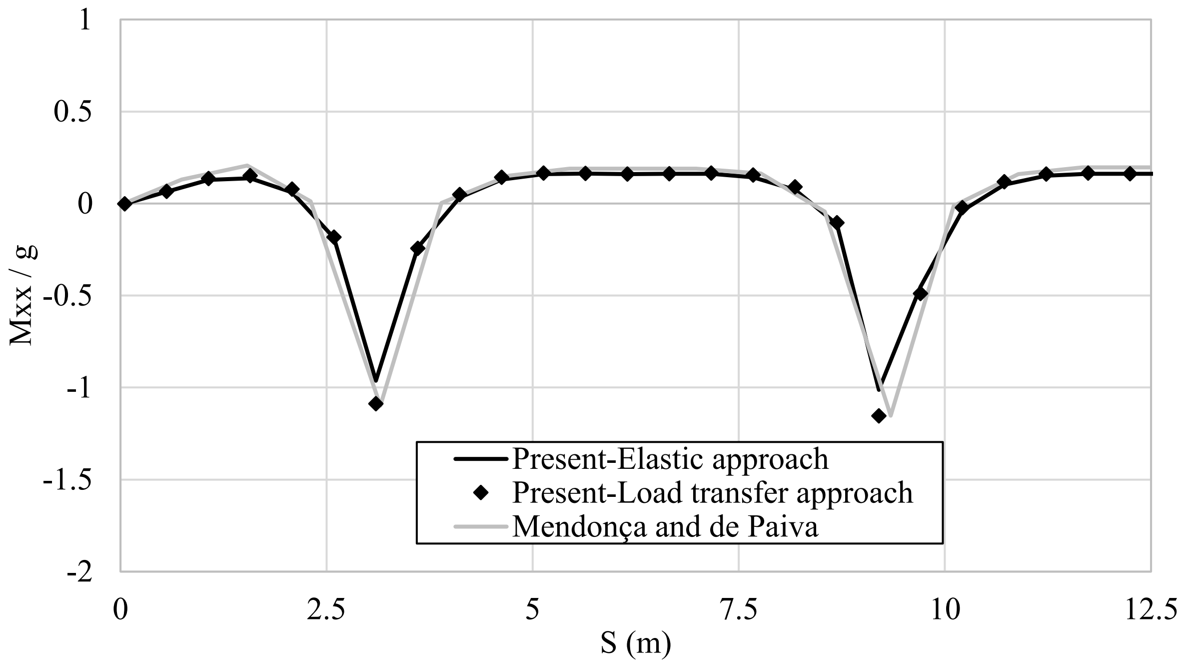

Figure 2.21: Bending moments along centerline strip for case t = 0.079 m in Example 2.13.

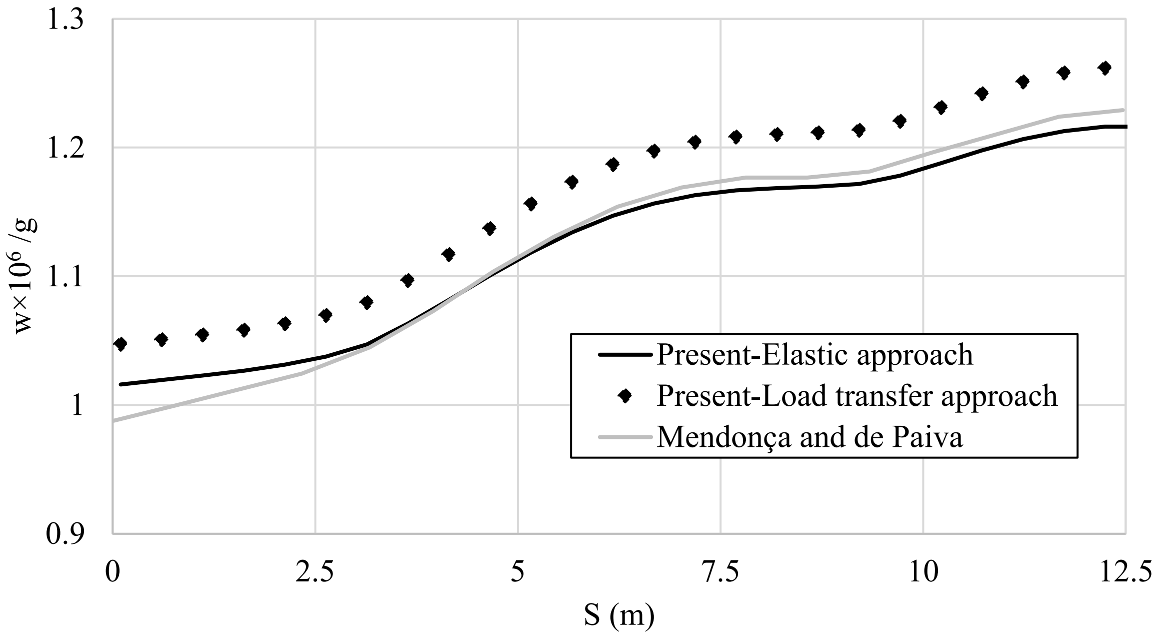

Figure 2.22: Deflection along centerline strip for case t = 0.37 m in Example 2.13.

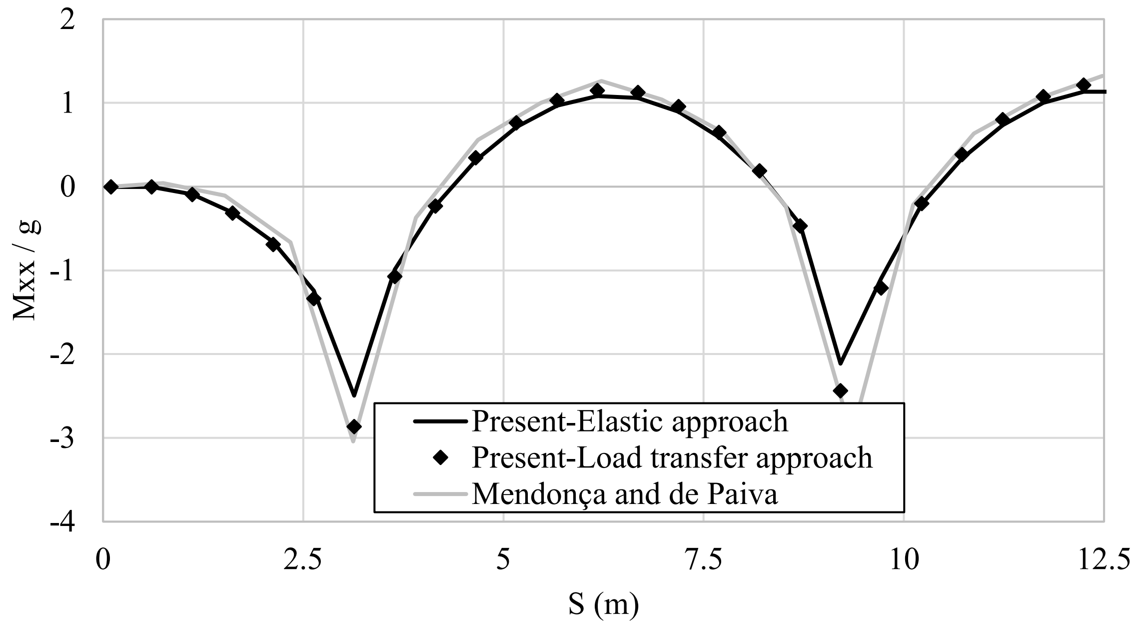

Figure 2.23: Bending moments along centerline strip for case t = 0.37 m in Example 2.13.

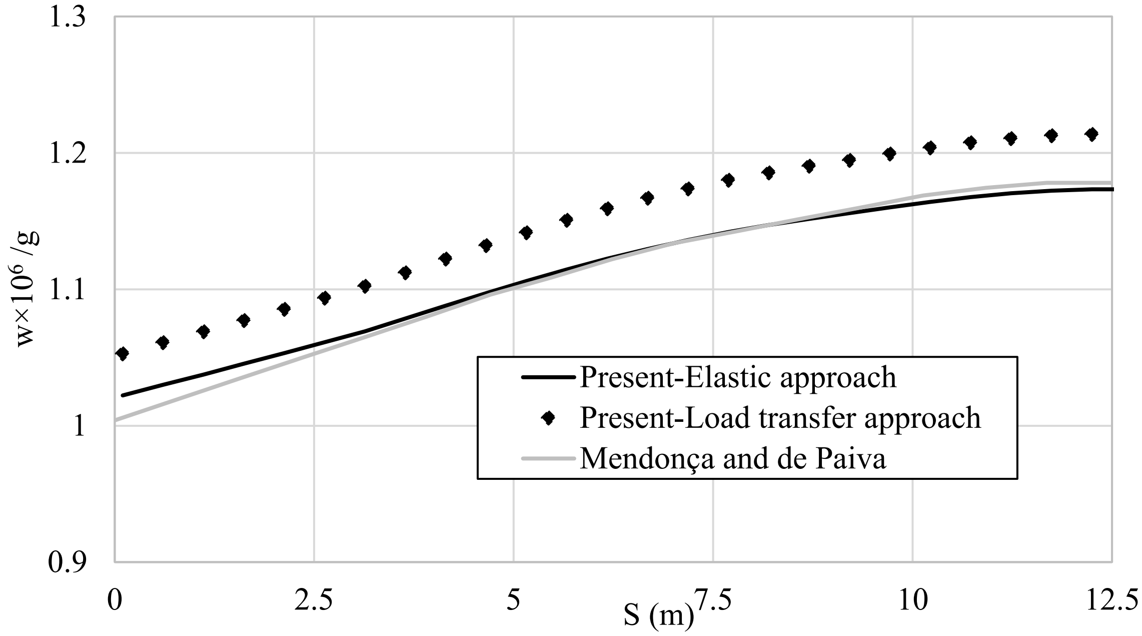

Figure 2.24: Deflection along centerline strip for case t = 0.79 m in Example 2.13.

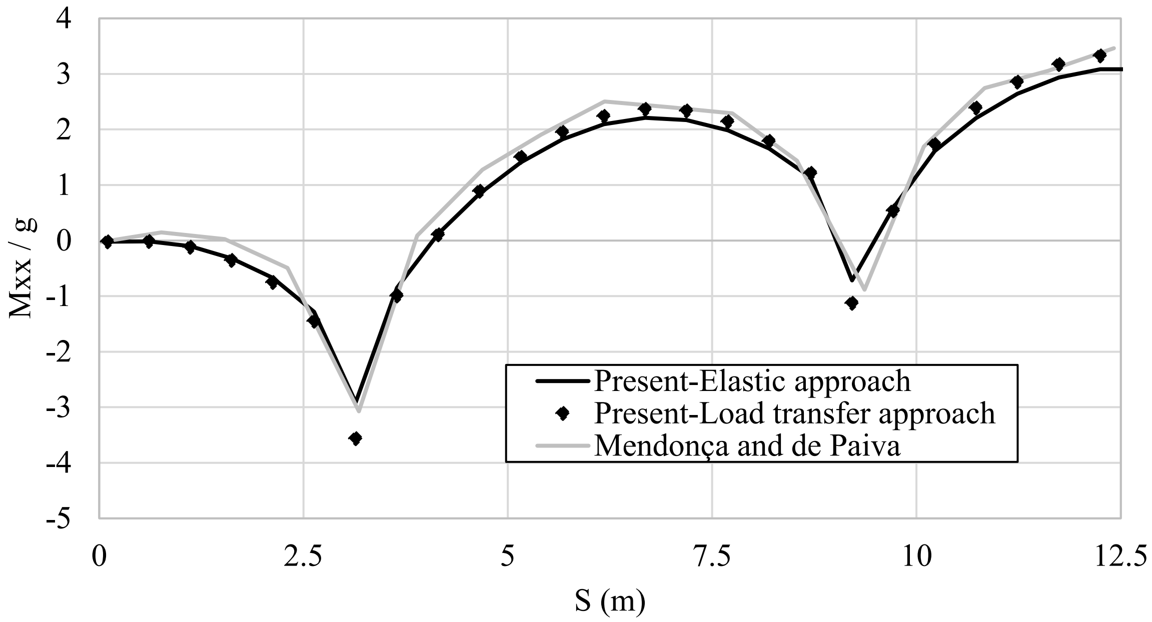

Figure 2.25: Bending moments along centerline strip for case t = 0.79 m in Example 2.13.

Example 2.14 [27]

Purpose : Comparing the results of a raft on nine piles under circular loads with a finite element software.

Description : The piled raft on nine piles shown in Figure 2.26 is considered in this example. Piles are 10 m in length and 0.5 m in diameter. The raft is 0.5 m in thickness and subjected to circular loads P_1 = 500 kN and P_2 = 1000 kN directly on piles as shown in Figure 2.26. The used modulus of elasticity for the raft and piles is 2×10^7 kN/m^2; whereas soil modulus of elasticity is 20,000 kN/m^2 and Poisson's ratio is 0.3. The raft is modeled as thick plate on elastic foundations and soil is divided into 10 × 6 rectangular elements and each pile is divided into 10 cylindrical elements and two circular elements for end bearing and coupling DOFs. The finite element method is used to model the raft as thin plate on elastic foundations using the ELPLA software, the raft is divided into 10 × 6 elements and each pile is divided into 10 elements.

Results : Results are presented along centerline strip of the raft. Figure 2.27 and Figure 2.28 demonstrate settlement and bending moments along centerline strip, respectively. It has been seen that proposed technique results are in good agreement with the FEM results. Table 2.8 presents the number of DOFs before and after condensation process.

Table 2.8: Number of DOFs before and after condensation process in Example 2.14.

	before condensation process	after condensation process
No. of DOFs	168	69

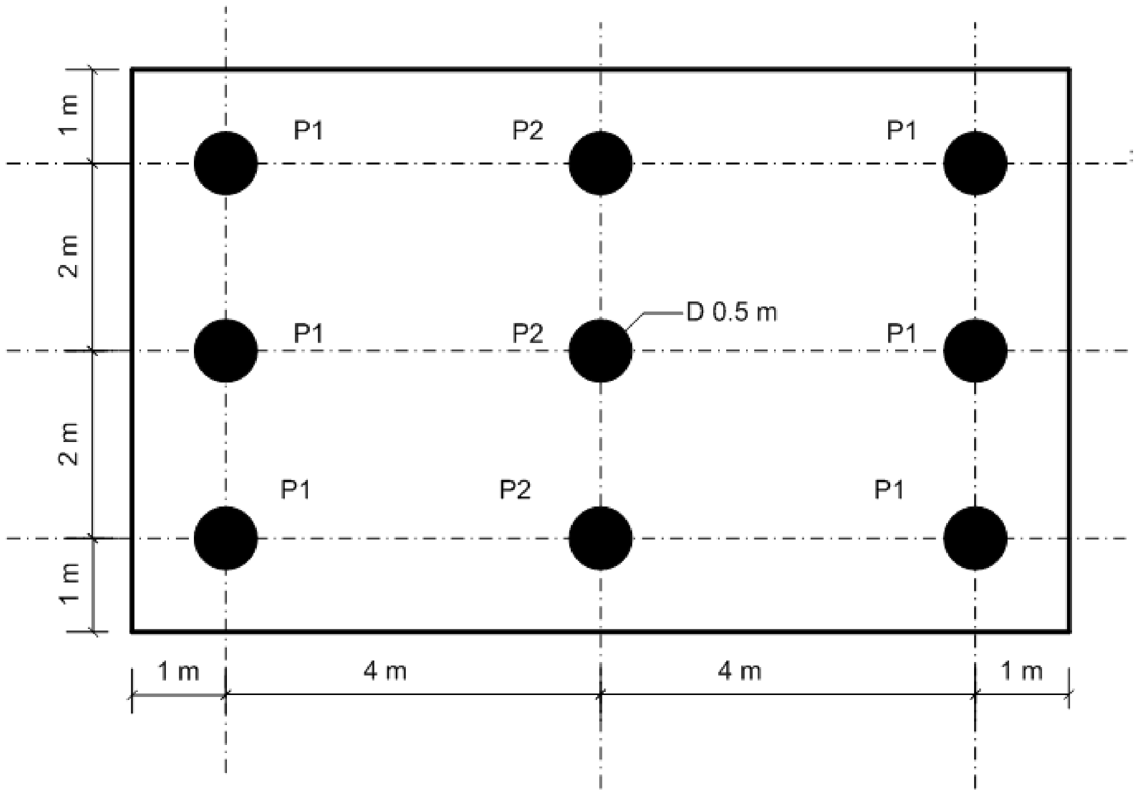

Figure 2.26: Piled raft geometry presented in Example 2.14.

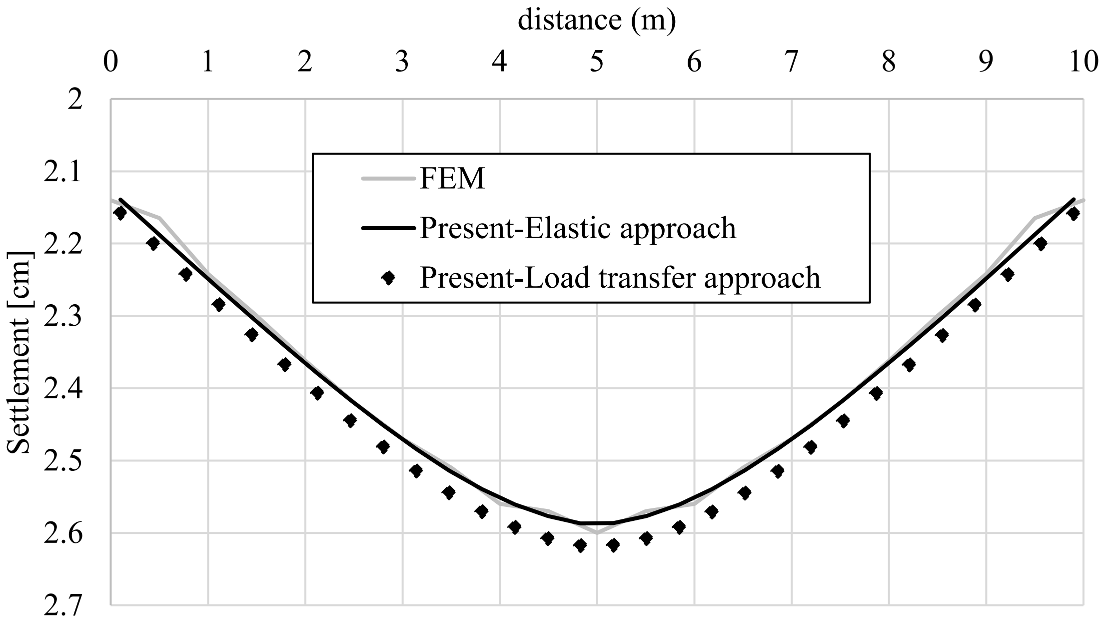

Figure 2.27: Settlement along centerline strip in Example 2.14.

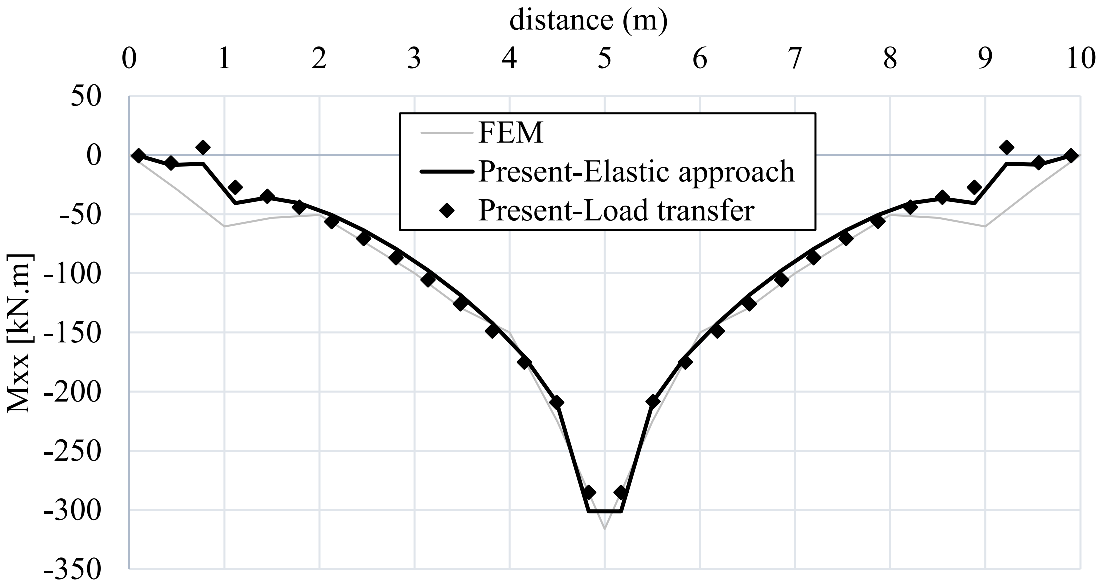

Figure 2.28: Bending moments along centerline strip in Example 2.14.

Example 2.15 [27]

Purpose : Comparing the results of a piled raft with variable lengths of piles with [29].

Description : A piled raft supported on nine piles and subjected to uniform load q_v (kN/m^2) is considered in this example. Piles are 0.5 m in diameter and classified as long and short piles with lengths 25, 5 m, respectively. The raft dimensions are 4.5 × 4.5 × 1.0 m. Modulus of elasticity of raft, long piles, and short piles are 3.0×10^7, 2.0×10^7, and 1.7×10^7 kN/m^2, respectively. Soil modulus of elasticity is 5000 kN/m^2 and Poisson's ratio is 0.35. The raft is modeled as thick plate on elastic foundations and soil is divided into 9 × 9 rectangular elements. Each pile is divided using 1 m cylindrical element and two circular elements for end bearing and coupling DOFs. It has to be noted that, the load transfer approach is not applicable for this case; therefore, this example is solved using the elastic approach only. In [29], the finite element method is used to model raft as thick plate on 3D finite elements using the ANSYS software. In this example, the four cases of pile configurations (see Figure 2.29) are solved.

Results : Table 2.9 presents the maximum settlement of the raft under three different uniform loads 100, 200, and 300 MPa. It has been seen that results are in a good agreement to those in [29]. Table 2.10 demonstrates the number of DOFs before and after condensation process.

Table 2.9: Maximum settlement value (m) for different piles pattern in Example 2.15.

	Load = 100 MPA		Load = 200 MPA		Load = 300 MPA	
	FEM	PLPAK	FEM	PLPAK	FEM	PLPAK
Case 1	0.0195	0.0201	0.0392	0.0402	0.0587	0.0603
Case 2	0.0213	0.0222	0.0427	0.0444	0.0643	0.0666
Case 3	0.0223	0.0225	0.0446	0.0451	0.0668	0.0676
Case 4	0.0446	0.0464	0.0883	0.0923	0.1327	0.1392

Table 2.10: Number of DOFs before and after condensation process in Example 2.15.

Case	DOFs before condensation process	DOFs after condensation process
1	324	90
2	244	90
3	224	90
4	144	90

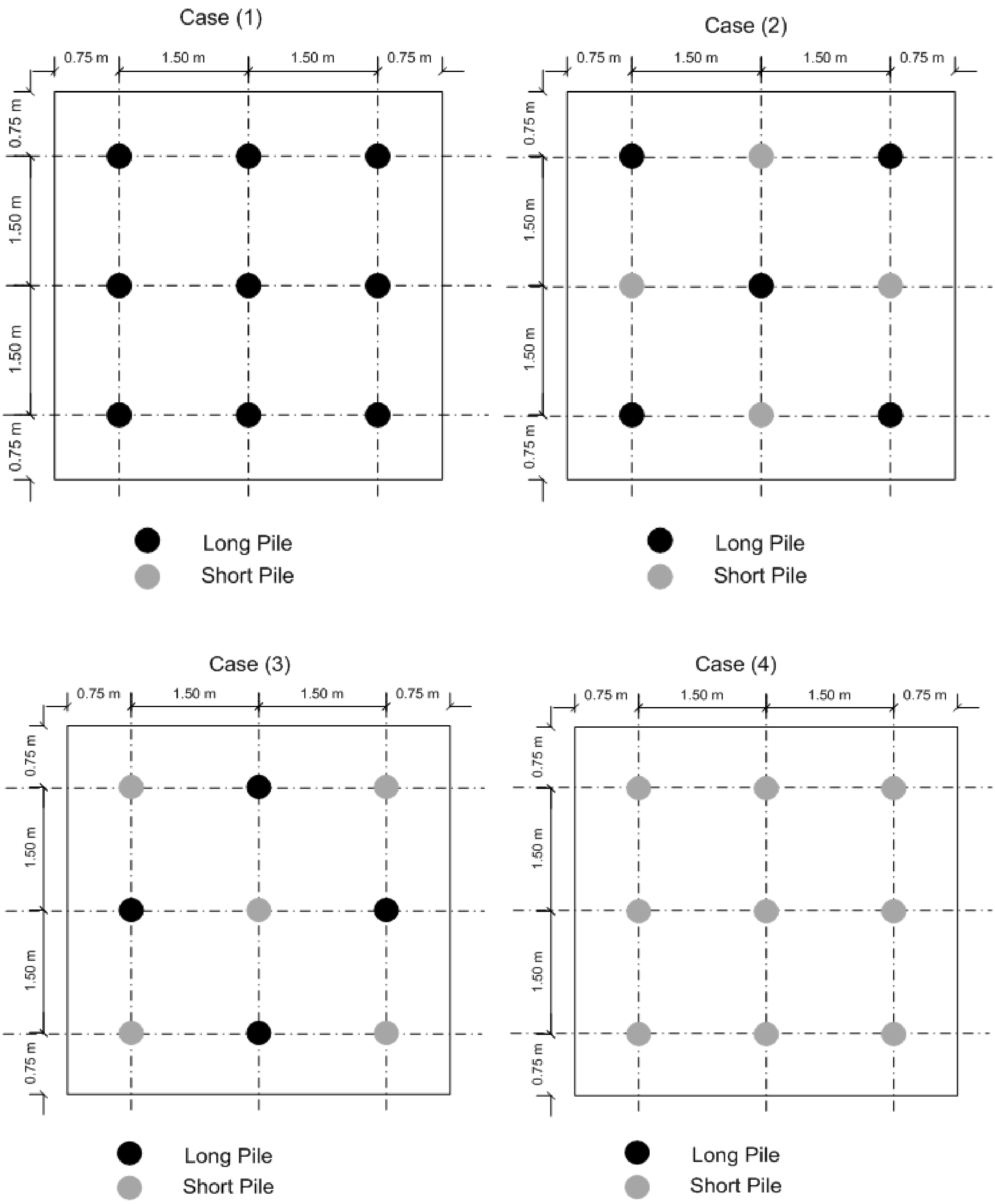

Figure 2.29: Four cases of piles configurations and raft geometry in Example 2.15.

Example 2.16 [27]

Purpose : Compare the results of solving a practical piled raft twice, without and with considering the interaction effects.

Description : In this example, the practical piled raft foundation shown in Figure 2.30 is analyzed. The raft thickness is $2.50\ m$ and rested on 231 piles with 0.8 diameter and $35\ m$ length. Soil modulus of elasticity is $2000\ t/m^2$ and Poisson's ratio is 0.3. Piles and raft modulus of elasticity is $2{,}210{,}000\ t/m^2$. The raft is subjected to columns and wall loads from superstructure with total vertical load of $58{,}714.9\ t$ as illustrated in Table 2.11 and Figure 2.31. Figure 2.32 demonstrates the used boundary element model. The raft is modeled as thick plate on elastic foundations, each pile is divided using $1\ m$ cylindrical element and two circular elements for end bearing and coupling DOFs. The following example is solved twice, without and with considering the interaction effects. Three different soil types [loose ($E = 2000\ t/m^2$), medium ($E = 5000\ t/m^2$), and dense ($E = 10000\ t/m^2$)] are used for the sake of comparison. It has to be noted that, in case of ignoring interaction effects, pile stiffness is calculated based on empirical equations used in building design code [30] to be $151{,}000\ t/m$. Four piles are selected as demonstration sample (see Figure 2.30). Piles 1 and 3 represent interior piles, whereas piles 2 and 4 represent exterior piles.

Results : Figure 2.33 demonstrates the selected piles reactions considering and ignoring the interaction effects. Figure 2.34 demonstrates pile force distribution considering and ignoring the interaction effects. It can be seen that considering the interaction effects redistributes pile forces by increasing pile reaction at exterior piles rather than those at interior piles. Therefore, including interaction effects is important in the design of practical examples. Figure 2.35 and Figure 2.36 demonstrate the deflection and bending moment values for different soil types (loose, medium, and dense) on a horizontal strip presented in Figure 2.30. It can be seen that considering interaction effects increases the predicted raft settlement. This is noticeable for loose soil. Table 2.12 demonstrates the advantages of the proposed condensation process to solve practical piled rafts, as DOFs decreased by about 97%. In order to demonstrate the strength of using the BEM together with the thick plate formulation, simple punching analysis is considered in this example. Regions S_1, S_2, S_3, and S_4 are considered to draw the shear stress distribution Q_x as contour maps in Table 2.13 for the case of loose soil. From the presented results, it can be seen that punching shear will be critical for external piles and internal loading zones (S_3 and S_4) in case of considering interactions effects. This is opposite to the case of ignoring interaction effects, which indicates that internal piles and external loading zones are the critical ones. This confirms the importance of considering interaction effects in design of practical examples.

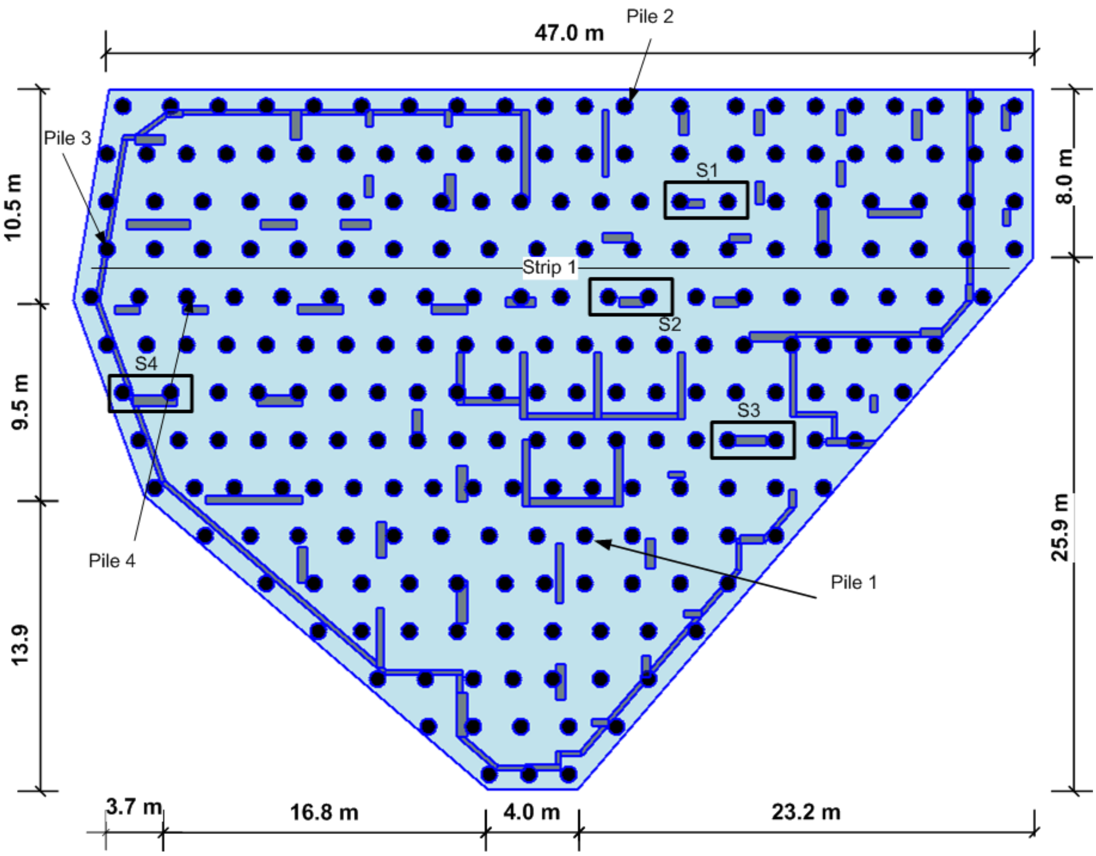

Figure 2.30: Practical piled raft foundation geometry in Example 2.16.

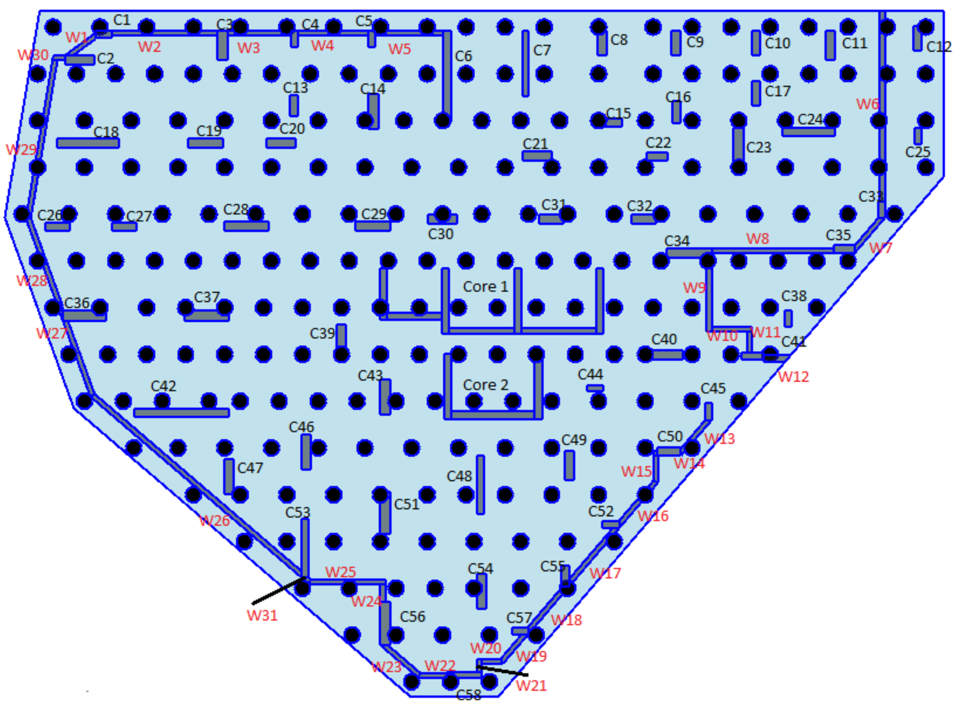

Figure 2.31: Columns and wall loads ID in Example 2.16.

Table 2.11: Columns, walls and cores loads in Example 2.16.

Column ID	Load (ton)	Column ID	Load (ton)	Wall ID	Load (t/m')
C1	247.8	C31	603.42	W1	1.67
C2	655.5	C32	603.42	W2	5.43
C3	745.02	C33	200.36	W3	3.27
C4	152.34	C34	1335.76	W4	3.69
C5	218.42	C35	410.54	W5	3.49
C6	1602.58	C36	1298.73	W6	9.75
C7	1085.1	C37	1335.24	W7	2.11
C8	637.08	C38	445.36	W8	6.24
C9	653.58	C39	938.4	W9	3.79
C10	583.2	C40	1268.32	W10	2.08
C11	835.2	C41	421.96	W11	1.05
C12	612.72	C42	2119.88	W12	1.778
C13	476.24	C43	938.4	W13	2.16
C14	1013.22	C44	324.48	W14	0.183
C15	664.12	C45	249.6	W15	1.34
C16	502.4	C46	1063.98	W16	2.87
C17	614.56	C47	1008.9	W17	3.7
C18	1168.2	C48	1265.6	W18	2.97
C19	1038.9	C49	780.06	W19	1.84
C20	847.38	C50	590.04	W20	1.04
C21	723.78	C51	1271.2	W21	0.67
C22	509.44	C52	326.93	W22	1.39
C23	998.52	C53	1340.1	W23	2.33
C24	1130.32	C54	996.06	W24	0.93
C25	236.64	C55	501.65	W25	3.86
C26	592.2	C56	1155.3	W26	14.11
C27	663.6	C57	248.08	W27	4.07
C28	1386.64	C58	555.56	W28	5.2
C29	1020.16	Core 1	3293.68	W29	8.23
C30	873.06	Core 2	184.32	W30	0.63
				W31	0.34

Table 2.12: Number of DOFs before and after condensation process in Example 2.16.

	before condensation process	after condensation process
No. of DOFs	8547	231

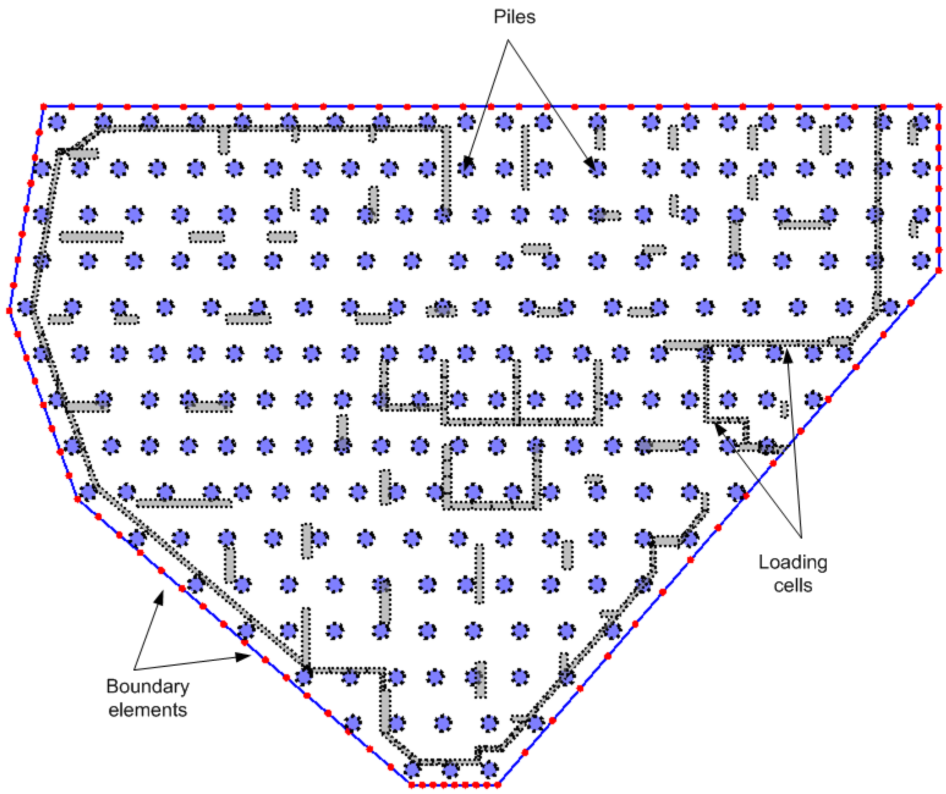

Figure 2.32: BEM model of practical piled raft foundation in Example 2.16.

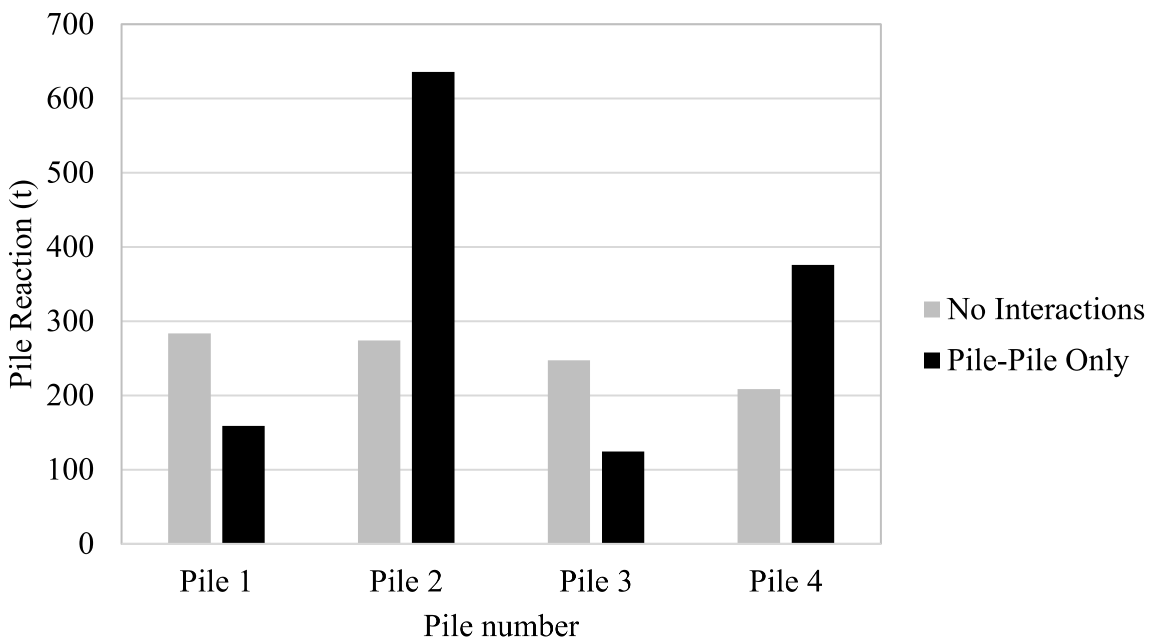

Figure 2.33: Sample pile forces in Example 2.16.

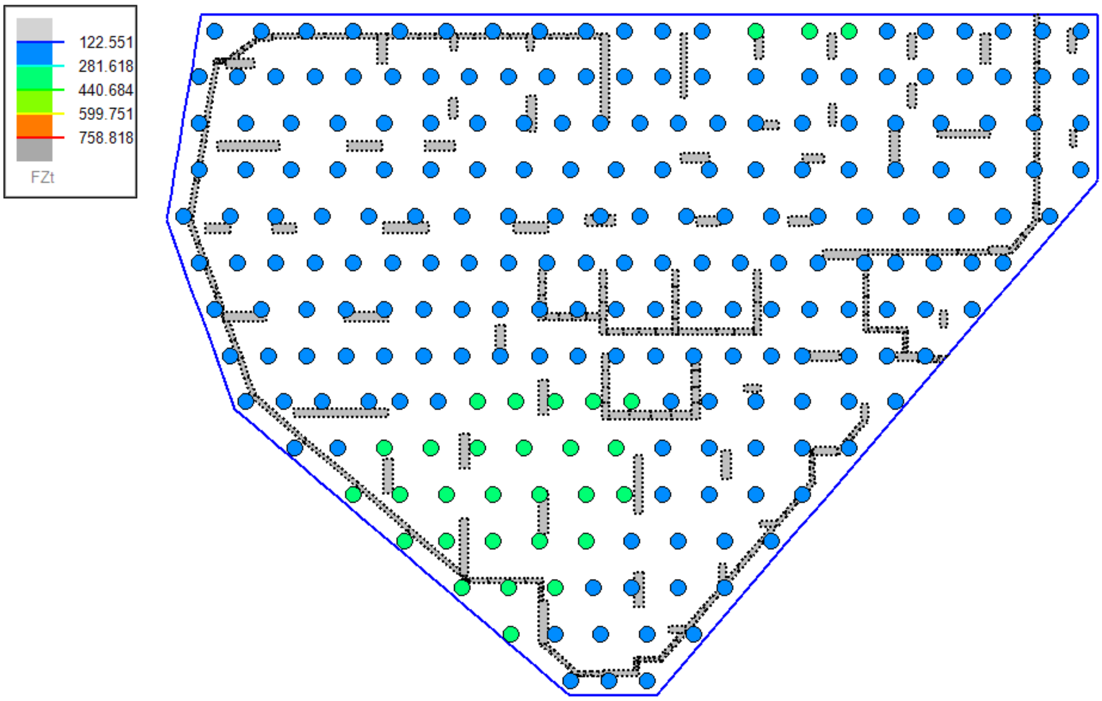

a: Without considering interaction effects.

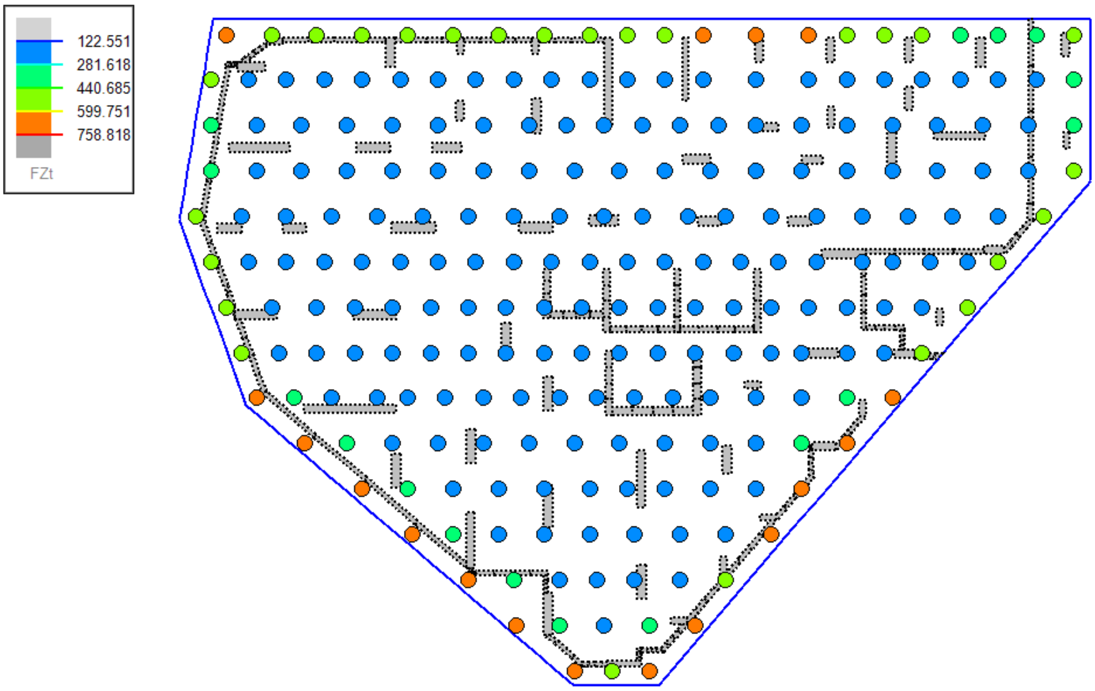

b: With considering interaction effects.

Figure 2.34: Pile forces distribution in Example 2.16. (a) Without considering interaction effects. (b) With considering interaction effects

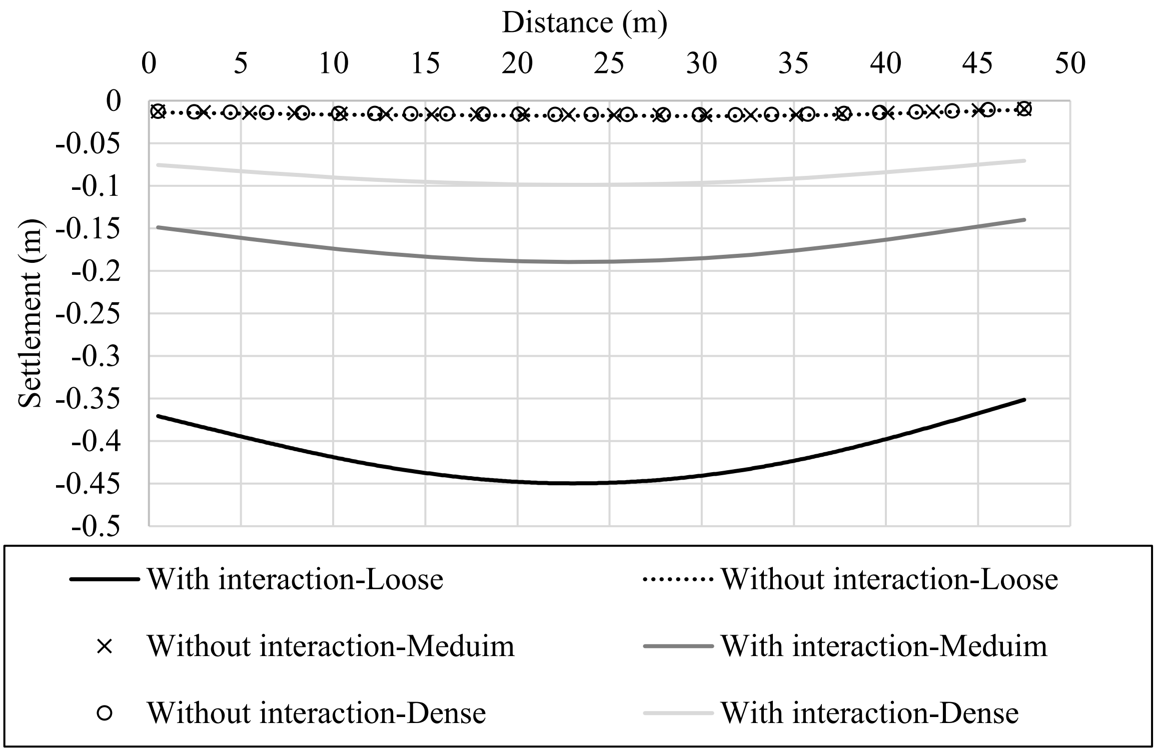

Figure 2.35: Deflection values along the horizontal strip 1 in Example 2.16.

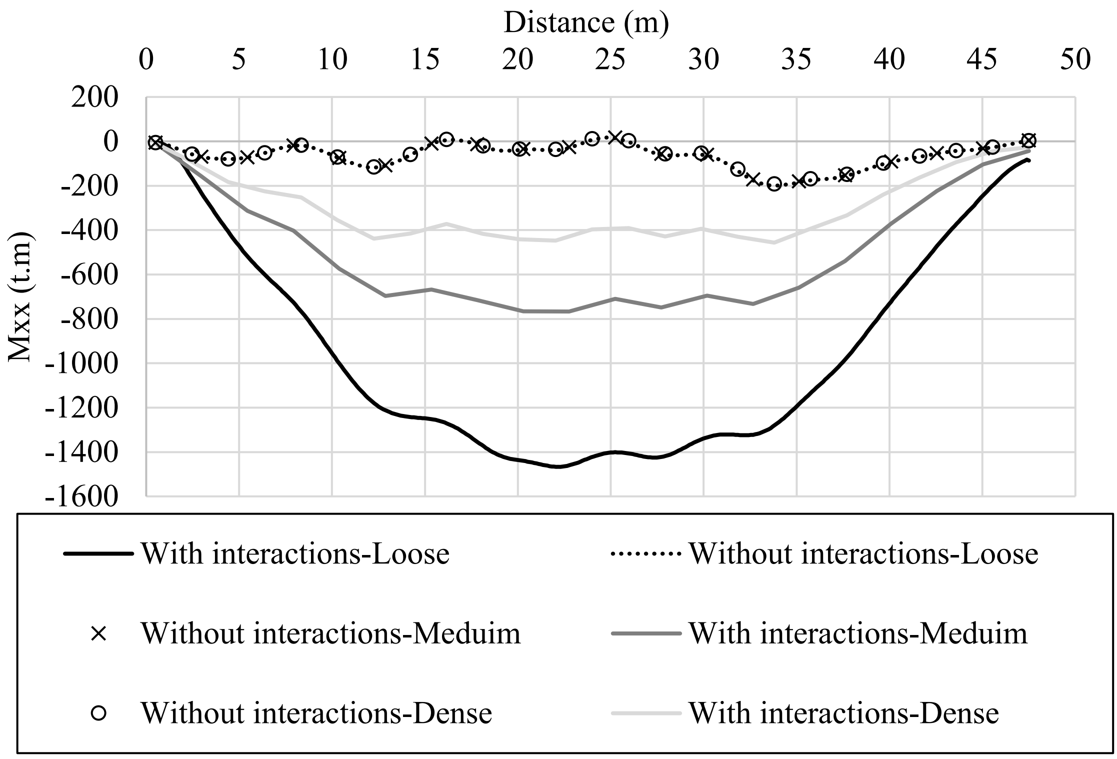

Figure 2.36: Bending moment values along the horizontal strip 1 in Example 2.16.

Table 2.13: Shearing force distribution over considered four regions in Example 2.16.

<table>
<tr><th>Region</th><th>Considering interactions</th><th>Legend</th><th>Ignoring interactions</th></tr>
<tr><td>S_1</td><td>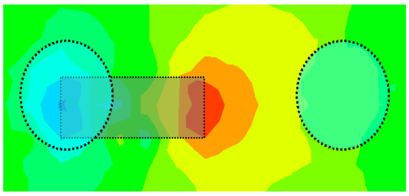</td><td>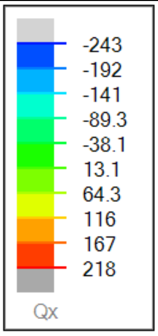
</td><td>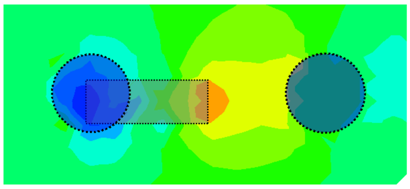</td></tr>
<tr><td>S_2</td><td>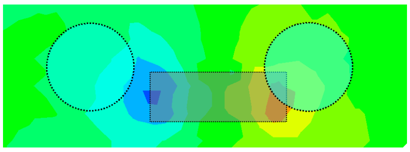</td><td>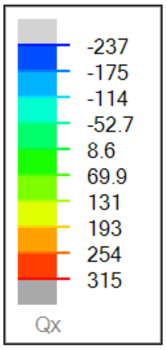
</td><td>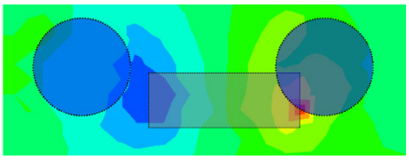</td></tr>
<tr><td>S_3</td><td>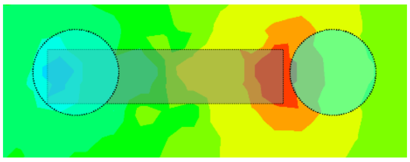</td><td>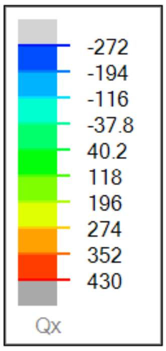
</td><td>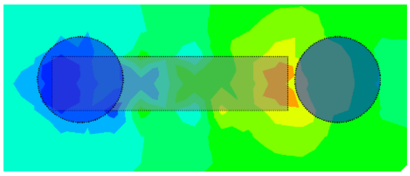</td></tr>
<tr><td>S_4</td><td>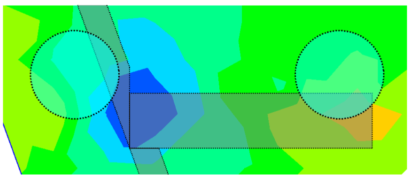</td><td>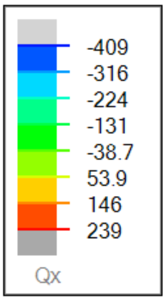
</td><td>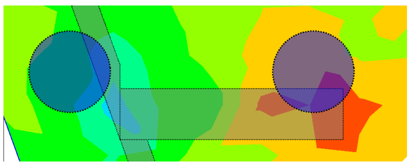</td></tr>
</table>

3. The Multiple-Floor Package:

The Multiple floor (fixed base) package can analyze tall building over fixed base. It is a BIM centered software; no GUI as the Autodesk Revit is its GUI. The preprocessing is done using Autodesk Revit where the structure is modelled with its real geometry.

For Example 3.1-Example 3.6:

In all these examples, "BEM model 1" denotes the modeling of beams as a part of the slab and "BEM model 2" denotes the modeling of beams as separate skeletal elements.

For Example 3.1-Example 3.4:

- Columns are 0.25m × 0.25m.
- Walls are 0.25m thick.
- Beams are 0.25m× 0.6m.
- Young's modulus is 2210000t/m^2.
- Poisson's ratio is 0.2
- Structure is 10 storeys; the storey height is 4 meters.
- Fifty tons load is applied in x-direction at the slab centerline of the top floor.

Please note that the fifty tons load is an exaggerated value that is going to lead to huge, non-realistic drifts. These values are only used for illustration purposes.

For Example 3.10-Example 3.12:

The finite element software used for the comparison are SAP2000 V16 and ETABS V15. In these examples:

- Young's Modulus is 2210000 t/m^2.
- Poisson's ratio is 0.2.
- Slab's thickness is 0.2 m.
- Columns' dimensions are 1 m x 1 m.
- Beams' dimensions are 0.4 m x 0.8 m.
- Walls are 0.35 m thick.
- Floor height is 4 m.

Example 3.1 [31]

Purpose : Compare drift and post-processing results for structure featuring columns only with the finite element method.

Description : The structural drawing of this example is presented in Figure 3.1. The boundary element model of the floor is presented in Figure 3.2. The finite element model is presented in Figure 3.3.

Results : The lateral drift comparison presented in Figure 3.4 demonstrate agreement between the PLPAK model results and traditional finite element results. However, the PLPAK model exhibits smaller values for lateral drifts; this originates from the real geometry modeling deployed in the boundary element model of plates. The boundary elements model considers the connection area between vertical elements and floors.

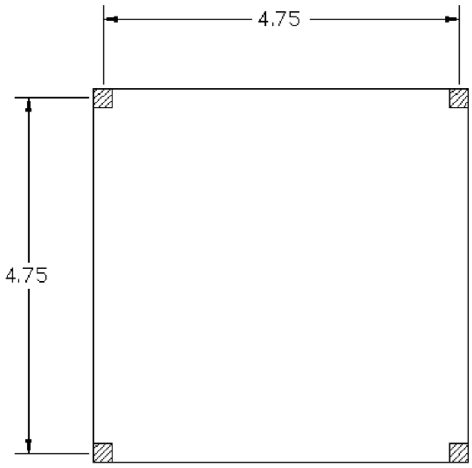

Figure 3.1: Example 3.1 structural drawing.

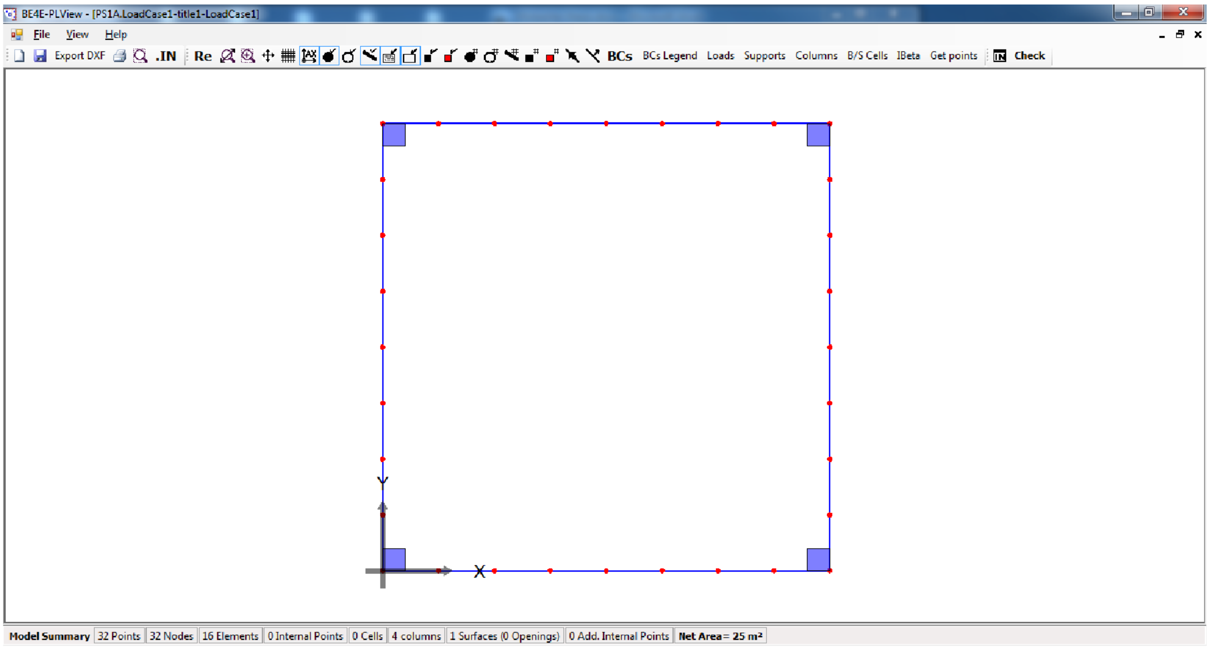

Figure 3.2: Example 3.1 BEM model.

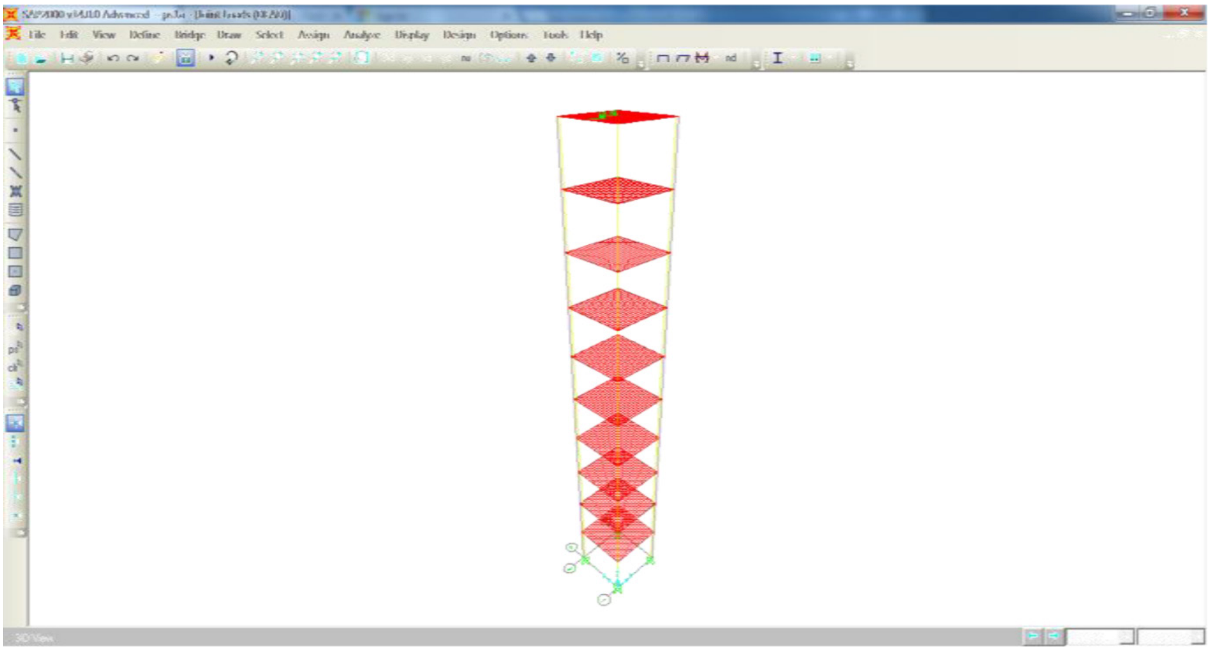

Figure 3.3: Example 3.1 FEM model.

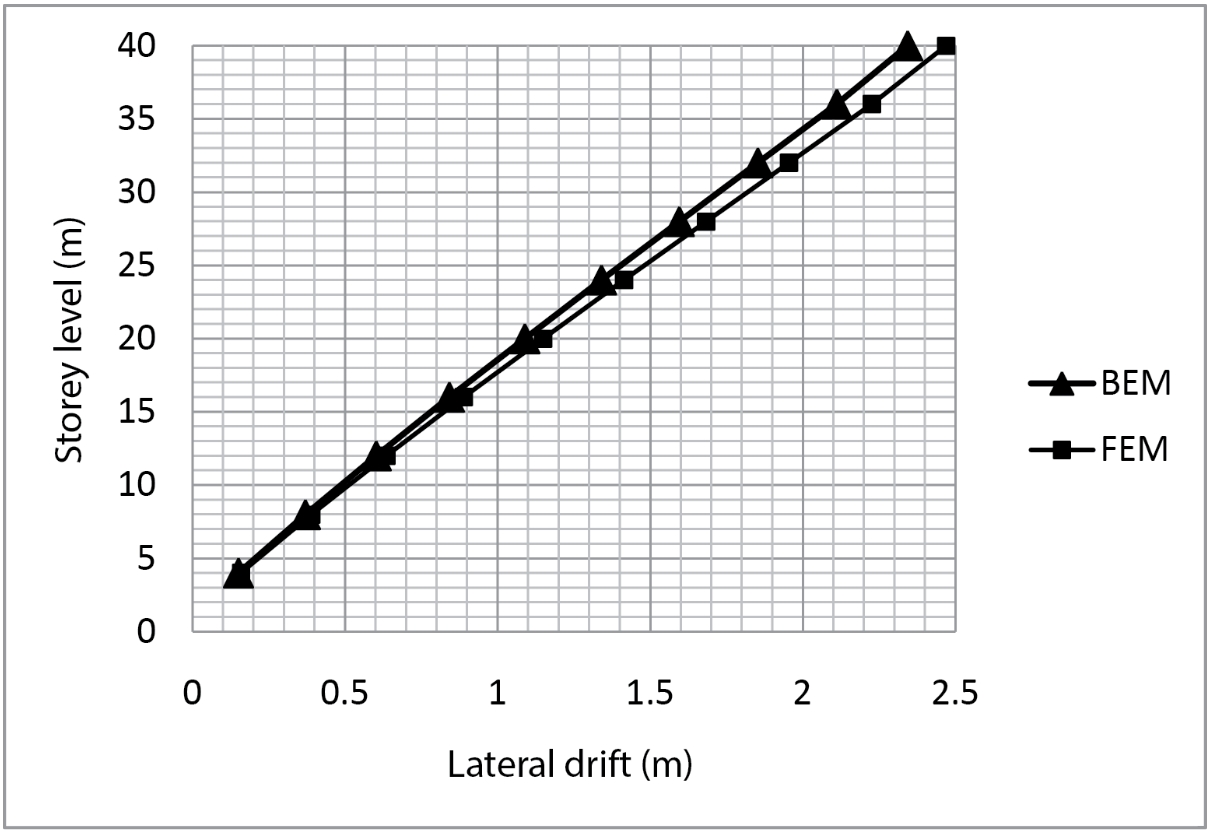

Figure 3.4: Example 3.1 lateral drift results.

Example 3.2 [31]

Purpose : Compare drift and post-processing results for structure featuring columns and beams with the finite element method.

Description : The structural drawing of this example is presented in Figure 3.5. The boundary element model of the floor is presented in Figure 3.6. The finite element model is presented in Figure 3.7.

Results : Top floor deflection comparison is provided in Figure 3.8 and Figure 3.9. The lateral drift comparison is demonstrated in Figure 3.10. Beam bending moment comparison is provided in Figure 3.11. Analyzing the results presented in Figure 3.8 to Figure 3.11, the following may be deduced:

- Lateral drift produced from the PLPAK model agrees with finite element values. However, the difference between BEM and FEM models is less than that in Example 3.1. Hence, it may be concluded that the PLPAK model captures reduced stiffness of the structure when beam elements are introduced. Further analysis on this point is presented in some succeeding examples.
- Slab deflection results produced from the new model agree with finite element values.
- Beam bending moments produced from the new model agree with finite element values.
- In this simple structural model, results from “BEM model 1” and “BEM model 2” are very similar.

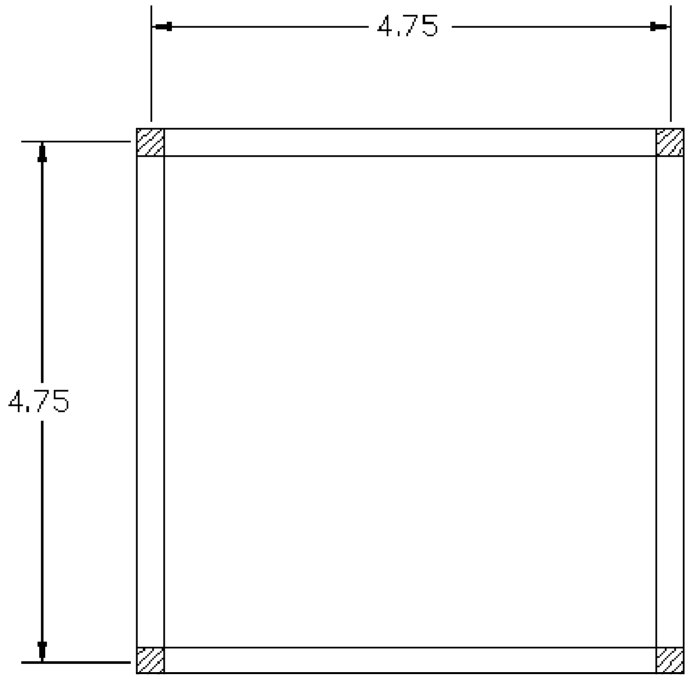

Figure 3.5: Example 3.2 structural drawing.

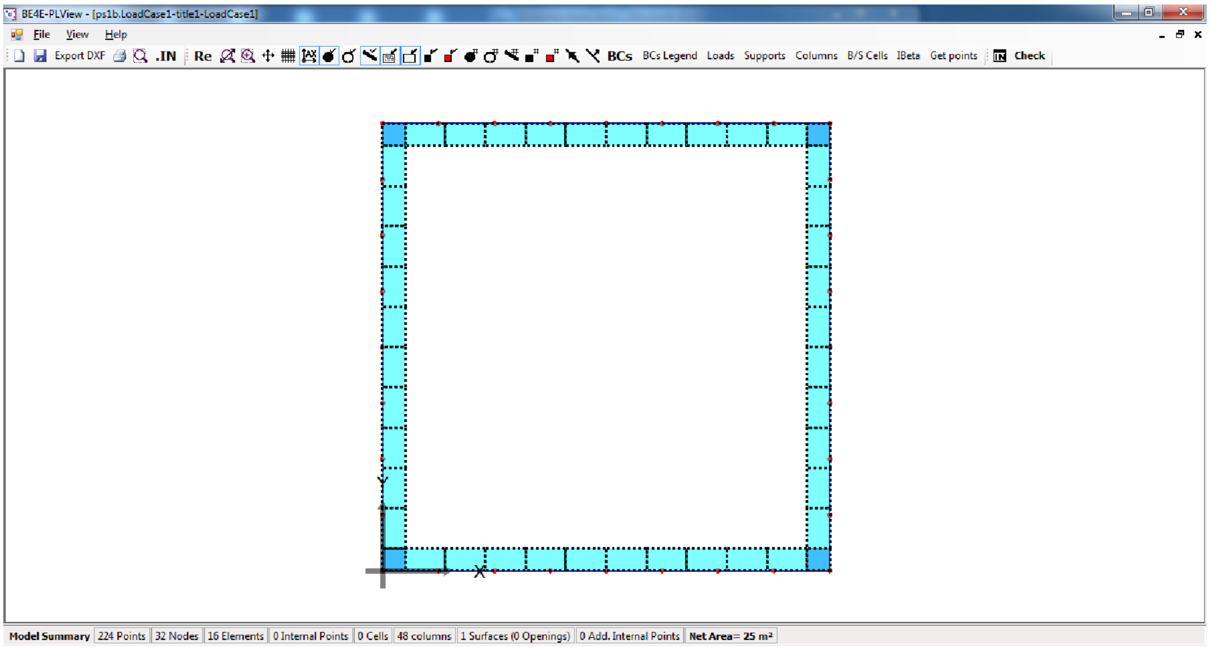

Figure 3.6: Example 3.2 BEM model.

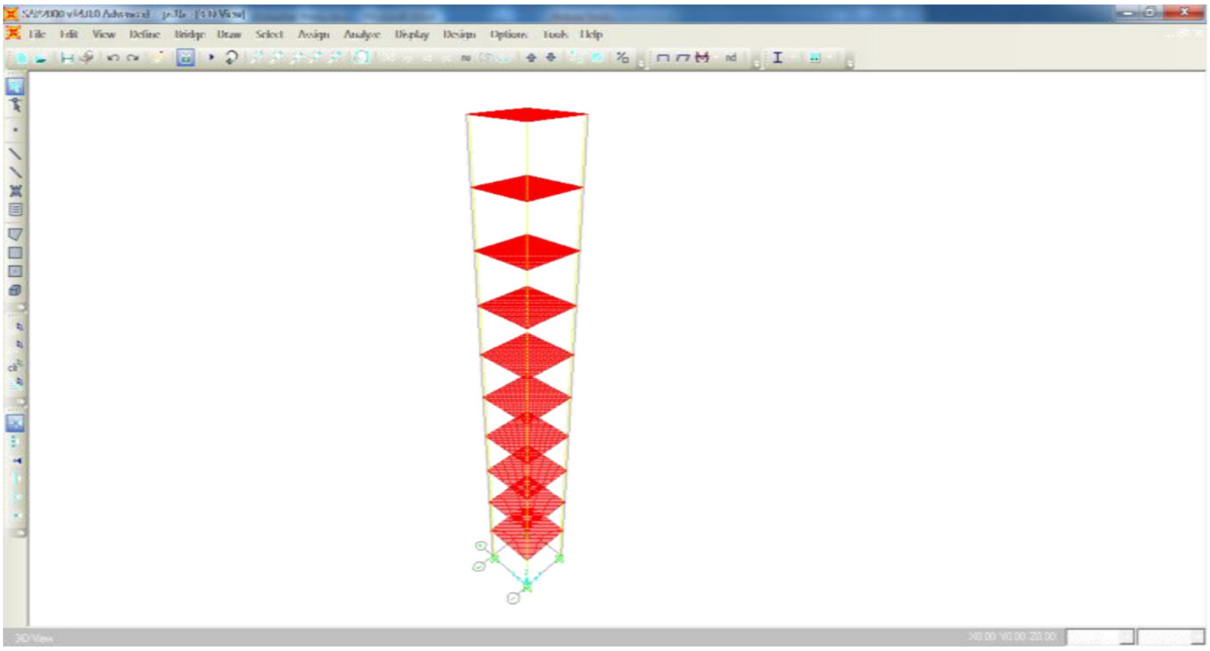

Figure 3.7: Example 3.2 FEM model.

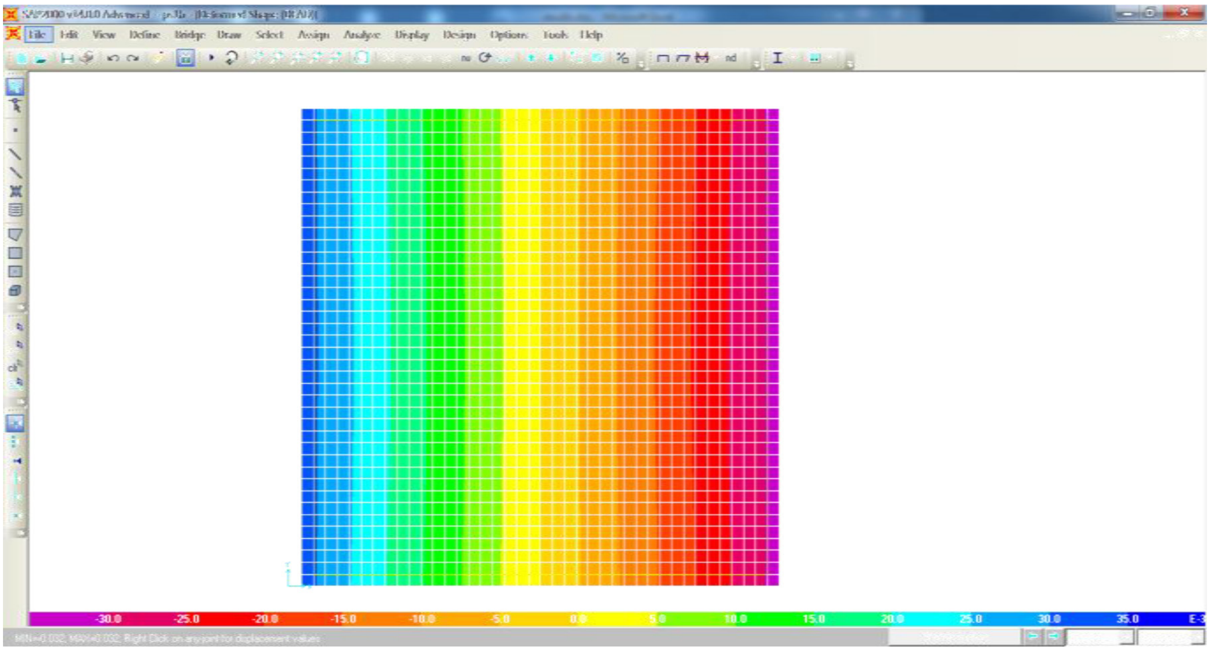

Figure 3.8: Example 3.2 FEM deflection results.

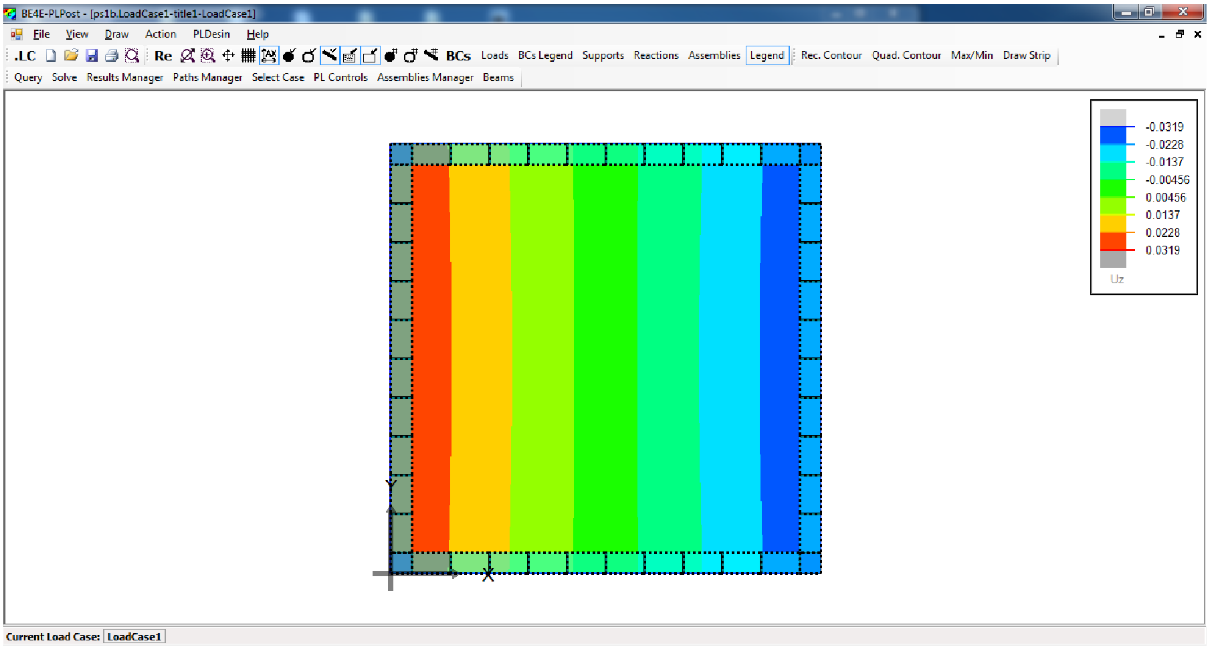

Figure 3.9: Example 3.2 BEM deflection results.

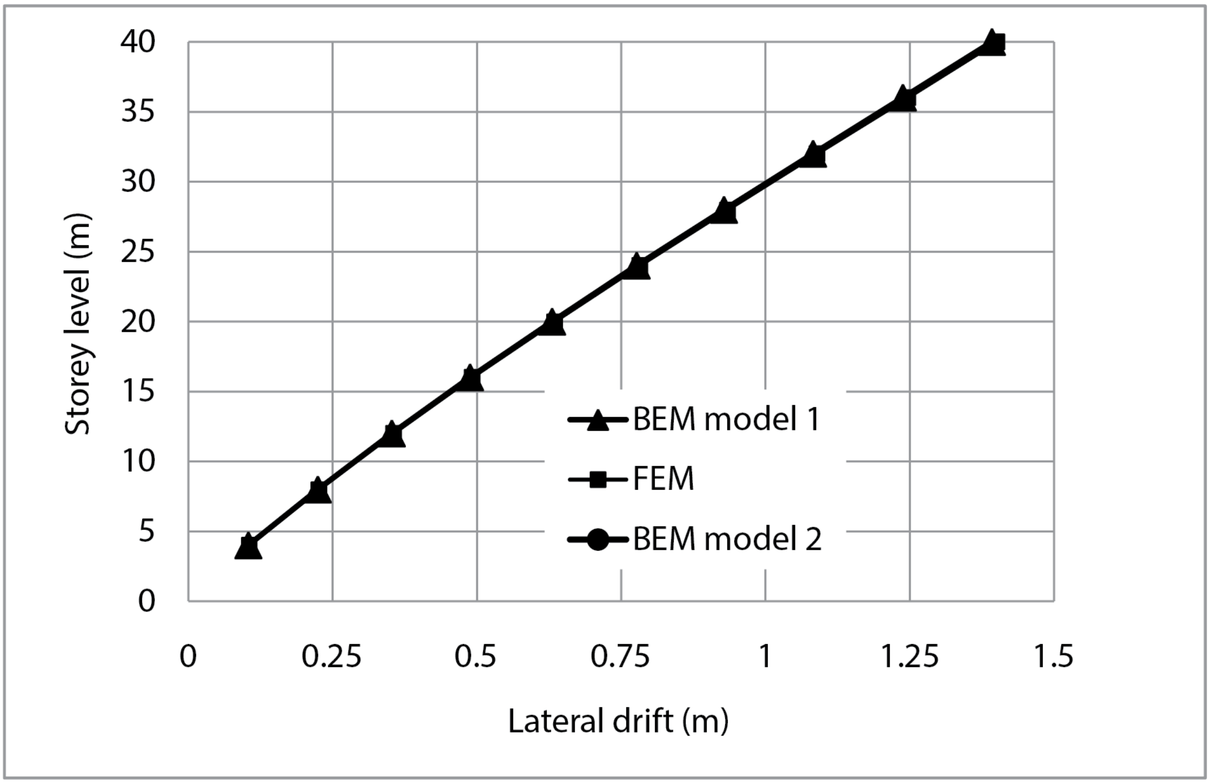

Figure 3.10: Example 3.2 lateral drift results.

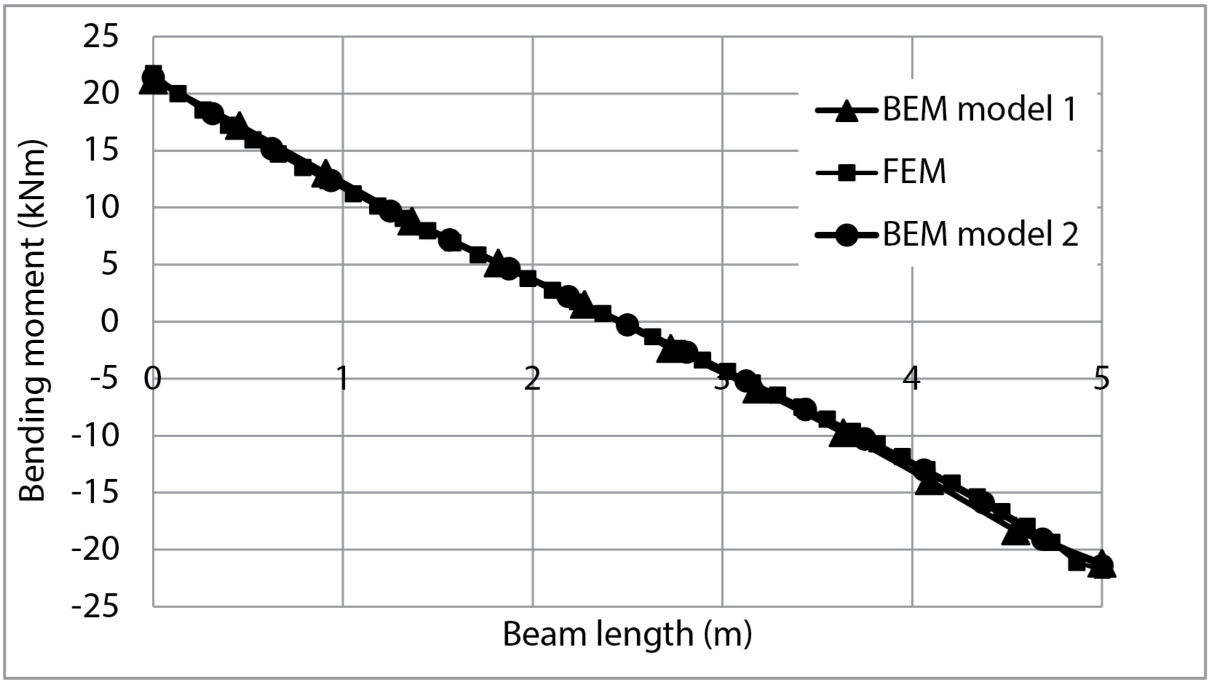

Figure 3.11: Example 3.2 beam bending moment results.

Example 3.3 [31]

Purpose : Compare drift and post-processing results for structure featuring walls only with the finite element method.

Description : The structural drawing of this example is presented in Figure 3.12. The boundary element model of the floor is presented in Figure 3.13. The finite element model is presented in Figure 3.14.

Results : The lateral drift comparison is demonstrated in Figure 3.15. In contrary to the conclusions derived from Example 3.1, the lateral drift calculated from the PLPAK model is larger than that calculated from the finite element model. This can be due to the different types of models used to model the vertical core. In the PLPAK model, walls are modeled as vertical frame elements which include warping effects. However, in the finite element model, the walls are modeled as shell elements. Thus, completely different stiffness is calculated for the vertical elements, leading to this variation in the lateral drift.

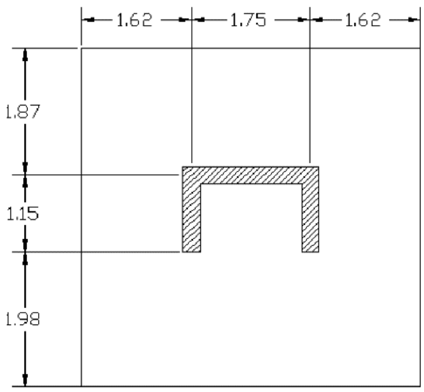

Figure 3.12: Example 3.3 structural drawing.

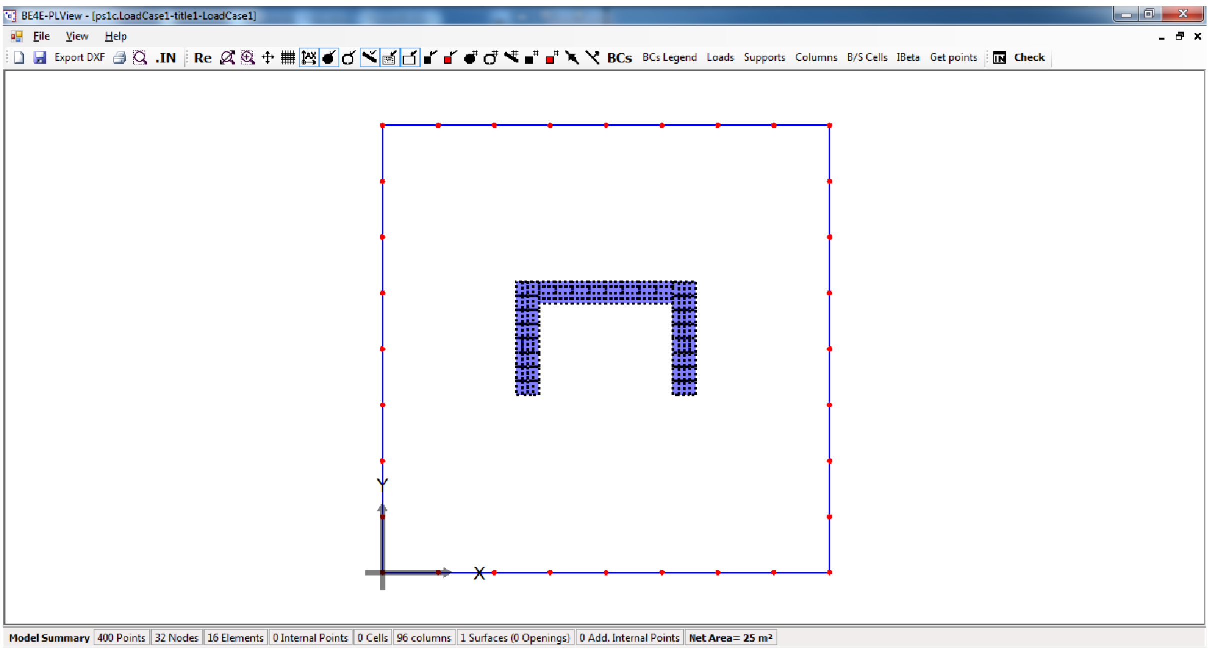

Figure 3.13: Example 3.3 BEM model.

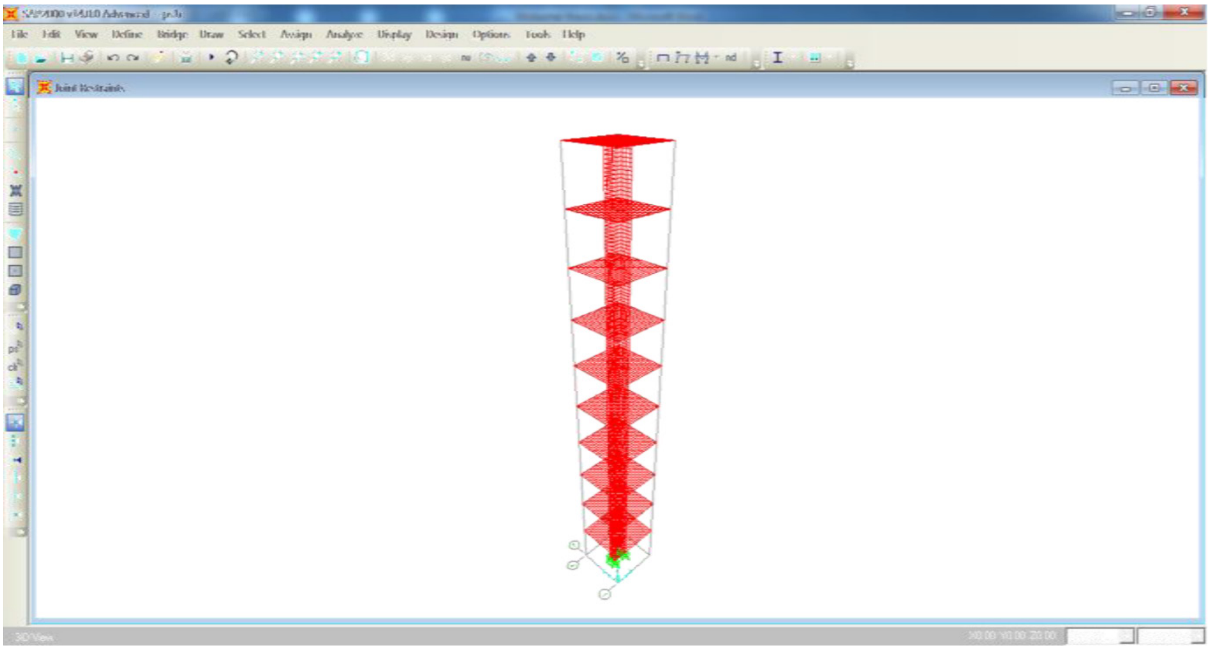

Figure 3.14: Example 3.3 FEM model.

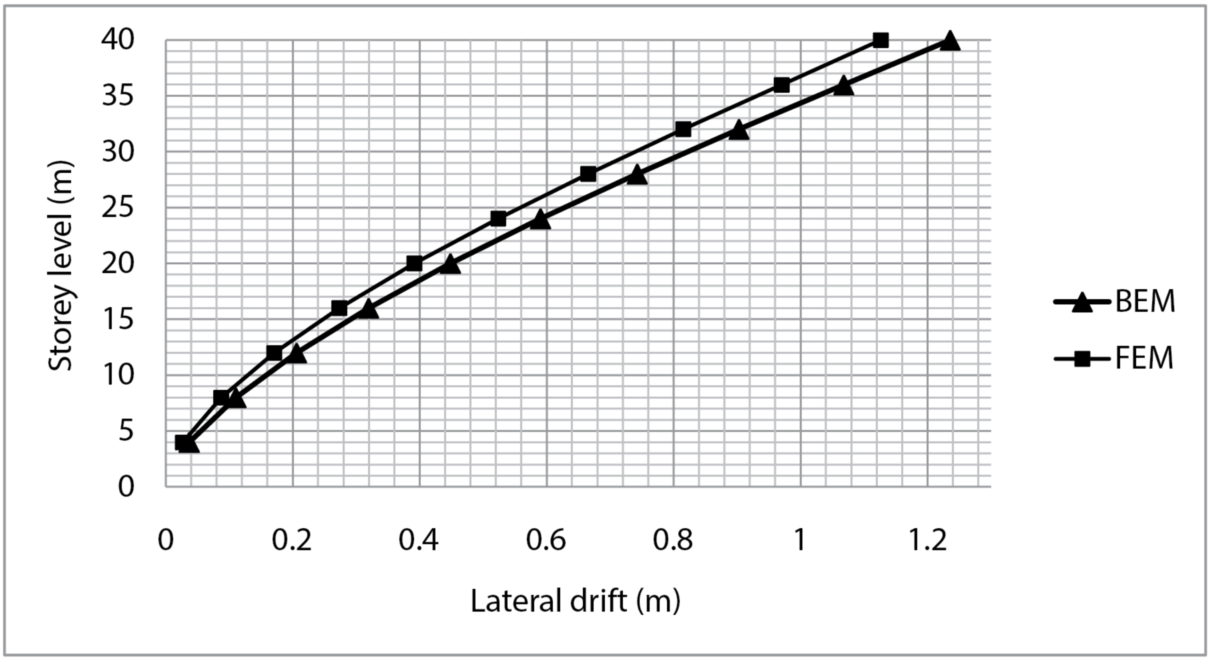

Figure 3.15: Example 3.3 lateral drift comparison.

Example 3.4 [31]

Purpose : Compare drift and post-processing results for structure featuring columns, beams, and walls with the finite element method.

Description : The structural drawing of this example is presented in Figure 3.16. The boundary element model of the floor is presented in Figure 3.17. The finite element model is presented in Figure 3.18.

Results : The lateral drift comparison is demonstrated in Figure 3.19 and the results from the PLPAK model are in acceptable agreement with finite elements. The same comments mentioned in Example 3.3 apply to this example.

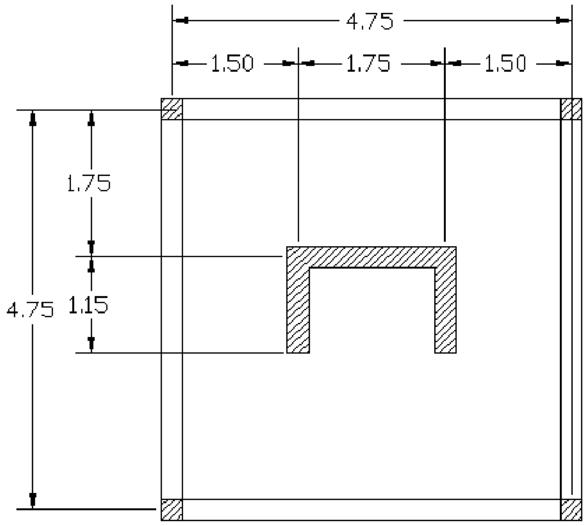

Figure 3.16: Example 3.4 structural drawing.

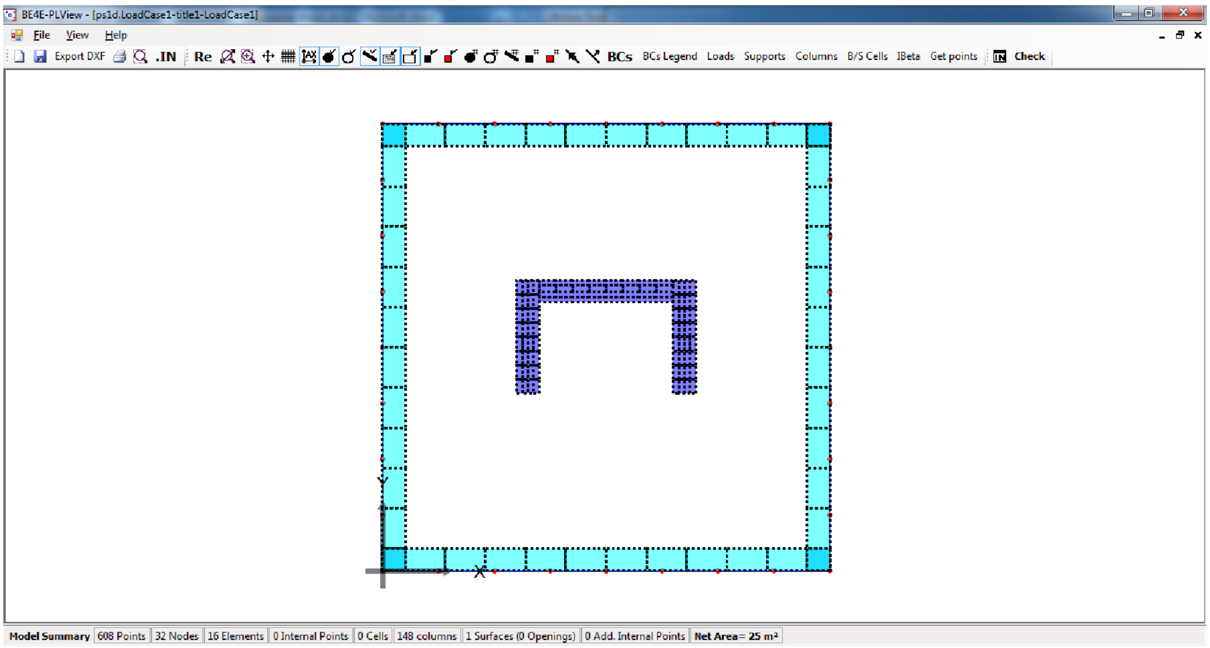

Figure 3.17: Example 3.4 BEM model.

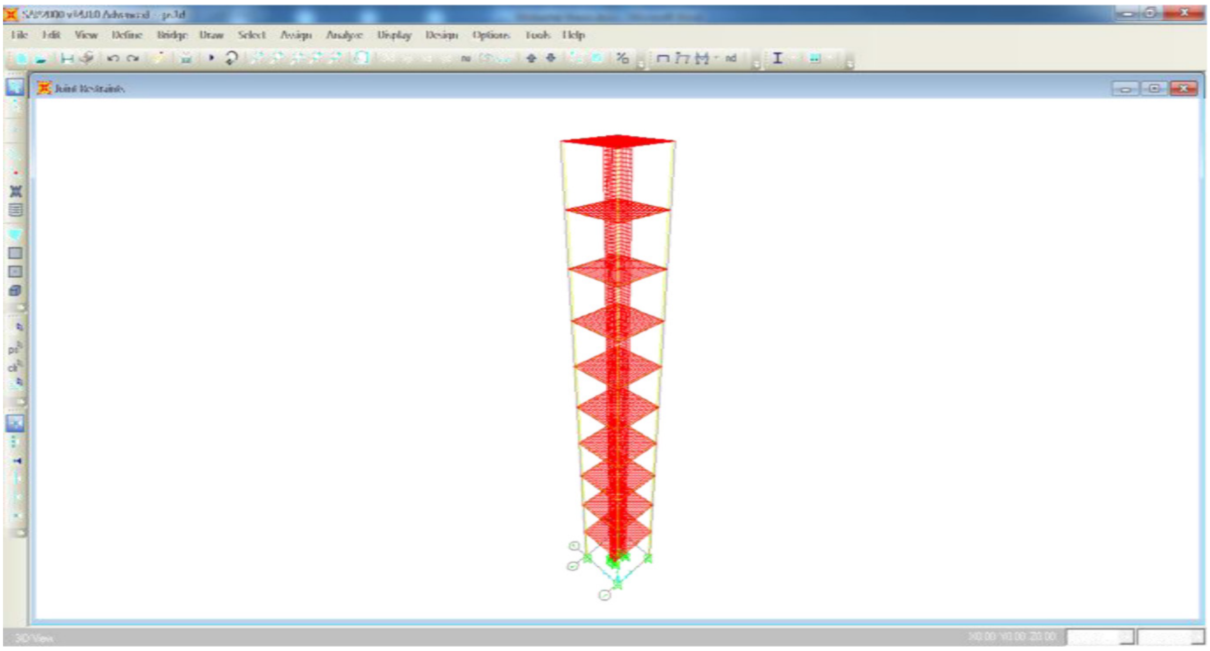

Figure 3.18: Example 3.4 FEM model.

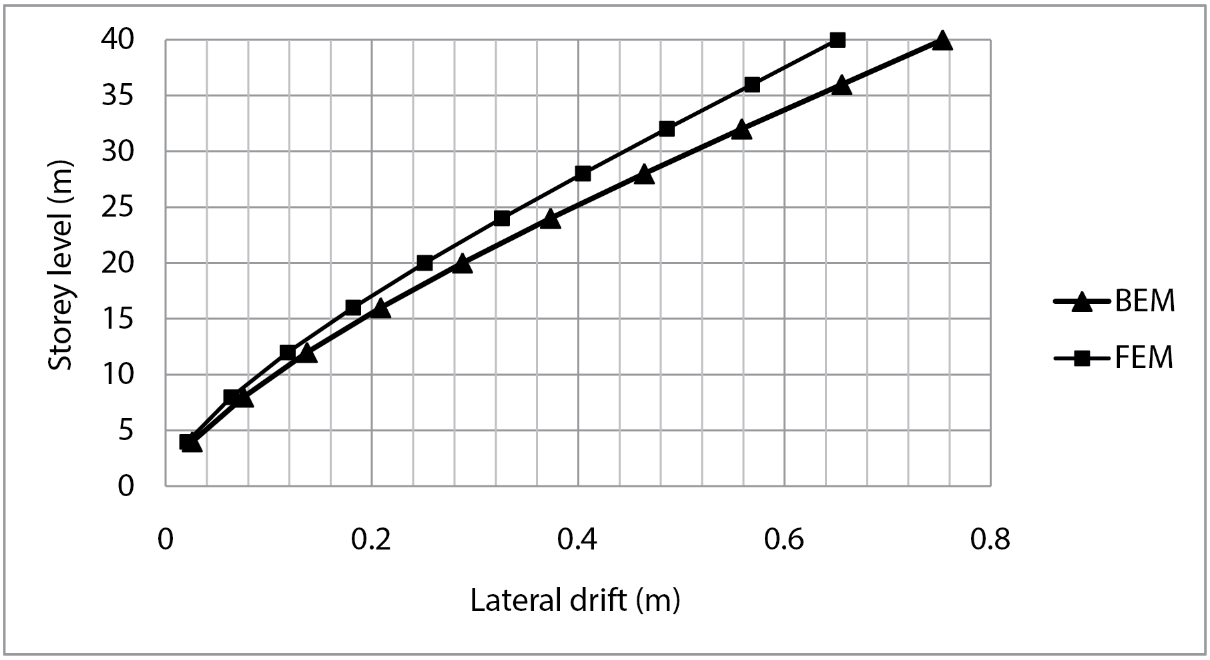

Figure 3.19: Example 3.4 lateral drift comparison.

Example 3.5 [31]

Purpose : Compare beam results in the lateral analysis in cases of beams that have irregular arrangement and overlapping with the finite element method.

Description : Figure 3.20 demonstrates the boundary element model of this example and Figure 3.21 demonstrates the finite element model. The structure is 2 storeys; each storey is 5 meters high. One hundred tons load is applied in x-direction at the slab centerline of the top floor. Young's modulus is 2210000 t/m^2 and Poisson's ratio is 0.2.

Results : Figure 3.22 demonstrates drift comparison against finite element model of the problem. Figure 3.23 illustrates comparison of bending moment results. Top floor deflection comparison is presented in Figure 3.24 and Figure 3.25. The results in Figure 3.22 demonstrate that modeling beams as skeletal elements lead lower drift values. This is expected because the modeling of the beams as separate skeletal elements will make the beams stiffness independent from the numerical BEM accuracy, hence, better capturing of the frame action resisting the lateral load will be achieved. The results presented in Figure 3.22-Figure 3.25 demonstrated agreement between the results produced from the PLPAK model and finite element analysis. This agreement validates the versatility of the PLPAK analysis in modeling beams and frame action in lateral resisting systems even in complicated beam-column arrangement.

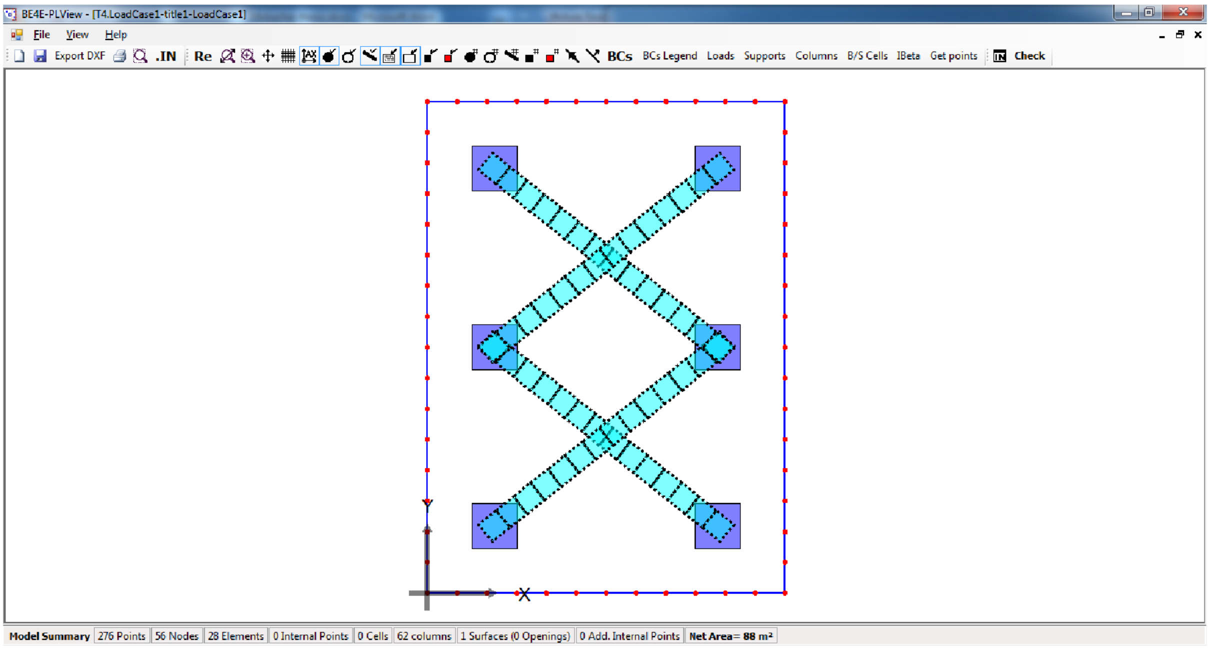

Figure 3.20: Example 3.5 BEM model.

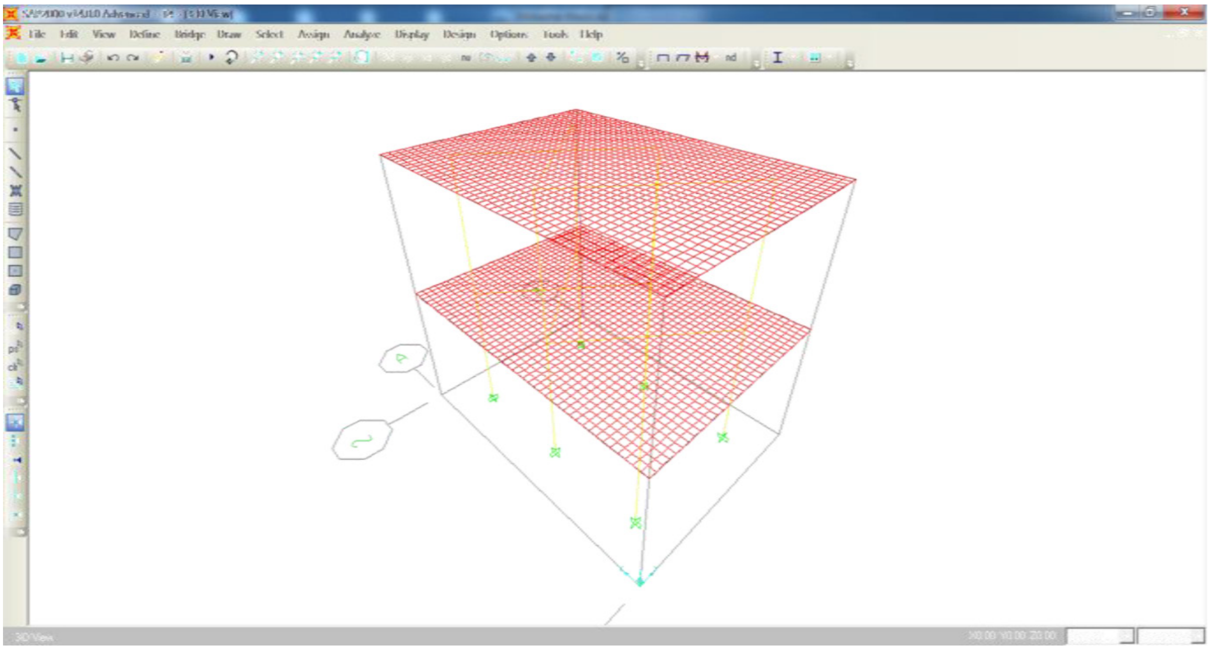

Figure 3.21: Example 3.5 FEM model.

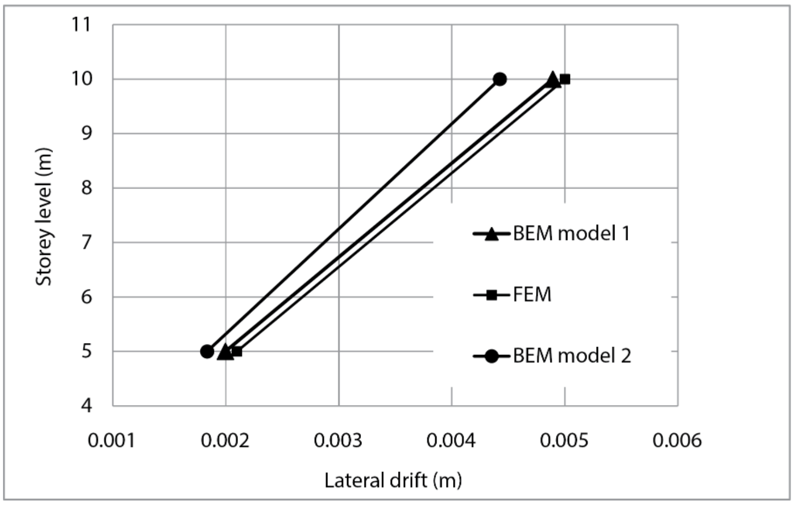

Figure 3.22: Example 3.5 lateral drift results.

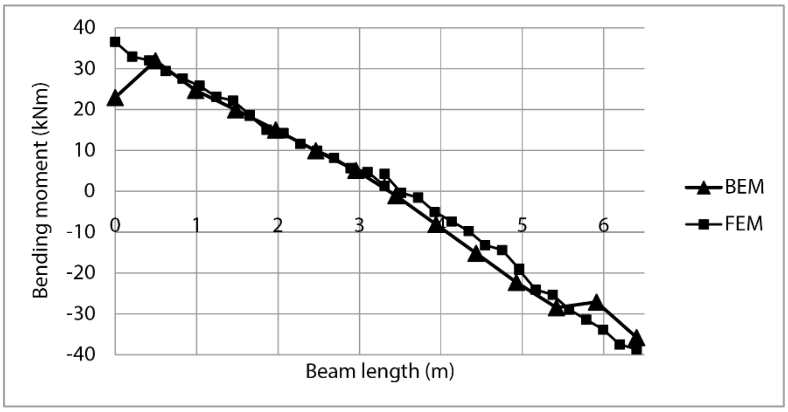

Figure 3.23: Example 3.5 Bending moment results.

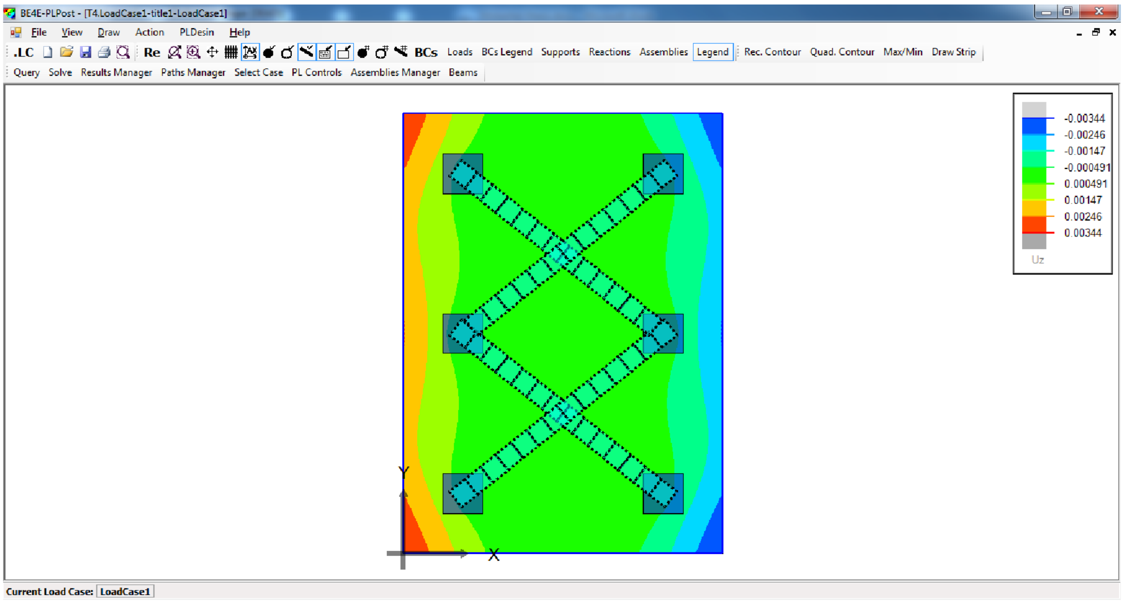

Figure 3.24: Example 3.5 BEM deflection results.

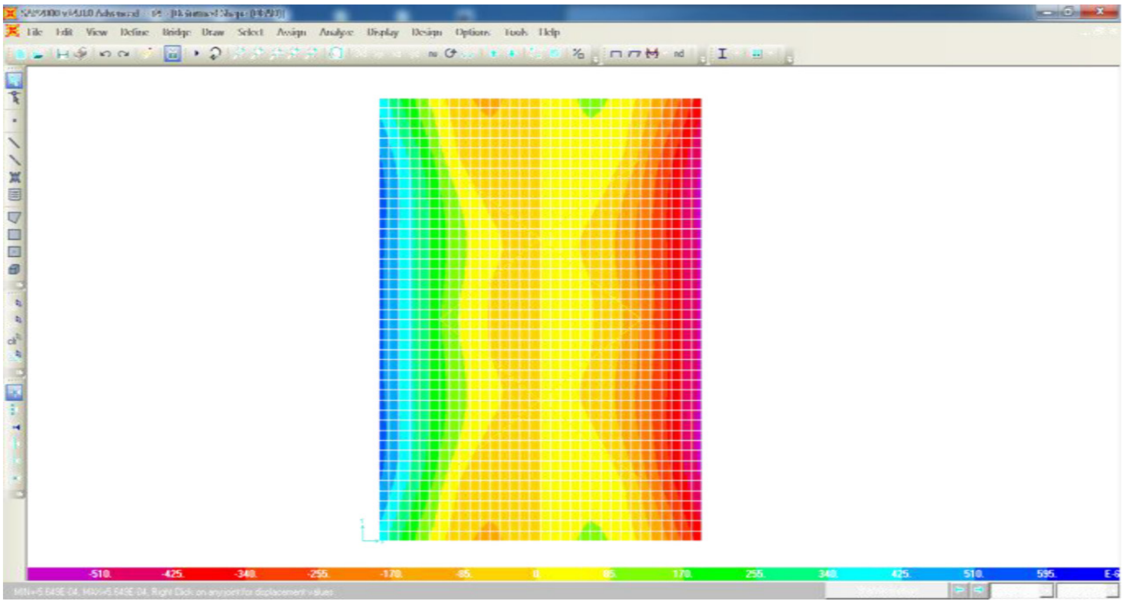

Figure 3.25: Example 3.5 FEM deflection results.

Example 3.6 [31]

Purpose : Test the efficiency of the PLPAK model in capturing the frame action by comparing several models with the finite element method.

Description : Eight models were created using the originally generated model and compared to finite element models. In these models, beam sizes thicknesses were varied from zero (no beams) to 1m. The boundary element and finite element models of the problem are presented in Figure 3.26 and Figure 3.27, respectively.

Results : Lateral drift comparison of the top floor is presented in Figure 3.28. Analyzing the results in Figure 3.28 it can be concluded that the "BEM model 1" captures less lateral stiffness of the frame action resistance of the structure in cases of large beam depths. In order to improve this defect, beam elements had to be modeled as skeletal as in "BEM model 2" which proved to be stiffer than FEM and "BEM model 1" for small beam sizes. "BEM model 2" is capable of capturing a higher stiffness of the structure for larger beam sizes upon increasing the discretization in the boundary element model.

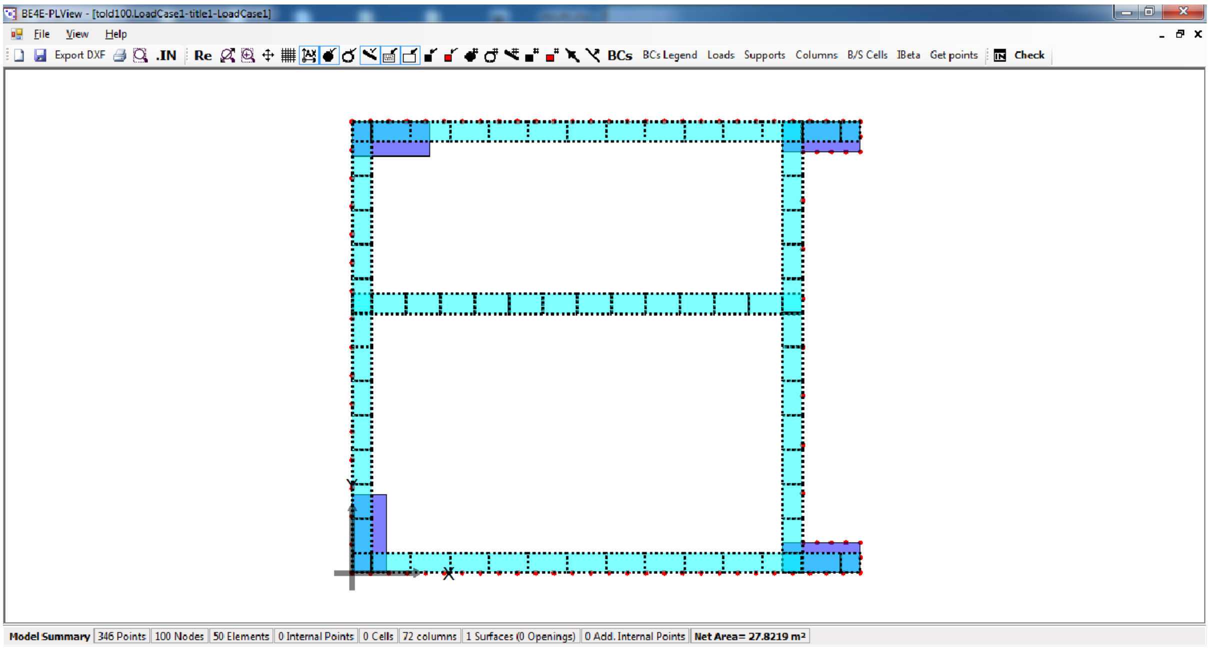

Figure 3.26: Example 3.6 BEM model.

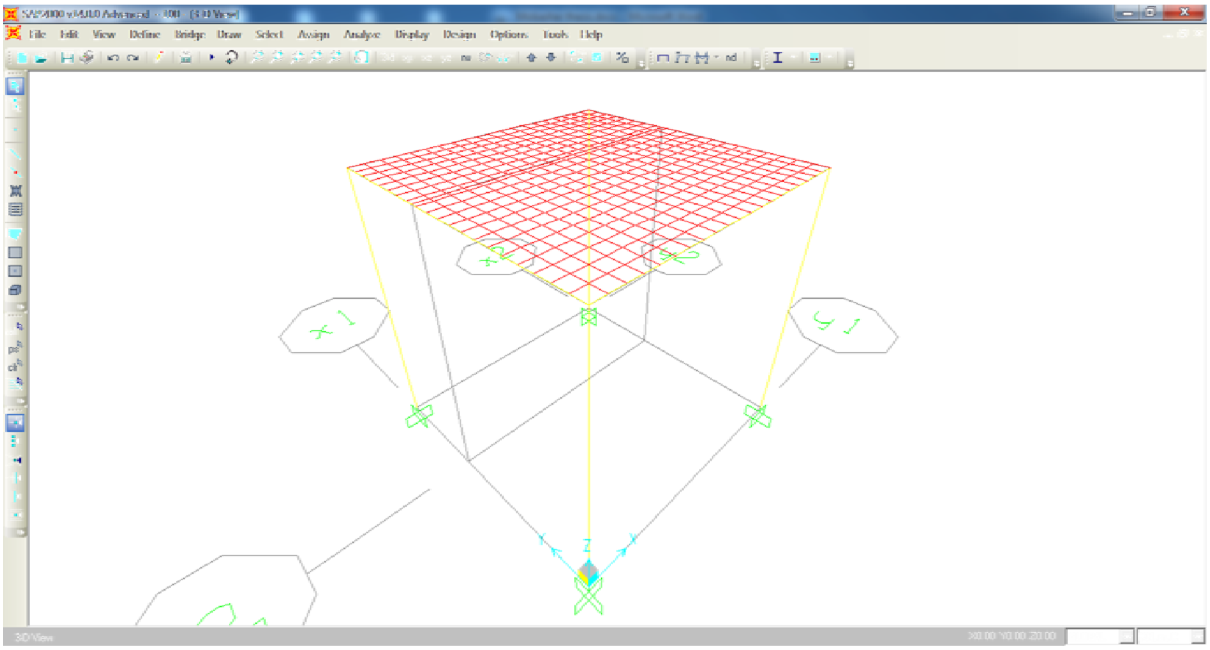

Figure 3.27: Example 3.6 FEM model.

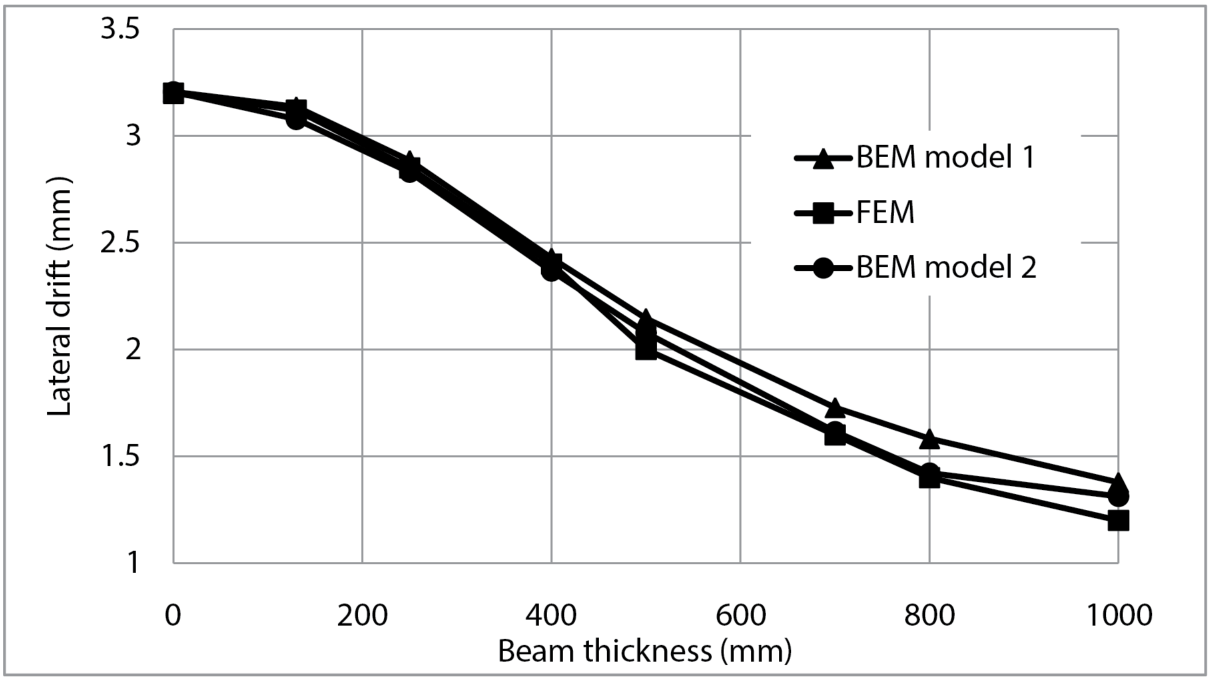

Figure 3.28: Example 3.6 lateral drift comparisons.

Example 3.7 [32]

Purpose : Compute the lateral drift of a single-story building by the PLPAK, hence, a comparison is made between the PLPAK results to those of the finite element method.

Description : Three numerical models are considered, two are based on the finite element method (FEM) and the third one is based on the boundary element method (BEM). The slab has a thickness of 0.2 m, and dimensions of 4x4m. Column dimensions are 0.5x0.5m as shown in Figure 3.29. The slab material has a modulus of elasticity equal to 2210000 t/m^2 and Poisson's ratio of 0.2. The columns modulus of elasticity is equal to 2210000 t/m^2. A 10 t is applied in the X direction at co-ordinates x=0, y=2 m at the level of the slab. The considered height of the story is 3m. The following three numerical models are considered:

1. Considers the PLPAK. The boundary element method is used to model slabs using continuous quadratic elements with element length of 1m as shown in Figure 3.30.
2. Considers columns as 3D solid finite elements with mesh of size 0.0625m. The slab is modeled using plate bending elements with a mesh size 0.0625m. A diaphragm constraint is enforced at the floor level as shown in Figure 3.31.
3. Considers columns as skeletal frame elements. The slab is modeled using the plate bending elements with a mesh size of 0.0625m. A diaphragm constraint at the floor level is enforced as shown in Figure 3.32.

It has to be noted that, in models 2 and 3 the Straus7 software is used to carry out the finite element analysis.

Results : Figure 3.33 to Figure 3.35 demonstrate the bending moment a contour map and strips for the three models. In order to compare the results, Figure 3.36 demonstrates the same strip results for the three models together. It can be seen that the frame model (the common model that is used in practice of structural engineering) produces peaking values for bending moments above support elements. If model 3 results are eliminated from Figure 3.36, then Figure 3.37 is obtained. It is clear that the PLPAK solution (model1) is as accurate as the (model2) in which columns are modeled as solid elements.

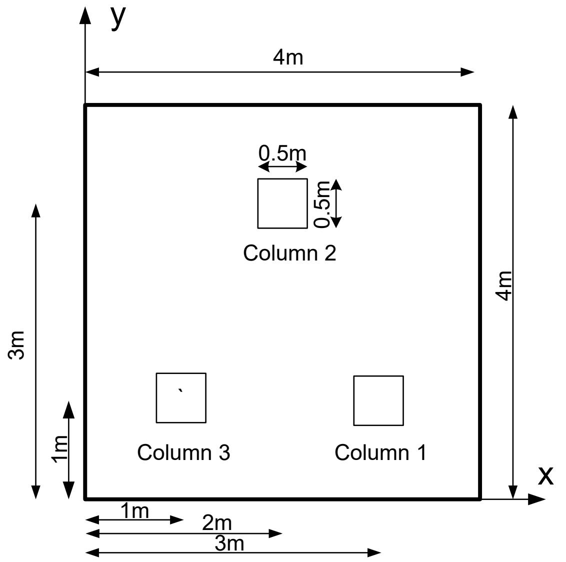

Figure 3.29: Dimensions considered for the slab in Example 3.7.

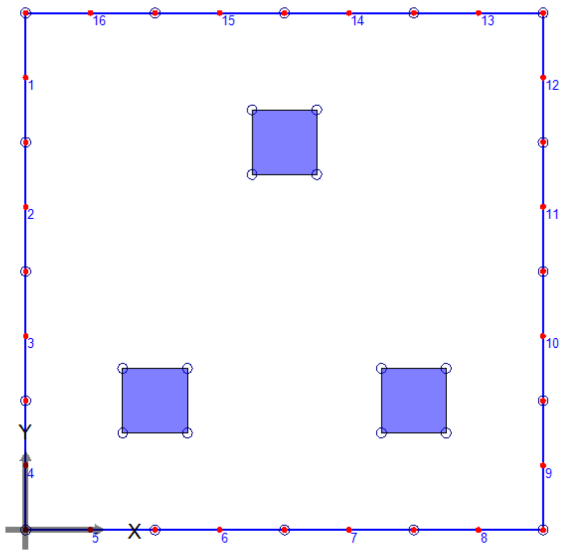

Figure 3.30: Boundary element model (model 1) in Example 3.7.

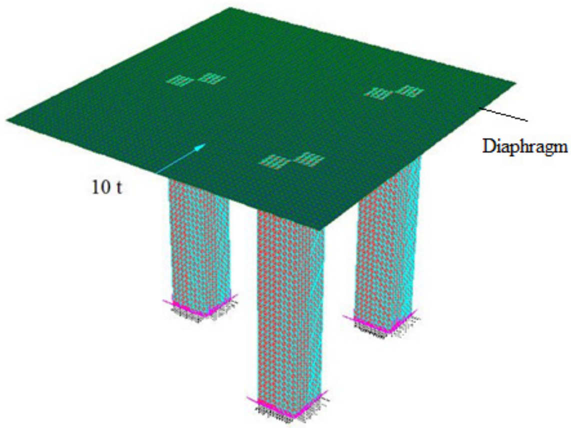

Figure 3.31: Solid element column model with slab plate bending finite element method (model 2) in Example 3.7.

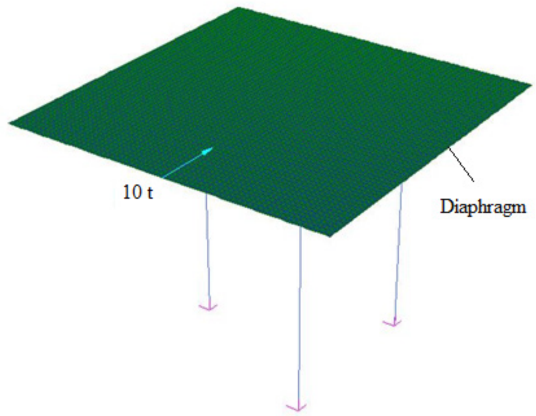

Figure 3.32: Frame element column model with slab plate bending finite element model (model 3) in Example 3.7.

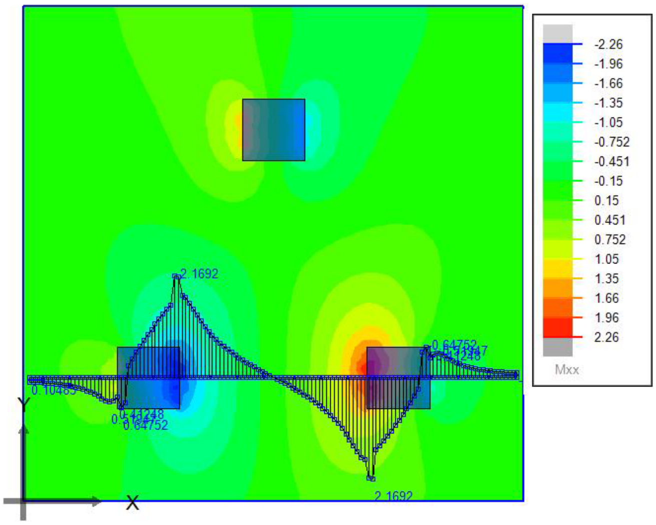

Figure 3.33: Bending moment Mxx contour in model 1 in Example 3.7.

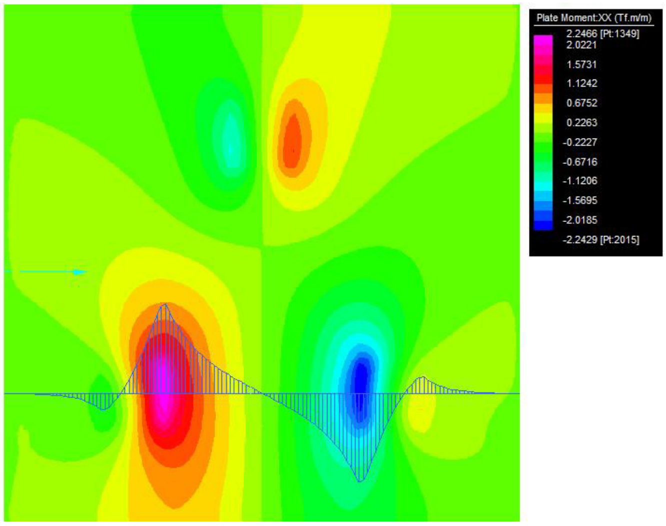

Figure 3.34: Bending moment Mxx contour map in the finite element model 2 in Example 3.7.

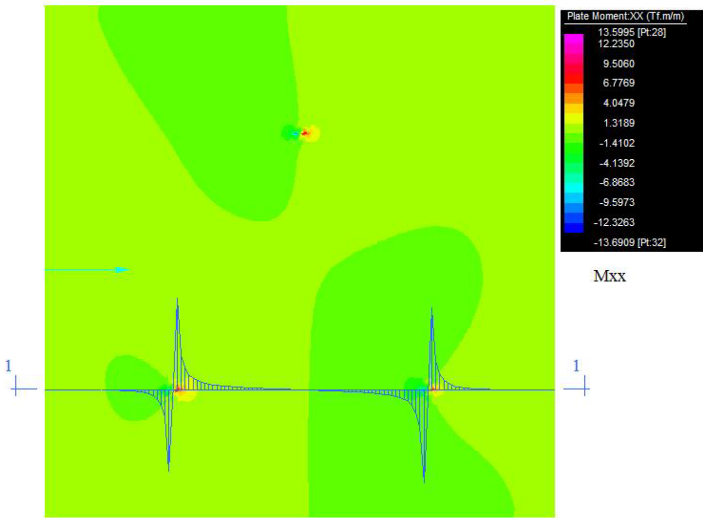

Figure 3.35: Bending moment Mxx contour map in the finite element model 3 in Example 3.7.

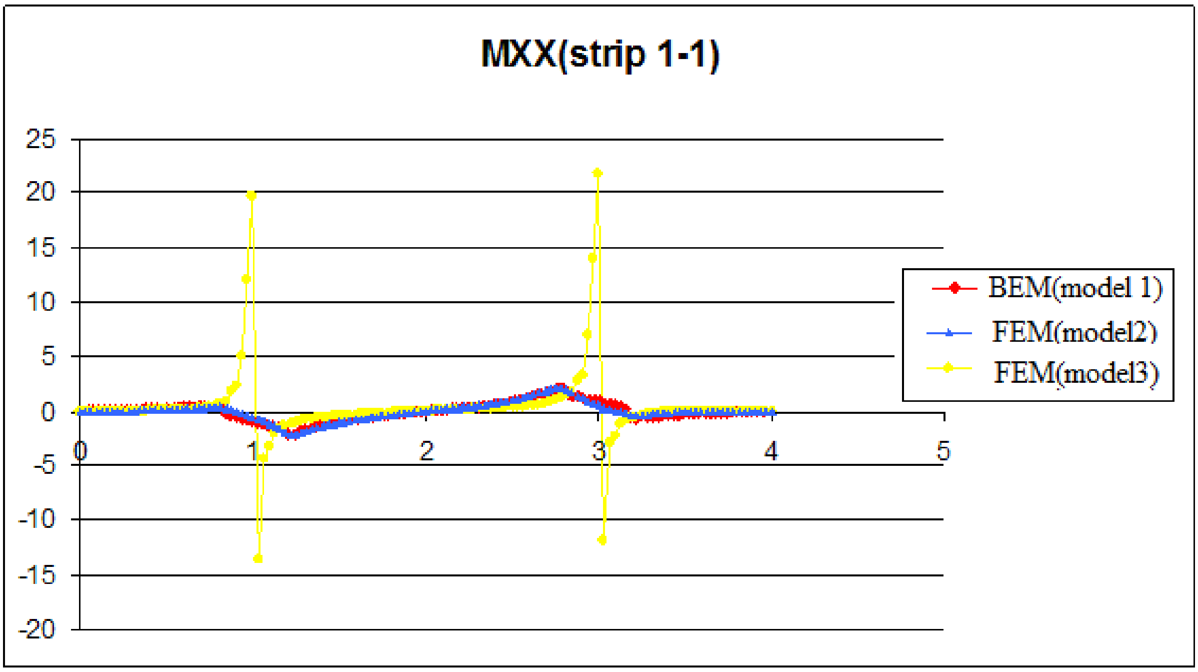

Figure 3.36: Comparison of bending moment M_{xx} for the considered three models in Example 3.7.

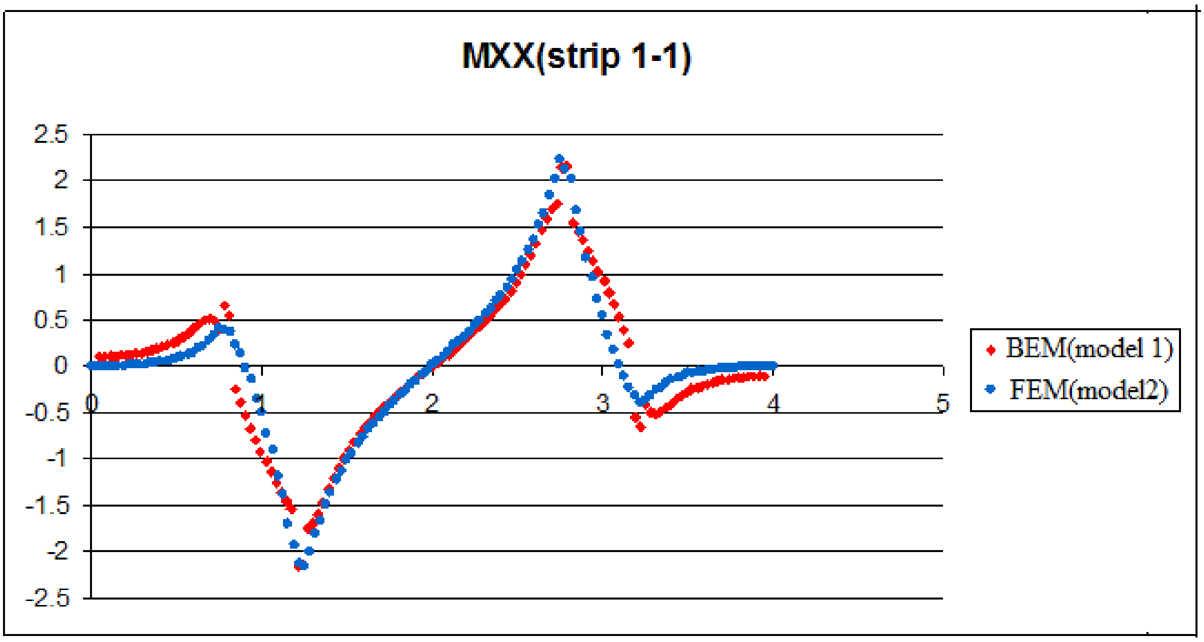

Figure 3.37: Comparison of bending moment M_{xx} for the considered two models in Example 3.7.

Example 3.8 [32]

Purpose : Demonstrate the effect of the consideration of real geometry of slab-column connection area.

Description : In order to demonstrate the effect of the consideration of real geometry of slab-column connection area, Example 3.7 is re-considered but with 20 stories. The applied load is applied at the top floor only (floor no. 20). Two BEM models are considered, whereas the first model considered the actual connection area of columns and slab (50×50cm), whereas in the second model, the connections area between the slab and the column is set to 10×10 cm with preserving the column's stiffness properties as a 50×50cm column. The drift results of the two models are demonstrated and compared to the FEM frame model (model3). It has to be noted that only the FEM model 3 is considered herein as it is difficult to run a 20-story building with solid elements using the currently used personal computers.

Results : It can be seen from Figure 3.38 to Figure 3.40 that both the FEM model3 and the PLPAK BEM model of the 10×10cm connecting area give similar results. That means that the contact area between the slab and the column affects the total drift of the structural.

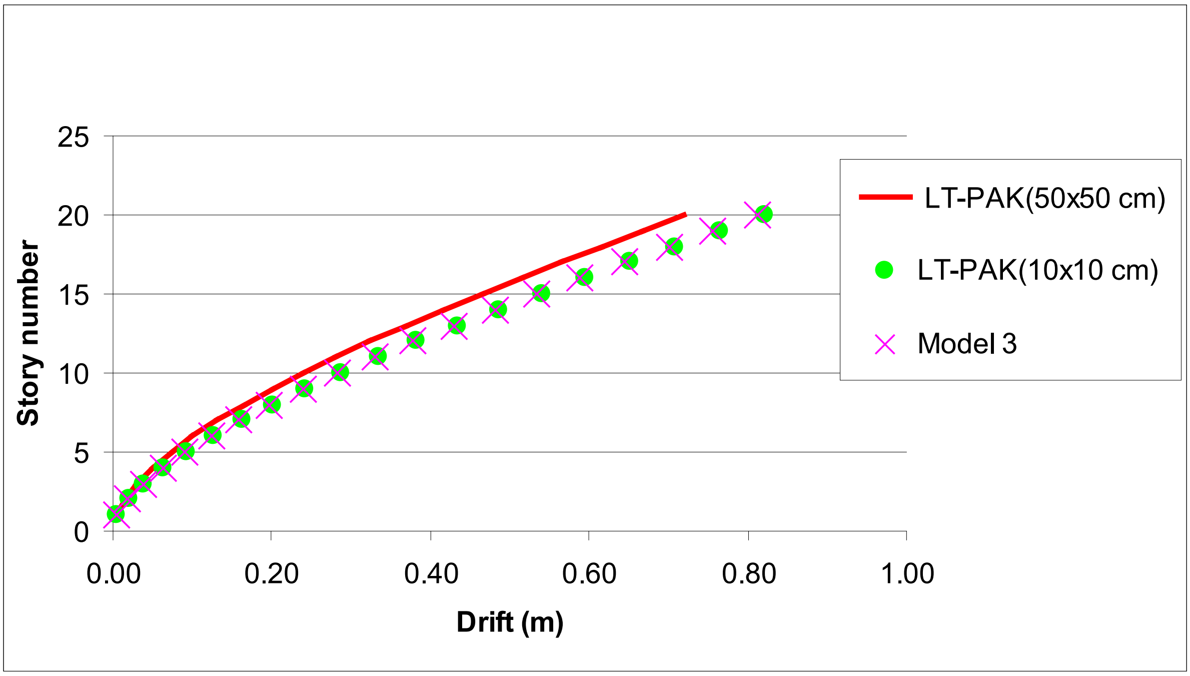

Figure 3.38: Drift in x axis in Example 3.8.

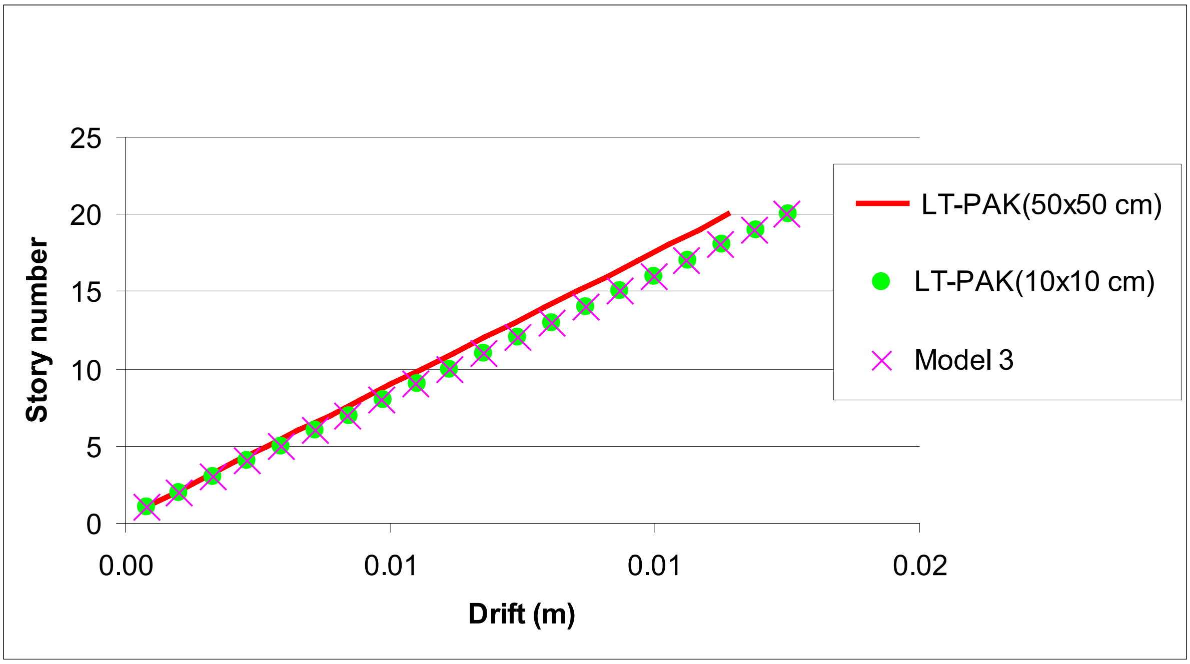

Figure 3.39: Drift in Y axes in Example 3.8.

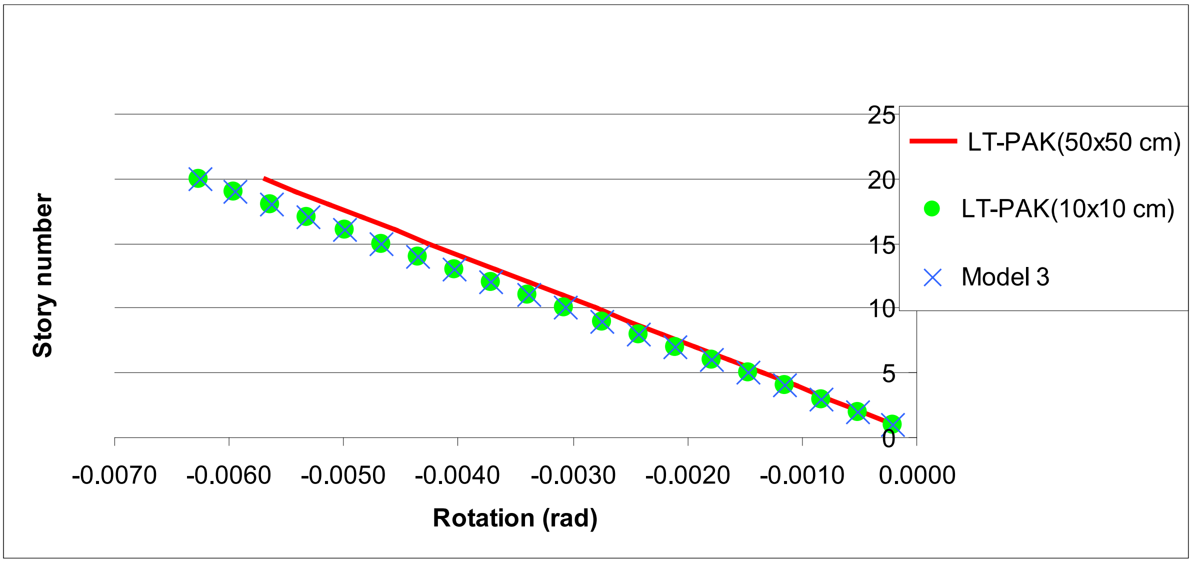

Figure 3.40: Rotation about Z axes in Example 3.8.

Example 3.9 [32]

Purpose : Compare the results of analyzing a practical multi-story building with the finite element method.

Description : A 10-storey building is analyzed using the PLPAK and the results are compared to those obtained from the finite element method. The slab shown in Figure 3.41 is analyzed. It has a thickness of 0.23 m. Both the slab and vertical element materials have a modulus of elasticity equal to 2210000 t/m^2 and Poisson's ratio equal to 0.2. The height of each storey is 3.4 m. A (1000 t) load is applied in the X-direction as shown in Figure 3.41 at all levels of the slabs. The boundary element mesh and associate discretization are shown in Figure 3.42. The used finite element mesh is shown in Figure 3.43 and Figure 3.44 with shell elements of size 0.5m. Columns are modeled using frame elements. A diaphragm constraint is applied at each floor level.

Results : The deflection of top slab as contour maps as shown in Figure 3.45 and Figure 3.46. Figure 3.48-Figure 3.53 demonstrate comparisons of deflections and lateral drifts. Noting that strips are demonstrated in Figure 3.47.

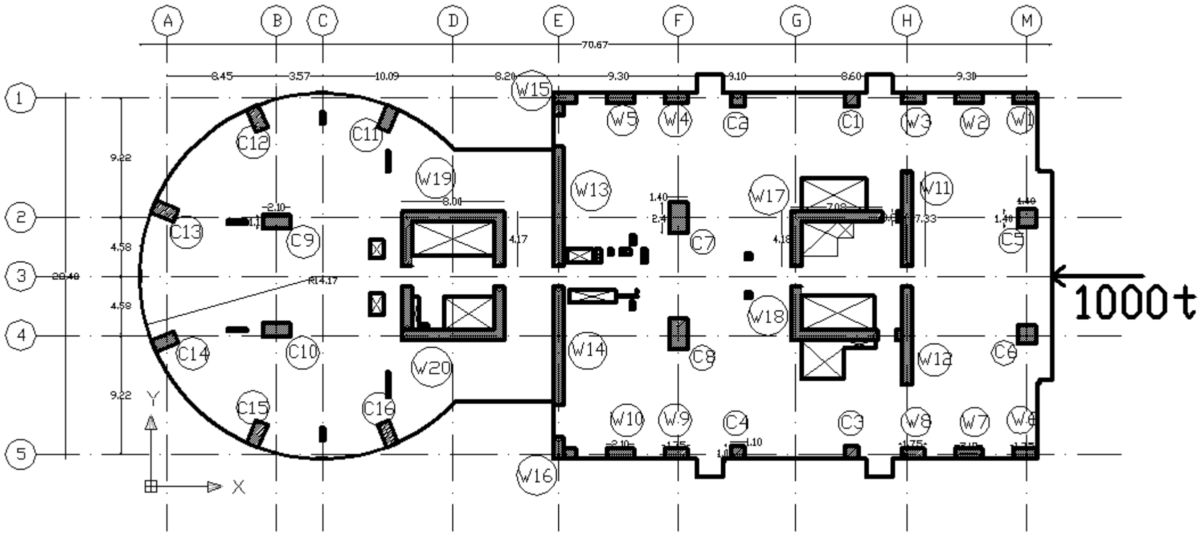

Figure 3.41: Dimensions of the Practical Building in Example 3.9.

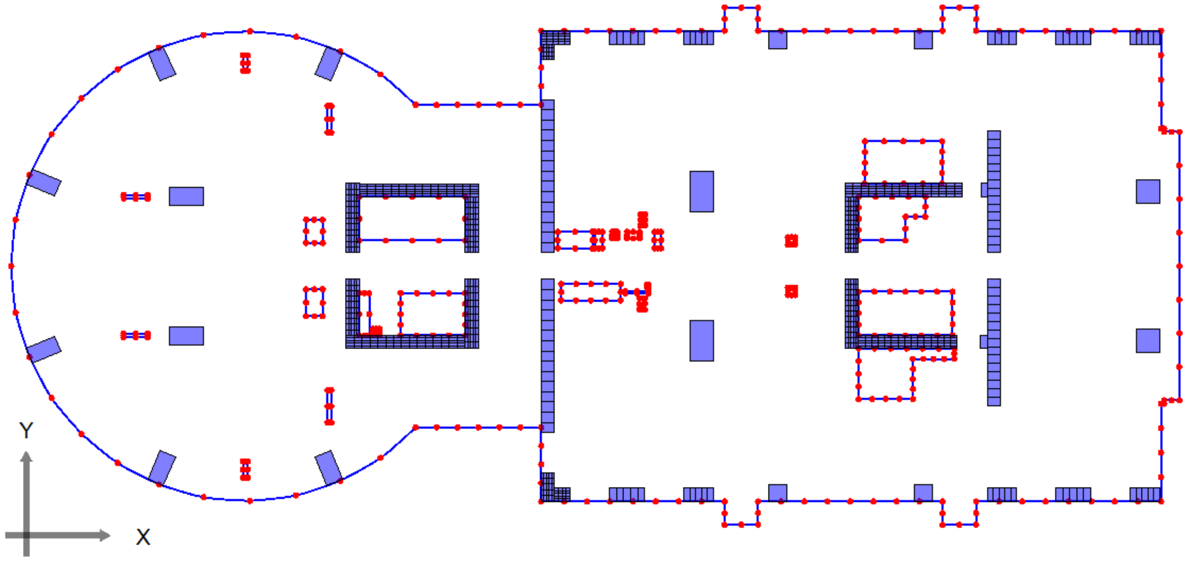

Figure 3.42: The used boundary element model in Example 3.9.

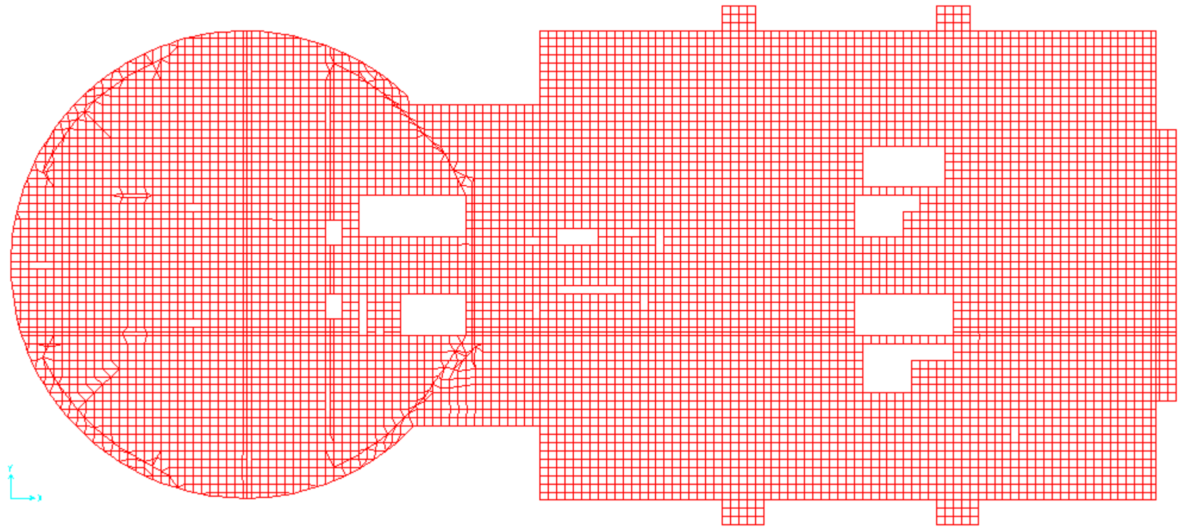

Figure 3.43: The finite element mesh used in Example 3.9.

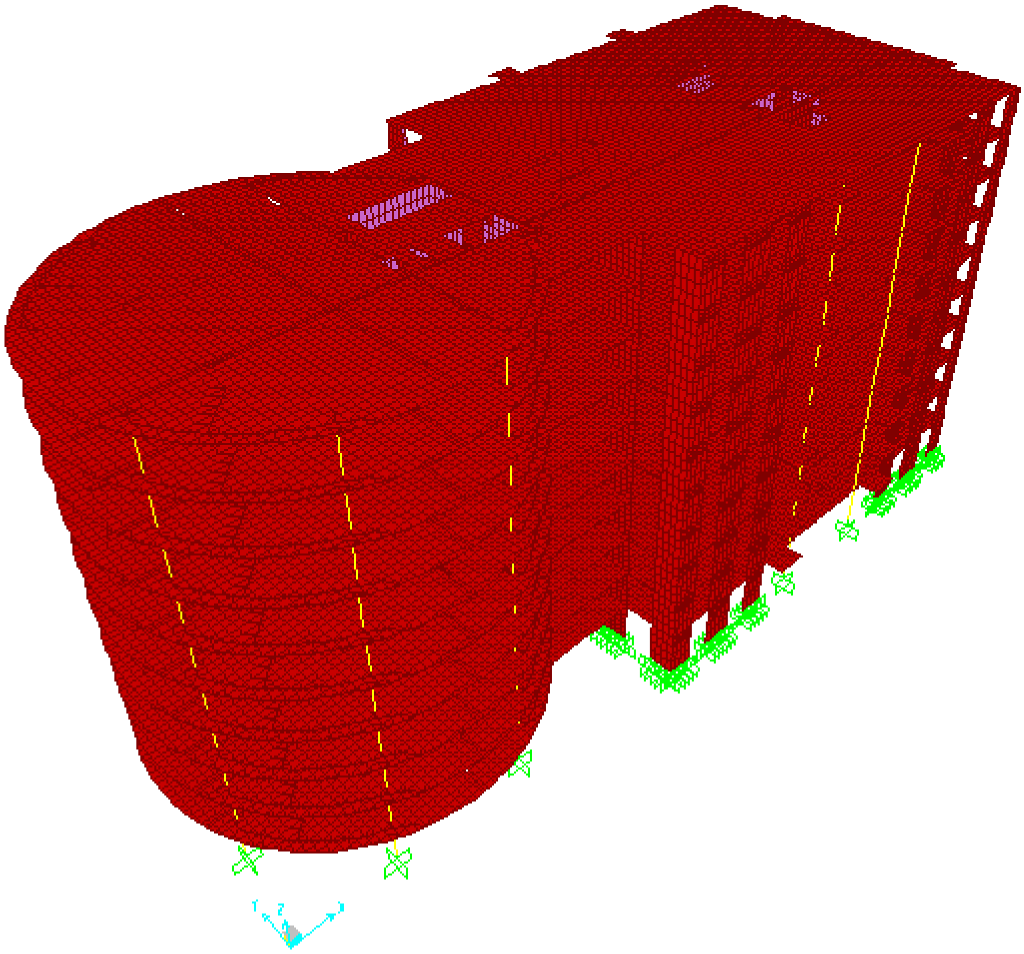

Figure 3.44: The multi-storey finite element model in Example 3.9.

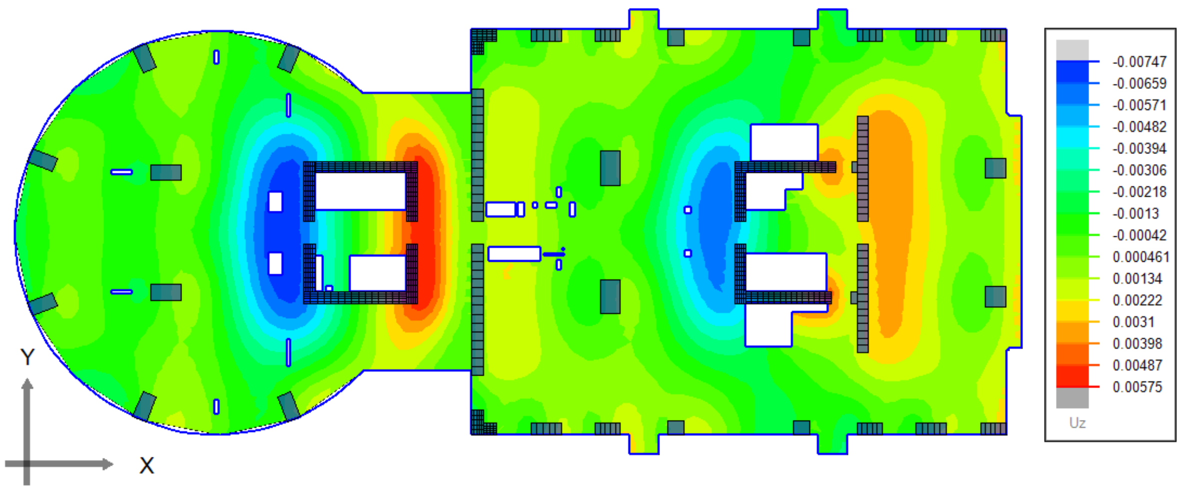

Figure 3.45: Slabs deflection U_Z_BEM_Model (1) in Example 3.9.

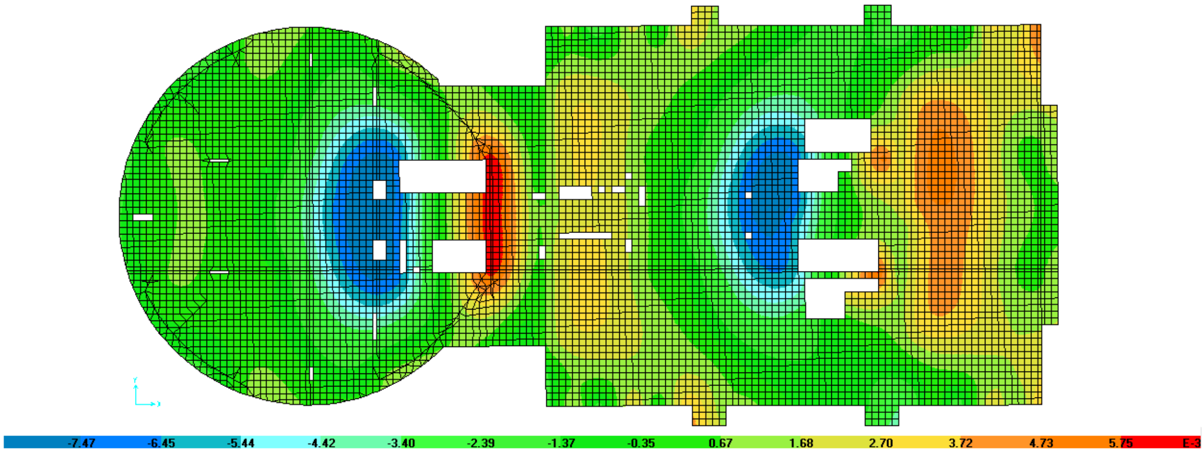

Figure 3.46: Slabs deflection U_Z- FEM-Model (2) in Example 3.9.

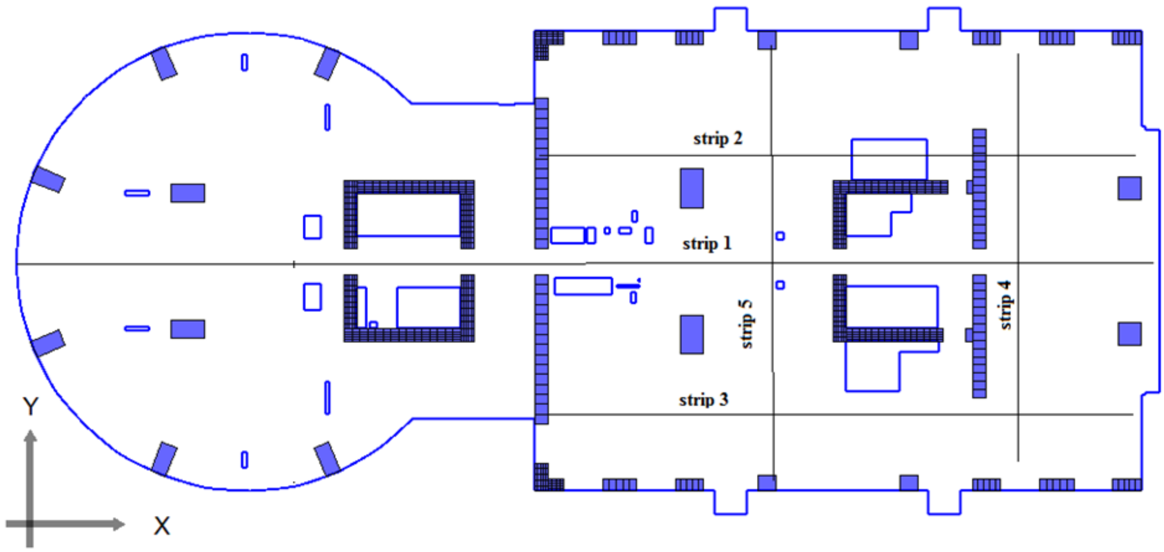

Figure 3.47: Strip guide in Example 3.9.

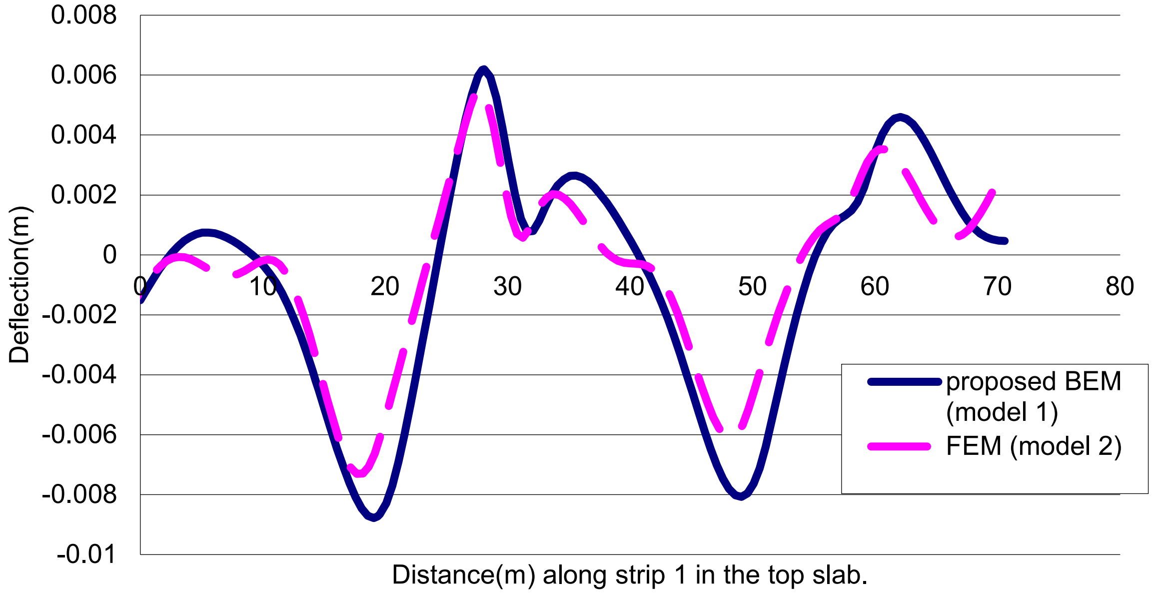

Figure 3.48: Comparison of deflection U_Z diagram between two models strip 1 in Example 3.9.

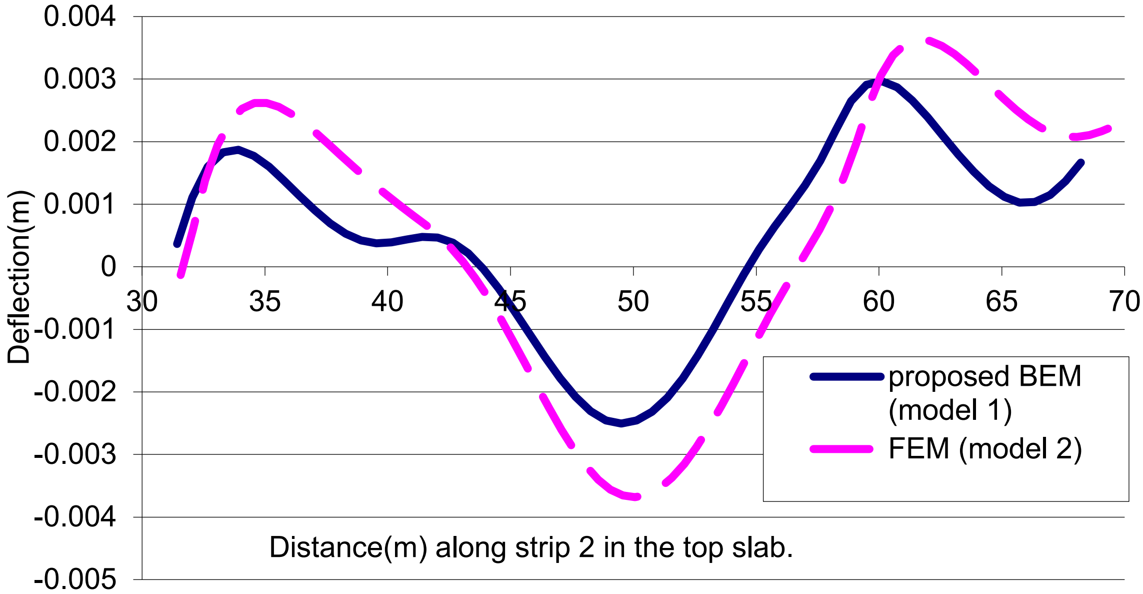

Figure 3.49: Comparison of deflection U_Z diagram between two models strip 2 in Example 3.9.

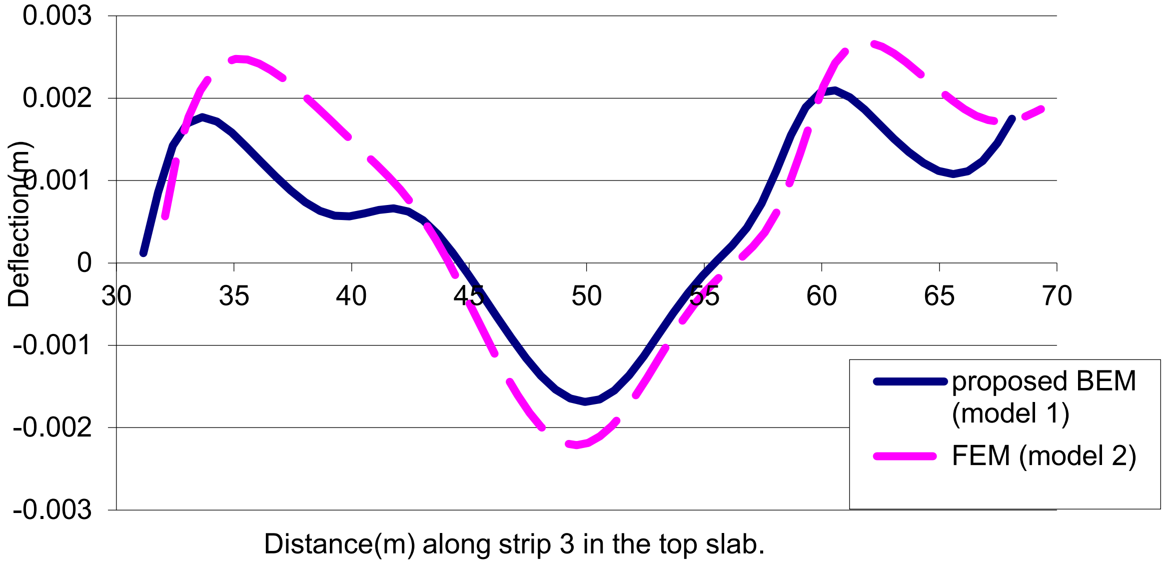

Figure 3.50: Comparison of deflection U_Z diagram between two models strip 3 in Example 3.9.

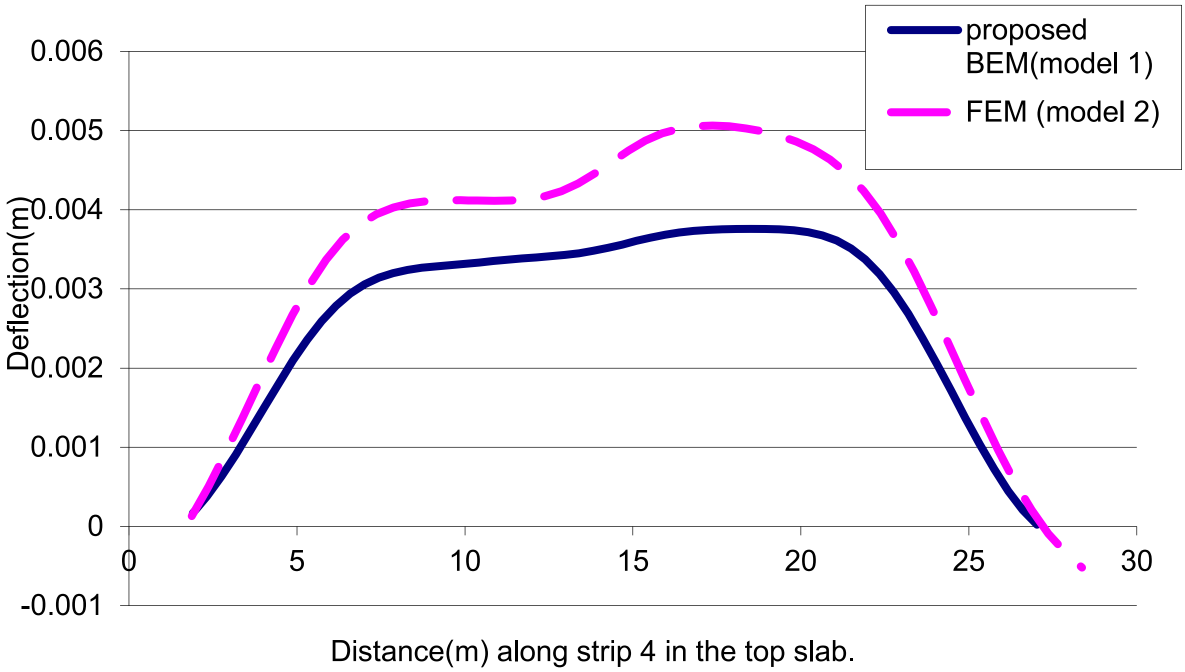

Figure 3.51: Comparison of deflection U_Z diagram between two models strip 4 in Example 3.9.

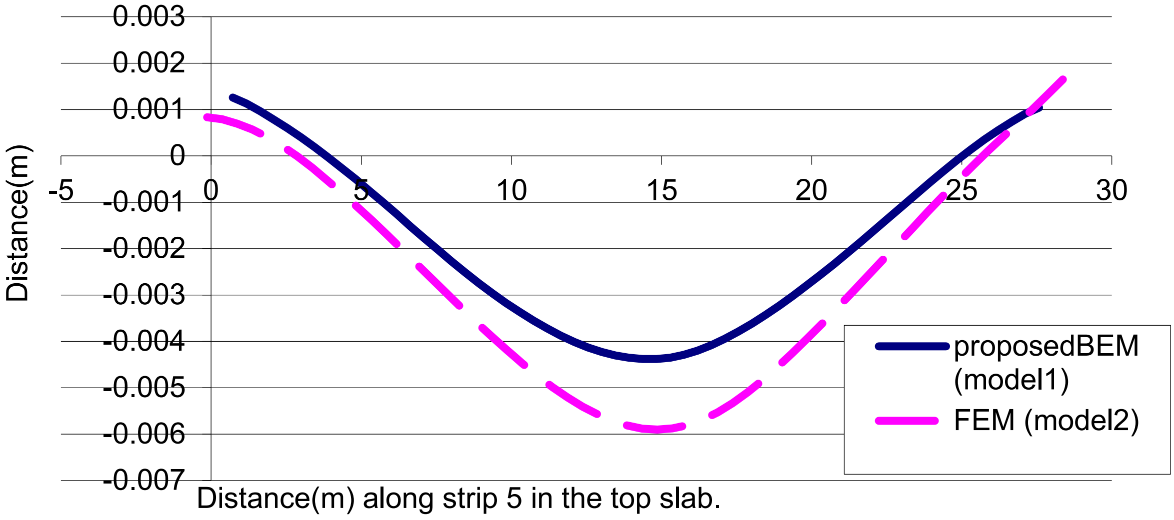

Figure 3.52: Comparison of deflection U_Z diagram between two models strip 5 in Example 3.9.

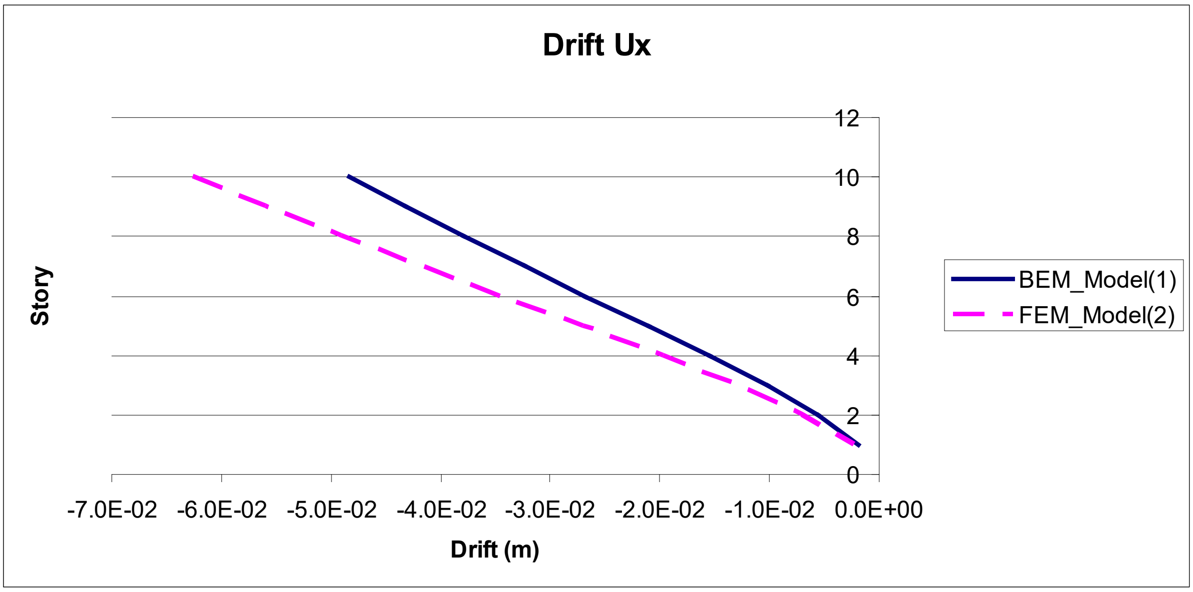

Figure 3.53: Comparison of lateral drifts in X direction in Example 3.9.

Example 3.10 [33]

Purpose : Comparing the results of applying gravity loads and applying lateral loads on single-story or multi-story building (slabs resting on four columns) with other finite element software.

Description : Figure 3.54 shows Example 3.10 structural plan. Figure 3.55 shows the BEM model of the PLPAK. Figure 3.56 and Figure 3.57 show the FEM model of the single story and the multi-story building with 1m x 1m slab mesh. Firstly, uniform gravity load of 1 t/m^2 is applied on the single-story building. Secondly, a lateral load of 100 t is applied in x-direction on the highest floor in the single-story model and the multi-story model of 10 floors as shown in Figure 3.60. For the multi-story building, in order to consider the effect of contact area in the FEM, another 2 FEM models are constructed. In the first one, Figure 3.63, the slab is modeled as thick plate element and columns are modeled as solid elements. In the second one, Figure 3.64, the slab and columns are modeled as solid elements.

Results : Figure 3.58 and Figure 3.59 show the bending moment M_{xx} for the FEM and the BEM respectively due to the gravity load. Also, the maximum deflection at the center of slab equals to 0.05631 m and 0.04733 m for the FEM and BEM respectively. For the lateral load on the single-story building, the lateral displacement U_x equals to 0.00277 m and 0.0027392 m for the FEM and BEM respectively. Figure 3.61 and Figure 3.62 show the bending moment M_{xx} for the FEM and the BEM respectively. It could be observed that lateral displacement in FEM is greater than in BEM due to the consideration of contact area effect in BEM. While for the multi-story building, lateral displacements U_x for the 3 FEM models and the BEM model is plotted against building elevation in Figure 3.65.

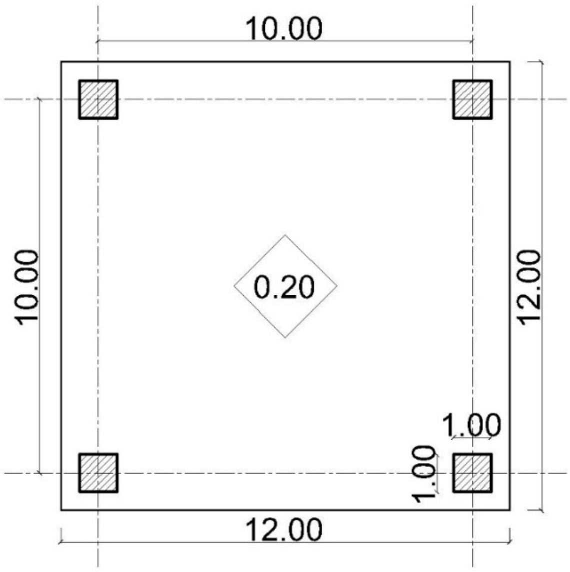

Figure 3.54: Example 3.10 structural Plan.

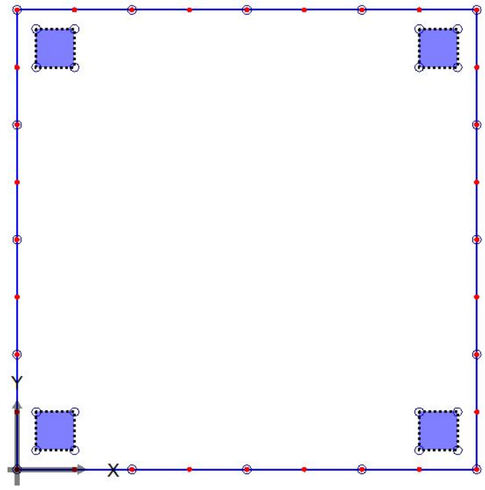

Figure 3.55: Example 3.10 BEM model.

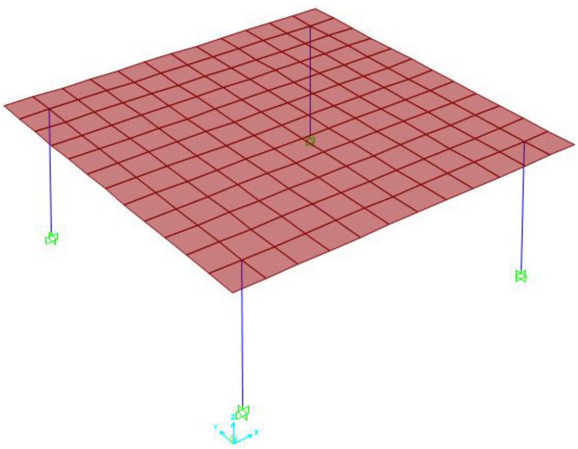

Figure 3.56: Example 3.10 single story FEM model.

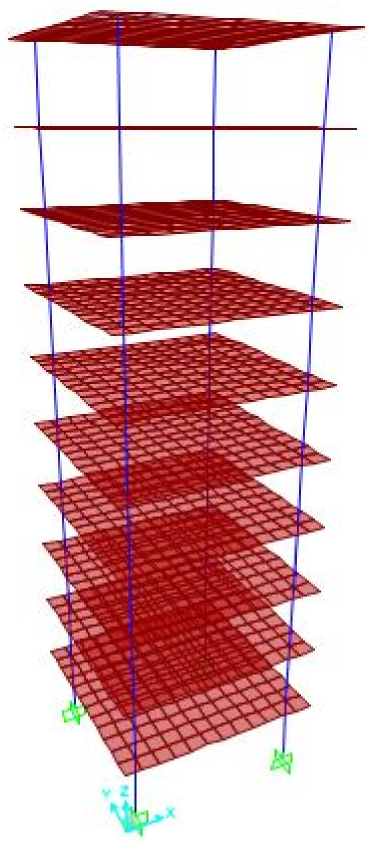

Figure 3.57: Example 3.10 multi-story FEM model.

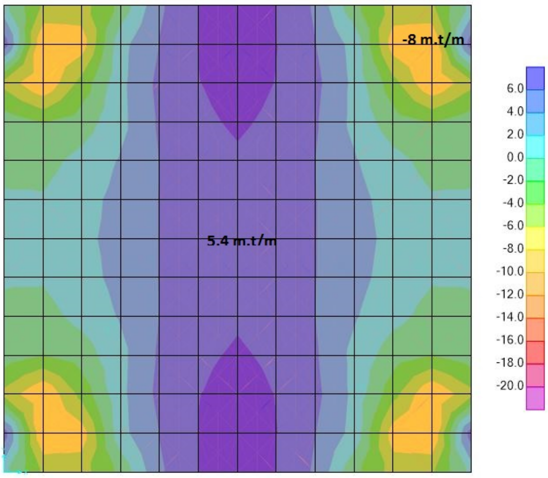

Figure 3.58: Example 3.10 bending moment M_{xx} for the FEM model due to gravity load 1 t/m².

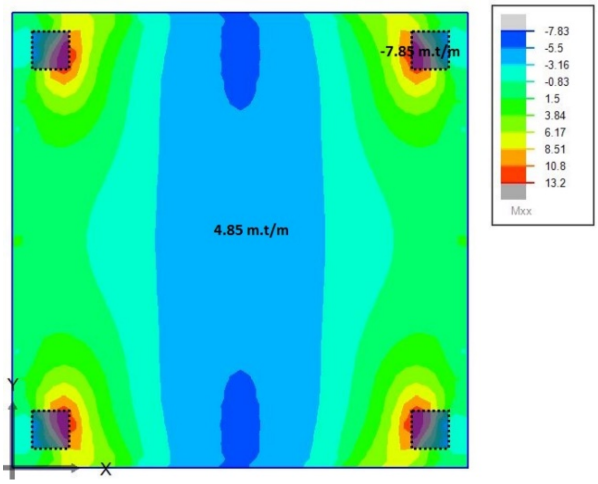

Figure 3.59: Example 3.10 bending moment M_{xx} for the BEM model due to gravity load 1 t/m².

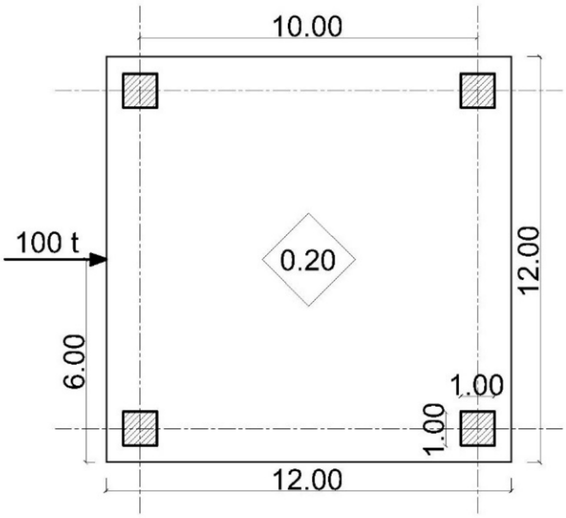

Figure 3.60: Direction, magnitude, and location of the applied lateral load in Example 3.10.

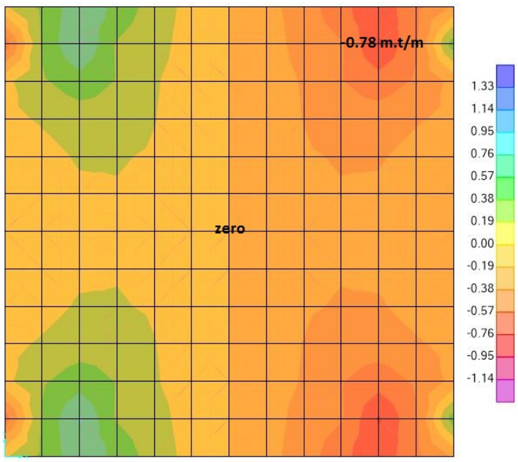

Figure 3.61: Example 3.10 bending moment M_{xx} for the FEM due to 100 t in x-direction.

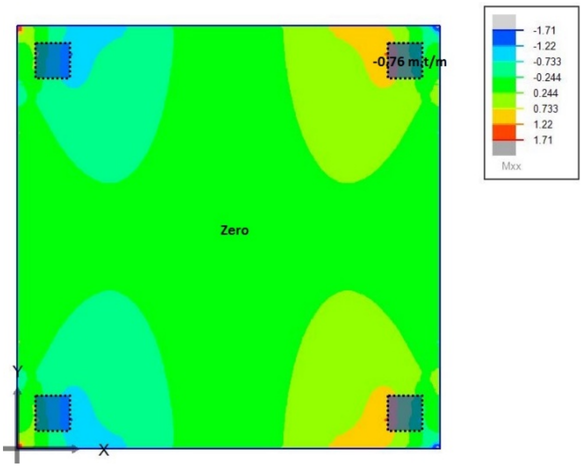

Figure 3.62: Example 3.10 bending moment M_{xx} for the BEM due to 100 t in x-direction.

Figure 3.63: Example 3.10 multi-story FEM solid & plate model.

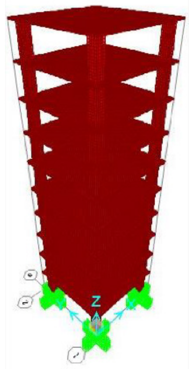

Figure 3.64: Example 3.10 multi-story FEM all solid model.

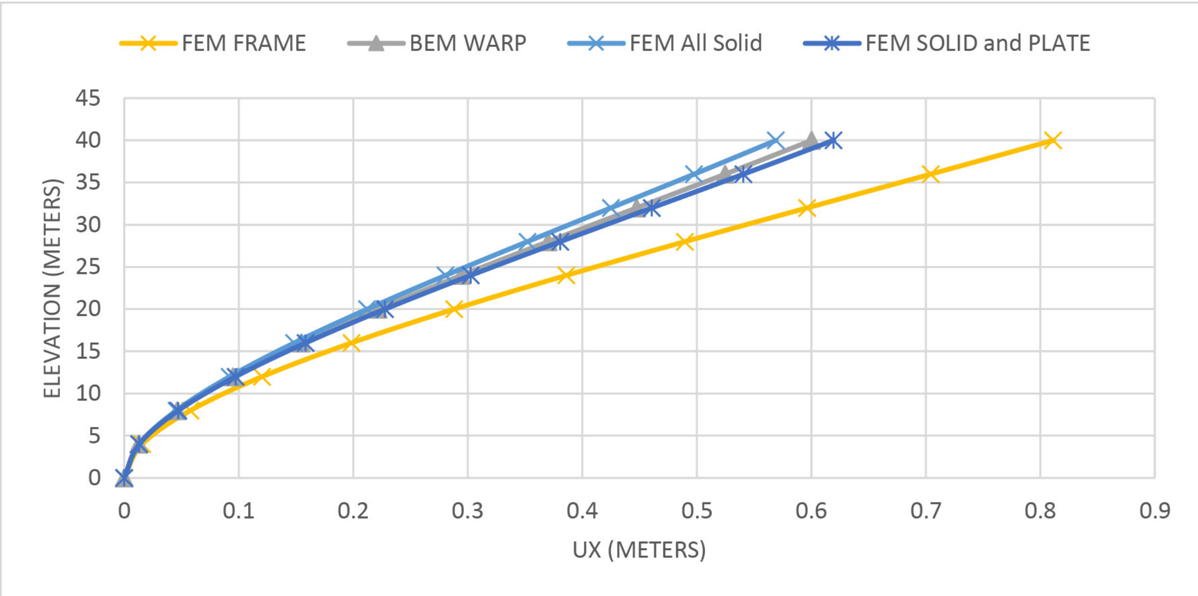

Figure 3.65: Example 3.10 U_x values along the building elevation.

Example 3.11 [33]

Purpose : Comparing the results of applying gravity loads and applying lateral loads on single-story or multi-story building (slabs resting on four beams and four columns) with other finite element software.

Description : Figure 3.66 shows Example 3.11 structural plan. Figure 3.67 shows the BEM model of the proposed technique. Figure 3.68 and Figure 3.69 show the FEM model of the single story and the multi-story building with 1m x 1m slab mesh. Firstly, uniform gravity load of 1 t/m^2 is applied on the single-story building. Secondly, a lateral load of 100 t is applied in x-direction on the highest floor in the single-story model and the multi-story model of 10 floors as shown in Figure 3.82.

Results : For the gravity loads, Figure 3.70-Figure 3.72 show the bending moment M_{xx} for the FEM, BEM mode 1 and BEM mode 2 respectively. Beams straining actions (bending moments, shearing force and torsional moments) are shown in Figure 3.73-Figure 3.81. The maximum deflection at the center of slab equals to 0.0173 m, 0.0156 m and 0.0154 m for the FEM, BEM mode 1 and BEM mode 2 respectively. For the lateral load on the single-story building, the lateral displacement U_x equals to 0.002105 m, 0.0020158 m and 0.0020103 m for the FEM, BEM mode 1 and BEM mode 2 respectively. It could be observed that lateral displacement in FEM is greater than in BEM due to the consideration of contact area effect in BEM. The lateral displacement for both BEM mode 1 and mode 2 is almost the same. While for the multi-story building, Figure 3.83 shows the values of the lateral displacement U_x versus floor's elevation for FEM, BEM mode 1 and BEM mode 2.

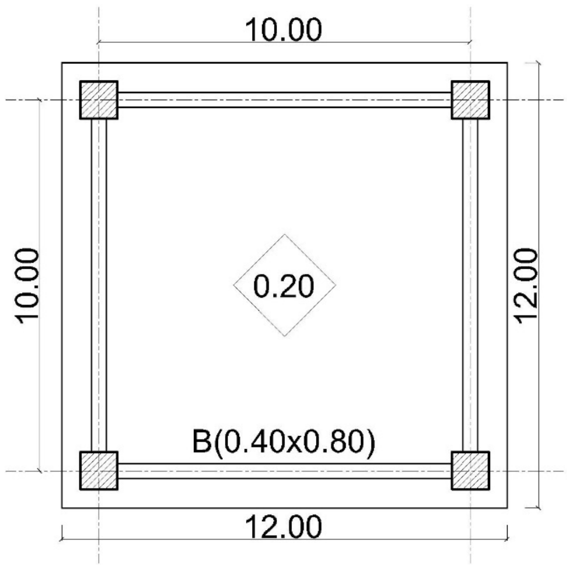

Figure 3.66: Example 3.11 structural Plan.

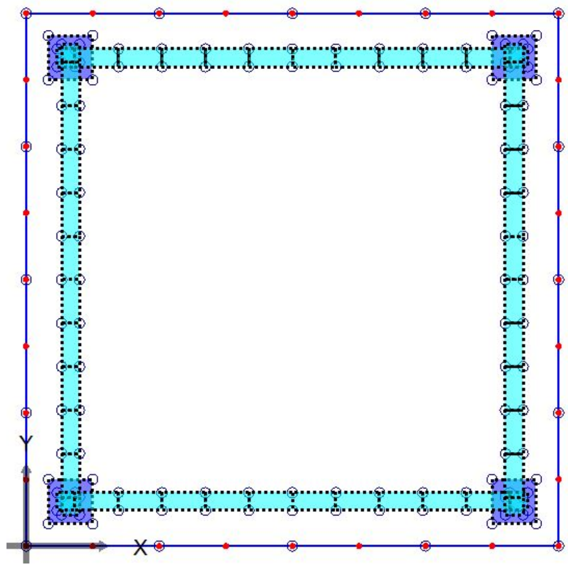

Figure 3.67: Example 3.11 BEM model.

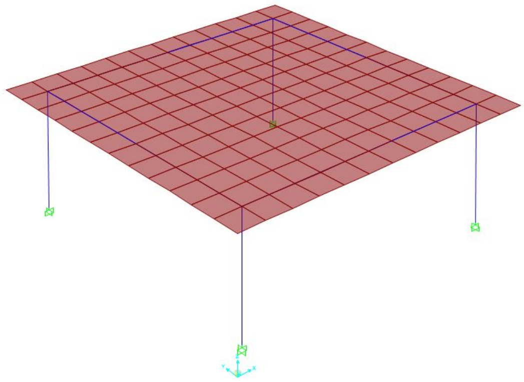

Figure 3.68: Example 3.11 single story FEM model.

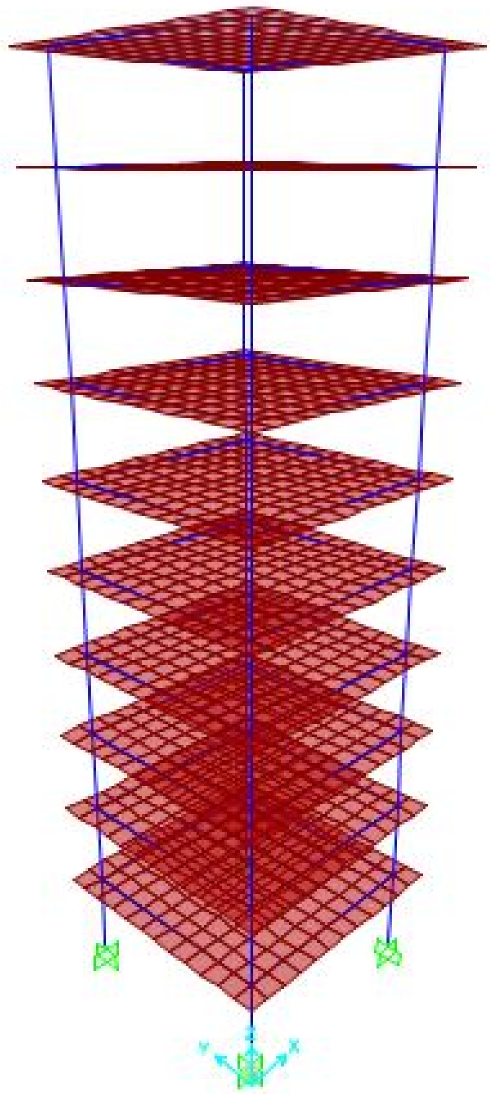

Figure 3.69: Example 3.11 multi-story FEM model.

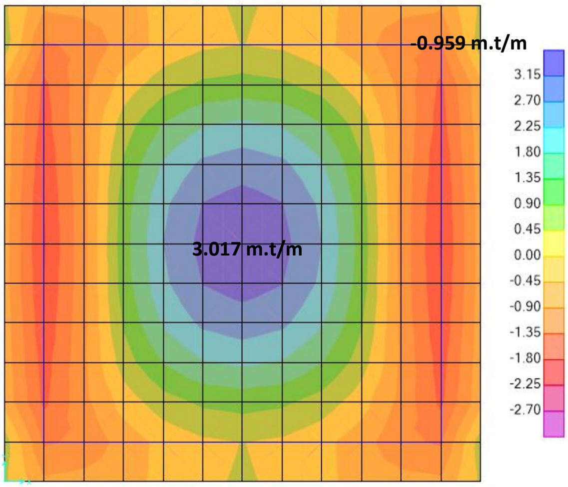

Figure 3.70: Example 3.11 bending moment M_{xx} for the FEM due to gravity load 1 t/m^2.

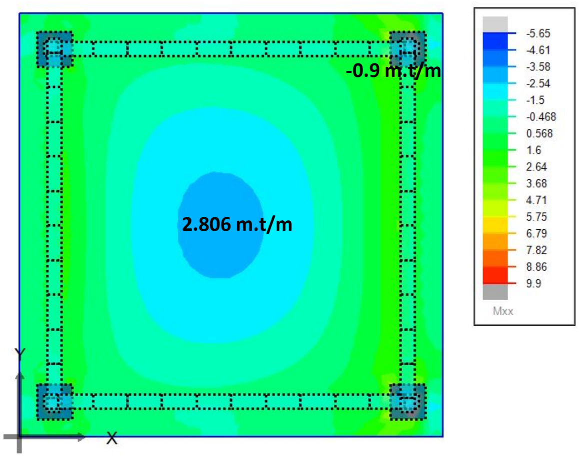

Figure 3.71: Example 3.11 bending moment M_{xx} for the BEM mode 1 due to gravity load 1 t/m^2.

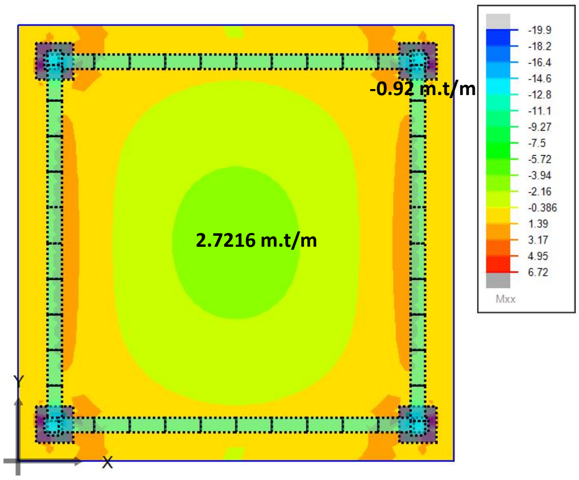

Figure 3.72: Example 3.11 bending moment M_{xx} for the BEM mode 2 due to gravity load 1 t/m^2.

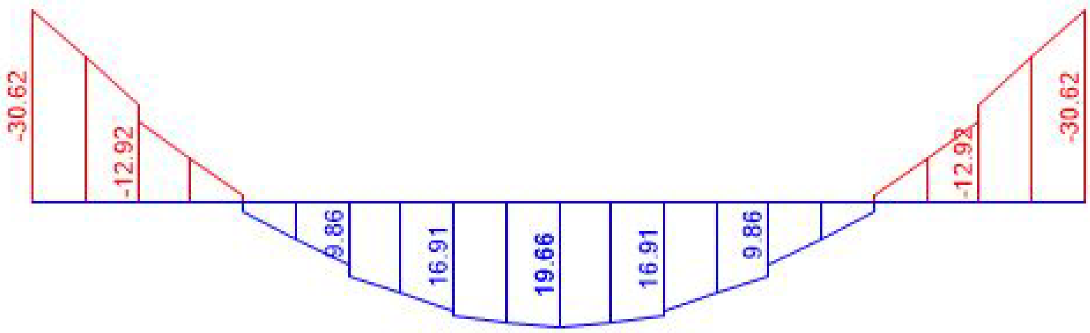

Figure 3.73: Example 3.11 beams bending moment in FEM due to gravity load 1 t/m².

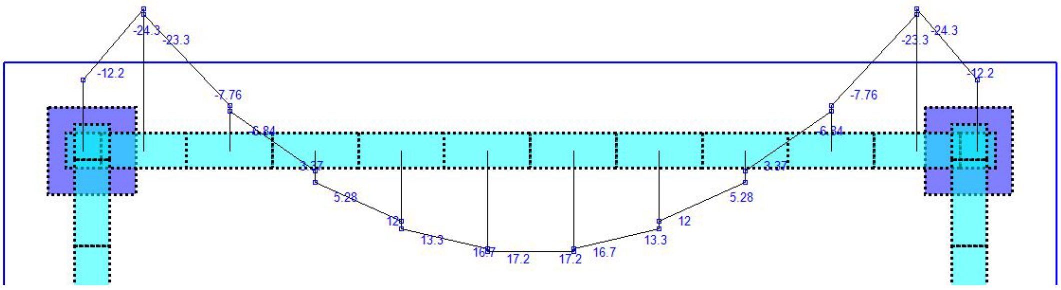

Figure 3.74: Example 3.11 beams bending moment in BEM mode 1 due to gravity load 1 t/m².

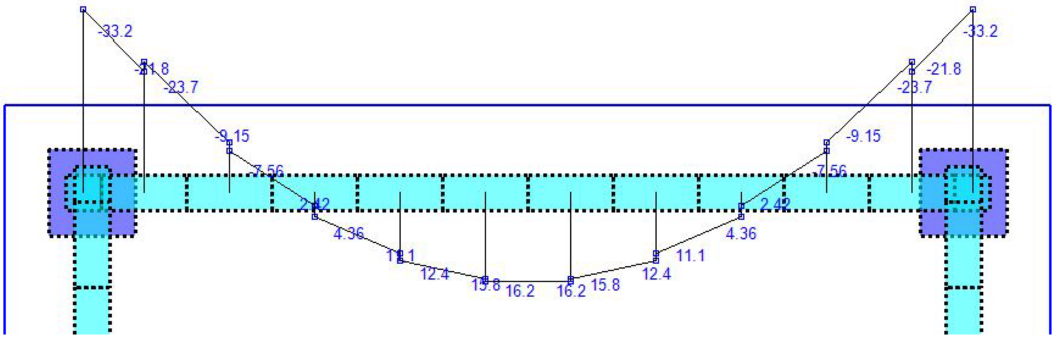

Figure 3.75: Example 3.11 beams bending moment in BEM mode 2 due to gravity load 1 t/m².

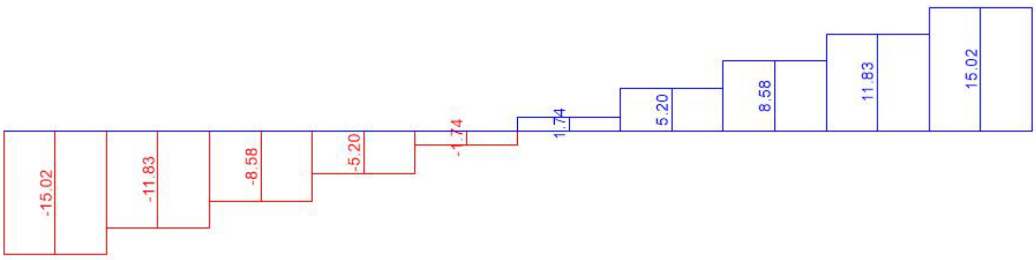

Figure 3.76: Example 3.11 beams shearing force in FEM due to gravity load 1 t/m².

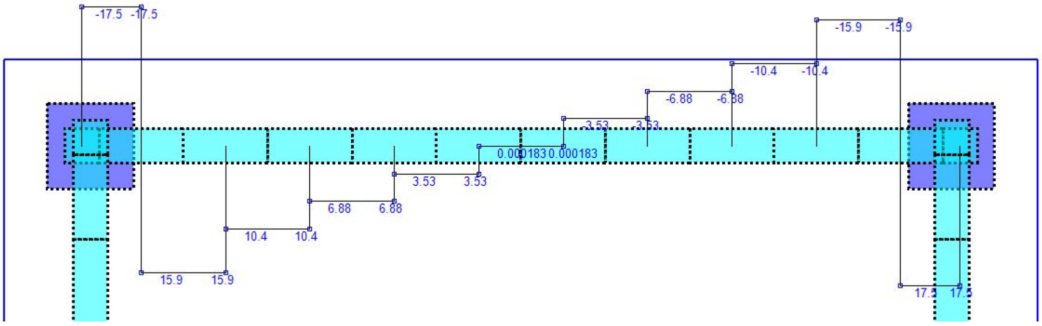

Figure 3.77: Example 3.11 beams shearing force in BEM mode 1 due to gravity load 1 t/m².

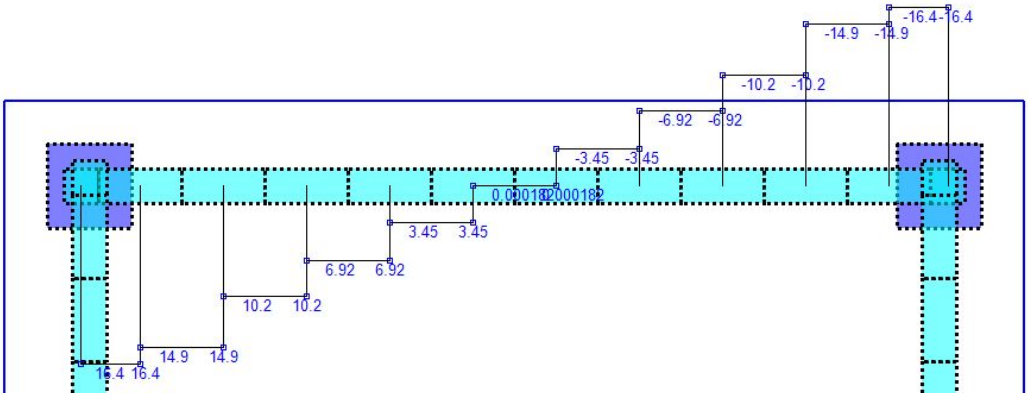

Figure 3.78: Example 3.11 beams shearing force in BEM mode 2 due to gravity load 1 t/m².

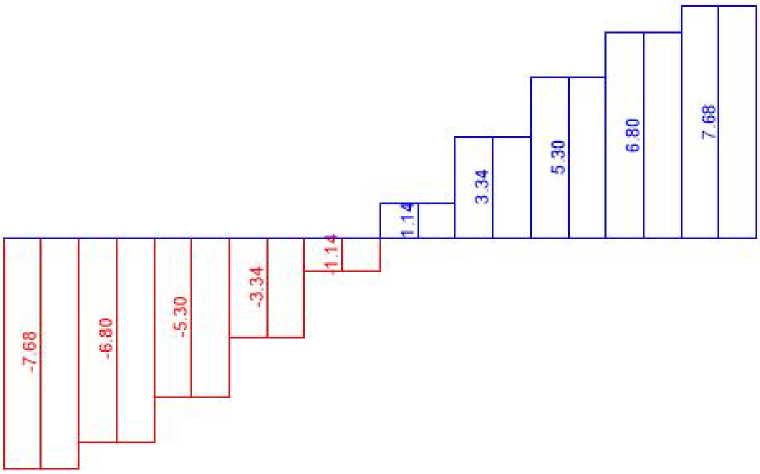

Figure 3.79: Example 3.11 beams Torsional moment in FEM due to gravity load 1 t/m².

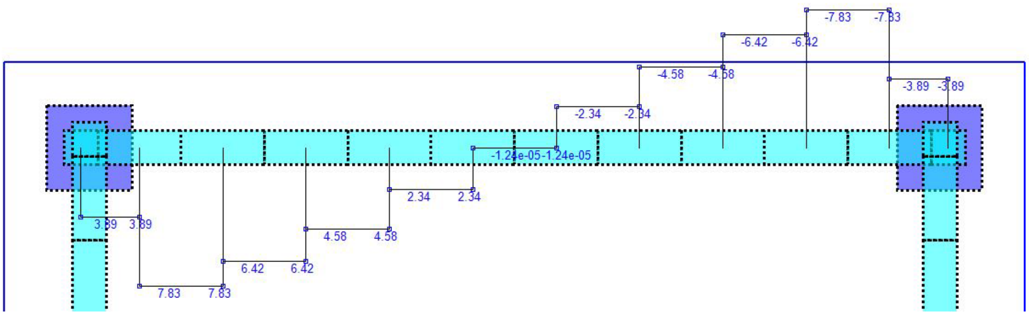

Figure 3.80: Example 3.11 beams Torsional moment in BEM mode 1 due to gravity load 1 t/m².

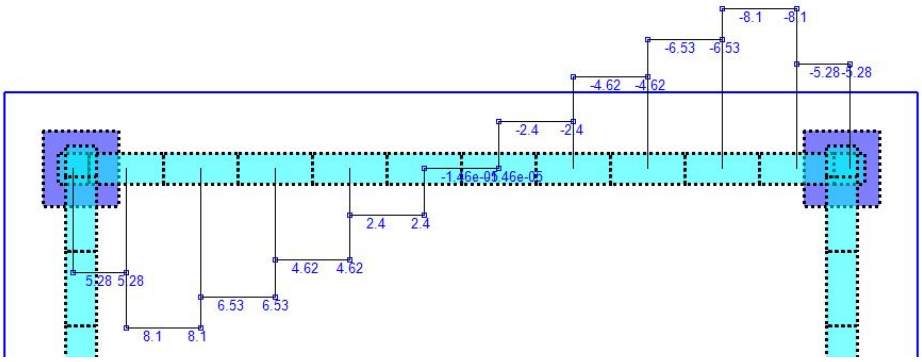

Figure 3.81: Example 3.11 beams Torsional moment in BEM mode 2 due to gravity load 1 t/m².

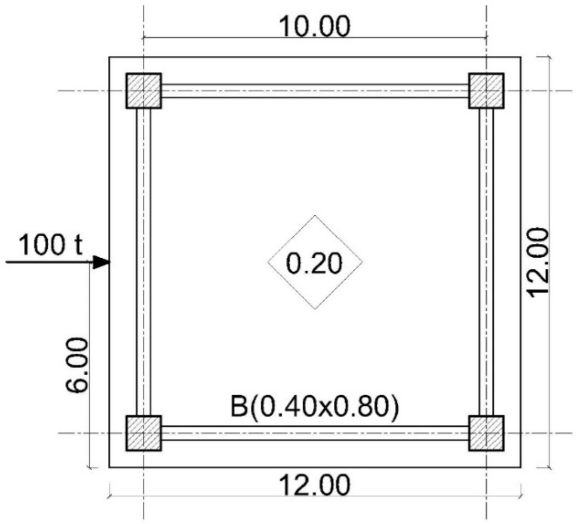

Figure 3.82: Direction, magnitude, and location of the applied lateral load in Example 3.11.

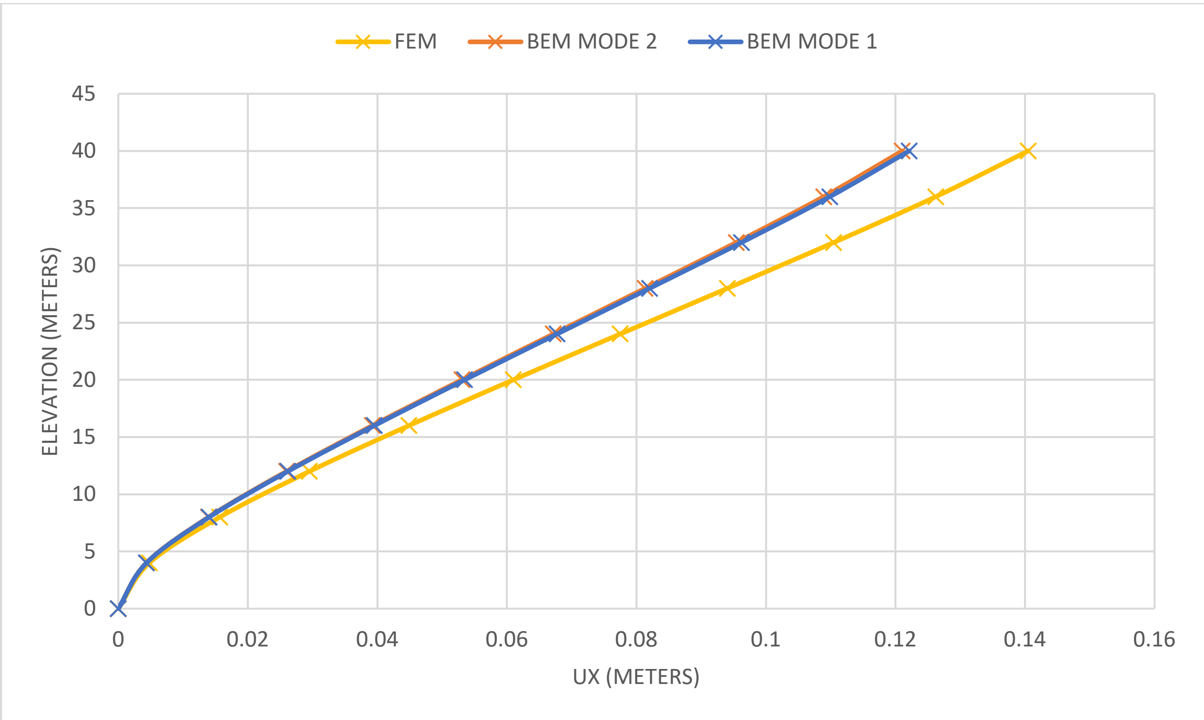

Figure 3.83: Example 3.11 U_x values along the building elevation.

Example 3.12 [33]

Purpose : Comparing the results of applying gravity loads and applying lateral loads on single-story or multi-story building (slabs resting on four beams, four columns, and a core) with other finite element software.

Description : Figure 3.84 shows Example 3.12 structural plan. Figure 3.85 shows the BEM model of the proposed technique. Figure 3.86 and Figure 3.87 show the FEM model of the single story and the multi-story building with 0.25m x 0.25m slab mesh. Firstly, uniform gravity load of 1 t/m^2 is applied on the single-story building. Secondly, a lateral load of 100 t is applied in x-direction on the highest floor in the single-story model and the multi-story model of 10 floors as shown in Figure 3.91.

Results : For the gravity loads, Figure 3.88-Figure 3.90 show the bending moment M_{xx} for the FEM, BEM mode 1 and BEM mode 2 respectively. The maximum deflection at the lower edge of the slab equals to 0.00196 m, 0.00167 m and 0.00164 m for the FEM, BEM mode 1 and BEM mode 2 respectively. For the lateral load on the single-story building, the lateral displacement U_x equals to 5.290E-04 m, 1.731E-04 m and 1.728E-04 m for the FEM, BEM mode 1 and BEM mode 2 respectively. It could be observed that lateral displacement in FEM is greater than in BEM due to the consideration of contact area effect in BEM. The lateral displacement for both BEM mode 1 and mode 2 is almost the same. While for the multi-story building, Figure 3.92 shows the values of the lateral displacement U_x versus floor's elevation for FEM, BEM mode 1 and BEM mode 2.

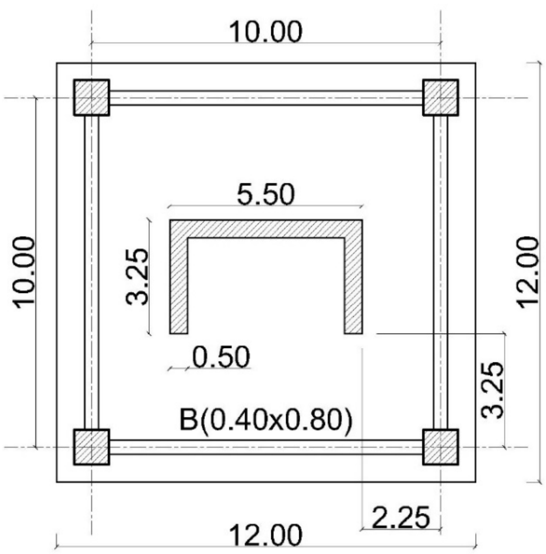

Figure 3.84: Example 3.12 structural Plan.

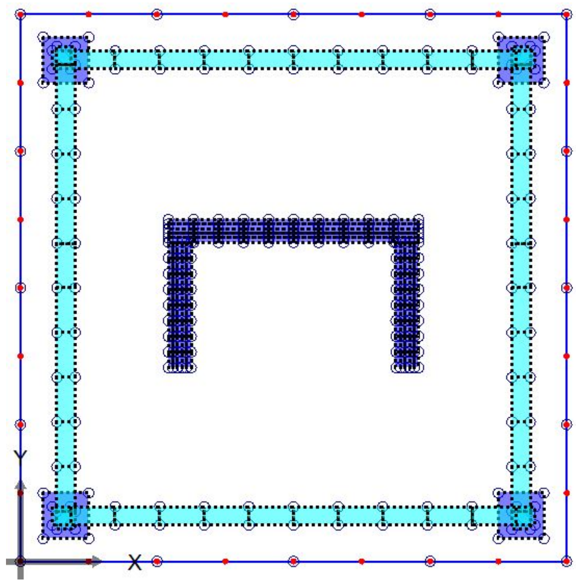

Figure 3.85: Example 3.12 BEM model.

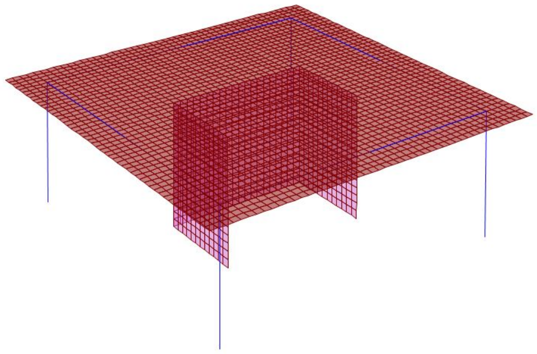

Figure 3.86: Example 3.12 single story FEM model.

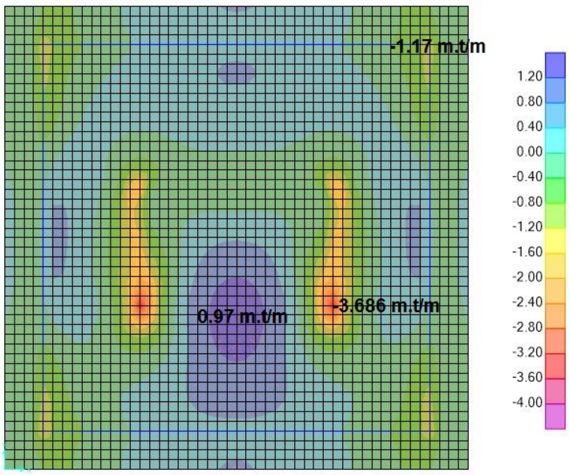

Figure 3.88: Example 3.12 bending moment M_{xx} for the FEM due to gravity load 1 t/m^2.

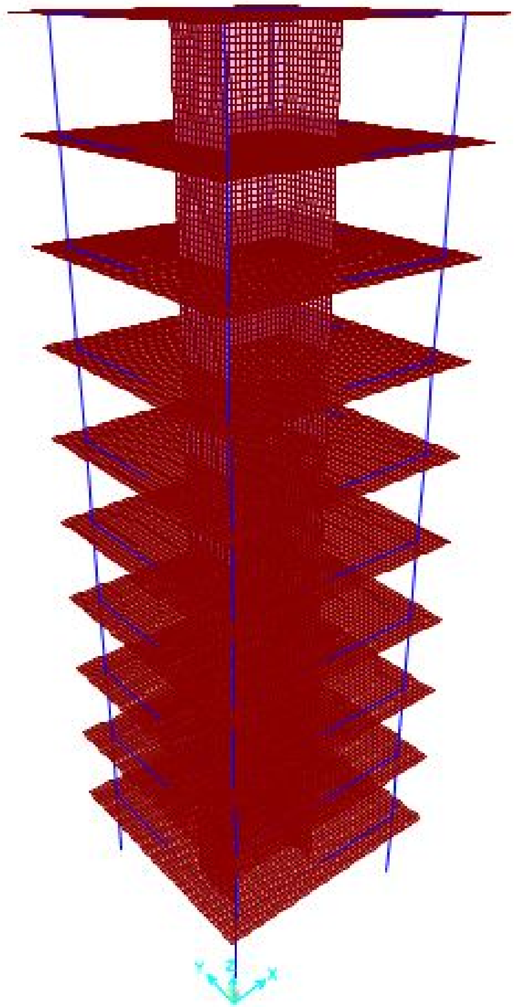

Figure 3.87: Example 3.12 multi-story FEM model.

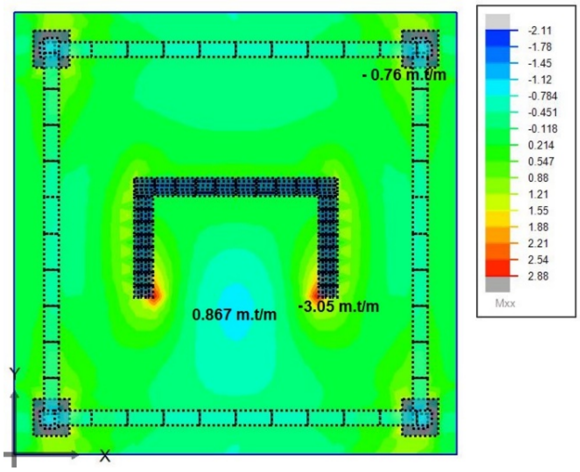

Figure 3.89: Example 3.12 bending moment M_{xx} for BEM mode 1 due to gravity load 1 t/m^2.

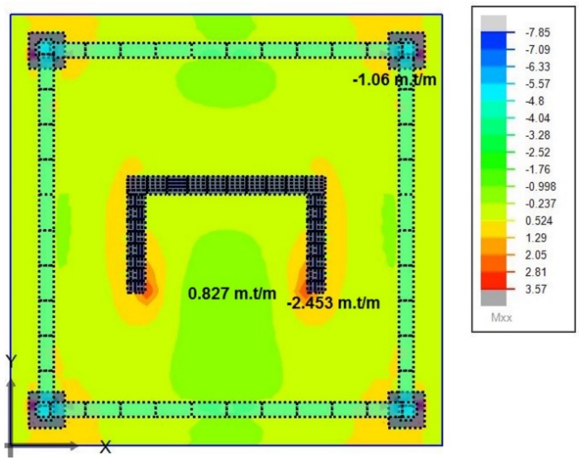

Figure 3.90: Example 3.12 bending moment M_{xx} for BEM mode 2 due to gravity load 1 t/m^2.

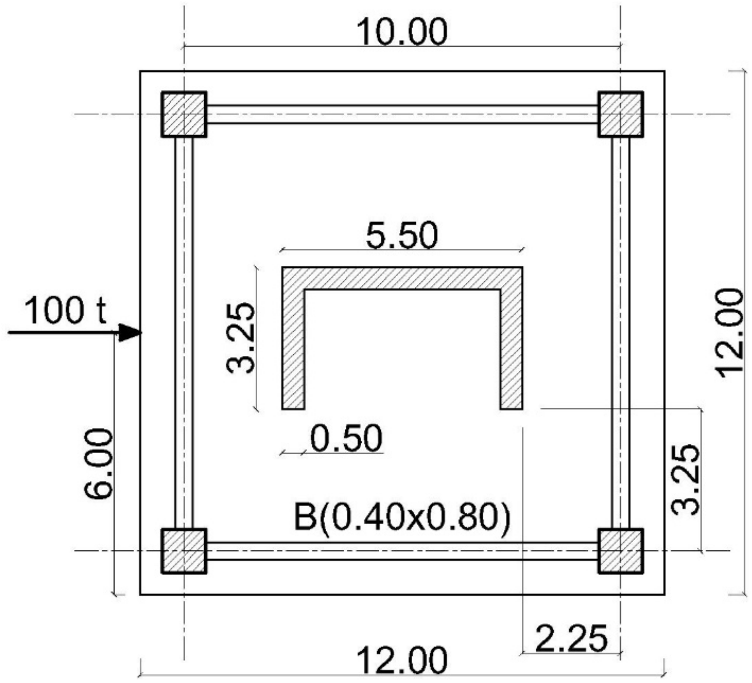

Figure 3.91: Direction, magnitude, and location of the applied lateral load in Example 3.12.

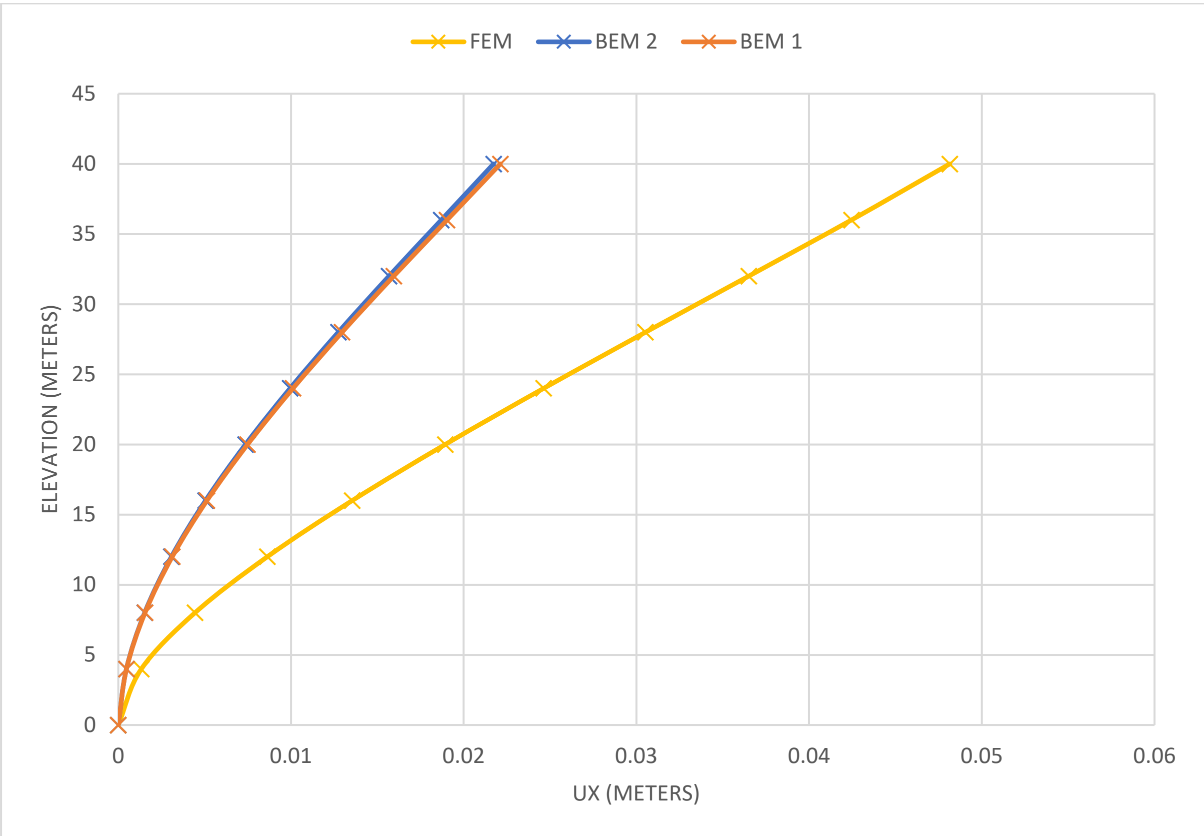

Figure 3.92: Example 3.12 U_x values along the building elevation.

Example 3.13

Purpose : Demonstrates the validation of the PLPAK in considering warping effects for warping wall of "L" shape.

Description : The slab, shown in Figure 3.93, has a thickness of 0.2 m and dimensions of 10x10 m. The wall dimensions are 4.5x4.5x0.5 m. The modulus of elasticity of the slab and wall material is taken equal to be 21680100 kPa and Poisson's ratio is set to 0.2 for the slab and zero for the wall. A 981 kN load is applied in the x-direction at a point which has x = 0 m, y = 5 m at the floor level. Only a single floor is considered with height equal to 3 m. The following numerical models are considered:

Model 1: The proposed formulation is employed to model the slab using continuous quadratic elements with element length of 1 m. In this model, the warping effect is neglected.

Model 2: is like model 1; but with considering the warping effects.

Model 3: walls are modeled as frame elements in this model. The slab is modeled as plate bending finite elements with a mesh size of 0.25 m. A diaphragm constraint is applied at the floor level. It should be noted that this model ignores warping.

Model 4: is like model 3 but the wall is modeled as shell finite elements with a mesh size of 0.25 m. It should be noted that this model considers warping effects.

Results : Figure 3.94 demonstrates deflection contour maps if warping is neglected. The contour maps of model 1 are in a good agreement with that of model 3. Figure 3.95 demonstrates deflection contour maps if warping is considered. The contour maps of model 2 are in a good agreement with that of model 4. It should be noted that, in this example, shell elements are considered to account for warping. Skeletal frame elements could be used; instead. However, when warping of angle cross section (as the case in this example) is considered, the use of shell finite elements (model 4) does not consider the warping of the angle cross section away from the angle center line. In the PLPAK, considering the cross-section area of the angle at the connection between column and slab, the sectorial coordinate away from the angle center line is calculated. Therefore, with single frame element, warping effects could be modeled as in model 2. This demonstrates the strength of the PLPAK in both warping modeling, and real connection between column and slab modeling.

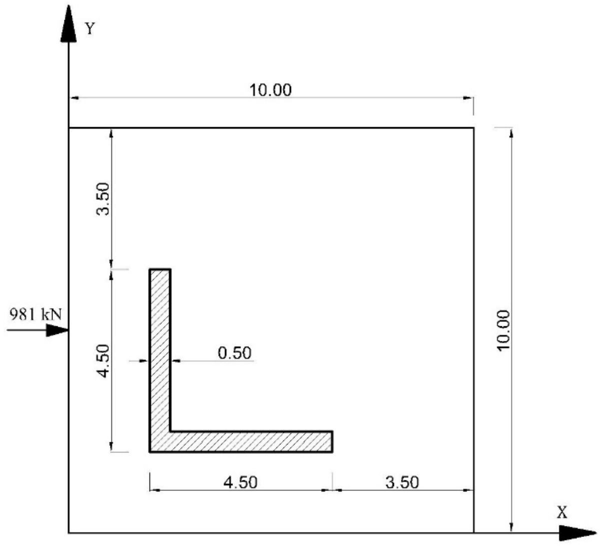

Figure 3.93: Dimensions of the considered slab in Example 3.13.

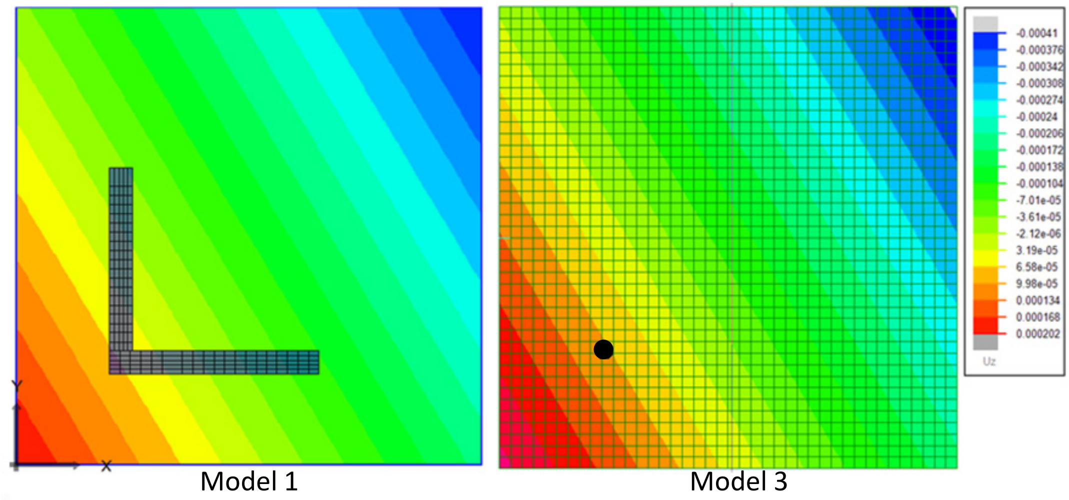

Figure 3.94: Comparison of deflection contour maps between model 1 and model 3 (warping is ignored) in Example 3.13.

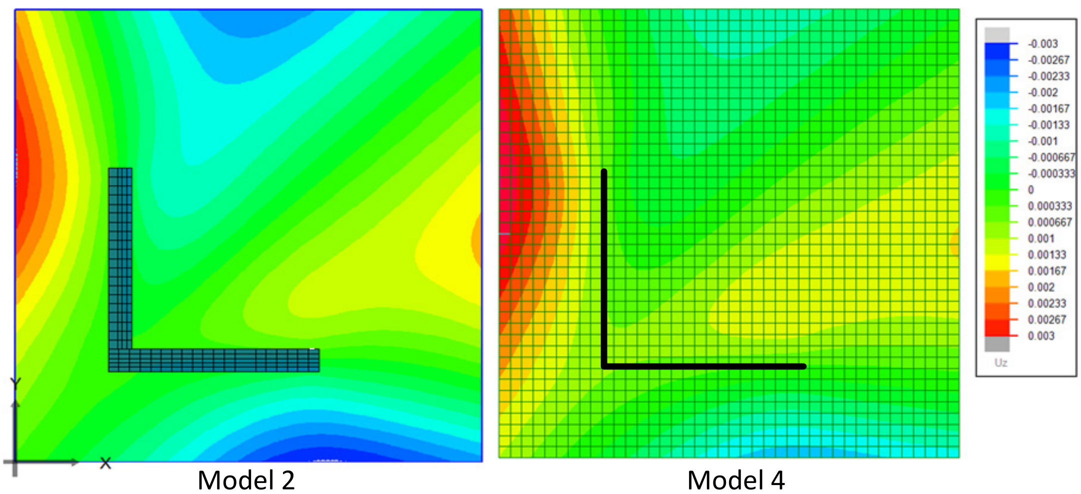

Figure 3.95: Comparison of deflection contour maps between model 2 and model 4 (warping is considered) in Example 3.13.

Example 3.14

Purpose : Demonstrates the validation of the PLPAK in considering warping effects for warping wall with "C" cross-section.

Description : In this example, the analysis of a 15-story building composed of an open C-section core is presented. The example is modeled based on the PLPAK both by considering the effect of warping deformations and by neglecting the floor stiffness effects. The PLPAK results are compared against the corresponding results of Taranath [34] which analyzed the same example based on the FEM. The example is shown in Figure 3.96. The core thickness is 0.3048 m (1 ft), story height is 3.81 m (12.5 ft), central core area = 6.5 m^2 (70 ft^2), I_x = 371.39 m^4 (43029.8 ft^4), I_y = 454.28 m^4 (52633.29 ft^4), I_w = 415.76 m^6 (518508.0 ft^6) and J = 0.201 m^4 (23.3 ft^4). The modulus of elasticity of core material is taken equal to be 27579024 kPa (576000 kip/sq.ft), and Poisson's ratio is taken equal to 0.2. A lateral load of 1.197 kPa (25 psf) is applied over the full height.

Results : Figure 3.97 and Figure 3.98 demonstrate the rotation and the bi-moment along the height of the central core. Both the rotation and the bi-moment results are in good agreement with results of [34].

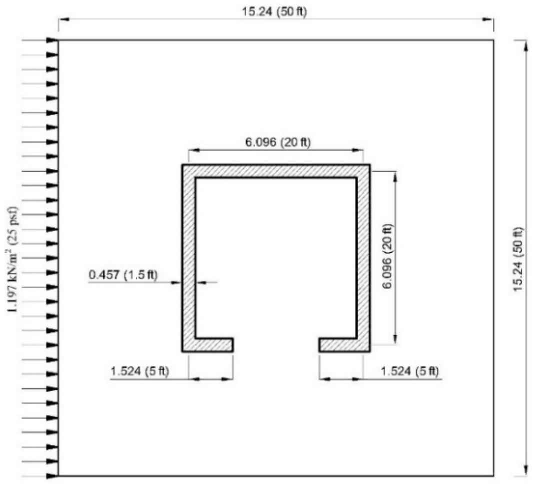

Figure 3.96: Dimensions of slab and core considered in Example 3.14.

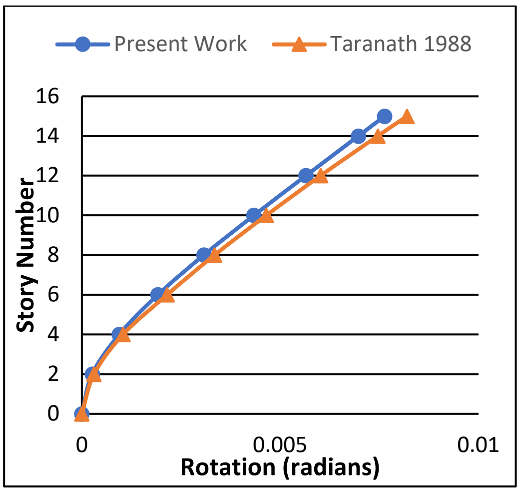

Figure 3.97: Rotation results at different story level in Example 3.14.

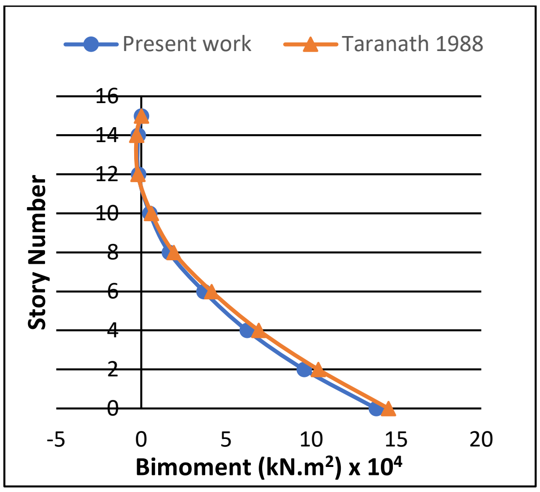

Figure 3.98: Bi-moment results at different story level in Example 3.14.

Example 3.15

Purpose : Demonstrates the validation of the PLPAK in considering warping effects for slab resting on three walls.

Description : In this example, a 20-story building composed of an open core and two I-shaped shear walls is analyzed as shown in Figure 3.99. The considered geometric data are:

All walls' thicknesses = 0.0508 m (2 in); Story height = 0.3175 m (12.5 in)

Central core: Area = 0.1445 m^2 (224 in^2), I_x = 0.0116 m^4 (27869.3 in^4), I_y = 0.02388 m^4 (57389.3 in^4), I_w = 3.261x10^{-3} m^6 (12143880 in^6) and J = 1.243x10^{-4} m^4 (298.7 in^4).

I-shaped walls: Area =0.1135 m^2 (176 in^2), I_x = 0.02685 m^4 (64512 in^4), I_y = 1.11x10^{-3} m^4 (2666.7 in^4), I_w = 4.124x10^{-4} m^6 (1536000 in^6) and J = 9.7689x10^{-5} m^4 (234.7 in^4). Modulus of elasticity of the slab, walls and core materials are taken equal to 2757889 kPa (400.0) ksi and Poisson's ratio is taken equal to 0.15. A unit clockwise torque is applied at the top slab.

Three numerical models are considered. The first model is based on the PLPAK as shown in Figure 3.100 by considering the effect of warping deformation together with the slab stiffness. The second one is like the first model but with ignoring the slab stiffness. The third one is like the first model but with ignoring the slab stiffness and the effect of warping. The same problem was analyzed by Taranath [35] using shell finite elements and by Gendy [36] using accuracy enhancement of hybrid/mixed models for thin-walled beam assemblages.

Results : Figure 3.101 and Figure 3.102 demonstrate a comparison of the displacements and the rotation at each floor level. The total internal torque and the bi-moment distributions along the height of the central core are demonstrated in Figure 3.103 and Figure 3.104. These results conclude that the PLPAK results agree with previous published results of Taranath [35] and Gendy [36]; which verify the PLPAK.

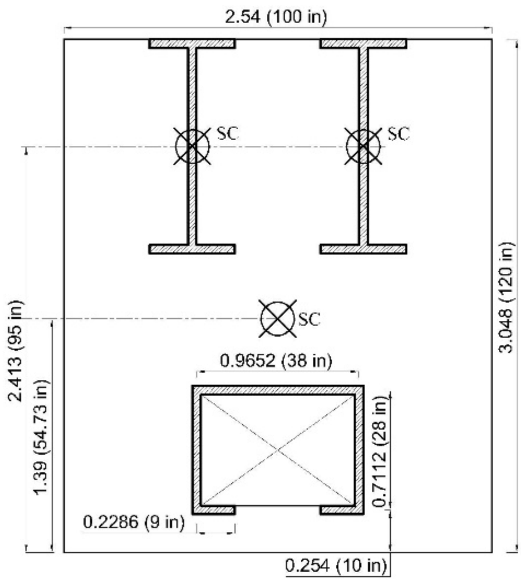

Figure 3.99: Dimensions of the considered slab in Example 3.15.

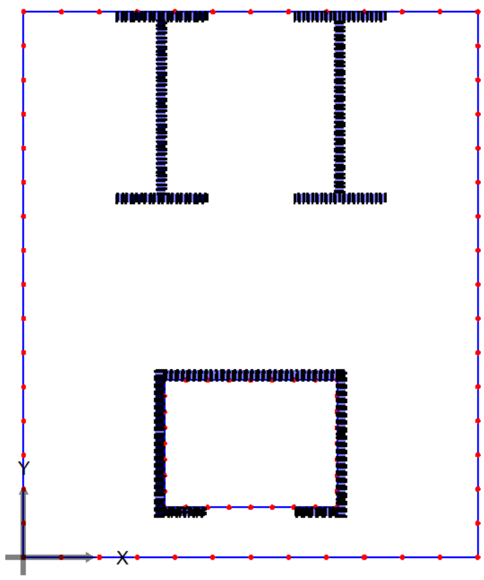

Figure 3.100: The considered boundary element discretization of the slab in Example 3.15.

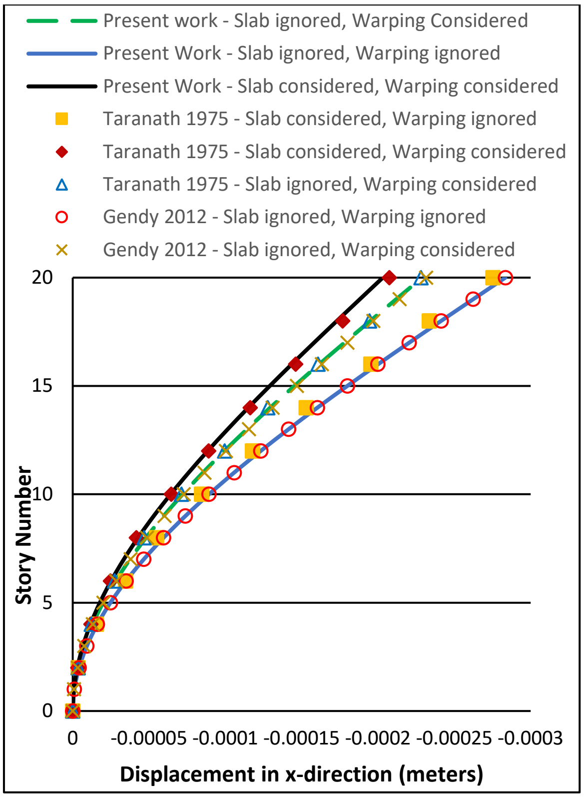

Figure 3.101: Displacement (meters) in x-direction in Example 3.15.

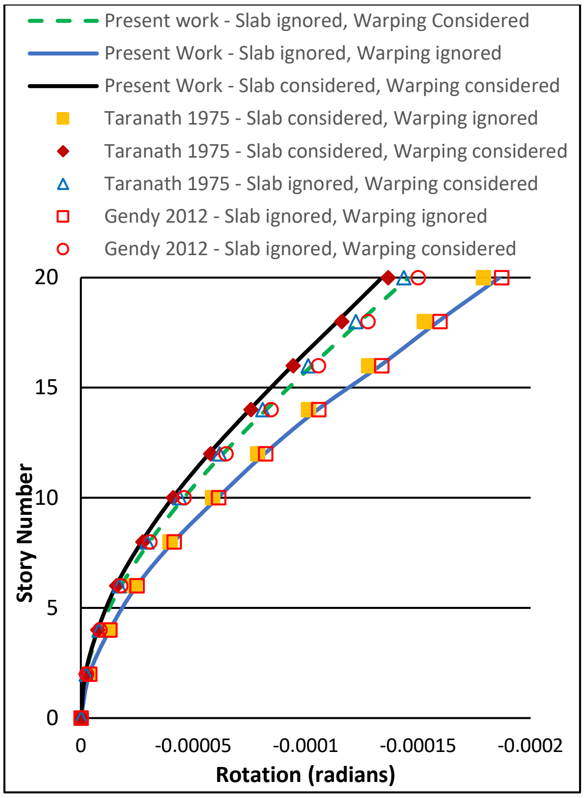

Figure 3.102: Distribution of the angle of twist along the shear wall building in Example 3.15.

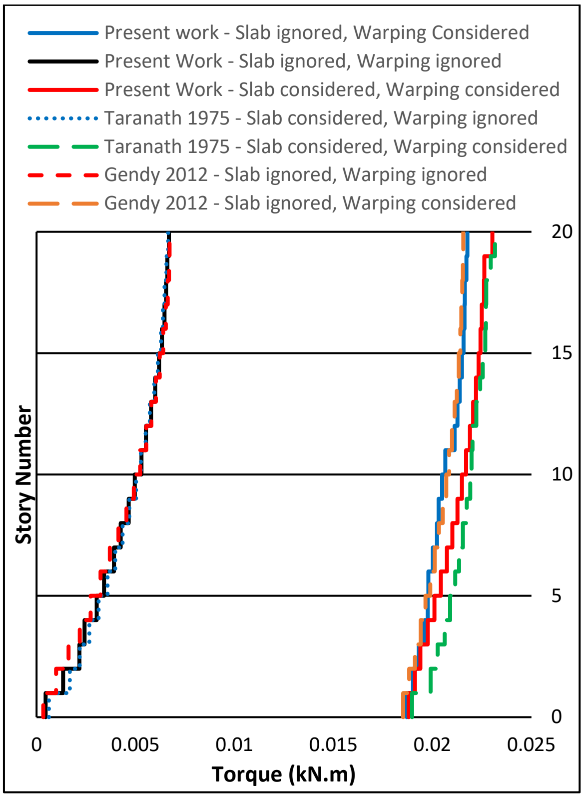

Figure 3.103: Distribution of total torque in the central core in Example 3.15.

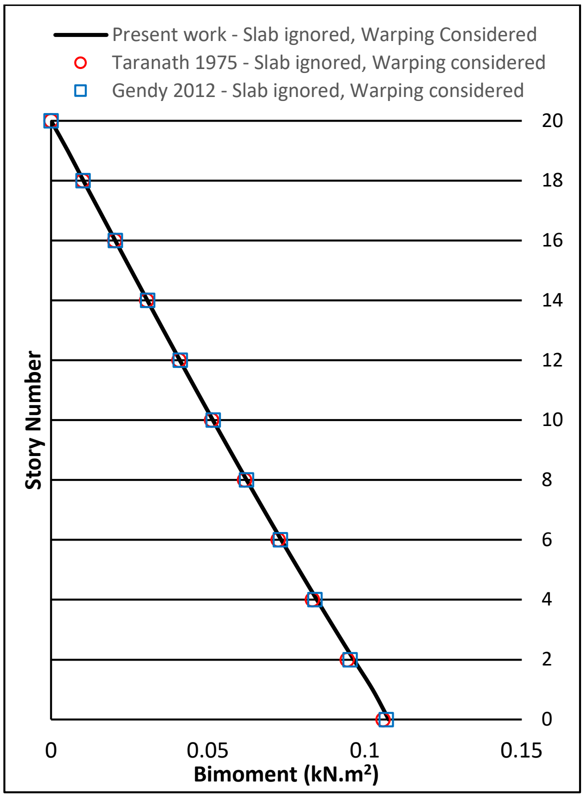

Figure 3.104: Distribution of bi-moment along the central core in Example 3.15.

Example 3.16

Purpose : Demonstrate the capability of the PLPAK to solve practical buildings and showing its efficiency from the point of view of value engineering.

Description : The floor plan shown in Figure 3.105 was analyzed. The slab has a thickness of 0.32m. Both slab and vertical elements material has modulus of elasticity equal to 21680100 kPa and Poisson's ratio equal to 0.2. The height of each story is 3.4m. Simplified seismic analysis is performed on this building in x-direction. The PLPAK (BEM) is used, and the results were compared to those obtained from finite element method (FEM) Figure 3.106 and Figure 3.107. Displacements obtained from both methods are used to check the adequacy of the lateral resisting system according to the Eurocode 8 [37]. Eurocode 8 [37] Clause 4.4.2.2(2) provides a limiting value of 0.3 to the inter-story drift sensitivity coefficient (θ):

$\theta = \frac{P_{tot} \times d_r}{V_{tot} \times h}$, where P_{tot} is the total gravity load at and above the story considered in the seismic design situation; d_r is the design inter-story drift, evaluated as the difference of the average displacements d_s at the top and bottom of the storey under considerations and calculated in accordance with Eurocode 8 (Eurocode8 1996) Clause 4.3.4; V_{tot} is the total seismic story shear; and h is the inter-story height. Base shear (F_b) can be estimated as a percentage from the total gravity loads, for simplicity, considered in the seismic design situation (5 to 10%), 10% is used here in this example. Distribution of the horizontal seismic forces is achieved using the following equation (Eurocode 8 [37] Clause 4.3.3.2.3(3)):

$F_i = F_b \times \frac{z_i m_i}{\sum z_j m_j}$, where F_i is the horizontal force acting on story i; z_i, z_j are the heights of the masses m_i m_j above the level of application of the seismic action (foundation or top of a rigid basement); and m_i, m_j are the story masses.

Results : Drift corresponding to the maximum value of θ obtained from both analysis methods is plotted against the number of stories in Figure 3.108. The value of drift obtained from the PLPAK is less than that obtained from FEM. The maximum value of θ is plotted also against the number of stories Figure 3.109. For the same building with same dimensions and same lateral resisting system, FEM exceeds the code limit for θ when it is 28 story-height only and BEM exceeds the code limit when it is 34 story-height. Additional 6 floors (21.4%) can be considered as a safe design just by including the effect of the real geometry of slab-column connecting area into the analysis of the building presented in this example.

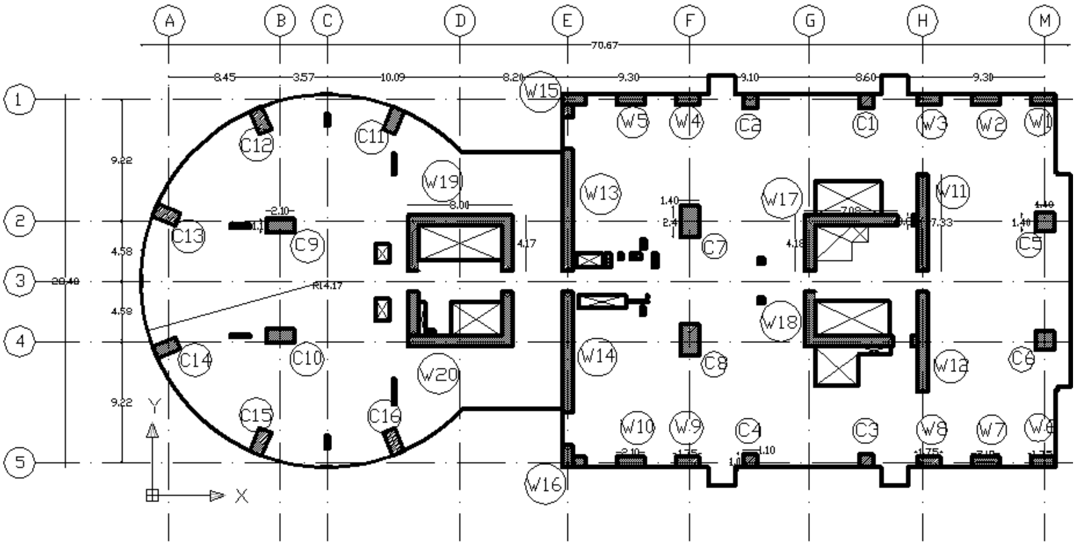

Figure 3.105: Plan of the typical floor in the building in Example 3.16.

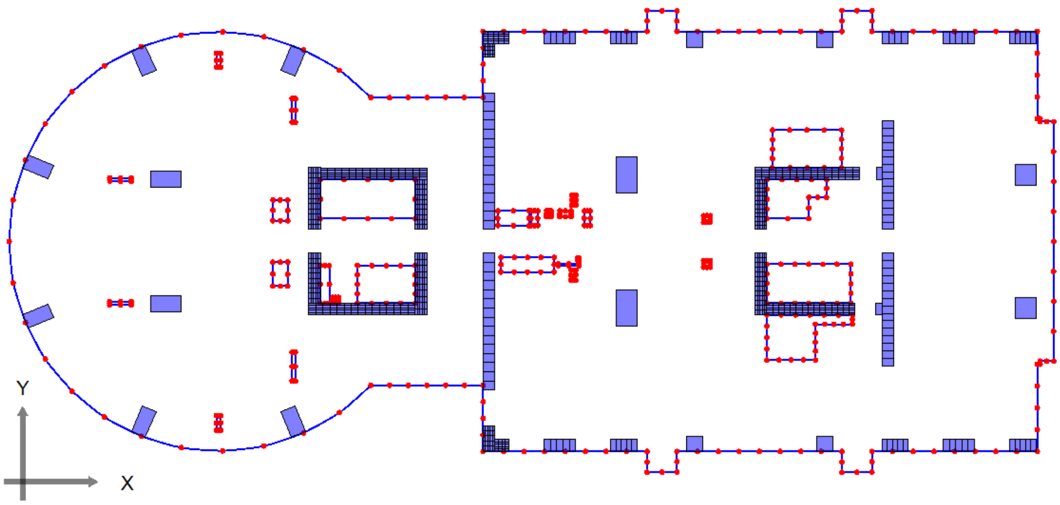

Figure 3.106: Boundary element model in Example 3.16.

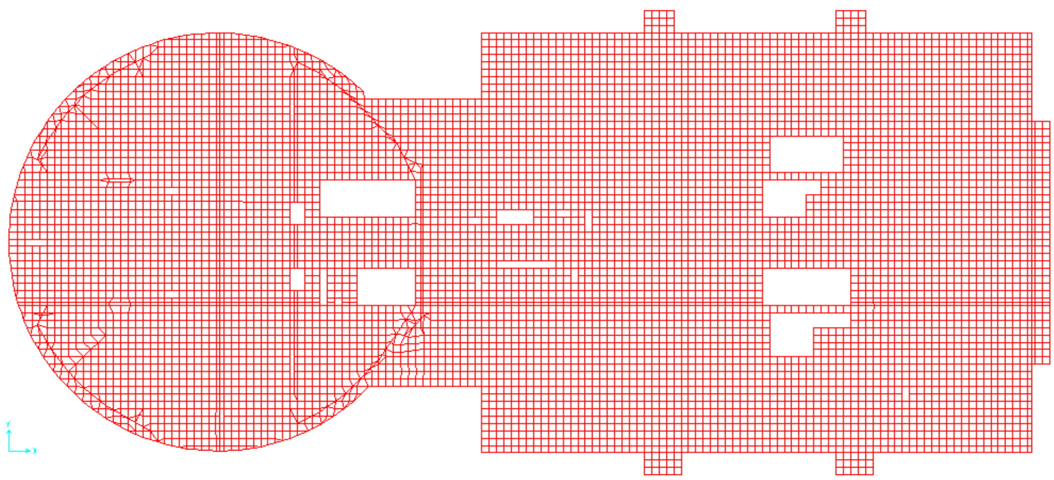

Figure 3.107: Finite element model in Example 3.16.

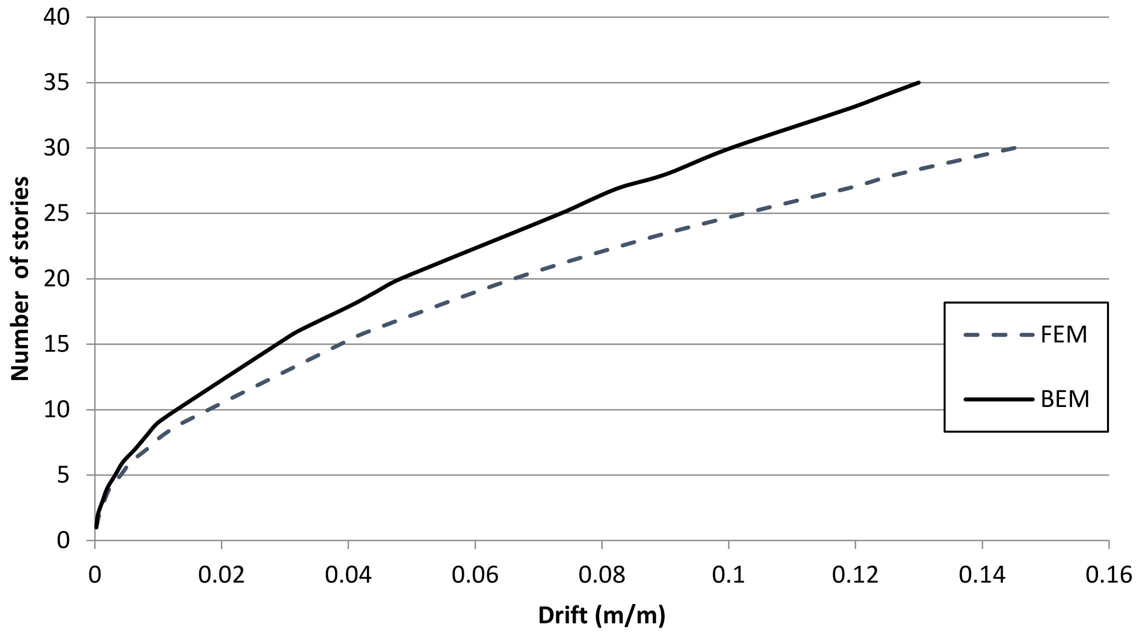

Figure 3.108: Shows the relation between the drift corresponding to the maximum value of theta and the number of floors in Example 3.16.

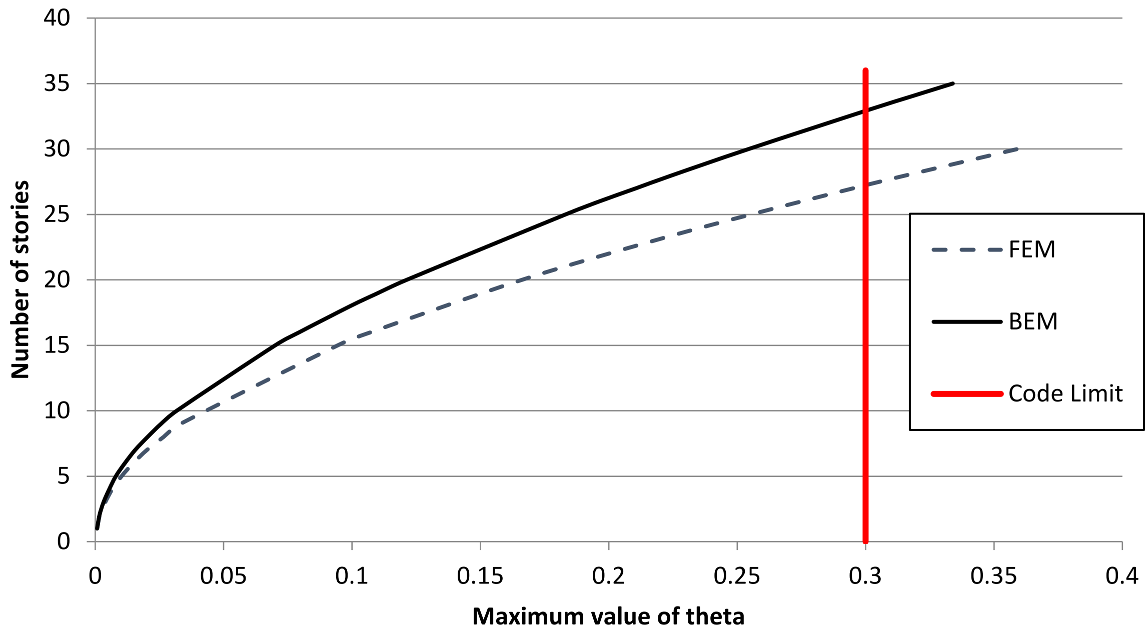

Figure 3.109: Shows the relation between the maximum value of theta and the number of stories in Example 3.16.. It shows also the code limit value (0.3).

4. The Design (PLDesign) Tool:

The Design tool is mainly used to design slabs, rafts, and beams. This tool supports:

- ACI, EN, ECP building codes.
- Different slab design methods (basic and additional reinforcement mesh, strip design, and multiple strip design).
- Punching check for regular and irregular columns' cross section with or without warping effects.
- Deflection check, even for irregular spans.
- Easy design for beams
- Works as post-processor for all PLPAK packages
- Save designs
- All designs and reinforcement details could be automatically exported to ACAD or Revit environment.
- Export calculation sheets and Auto CAD drawings
- Import and export DXF, text and Excel files

To verify the applicability of the proposed standards for solving practical structural engineering applications (slabs and foundations), the standards were implemented into prototype software using object-oriented programming. The software included preprocessing, postprocessing, and automated design modules. The prototype was utilized in many research projects; in addition, it was also applied for the structural analysis and design of practical structural engineering applications. Three examples are presented to demonstrate the applicability of the standards to be implemented into software that may be utilized for the solution of practical structural engineering problems. The assessment criteria presented in Table 4.1 is used to verify the applicability of the proposed standards to be implemented into structural engineering software. The performance of the proposed prototype is compared to standard FEM-BIM engines via comparing modeling time; the results are demonstrated in Table 4.2. The modeling times in Table 4.2 are the average of 10–15 engineers who were asked to model the problem using both approaches.

Table 4.1: Verification Criteria for Example 4.1-Example 4.3.

SW module	Assessment aspect	Assessed in	Achieved in prototype
Pre-processor	BIM object structure	Example 4.1	✓
	GUI operation	Example 4.1	✓
	Interconnectivity	Example 4.1	✓
Post-processor	BIM object structure	Example 4.2	✓
	GUI operation	Example 4.2	✓
	Control of BE solution	Example 4.2	✓
	Interconnectivity	Example 4.2	✓
Automated design	BIM object structure	Example 4.3	✓
	GUI operation	Example 4.3	✓
	Various design methodologies	Example 4.3	✓
	Detailing options	Example 4.3	✓
	Interconnectivity	Example 4.3	✓

Table 4.2: Performance Evaluation for Example 4.1-Example 4.3.

Example	Standard FEM-BIM modeling time (min)	Proposed BEM-BIM modeling time (min)
Example 4.1	60	50
Example 4.2	180	45
Example 4.3	120	100

Example 4.1 [38]

Purpose	:	Input of High-Rise Building Floor
Description	:	The high-rise building presented in Figure 4.1 was imported from a CAD drawing into the prototype preprocessor automatically to produce the BIM demonstrated in Figure 4.2. The 3D view of the floor and the BEM of the floor are presented in Figure 4.3 and Figure 4.4, respectively.
Results	:	The input of this example verifies the object structure, GUI operation, and interconnectivity requirements of the BIM-based preprocessor stated in section “Proposed BIM-Based Preprocessing,” (Table 4.1). Table 4.2 indicates that it takes less time for engineers to model the problem using this approach than commercial FEM-BIM packages.

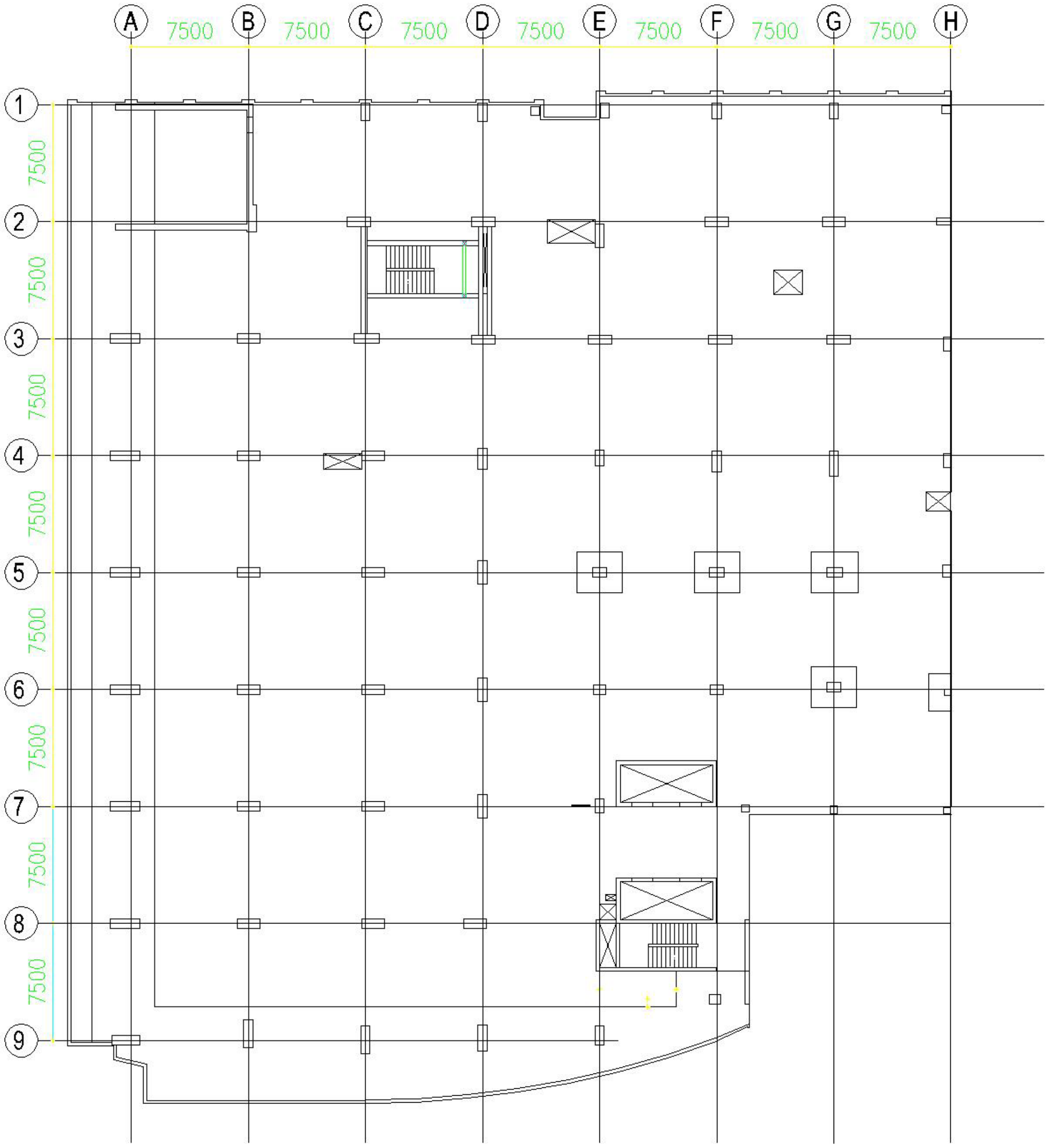

Figure 4.1: High-rise building structural drawing in Example 4.1.

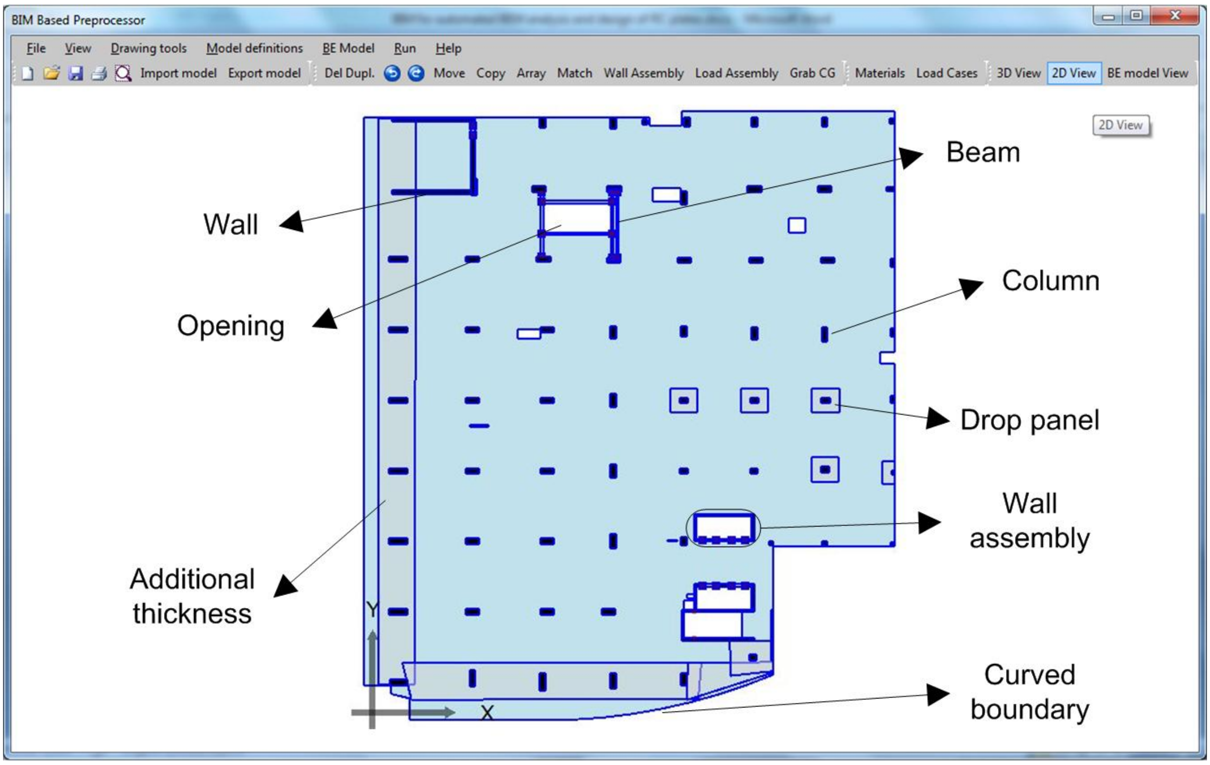

Figure 4.2: BIM of the high-rise building in the preprocessing stage in Example 4.1.

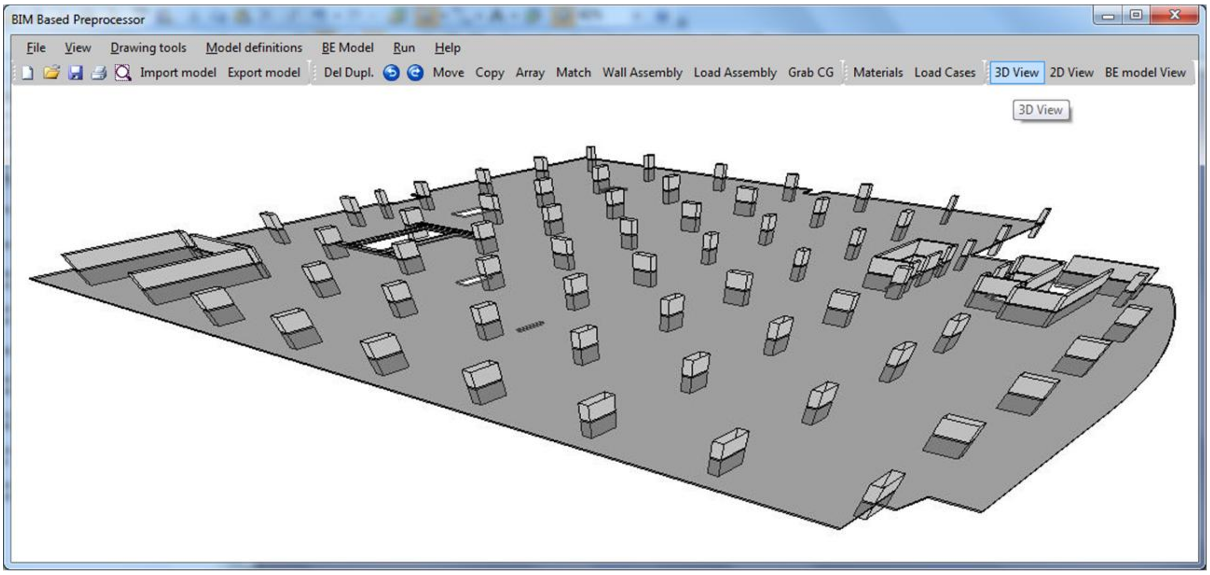

Figure 4.3: 3D model building in the preprocessing stage in Example 4.1.

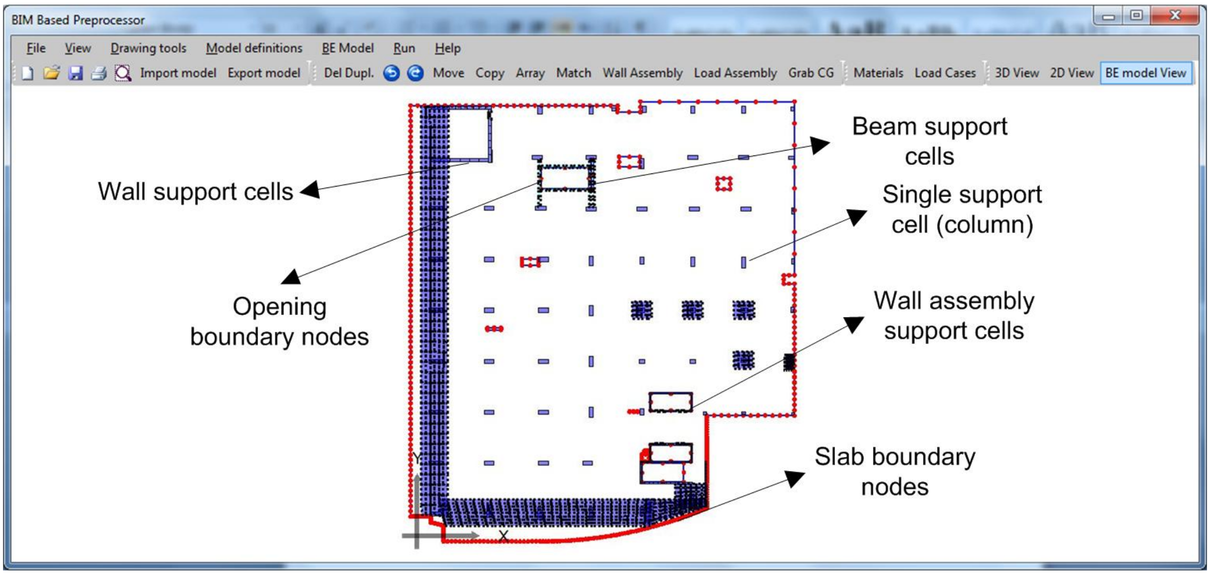

Figure 4.4: BIM-BEM model view of the high-rise building in Example 4.1.

Example 4.2 [38]

Purpose : Piled Raft Foundation Analysis Results

Description : The analysis results for the piles and soil support are captured from GUI and presented in Figure 4.5. Slab results in the forms of analysis strips and local and global contours are demonstrated in Figure 4.6.

Results : The analysis results depicted in these figures verify the requirements of the BIM results' objects, GUI, data flow, and control of second mode of BE solution (Table 4.1). The comparison in Table 4.2 for this problem shows a large difference in modeling time; the difference is in favor of the proposed BEM-BIM prototype because the commercial FEM-BIM packages require a lot of effort from engineers in modeling, mainly due to mesh adjustment requirements.

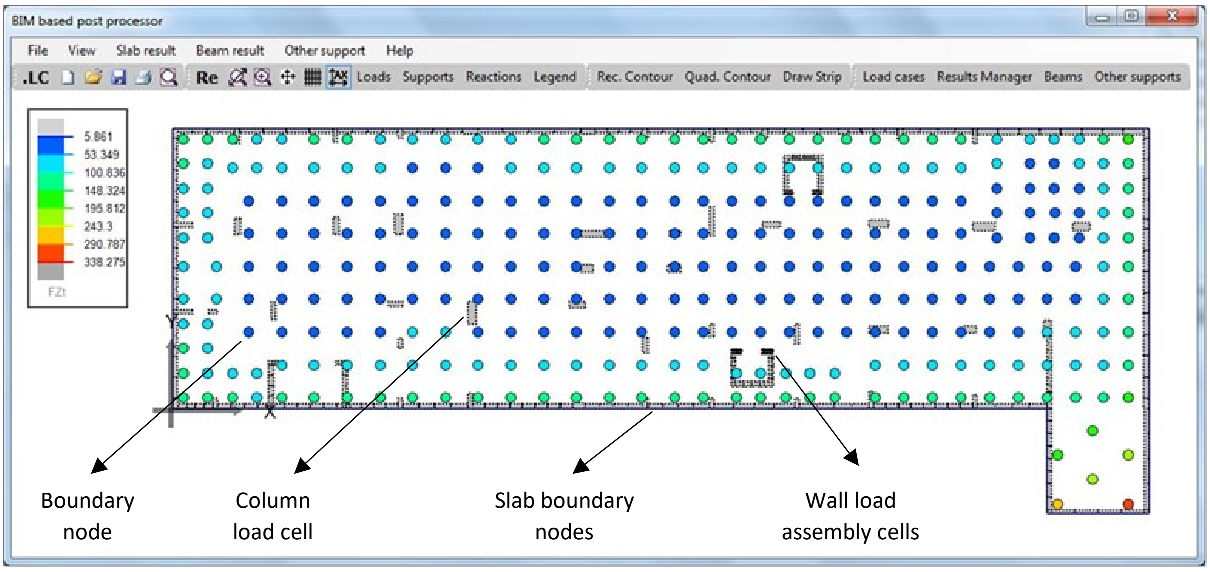

Figure 4.5: Pile reactions captured from the postprocessor GUI in Example 4.2.

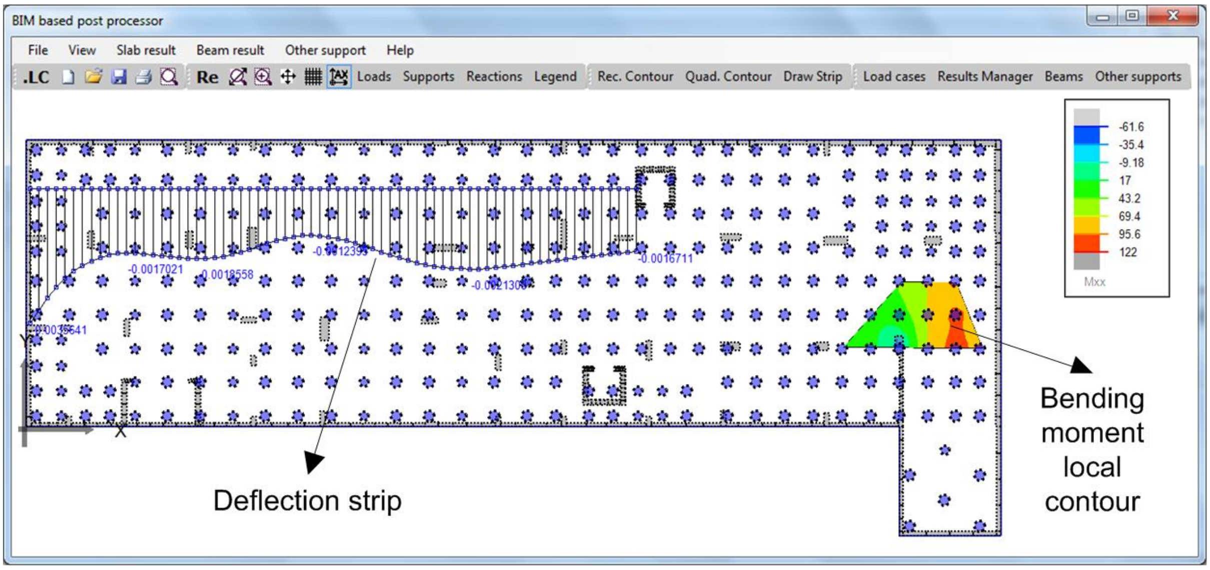

Figure 4.6: Piled raft strips and local contour results captured from the postprocessor GUI in Example 4.2.

Example 4.3 [38]

Purpose	:	Design of Building Floor
Description	:	First, the BE analysis model is created as presented in Figure 4.7. Slab design using methods III and IV are demonstrated in Figure 4.8 and Figure 4.9. The beam design and detailing options are presented in Figure 4.10. The design output in the form of calculation notes, summary spreadsheets, and detail drawings are presented in Figure 4.11-Figure 4.13, respectively.
Results	:	The design process described herein verifies the application of the specifications stated in section "BIM-Based Automated Design" for the BIM automated design including object structure, GUI, various design methodologies, detailing options, and interconnectivity (Table 4.1). The modeling time comparison is presented in Table 4.2 for the design process. In addition to the flexibility and applicability of design methodologies provided in the prototype, the proposed prototype required less modeling time than commercial FEM-BIM packages.

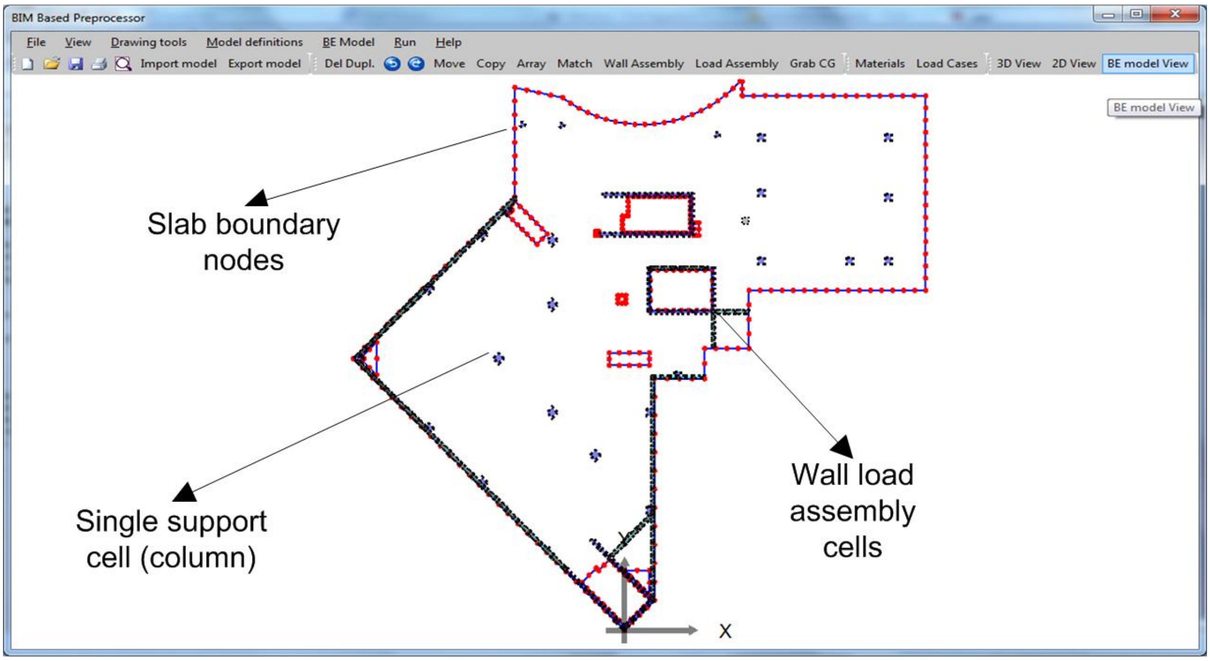

Figure 4.7: BIM-BEM model view of the building floor in Example 4.3.

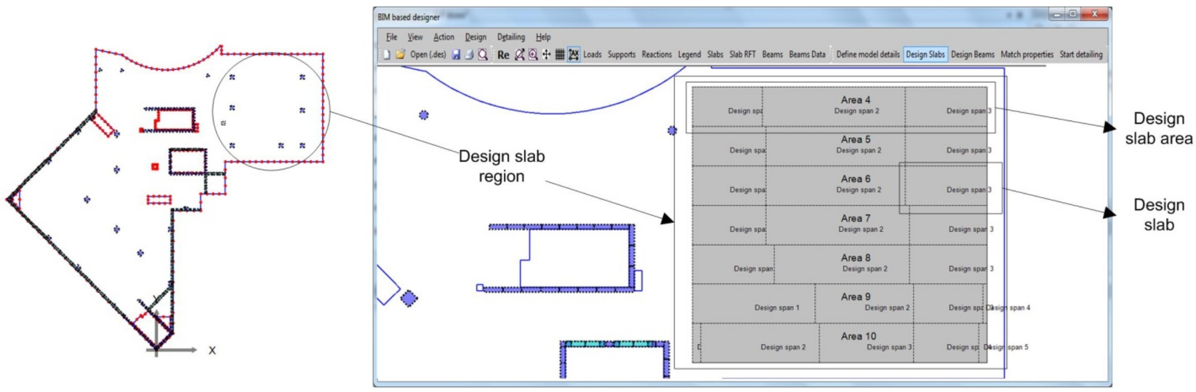

Figure 4.8: Example 4.3 slab design using method III.

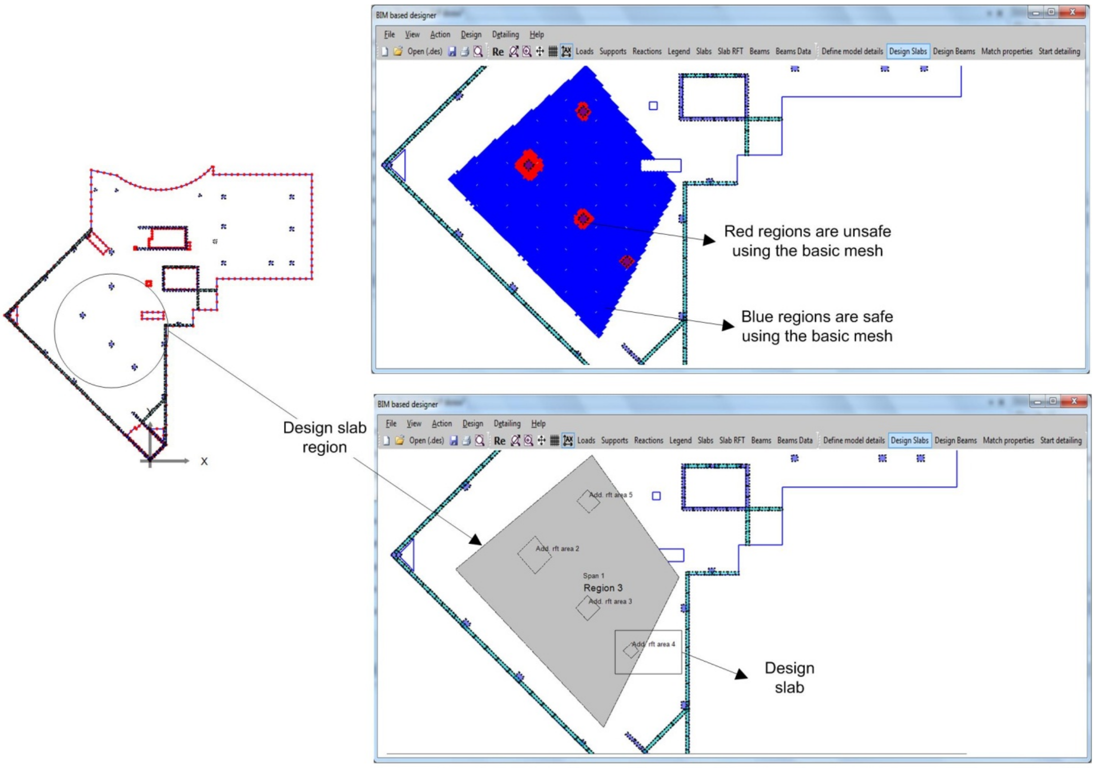

Figure 4.9: Example 4.3 Slab design using method IV.

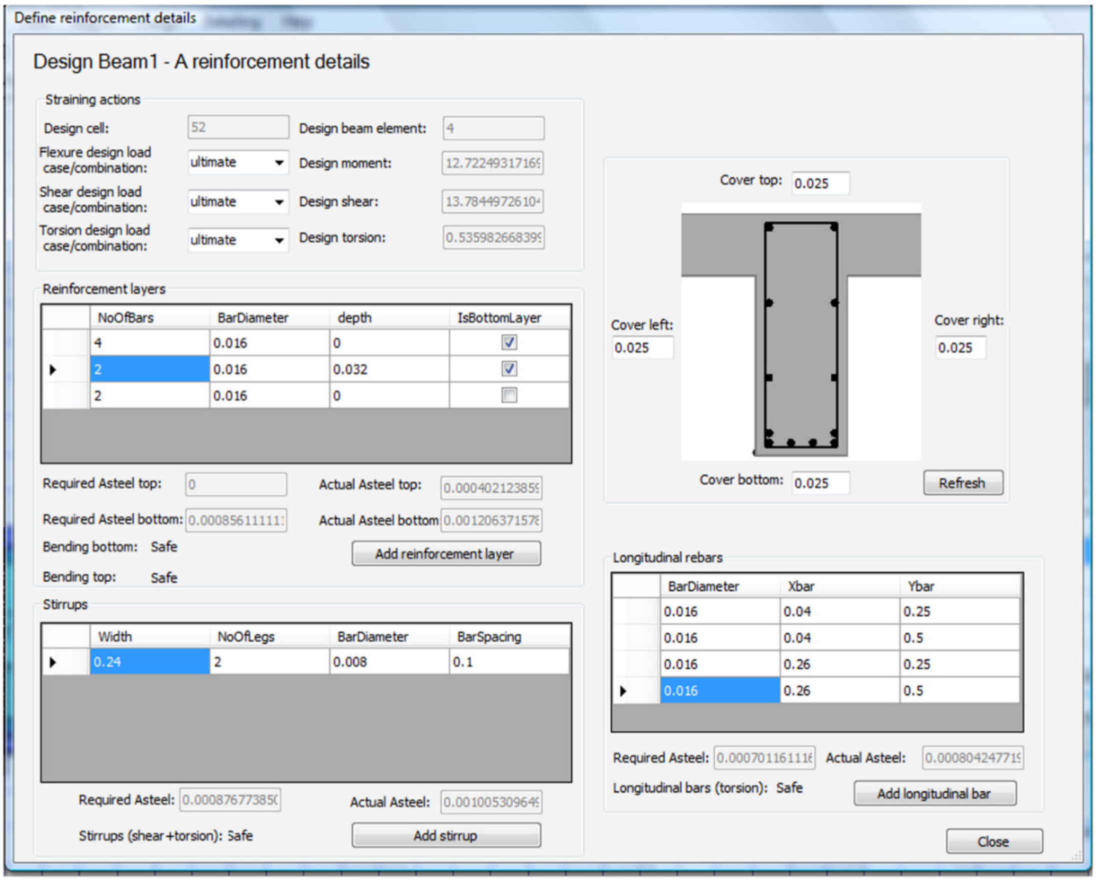

Figure 4.10: Example 4.3 BIM beam detailing.

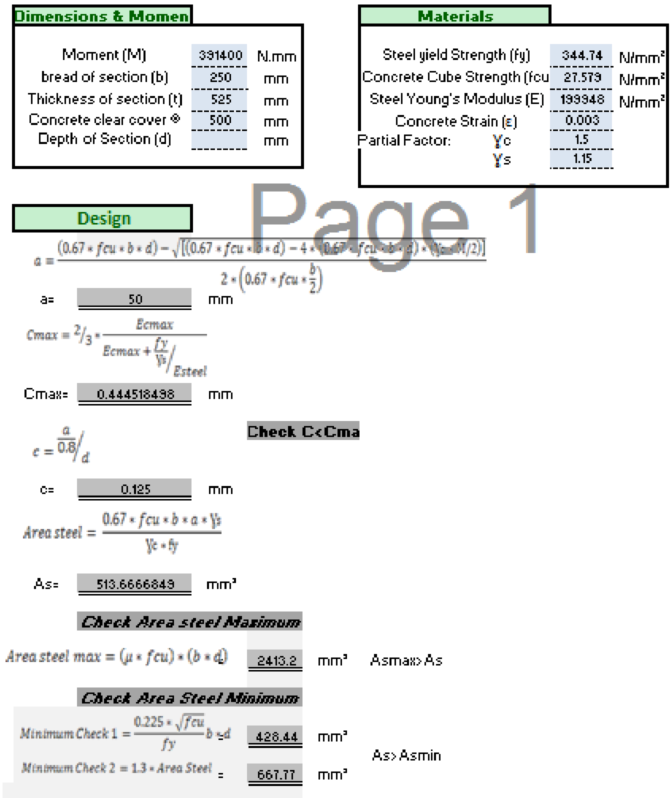

Dimensions & Momen

Moment (M)	391400	N.mm
bread of section (b)	250	mm
Thickness of section (t)	525	mm
Concrete clear cover ®	500	mm
Depth of Section (d)		mm

Materials

Steel yield Strength (fy)	344.74	N/mm²
Concrete Cube Strength (fcu	27.579	N/mm²
Steel Young's Modulus (E)	199948	N/mm²
Concrete Strain (ε)	0.003	
Partial Factor: γc	1.5	
γs	1.15	

Page 1

Design

$$a = \frac{(0.67 * fcu * b * d) - \sqrt{[(0.67 * fcu * b * d) - 4 * (0.67 * fcu * b * d) * (\gamma c * M/2)]}}{2 * \left(0.67 * fcu * \frac{b}{2}\right)}$$

a= 50 mm

$$Cmax = {}^{2}/_{3} * \frac{\varepsilon cmax}{\varepsilon cmax + \frac{fy/\gamma s}{Esteel}}$$

Cmax= 0.444518498 mm

$$c = \frac{a/0.8}{d}$$

Check C<Cma

c= 0.125 mm

$$Area\ steel = \frac{0.67 * fcu * b * a * \gamma s}{\gamma c * fy}$$

As= 513.6666849 mm²

Check Area steel Maximum

$Area\ steel\ max = (\mu * fcu) * (b * d)$ 2413.2 mm² Asmax>As

Check Area Steel Minimum

$Minimum\ Check\ 1 = \frac{0.225 * \sqrt{fcu}}{fy} b * d$ 428.44 mm²

$Minimum\ Check\ 2 = 1.3 * Area\ Steel$ = 667.77 mm²

As>Asmin

Figure 4.11: Example 4.3 sample design calculation note.

Slab summary

Area name	Major design moment	Strip name	Top major rft.	Bot. major rft.	Top minor rft.	Bot minor rft.
Area 1	Mxx	Span 1	5 Φ 0.018	5 Φ 0.018	5 Φ 0.018	5 Φ 0.018
		Add. rft area 2	6 Φ 0.018	0 Φ 0.018	**5 Φ 0.018**	0 Φ 0.018
		Add. rft area 3	3 Φ 0.018	0 Φ 0.018	3 Φ 0.018	0 Φ 0.018
		Add. rft area 4	2 Φ 0.018	0 Φ 0.018	2 Φ 0.018	0 Φ 0.018

Beam summary

Beam name	Beam size	Beam section	Flexure reinforcement	Stirrups	Longitudinal steel
Design Beam1	0.25 X 0.6	1	Top (2 Φ 0.016) Bot (4 Φ 0.018)	2L Φ 0.01 @ 0.2	Φ 0.012 @ (0.035,0.3) Φ 0.012 @ (0.215,0.3)
		2	Top (4 Φ 0.016) Bot (2 Φ 0.016)	2L Φ 0.01 @ 0.2	Φ 0.012 @ (0.035,0.3) Φ 0.012 @ (0.215,0.3)
Design Beam2	0.25 X 0.5	1	Top (2 Φ 0.016) Bot (2 Φ 0.016)	2L Φ 0.008 @ 0.2	Φ 0.012 @ (0.035,0.25) Φ 0.012 @ (0.215,0.25)
		2	Top (2 Φ 0.016) Bot (2 Φ 0.016)	2L Φ 0.008 @ 0.2	Φ 0.012 @ (0.035,0.25) Φ 0.012 @ (0.215,0.25)

Figure 4.12: Example 4.3 design summary spreadsheet.

Slab Detailing

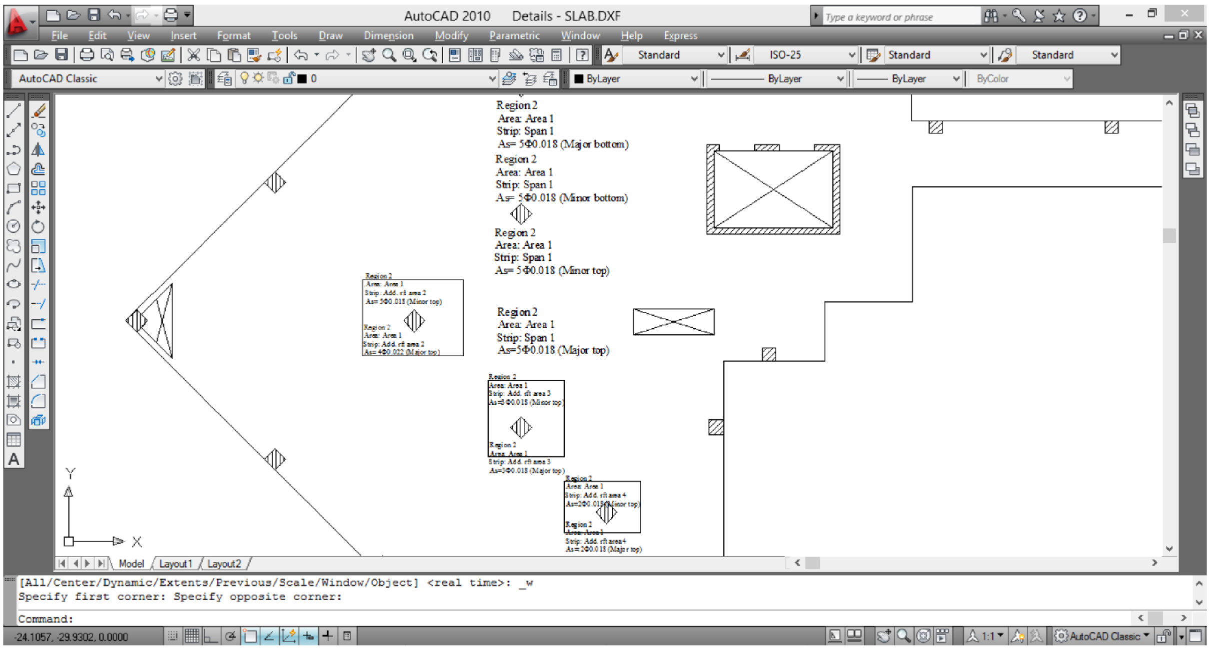

Beam Detailing

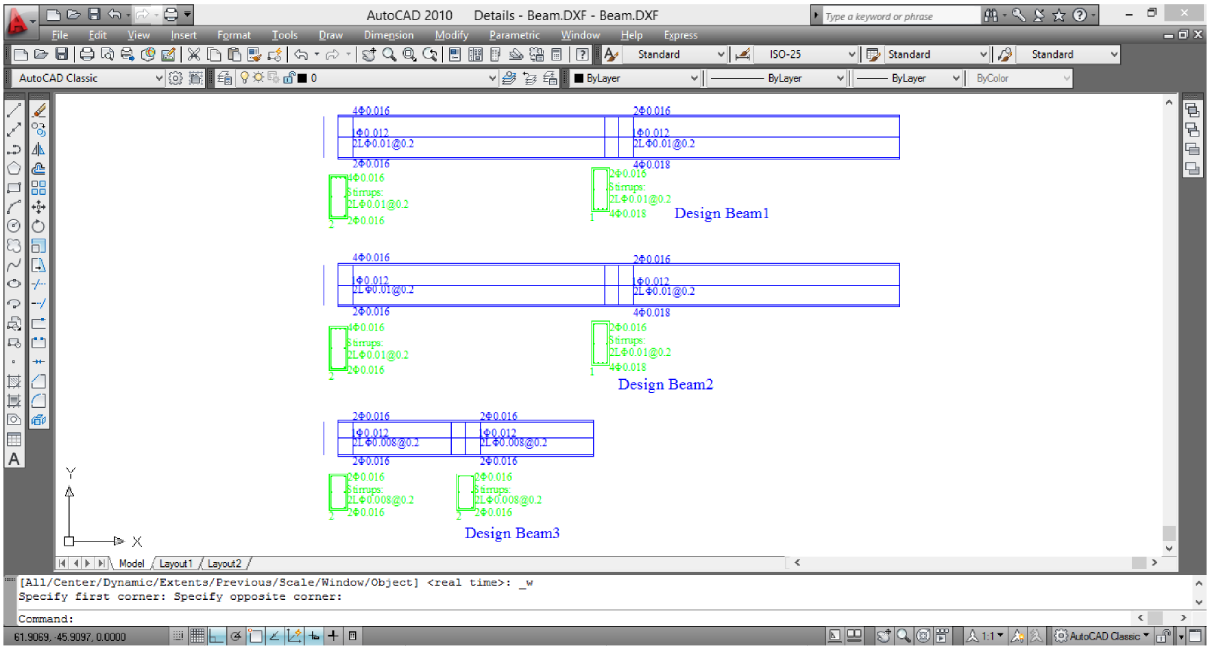

Figure 4.13: Example 4.3 slab and beam detail drawing.

5. The Dynamics Tool:

This tool should be installed with Multiple floor (fixed base) package to:

- Perform boundary elements free vibration, or forced vibration, or modal analysis of multiple floor building over fixed base.
- Time history analysis can be performed for the building under earthquake loads.
- Damping effects are easily considered using two techniques (Rayleigh and Caughey methods).

Example 5.1 [39]

Purpose : Analysis of multi-story building under free vibrations and comparing results with finite element.

Description : Figure 5.1 represents a 10-story flat slab building with the shown geometry supported on 4 square columns. The slab is 200mm thick. The modulus of elasticity E of the slabs and the vertical elements is $2210000\ t/m^2$ and Poisson's ratio v is 0.3. The story height is $3.0\ m$. The columns are fixed at the base. The modal periods obtained from the eigen value analysis [40] are computed, and the fundamental modes are plotted for comparison. It is solved two times, Example 5.1 A has columns with dimensions $500 \times 500\ mm^2$, and Example 5.1 B has columns with dimensions $100 \times 100\ mm^2$.

Results : The results and comparisons with finite element are presented in Table 5.1 and Table 5.2 for Example 5.1 A and Example 5.1 B respectively. Analysis of the results of Example 5.1 A shows that the proposed boundary element method approaches the solid column finite element model, while the skeletal column finite element models give higher time periods due to ignoring the area modeling which is accounted for naturally in the boundary element method. As for Example 5.1 B the effect of area modeling is minimized, thus the results of both boundary element and skeletal column finite element models were almost the same.

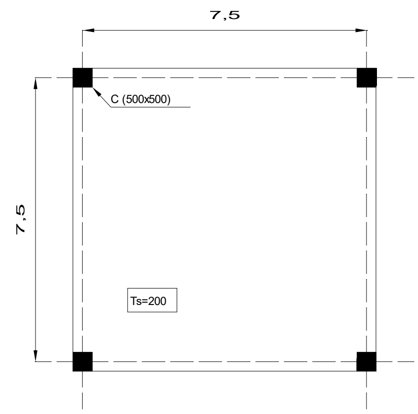

a. Dimensions of the Slab

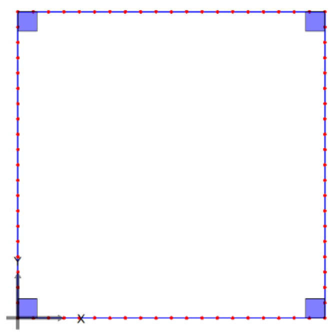

b. The Boundary Element Model

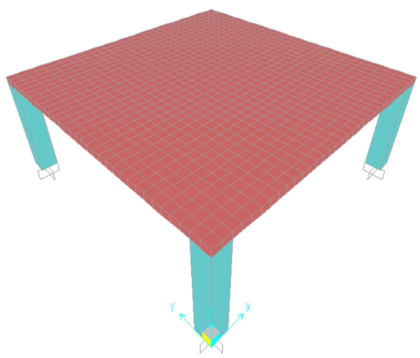

c. The Finite Element Model

Figure 5.1: Slab, boundary element model and finite element model of Example 5.1.

Table 5.1: Natural periods "Example 5.1 A".

Mode	Period (T) in seconds			% Error relative to F.E.M.	
	Boundary Element	F.E. Skeletal Column	F.E. Solid Column	Skeletal Column	Solid Column
1	2.4792	2.6085	2.3090	-5.60	-3.04
2	2.4792	2.6085	2.3090	-5.60	-3.04
3	1.8061	1.5760	1.4433	15.94	2.28
4	0.7415	0.7717	0.6969	-4.33	-1.03
5	0.7415	0.7717	0.6969	-4.33	-1.03
6	0.5374	0.4804	0.4446	12.82	0.72
7	0.3744	0.3834	0.3563	-2.53	-0.72
8	0.3744	0.3834	0.3563	-2.53	-0.72
9	0.2704	0.2487	0.2339	9.28	0.39
11	0.2231	0.2251	0.2145	-0.93	-0.92

Table 5.2: Natural periods "Example 5.1 B".

Mode	Period (T) in seconds		% Error relative to F.E.M.
	Boundary Element	F.E. Skeletal Column	
1	13.7913	13.7025	0.65
2	13.7913	13.7025	0.65
3	8.1044	7.9809	1.55
4	4.6213	4.5928	0.62
5	4.6213	4.5928	0.62
6	2.7941	2.7783	0.57
7	2.7941	2.7783	0.57
8	2.7170	2.6766	1.51
9	2.0318	2.0218	0.49
11	2.0318	2.0218	0.49

Example 5.2 [41]

Purpose	:	Analysis of multi-story building under forced vibrations and using the HHT finite difference technique [42] for the time history analysis, and assuming un-damped condition. Results are compared with finite element.
Description	:	The same building in Example 5.1 is considered. A constant force of 1000 tons in magnitude is applied in the center of mass of the topmost level with a time step of 0.01 second for a total of 10 seconds. It is analyzed using the finite element twice, where the columns are modeled in the first model as skeletal elements and the other as solid elements, then the problem is solved using the PLPAK.
Results	:	The time history results for the topmost displacement and the base shear are presented in Figure 5.2 and Figure 5.3, respectively. From Figure 5.2, it is clear that the response time history for top displacement obtained by the PLPAK is in good agreement with that obtained using the solid frame elements, also the results show that the skeletal finite element model gives over-estimated displacement values compared to the solid finite element model. Also, Figure 5.3 shows a good agreement for the base shear obtained by the PLPAK relative to the finite element method.

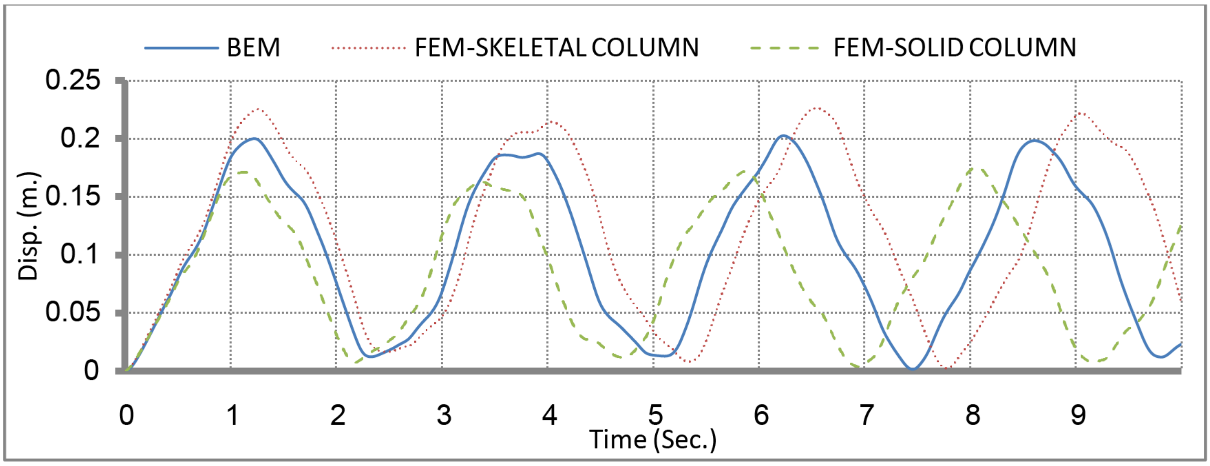

Figure 5.2: Time History for Topmost "x" Displacement for Example 5.2 (m).

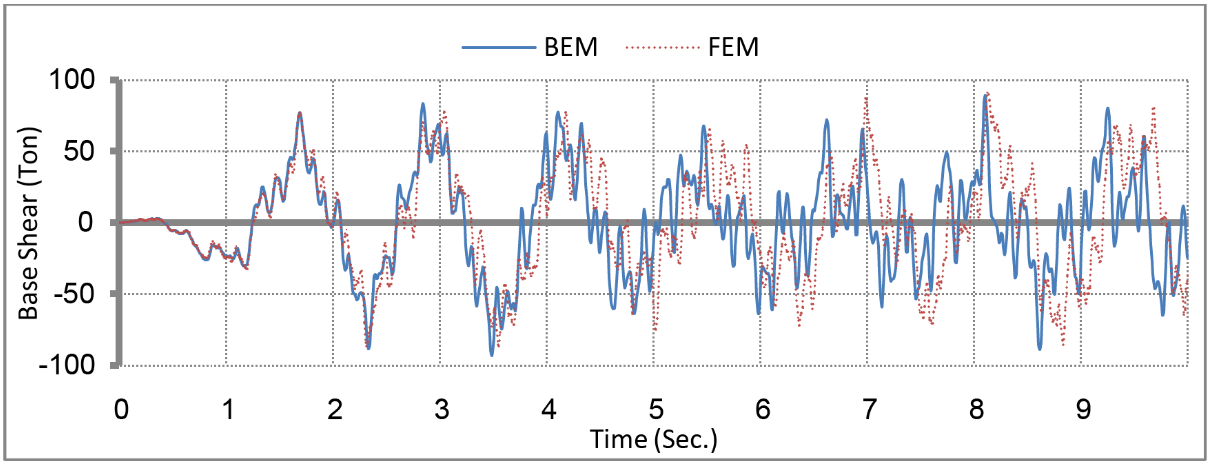

Figure 5.3: Time History for Base Shear for Example 5.2 (Tons).

Example 5.3 [39]

Purpose : Analysis of multi-story building under free vibrations and comparing results with finite element.

Description : Figure 5.4 represents a 10-story flat slab building on a wall pattern of 250 mm thickness. The slab has a thickness of 0.20 m. The modulus of elasticity E of the slabs and the vertical elements is $2210000\ t/m^2$ and Poisson's ratio v is 0.3. The story height is $3.0\ m$. The columns are fixed at the base. The modal periods obtained from the eigen value analysis [42] are computed, and the fundamental modes are plotted for comparison. The results of the PLPAK B.E. model are compared to those obtained by the F.E. method.

Results : The results are shown in Table 5.3. From the results it is clear that the natural periods obtained by the proposed method are in good agreement with those of the finite element method. As for the higher modes the difference between the 2 methods is more pronounced due to the effect of area modeling and the variation of the degrees of freedom of the B.E. and the F.E. models. yet this difference will not affect the dynamic behavior of the structure due to the fact that the higher modes have insignificant contribution in the structure vibration.

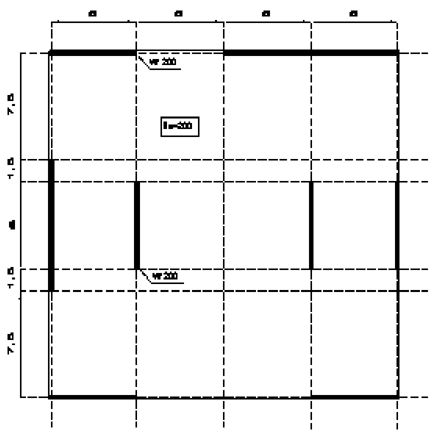

a. Dimensions of the Slab

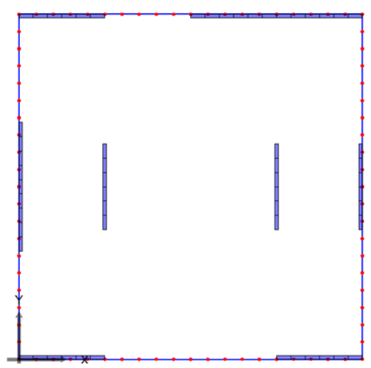

b. The Boundary Element Model

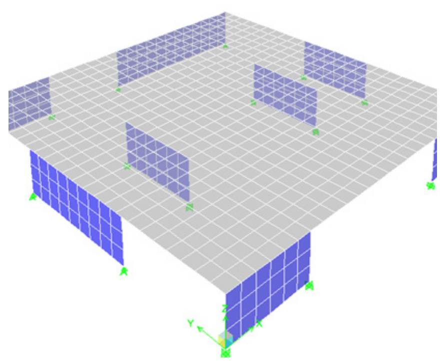

c. The Finite Element Model

Figure 5.4: Slab, boundary element model and finite element model of Example 5.3.

Table 5.3: Natural periods "Example 5.3".

Mode	Period (T) in sec. B.E.M	Period (T) in sec. F.E.M.	% Error relative to F.E.M.
1	0.8831	0.8063	9.52
2	0.7072	0.6803	3.95
3	0.3895	0.3994	-2.48
4	0.1431	0.1541	-7.14
5	0.1152	0.1333	-13.58
6	0.0634	0.0815	-22.21
7	0.0515	0.0632	-18.51
8	0.0437	0.0565	-22.65
9	0.0437	0.0376	16.22
11	0.0437	0.0358	22.07

Example 5.4 [41]

Purpose : Analysis of multi-story building under forced vibrations and using the HHT finite difference technique [42] for the time history analysis, and assuming un-damped condition. Results are compared with finite element.

Description : The same building in Example 5.3 is considered. The ground motion of Elcentro earthquake “Elcentro-EW” shown in Figure 5.5 is applied with a time step of 0.02 second for a total of 20 seconds. A finite element model is prepared for comparison with the boundary element model, where the walls in the finite element model are represented as shell elements. This example demonstrates the applicability of the proposed method to solve buildings on walls as well as columns and also to solve irregular wall patterns where the centers of mass and rigidity do not coincide thus generating twisting moment on the building.

Results : From Figure 5.6, it is clear that the response time history for top displacement obtained by the proposed method is in good agreement with that obtained using the finite element method for the first 3 seconds, and then a phase shift appears. The explanation provided for this phase shift is the effect of area modeling which is present in the BEM model, and this explanation is strengthened by comparing the natural periods of the mode shapes of the 2 models in [39]. The maximum displacements for the BEM model and the FEM model are 0.0124 m and 0.114 m, respectively. For the sake of completeness Figure 5.7 displays a comparison between fundamental mode shapes for the two case studies for both the proposed method and the FEM [39].

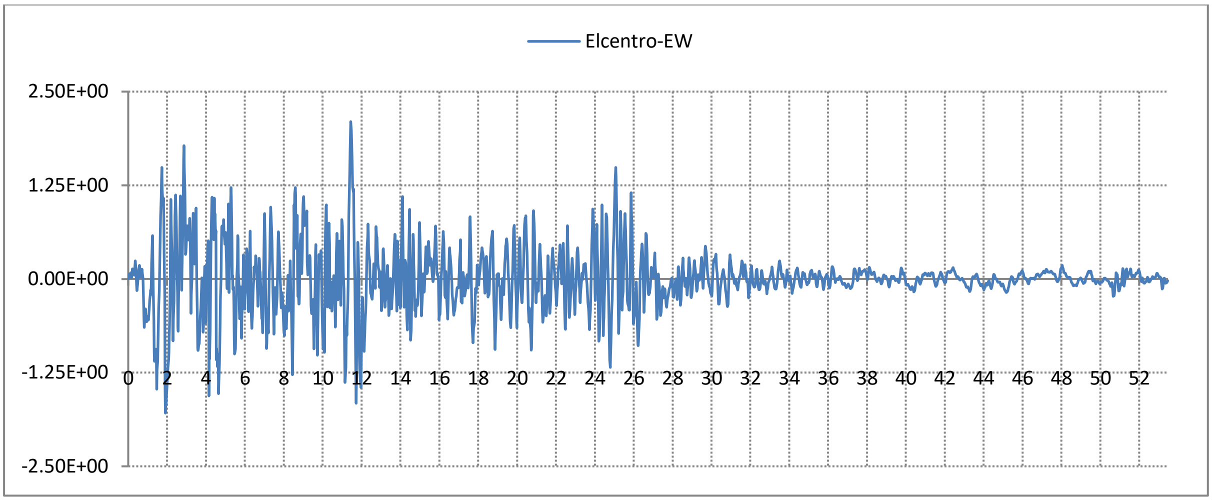

Figure 5.5: Elcentro-EW acceleration time history in G units

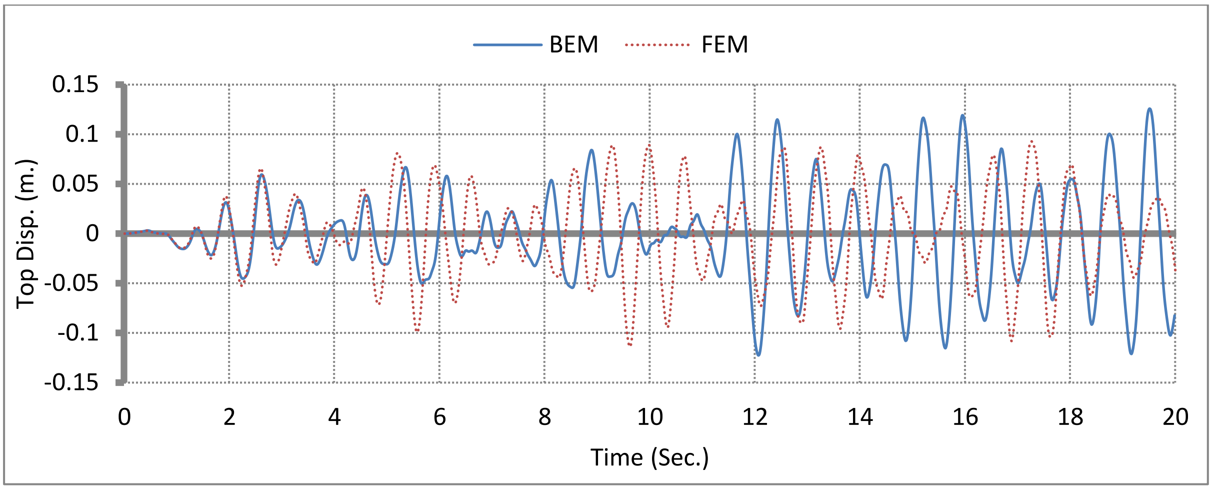

Figure 5.6: Time History for Topmost (x) Displacement for Example 5.4 (m).

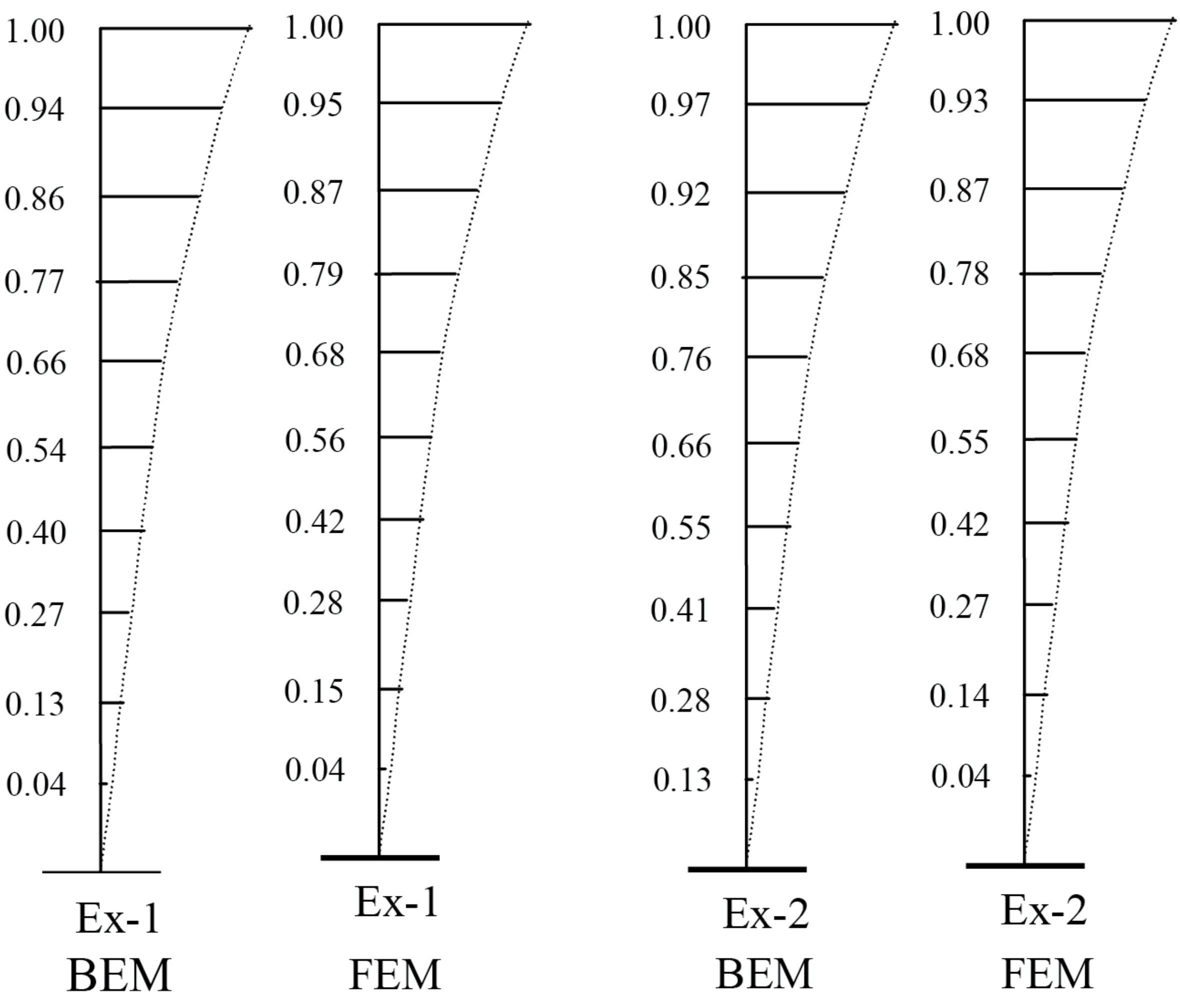

Figure 5.7: Time History for Topmost (x) Displacement for Example 5.4 (m).

Example 5.5 [43]

Purpose : Analysis of multi-story building under forced vibrations with damped conditions. Results are compared with finite element.

Description : A 30-story building as shown in Figure 5.8 and Figure 5.9 was analyzed using FEM (SAP2000) with level of discretization of the shell and solid elements 0.5X0.5 m by defining the columns as frame elements and solid elements. And solved by BEM (The PLPAK) with the different damping techniques. El-Centro earthquake was used for analysis as shown in Figure 5.5. The material properties are as shown in Table 5.4.

Results : The resulted time history of the top story displacement, top story displacement with no damping, base shear and maximum inter story drifts was as shown in Figure 5.10-Figure 5.13. As shown in the graph the BEM Models response matches well with the FEM solid model than the frame elements model. So, the BEM is more accurate and practical. Giving closer solution to the solution with less time and storage usage. Caughey model was calculated using damping ratio 5% for the first two mode shapes, while for the third mode shape the damping ratio was taken 10%. Results from Caughey model was noticed to be closer to the FEM solid element model so it is more accurate than Rayleigh model. The resulted time periods of the models were as shown in the following Table 5.5. As shown in the table the natural periods of the BEM is in good match with the solid element model. From the periods it can be deduced that the frame element model is more flexible than the BEM model and the solid model.

Table 5.4: Material properties for Example 5.5.

Γ	2.5 t/m^3
Modulus of Elasticity	2210000 t/m^2
Damping ratio for the first two mode shapes	5%
Slab thickness	200
Damping ratio for the third mode shape	10%
Supports	Fixed

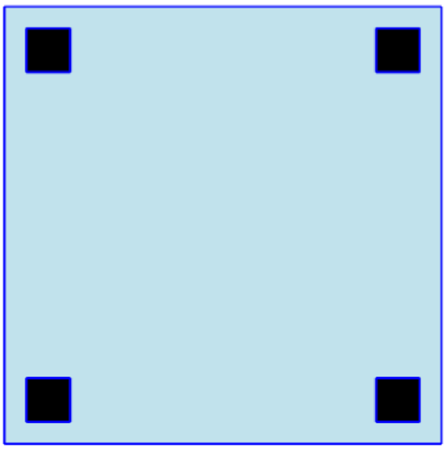

Figure 5.8: BEM slab model of Example 5.5.

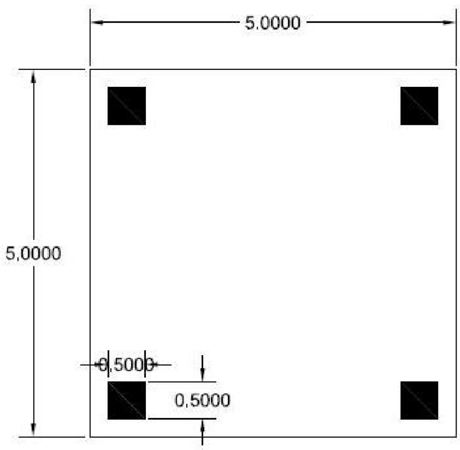

Figure 5.9: Slab plan of Example 5.5.

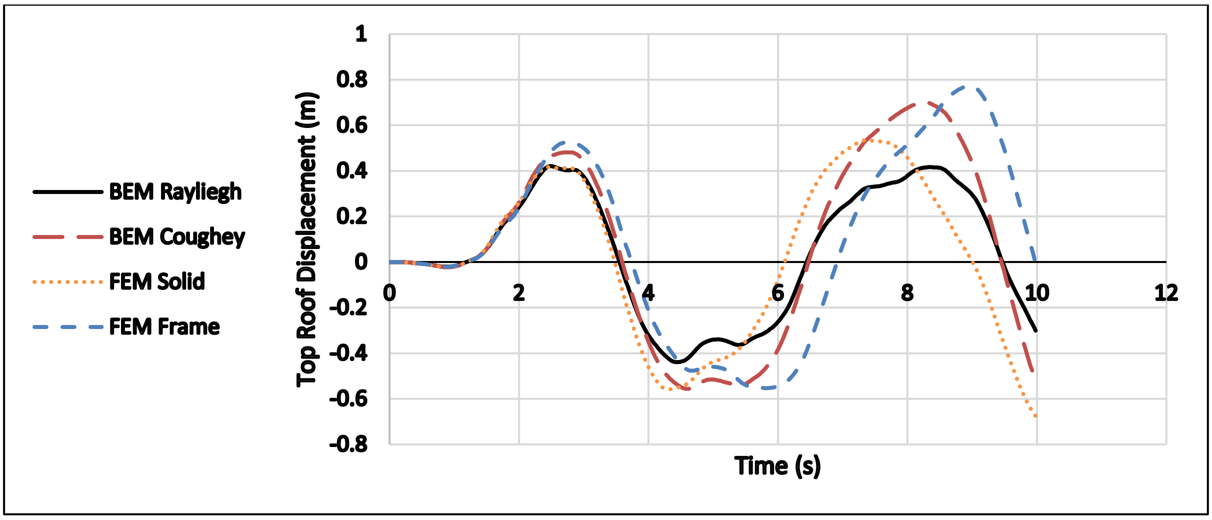

Figure 5.10: Top Displacement time history with damping in Example 5.5.

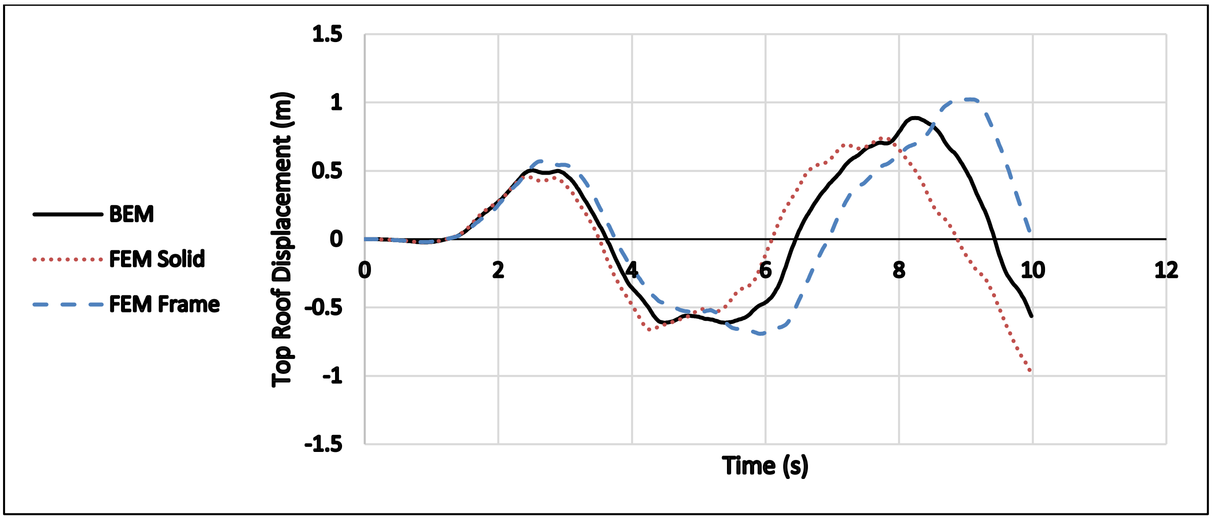

Figure 5.11: Top Displacement time history with no damping in Example 5.5.

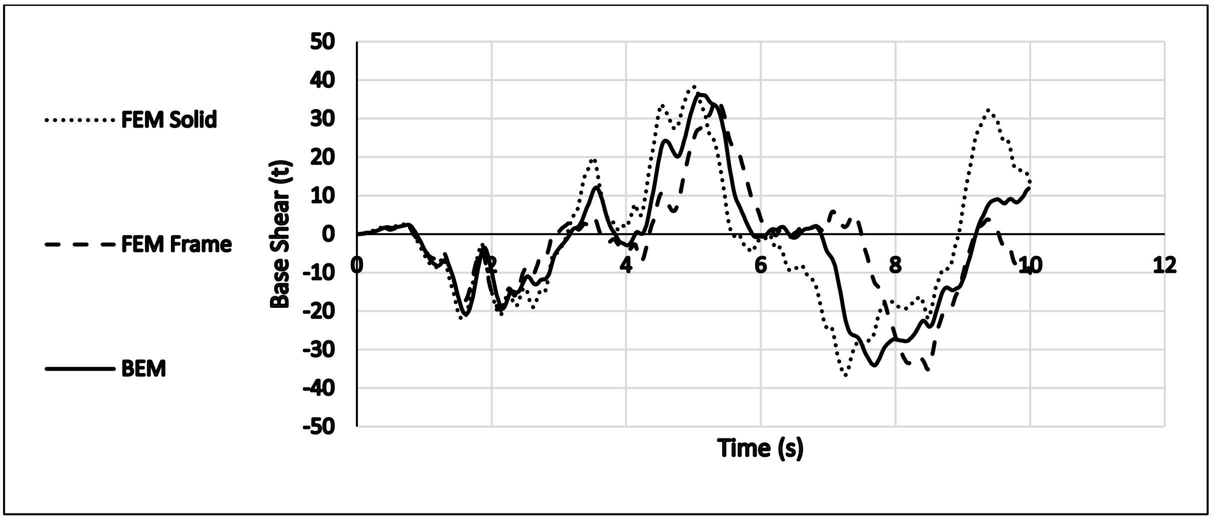

Figure 5.12: Base Shear time history in Example 5.5.

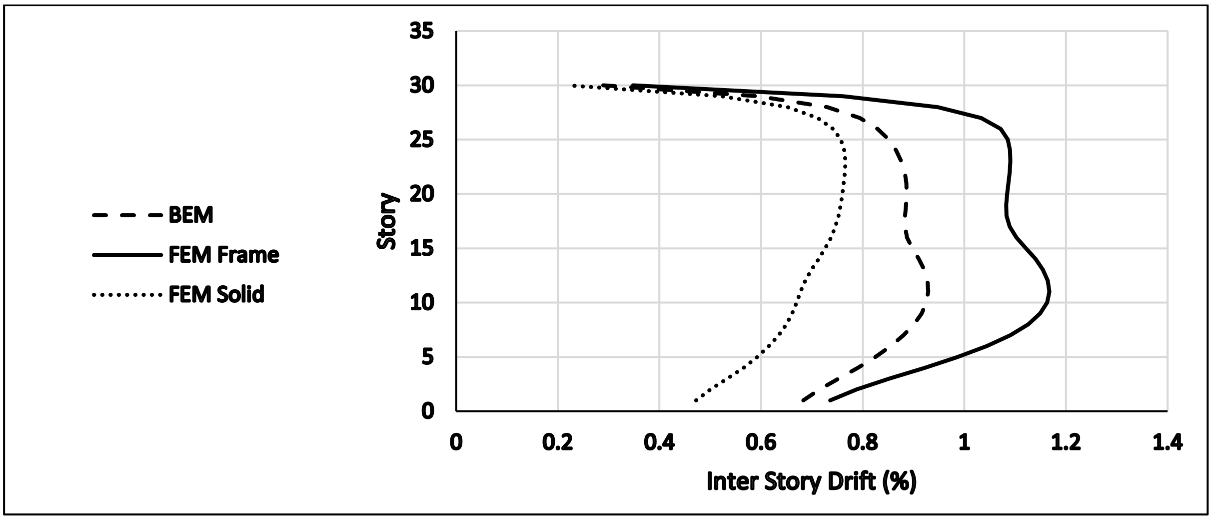

Figure 5.13: Maximum inter story drift in Example 5.5.

Table 5.5: Time period of the models (Example 5.5).

Mode	Period		
	Sec		
	FEM SOLID	BEM	FEM FRAME
1	5.16113	5.719482613	6.441816
2	1.516741	1.656250918	1.935619
3	0.784252	0.850225286	1.012103
4	0.531077	0.575712167	0.682878
5	0.391329	0.425434432	0.49986
6	0.304341	0.332295061	0.385912
7	0.243694	0.267652385	0.307083
8	0.199642	0.220804319	0.250414
9	0.166035	0.185208865	0.207784
10	0.139914	0.15758397	0.175122

Example 5.6 [43]

Purpose	:	Analysis of multi-story building under forced vibrations with damped conditions. Results are compared with finite element.
Description	:	A 30-story building as shown in Figure 5.14 was analyzed using FEM (SAP2000) with level of discretization of the shell and solid elements 0.5X0.5 m by defining the columns as frame elements and solid elements. And solved by BEM with the Rayleigh damping technique. El-Centro earthquake was used for analysis as shown in Figure 5.5. The material properties are as shown in Table 5.4.
Results	:	The resulted time history of the top story displacement was as shown in Figure 5.15. As shown in the graph the BEM Model is in between the FEM solid and frame elements. It is noticed that the assumption for the damping ratio of the third natural mode is 10% is not accurate one. So, the Caughey damping is calculated to be negative which is illogical. The damping ratio needs to be assumed according to the building. The resulted time periods of the models were as shown in Table 5.6.

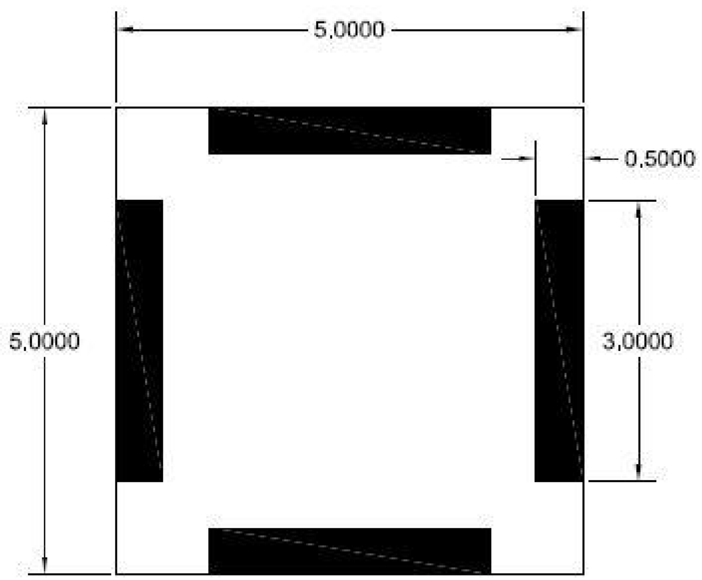

Figure 5.14: Slab plan of Example 5.6.

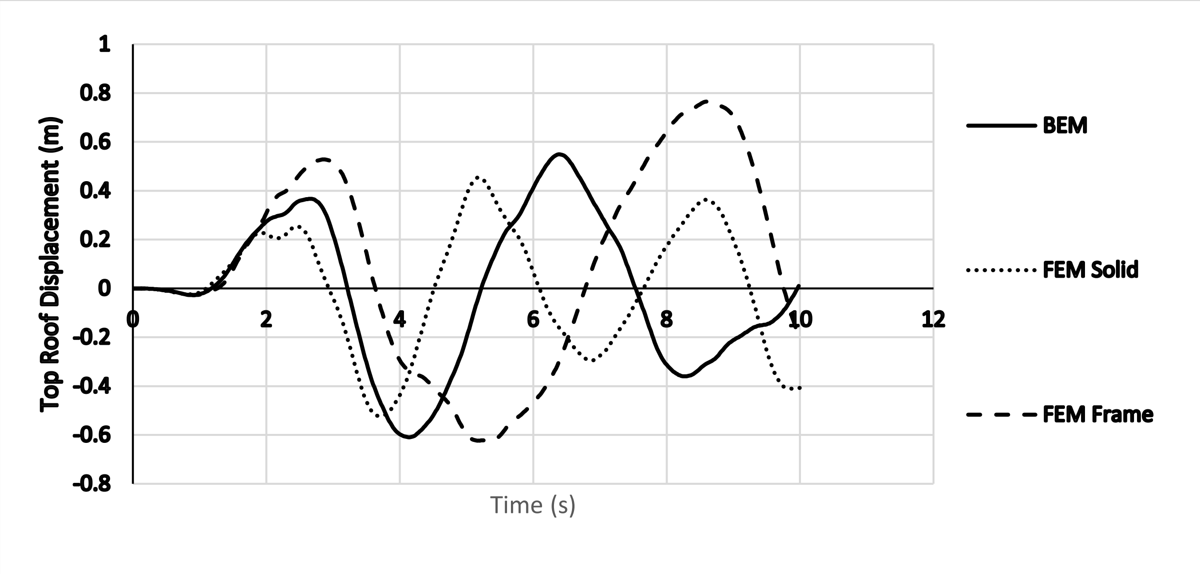

Figure 5.15: Top Displacement time history of Example 5.6.

Table 5.6: Time period of the models of Example 5.6.

Mode	Period Sec		
	FEM SOLID	BEM	FEM FRAME
1	3.24895	4.19847263	6.183891
2	0.67024	0.985063419	1.302294
3	0.289839	0.418739108	0.501773
4	0.172867	0.233163368	0.263893
5	0.116639	0.146979429	0.163329
6	0.084759	0.100751493	0.111962
7	0.064673	0.073174903	0.082486
8	0.051286	0.055496498	0.064122
9	0.041999	0.044921665	0.052038
10	0.034822	0.043503149	0.048352

Example 5.7 [43]

Purpose	:	Analysis of multi-story building under forced vibrations with damped conditions. Results are compared with finite element.
Description	:	A 30-story building as shown in Figure 5.16 was analyzed using FEM (SAP2000) with level of discretization of the shell and solid elements 0.5X0.5 m by defining the columns as frame elements and solved by BEM with Rayleigh and Caughey damping techniques. El-Centro earthquake was used for analysis as shown in Figure 5.5. The material properties are as shown in Table 5.4.
Results	:	The resulted time history of the top story displacement was as shown in Figure 5.17. The phase difference between FEM and BEM responses as shown in Figure 5.15 and Figure 5.17 can be due to the difference in the calculation of the time period for the two approaches, which results in the different response during vibration and different phases.

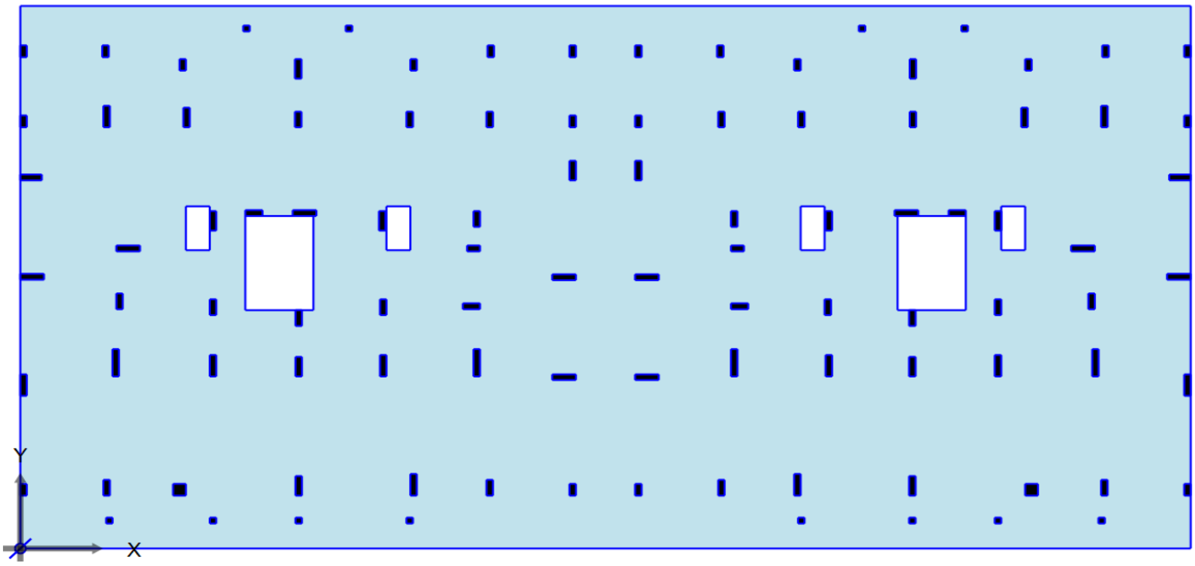

Figure 5.16: Slab model in Example 5.7.

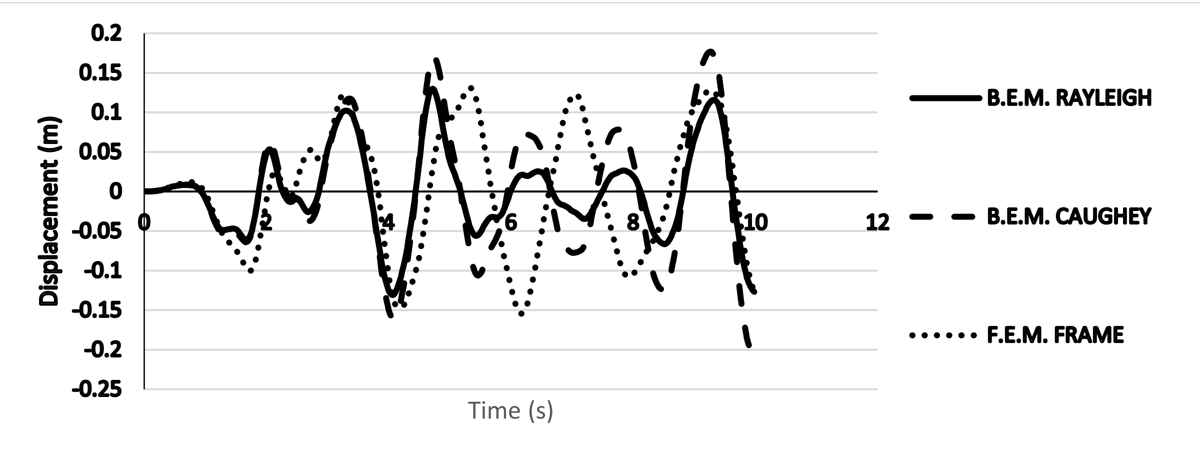

Figure 5.17: Top Displacement time history in Example 5.7.

Example 5.8 [43]

Purpose : Analysis of multi-story building under forced vibrations with damped conditions. Results are compared with finite element.

Description : A 30-story building as shown in Figure 5.18 was analyzed using FEM (SAP2000) with level of discretization of the shell and solid elements 0.5X0.5 m by defining the columns as frame elements and then solved using the BEM with Rayleigh and Caughey damping techniques. El-Centro earthquake was used for analysis as shown in Figure 5.5. The material properties are as shown in Table 5.4.

Results : The resulted time history of the top story displacement was as shown in Figure 5.19. As shown in Figure 5.17 and Figure 5.19 of Example 5.7 and Example 5.8 respectively, the BEM results agree with those of the FEM for the first 4 seconds, then the response differs significantly after that. As was shown in the previous examples the BEM gives results that are near the solid FEM model, so the differences in the responses of Example 5.7 and Example 5.8 are due to the effect of the area modeling which is neglected in the FEM.

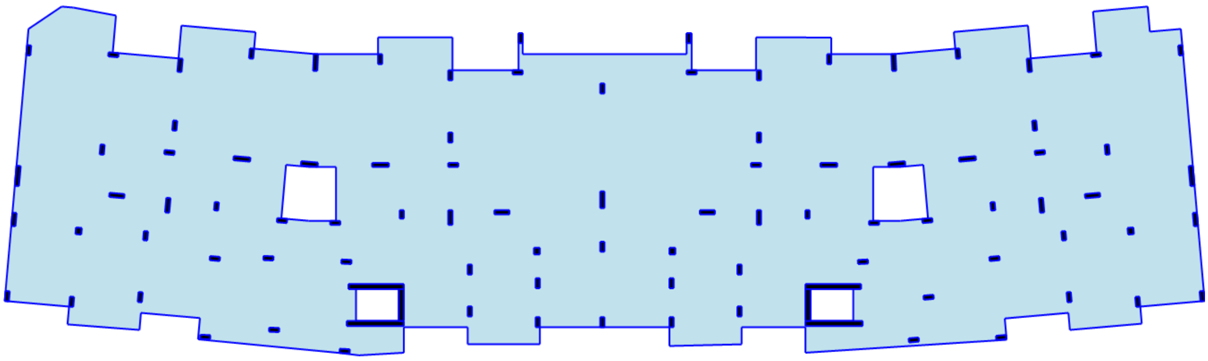

Figure 5.18: Slab model in Example 5.8.

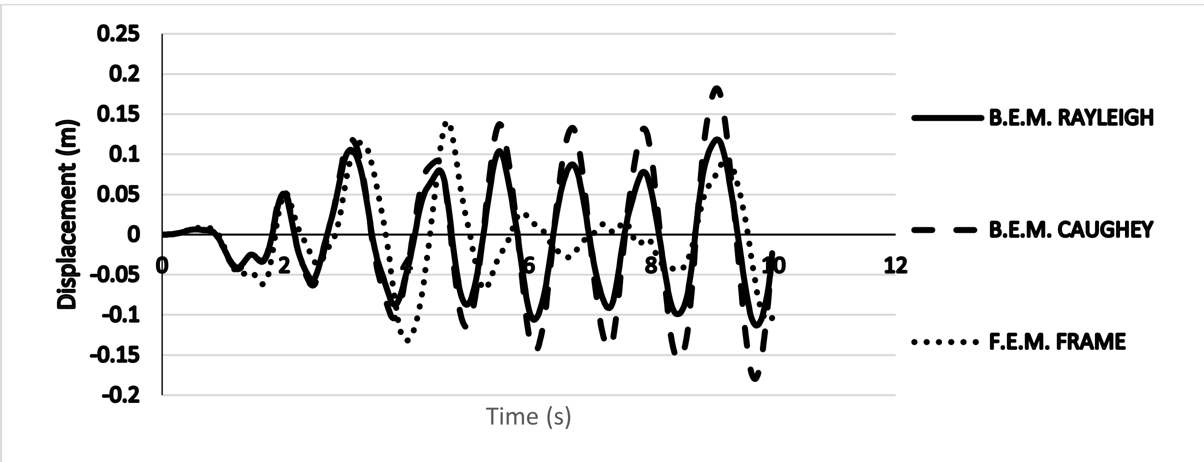

Figure 5.19: Top Displacement time history in Example 5.8.

6. The Post-Tension Tool:

With this tool post-tension slabs are analyzed and designed. The slab can be constructed using either PLGEN or using Autodesk Revit.

Example 6.1 [44]

Purpose : Load balancing of simply-supported slab own weight.

Description : In this example, the slab shown in Figure 6.1 is considered. The slab has cross-section dimensions of $1.0 \times 0.6\ m$. The material properties taken are $E = 2.21 \times 10^6\ t/m^2, t = 0$ to allow comparison against results for the beam theory. The slab is pre-stressed with one cable of force equal to the balancing force $23.4\ tons$. The cable profile and eccentricity are shown in Figure 6.1. The slab is supported on two supports of $0.1 \times 1.0\ m$ in cross section and $1.5\ m$ in height as shown in Figure 6.1. The slab boundary is modeled (see Figure 6.2) using 16 boundary elements. A simply supported boundary condition is employed. Such conditions are simulated using two column support of $1.0 \times 0.1\ m$ with zero rotational stiffnesses and high value of (10^{10}) for the axial stiffness. Eleven internal cells are used to represent the cable equivalent loading. The numbers of Gauss points used for integration purposes are ten. The total number of extreme points is 52. The results are calculated along a strip along the cable center line.

Results : Figure 6.1 demonstrates the deflection and bending moment distributions along the slab center line under its own weight only. Figure 6.2 demonstrates the same deflection and bending moment distributions under both own weight plus the balancing pre-stressing force. It can be seen that defection approaches zero compared to the deflection distribution in Figure 6.1. The bending moment in Figure 6.2 approaches zero also; except near the end supports as such supports are not knife edge and has width of $0.1\ m$; therefore, small negative moment is expected.

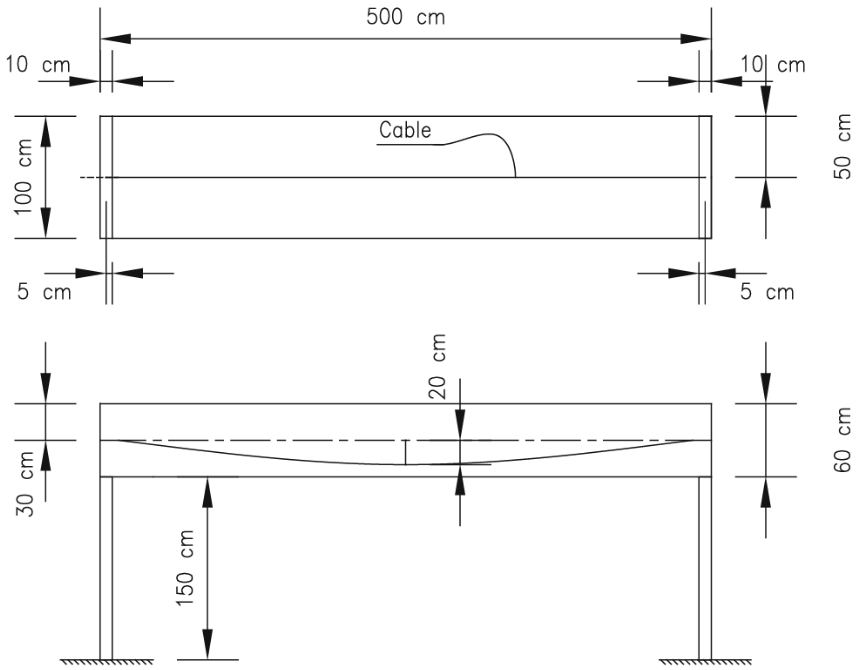

Figure 6.1: The simply supported slab considered in Example 6.1.

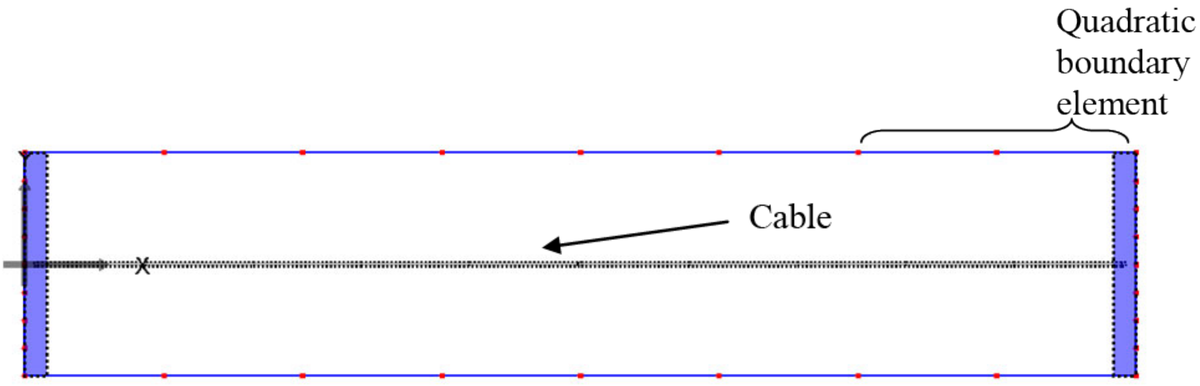

Figure 6.2: Boundary element and cable internal cells for the simply supported slab considered in Example 6.1.

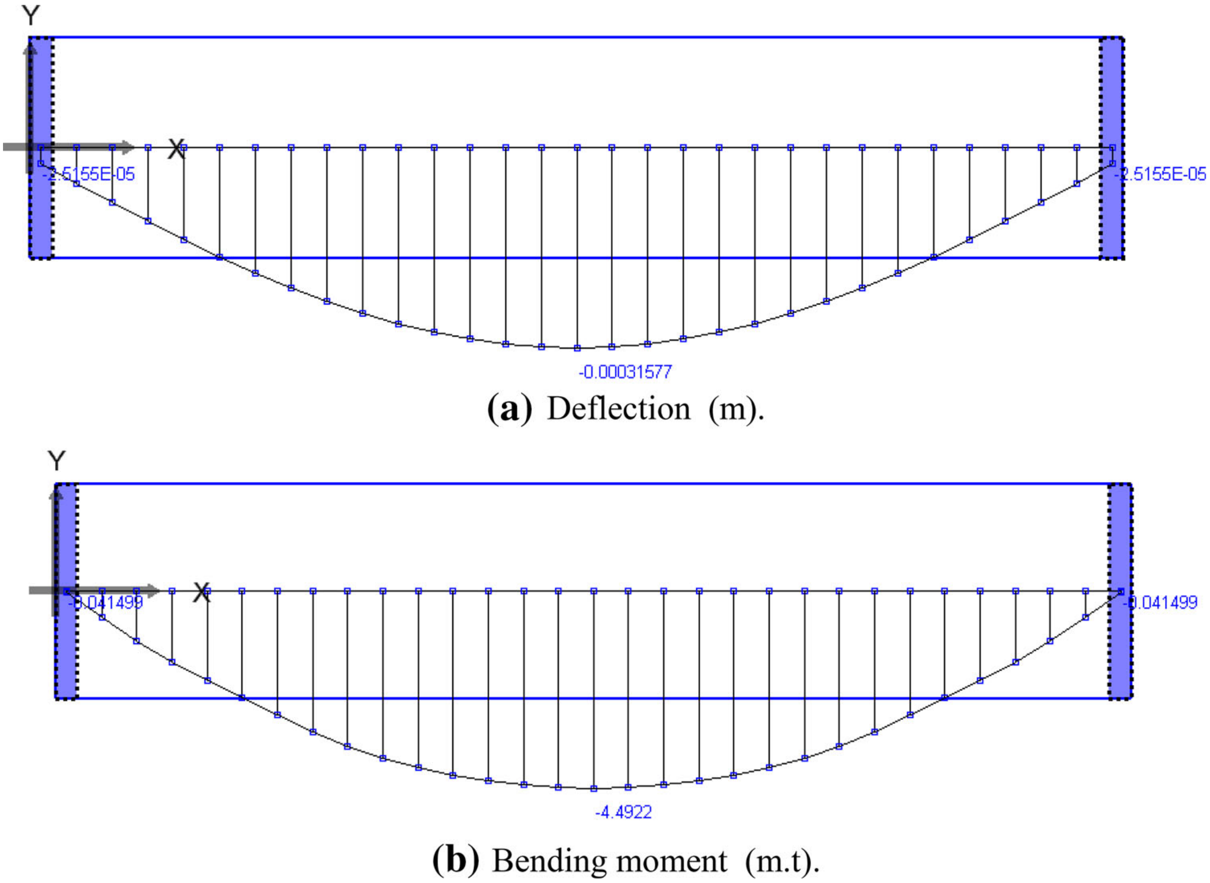

Figure 6.3: Deflection and bending moment distribution under the slab own weight along the slab center line in the simply supported slab considered in Example 6.1.

Example 6.2 [44]

Purpose : Comparison of central deflection against analytical values

Description : Example 6.1 is reconsidered herein using different cable profile (see Table 6.1). The symbols used in Table 1 are: P is pre-stressing force, e, e_c are the centerline eccentricity, e_e is end eccentricity, E is modulus of elasticity, I is section moment of inertia, β is the ratio of the distance from the harping point to the beam end, to the beam length. This ratio is equal to 1.4/4.9 in the considered case (Figure 6.4).

Results : The PLPAK results for the deflection at the mid span are shown in Table 6.1. It can be seen from Table 6.1 that the results for the central deflection are in excellent agreement with analytical values obtained from [45].

Table 6.1: Comparison of central deflection against analytical values (m) in Example 6.2.

Case description	Analytical equation for central deflection[16]	Analytical value	Present result	Profile
Parabolic profile	$\frac{5}{48}\frac{Pe\ell^2}{EI}$	6.29E-04	6.50E-04 (Error of 3.33%)	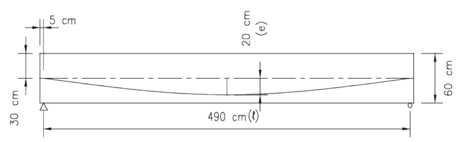
Constant eccentricity	$\frac{1}{8}\frac{Pe\ell^2}{EI}$	7.54E-04	7.61E-04 (Error of 0.93%)	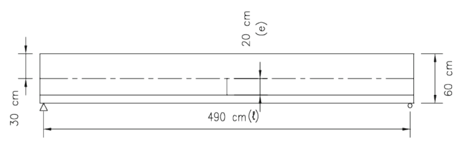
Single harping point	$\frac{(2e_c+e_e)}{24}\frac{P\ell^2}{EI}$	6.29E-04	6.46E-04 (Error of 2.70%)	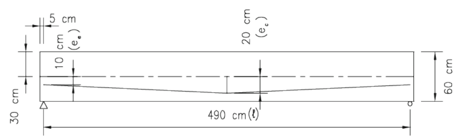
Double harping point	$\left[\frac{e_c}{8}-\frac{\beta^2}{6}(e_c-e_e)\right]\frac{P\ell^2}{EI}$	7.13E-04	7.29E-04 (Error of 2.24%)	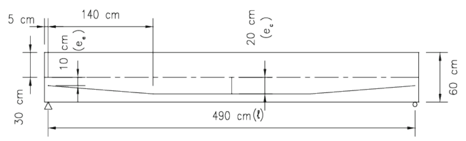

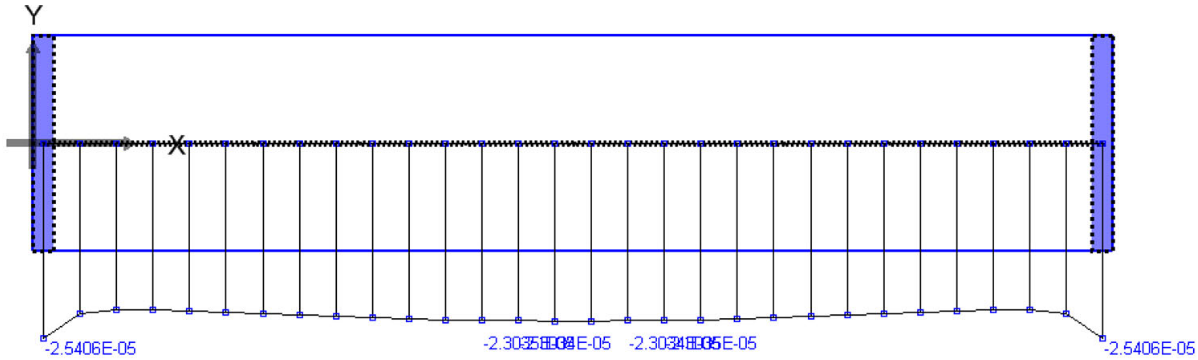

(a) Deflection (m).

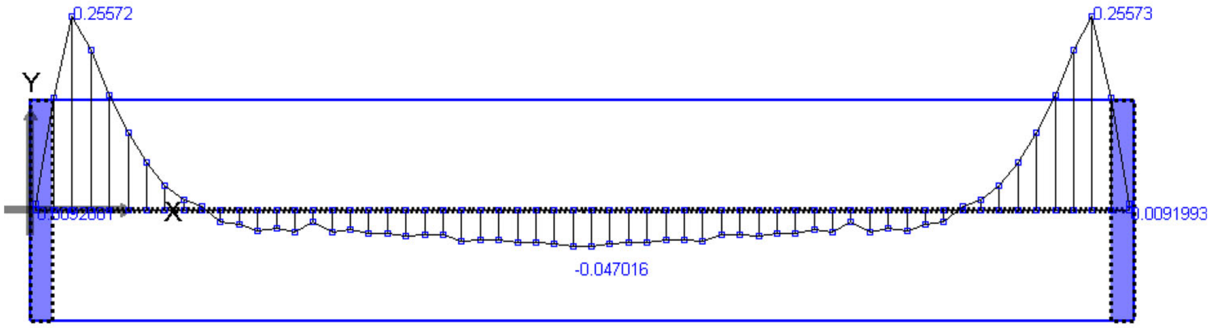

(b) Bending moment (m.t).

Figure 6.4: Deflection and bending moment distributions under the slab own weight plus the balancing force prestressing cable along the slab center line in the simply supported slab considered in Example 6.1.

Example 6.3 [44]

Purpose : Comparison of fixed end moments against analytical values.

Description : Using the same slab in Example 6.1, alternative cases are considered herein to verify values of the fixed end moments. The cable profiles shown in Table 6.2 are considered. In this case the fixed–fixed boundary condition is employed. Such conditions are simulated within the boundary element model using the same previous columns but with very high value of (10^{10}) for the axial and the rotational stiffnesses in the two directions. It is worth mentioning that in the last case, the end fixations are spaced by distant $5.0\,m$ away from the cable end to avoid the placement of the concentrated moment near the fixed column.

Results : The results of the PLPAK fixed end moments together with the analytical values obtained from [45] are given in Table 6.2. It can be seen that the obtained results are in excellent agreement with analytical values.

Table 6.2: Comparison of fixed end moments against analytical values (m.t) in Example 6.3.

Case description	Analytical equation[16]	Analytical Value	Result (%Error)	Profile
Single harping point with no end eccentricity	$M_1 = M_2 = P\frac{e}{2}$	5.00	5.03 (0.60%)	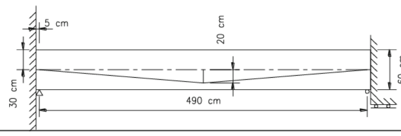
Parabolic profile with no end eccentricity	$M_1 = M_2 = P\frac{2}{3}e$	6.67	6.72 (0.75%)	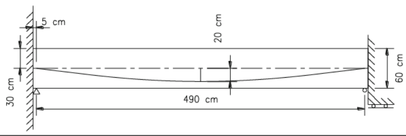
Single harping point with end eccentricity	Obtained based on stiffness analysis	M_1=0.26 M_2=1.42	M_1=0.24 (7.69%) M_2=1.40 (1.41%)	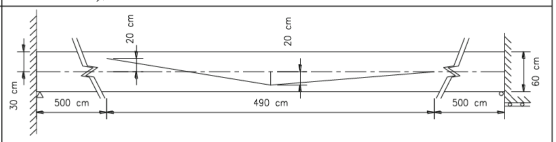

Example 6.4 [44]

Purpose : Demonstrate that capabilities of the PLPAK to solve practical slabs compared to the existing finite element-based software packages.

Description : The slab has maximum dimensions of $61 \times 26\ m$ with spans about 7 to 11 m and thickness of $0.24\ m$. The material properties taken are $E = 2.1 \times 10^6\ t/m^2$, $v = 0.16$. The slab is pre-stressed with cables in X & Y directions as shown in Figure 6.6 and Figure 6.7, respectively. Cables spacing varies from 0.6 to $1.6\ m$ and cable force are equal to $12\ ton$. Cable groups are used. Each group contains 2 to 5 cables. Cable layout and eccentricity are shown in Figure 6.6 and Figure 6.7, respectively. The slab is supported on group of irregular columns (cross section varies from 2 to 4 m^2) and central core as shown in Figure 6.5. The floor height is $3\ m$. The slab boundary is modeled using the PLPAK using 159 boundary elements and 4124 internal cells are used to represent the equivalent loading of cables as shown in Figure 6.8. The number of Gauss points used is 4. Total number of extreme points is 8787. The results are calculated along several sections using 515 internal points and internal point meshes of $1 \times 1\ m$ are used for contour map calculations. The internal columns and cores are represented by multiple supporting cells (2 to 4 cells).

The same slab is considered using finite element analysis with $0.2 \times 0.2\ m$ mesh, columns are represented as 3D solids, shear walls and cores are represented using shell element. The used finite element model has $87{,}003$ nodes and $22{,}098$ four-node plate-bending elements as well as $48{,}990$ solid elements as shown in Figure 6.9. It has to be noted that results presented here will concentrate on slab results. Discussions on results for supporting elements are similar to those of slabs without pre-stressing cables which have been already considered by [1], [10].

Results : Figure 6.10-Figure 6.23 demonstrate the distribution of bending moment and deflection results along sections A, B, C, D, E, F and G in the considered slab (see Figure 6.5). It can be seen that the PLPAK (BEM) results are in good agreement when compared to results obtained from finite element analysis (FEM). Figure 6.24-Figure 6.29 demonstrate the contour map results of bending moment and deflection, respectively. An effort is made to have as much a similar color range as possible in the two analyses (BEM and FEM). It can be seen that the results of the PLPAK (BEM) agree with those obtained from the (FEM) results. Table 6.3 demonstrates a comparison in terms of computer running time and computer storage requirements between the PLPAK (BEM) and (FEM). The superiority of the PLPAK can be seen from this table.

Table 6.3: A comparison between the present BEM and FEM results in Example 6.4.

	FEM	BEM
Time (min)	75	1 (98.67% less in time)
Size (MB)	2530	4.5 (99.82% less in storage)

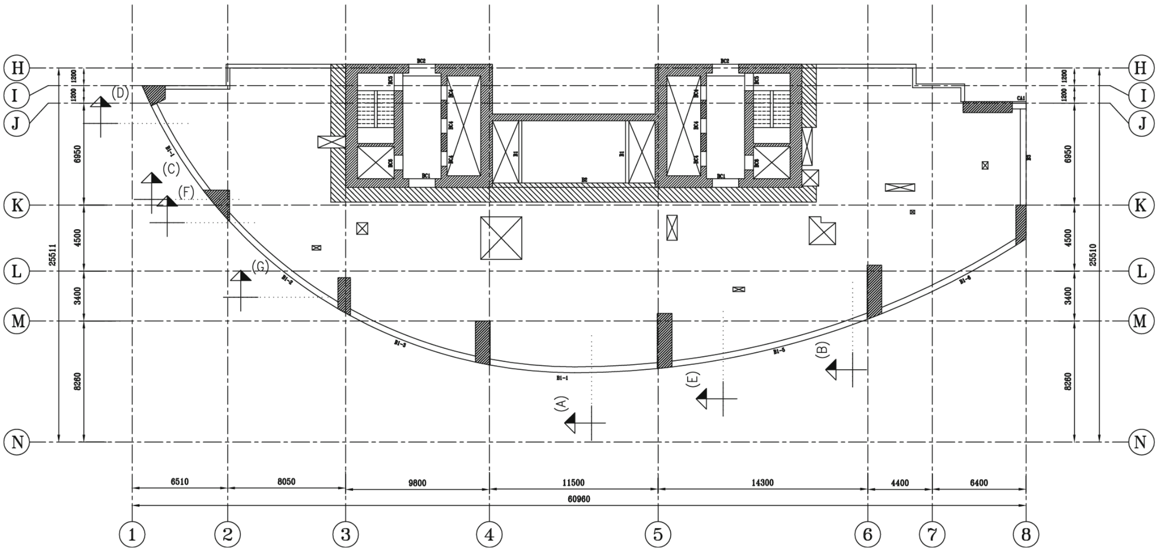

Figure 6.5: The practical slab geometry and section locations in Example 6.4 (dimensions are in mm).

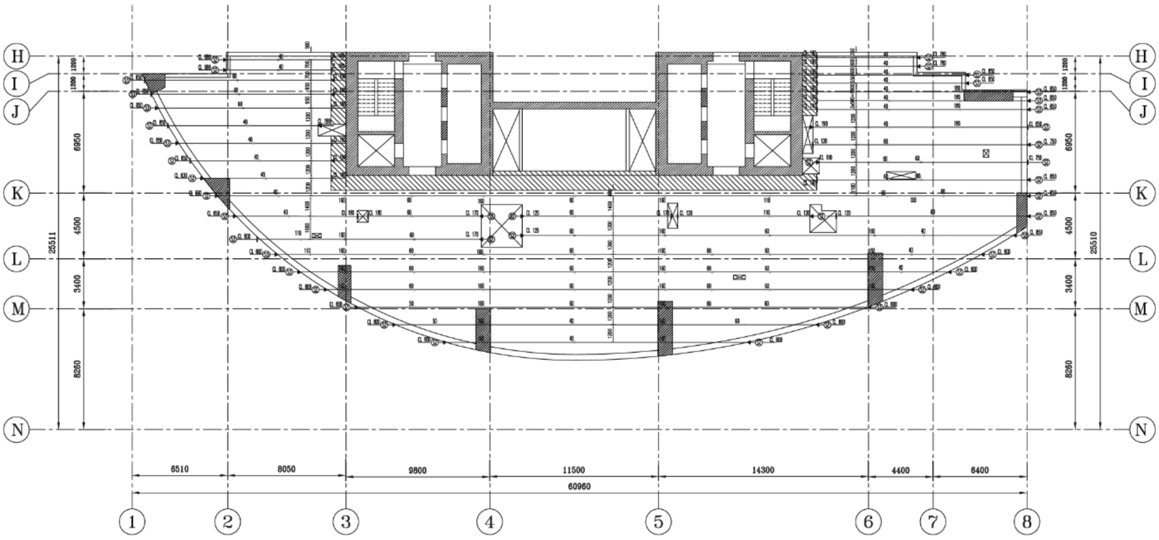

Figure 6.6: Cables layout in the X-direction in Example 6.4.

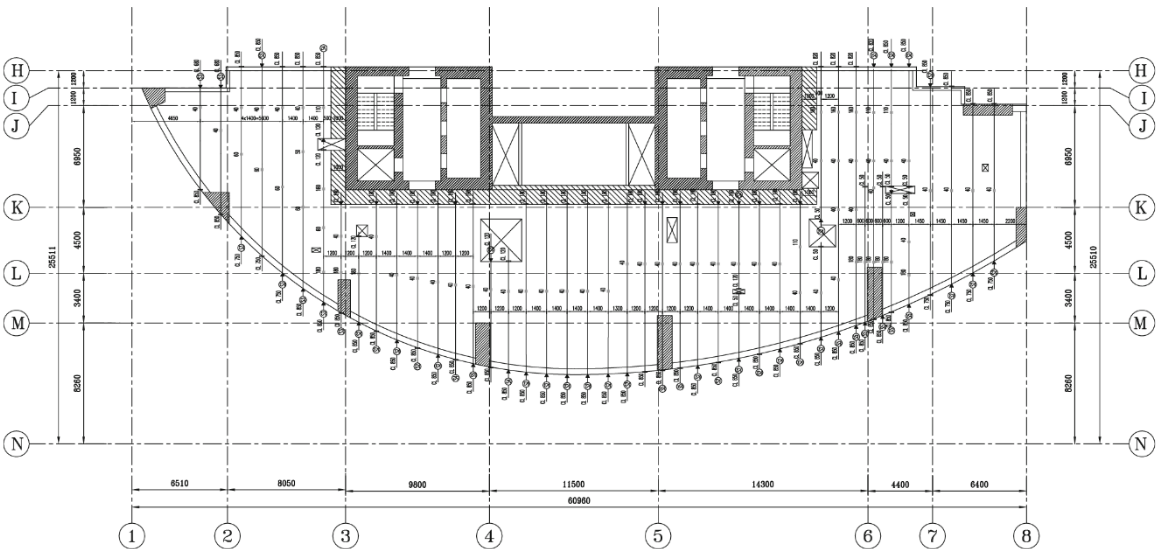

Figure 6.7: Cables layout in the Y-direction in Example 6.4.

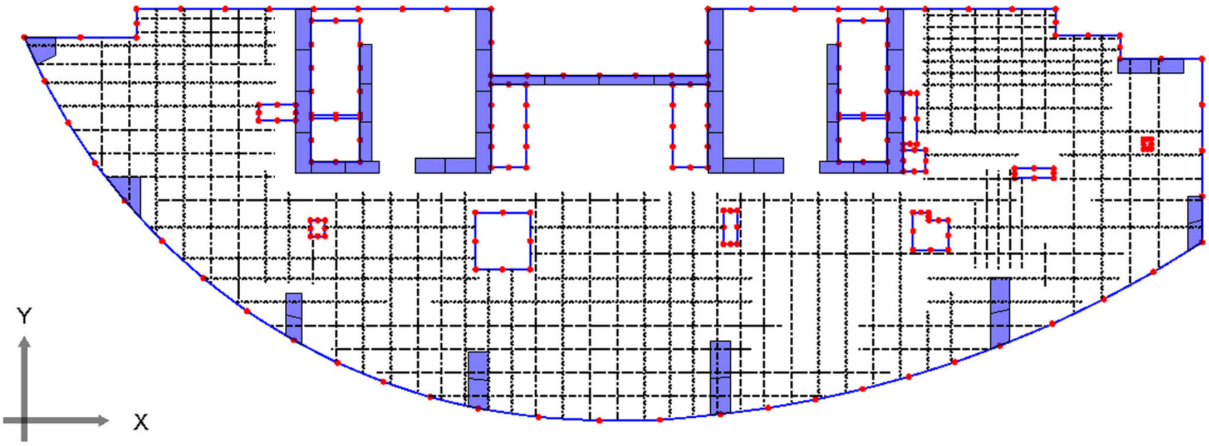

Figure 6.8: The boundary element model with cable cells and support cells in Example 6.4.

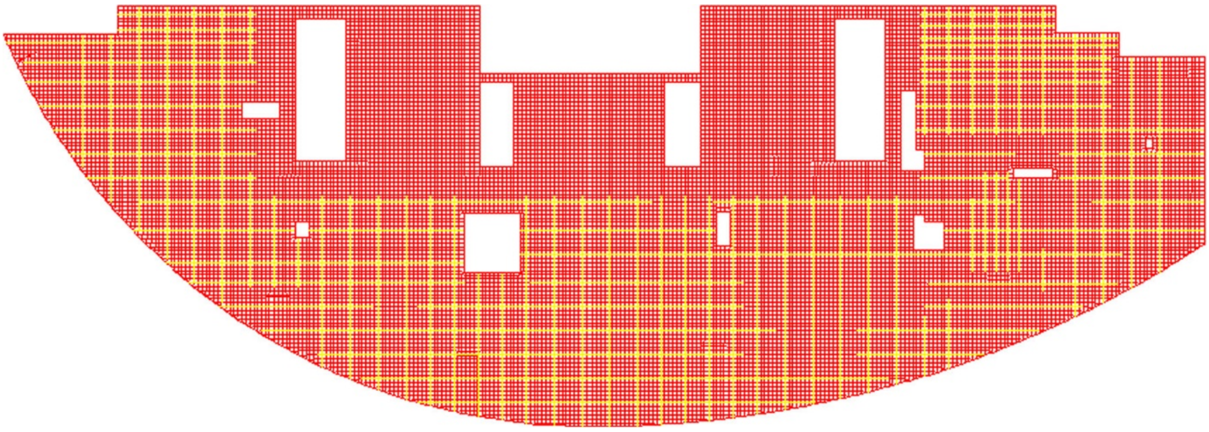

Figure 6.9: The finite element model in Example 6.4.

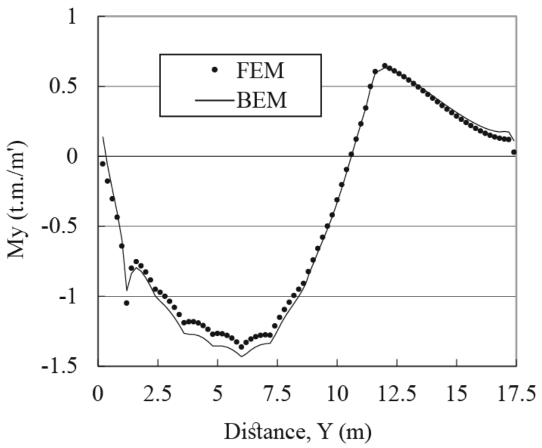

Figure 6.10: Example 6.4 bending moment along section A (m.t).

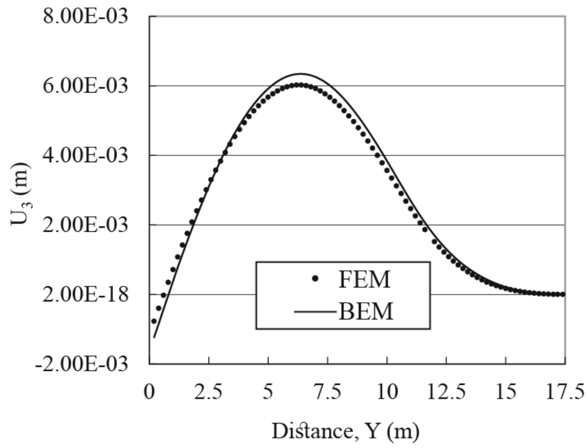

Figure 6.11: Example 6.4 deflection along section A (m).

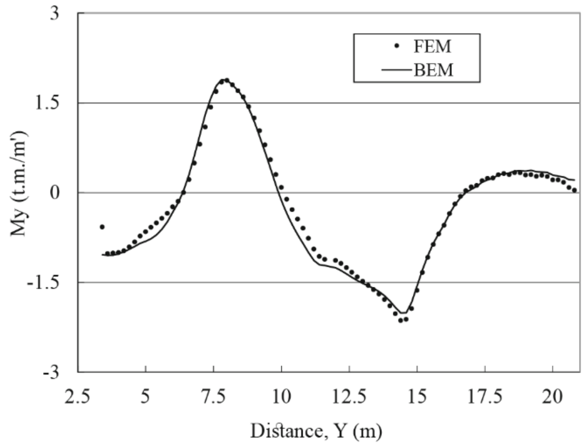

Figure 6.12: Example 6.4 bending moment along section B (m.t).

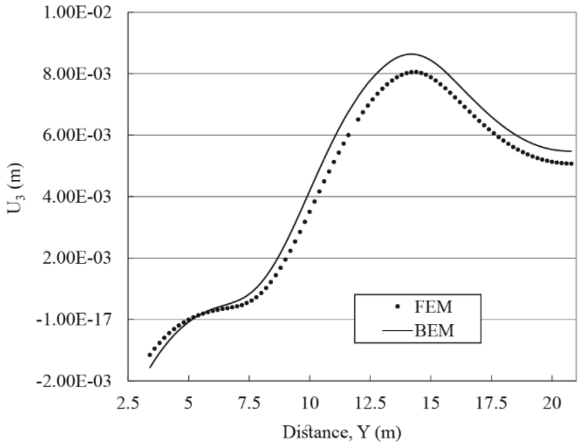

Figure 6.13: Example 6.4 deflection along section B (m).

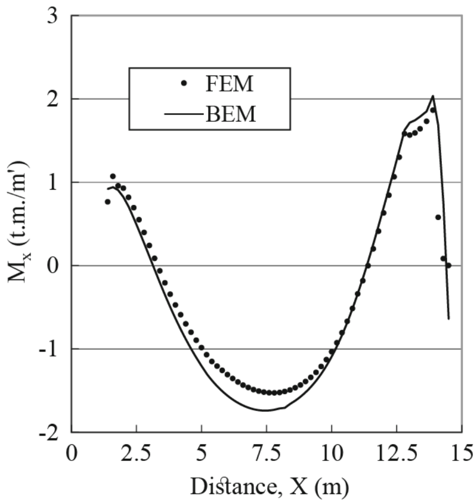

Figure 6.14: Example 6.4 bending moment along section C (m.t).

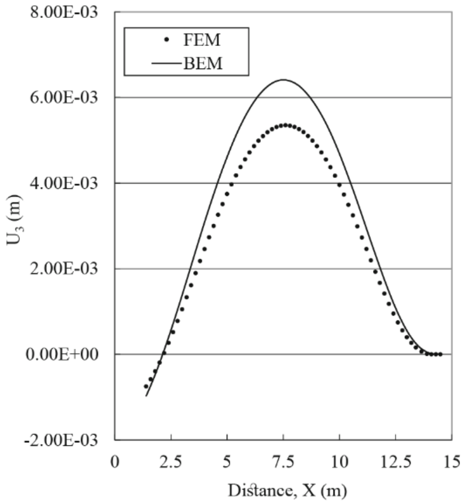

Figure 6.15: Example 6.4 deflection along section C (m).

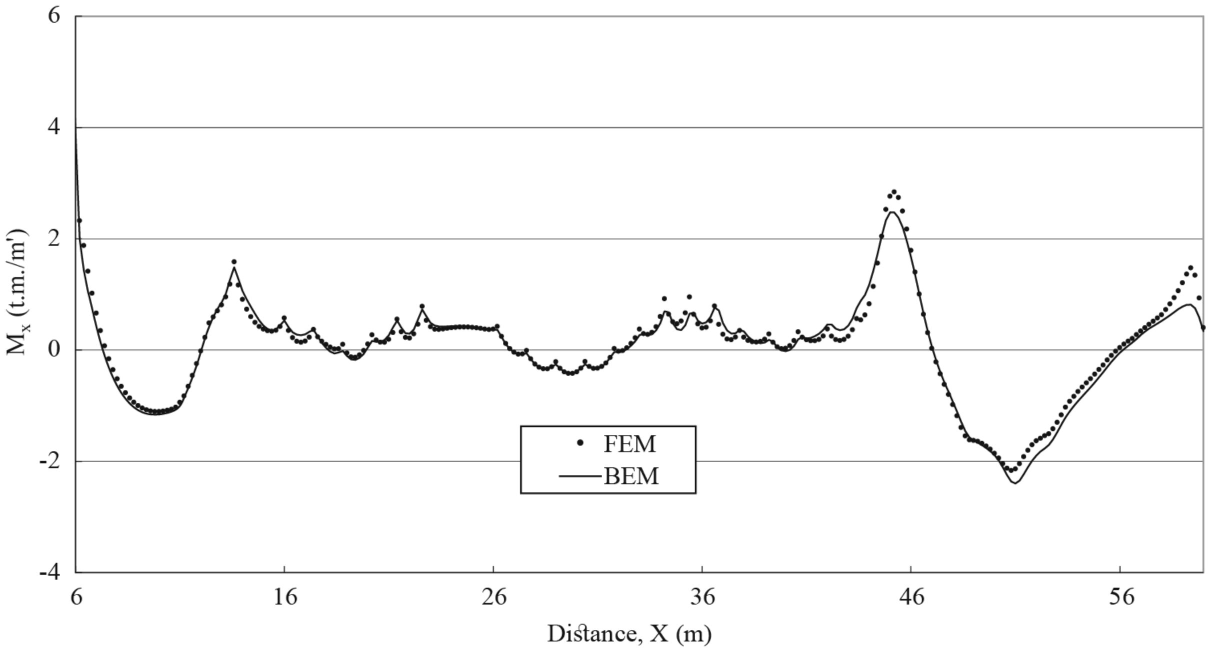

Figure 6.16: Example 6.4 bending moment along section D (m.t).

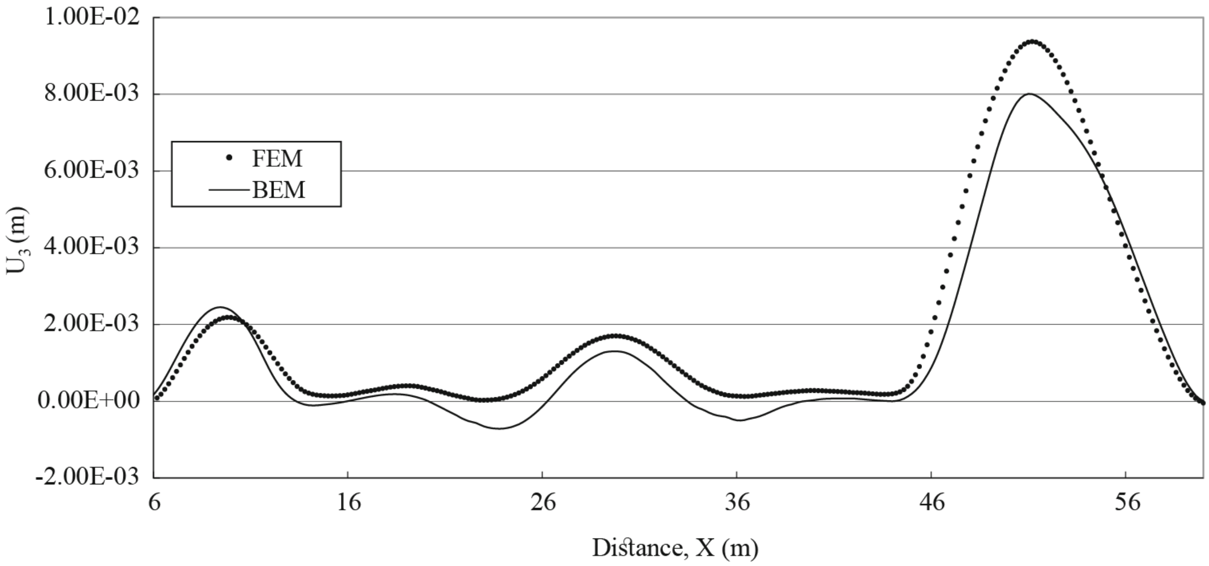

Figure 6.17: Example 6.4 deflection along section D (m).

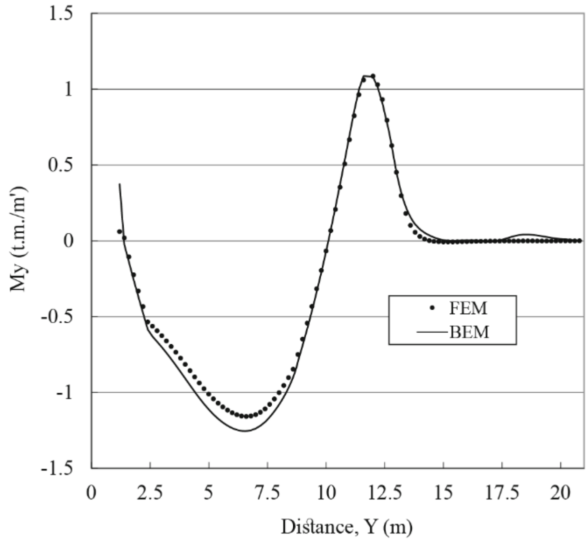

Figure 6.18: Example 6.4 bending moment along section E (m.t).

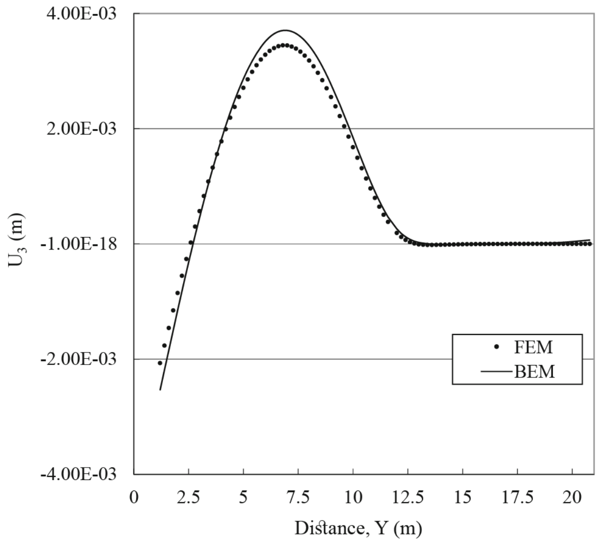

Figure 6.19: Example 6.4 deflection along section E (m).

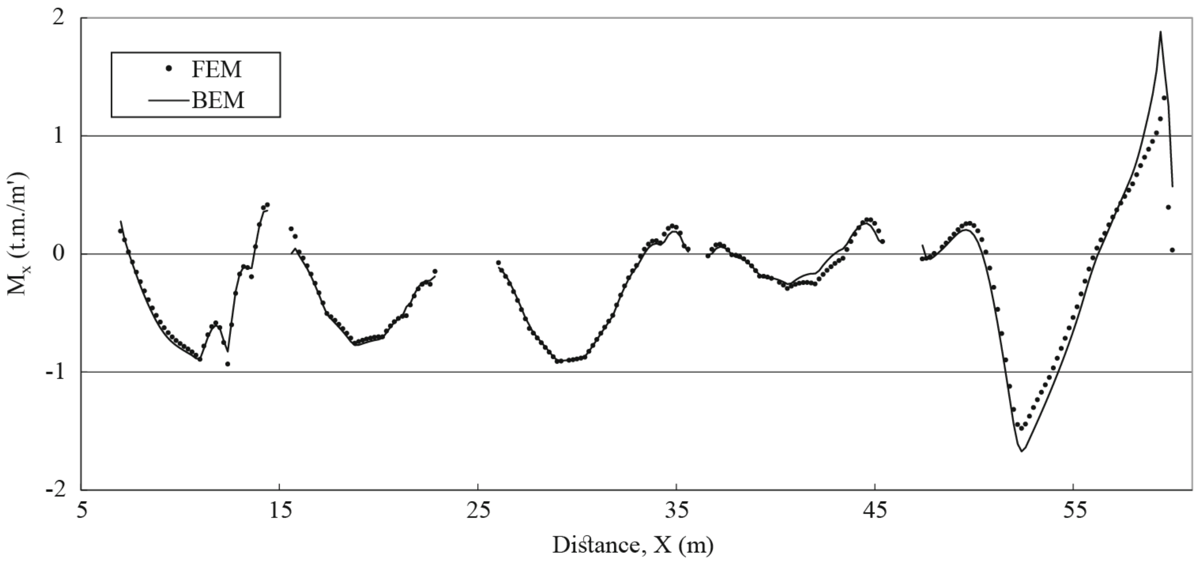

Figure 6.20: Example 6.4 bending moment along section F (m.t).

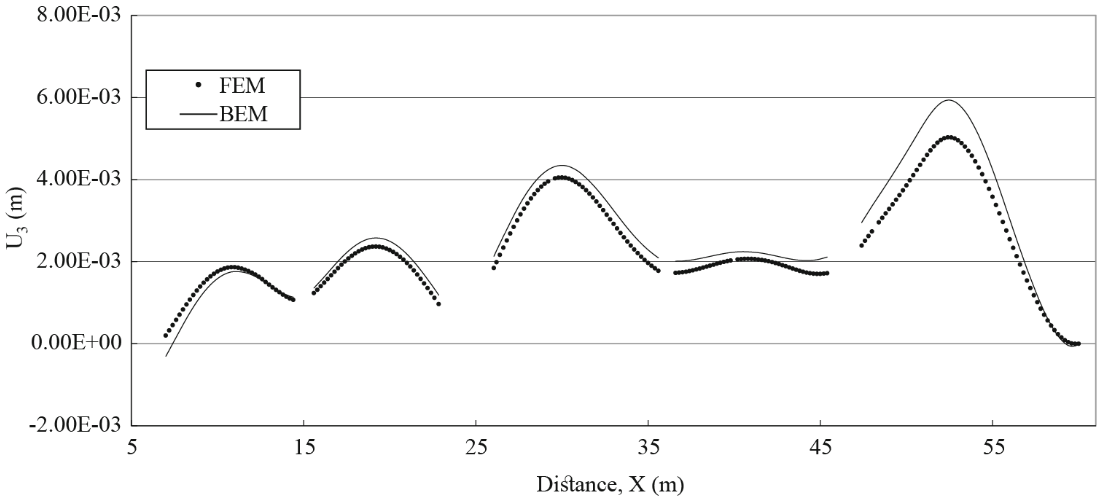

Figure 6.21: Example 6.4 deflection along section F (m).

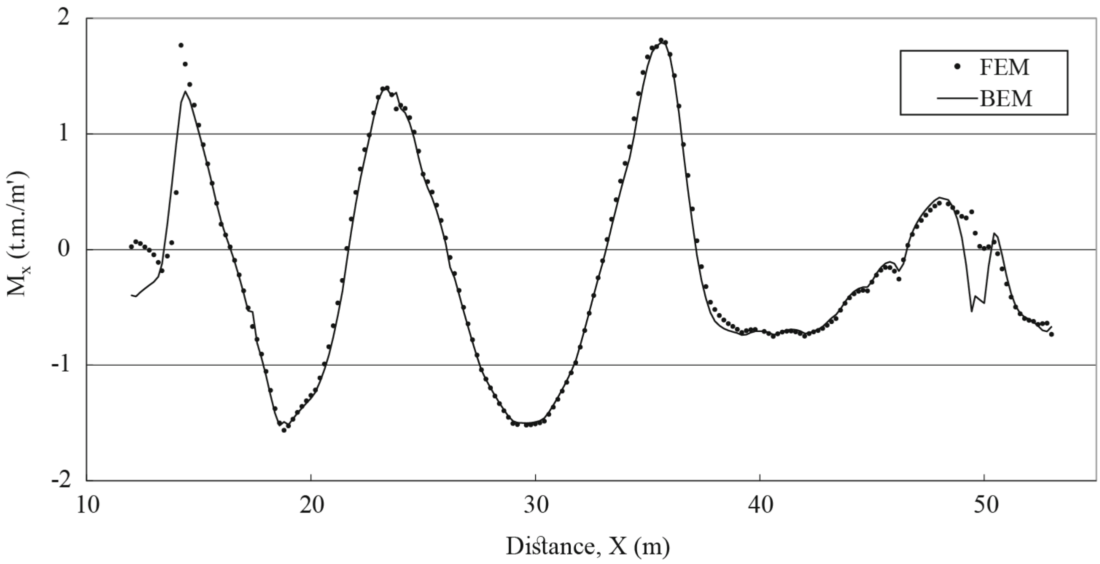

Figure 6.22: Example 6.4 bending moment along section G (m.t).

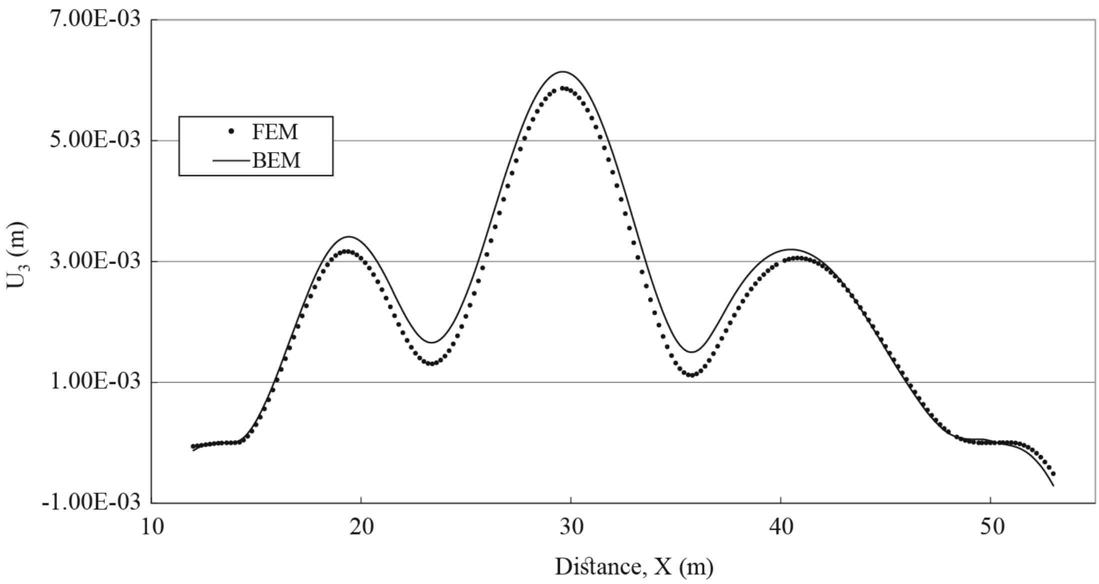

Figure 6.23: Example 6.4 deflection along section G (m).

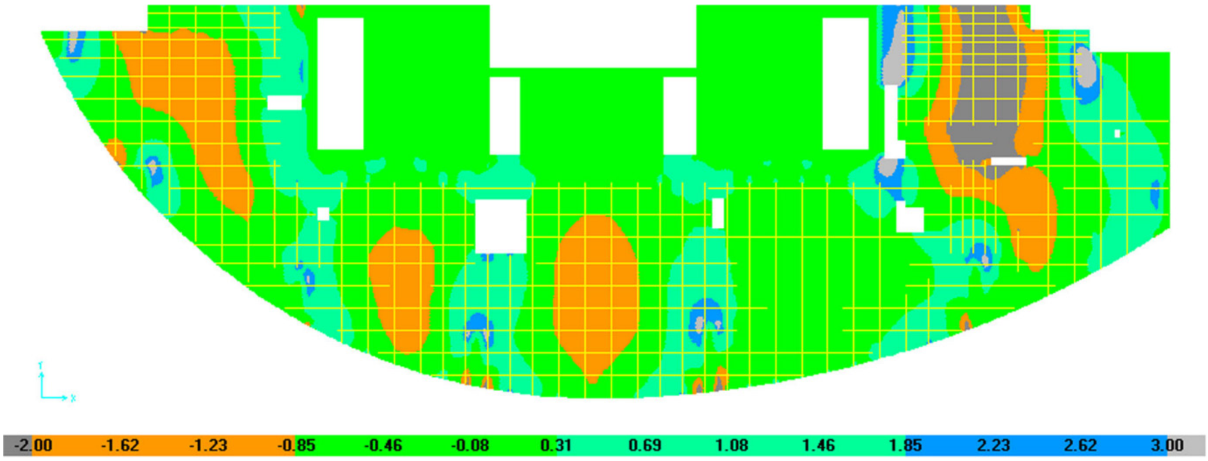

Figure 6.24: Example 6.4 contour map for bending moment Mxx in the finite element model (m.t).

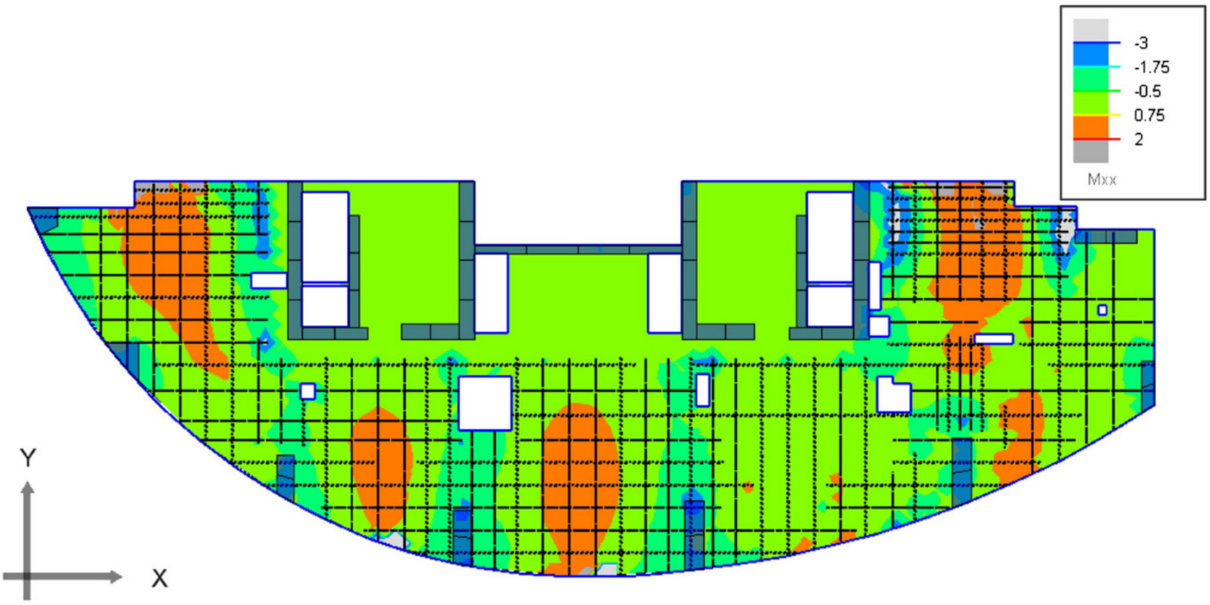

Figure 6.25: Example 6.4 contour map for bending moment Mxx in the boundary element model (m.t).

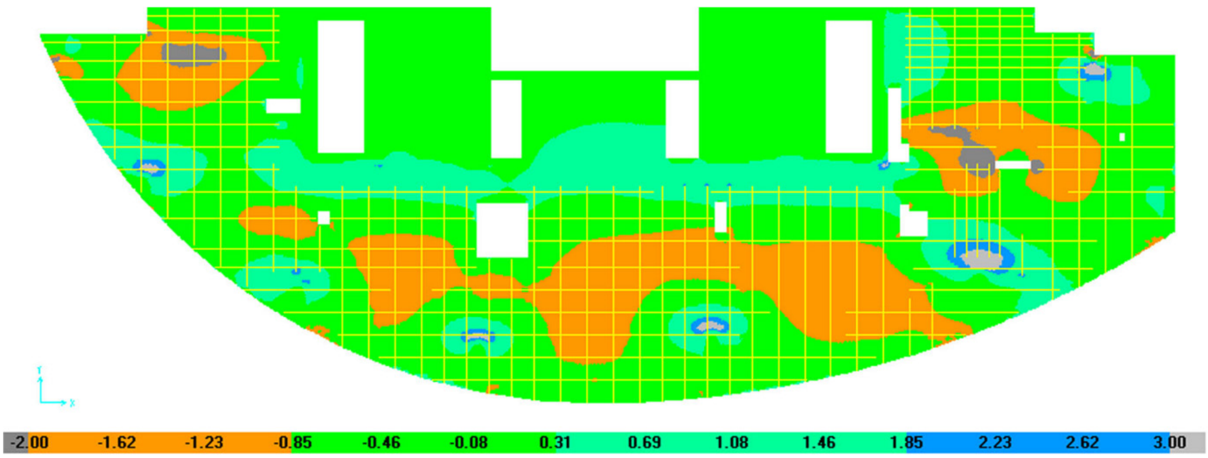

Figure 6.26: Example 6.4 contour map for bending moment Myy in the finite element model (m.t).

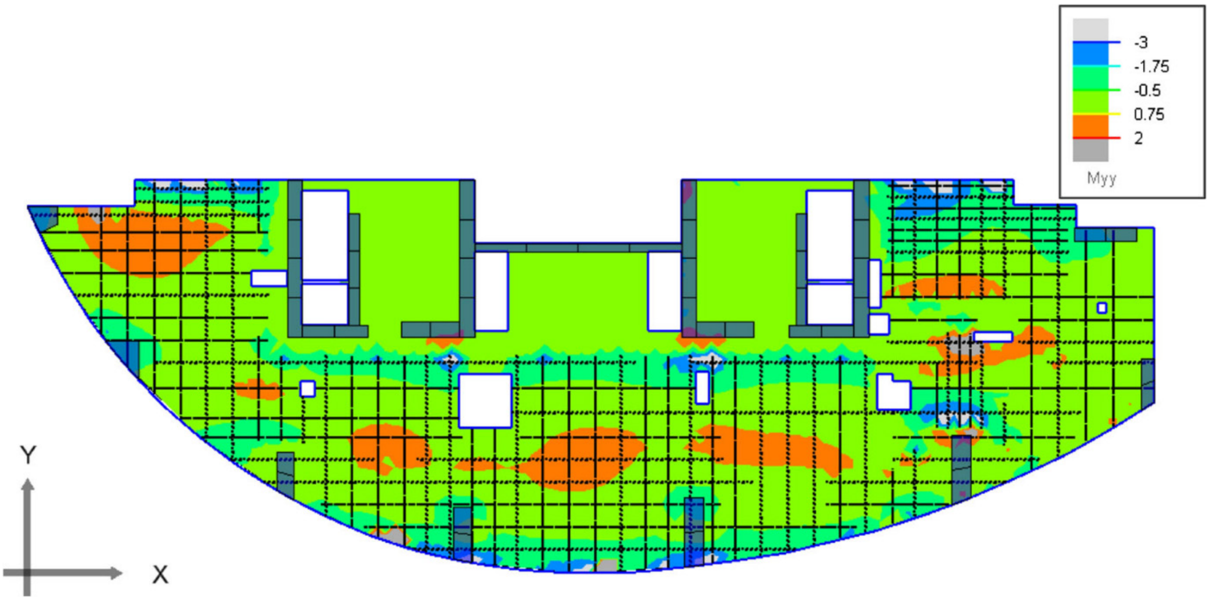

Figure 6.27: Example 6.4 contour map for bending moment Myy in the boundary element model (m.t).

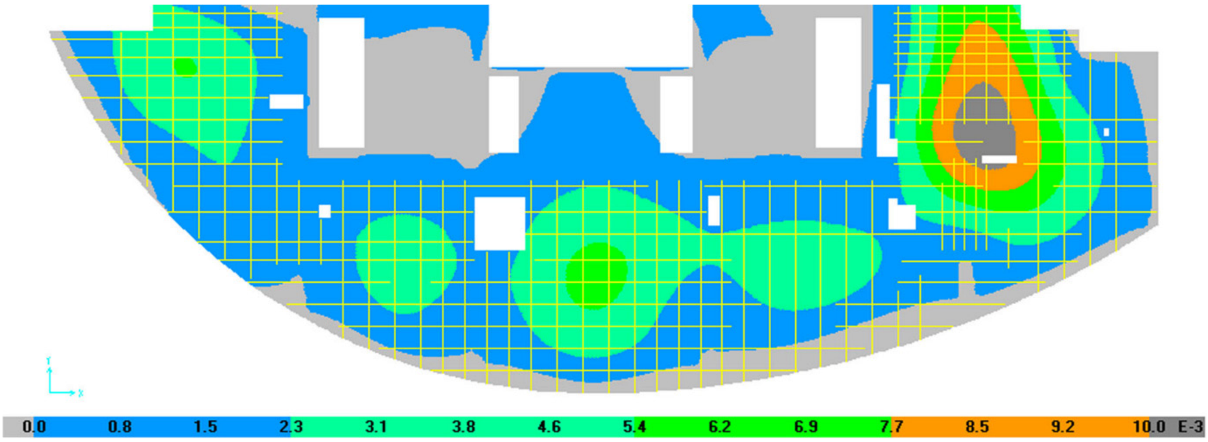

Figure 6.28: Example 6.4 contour map for vertical deflection Uz in the finite element model (m).

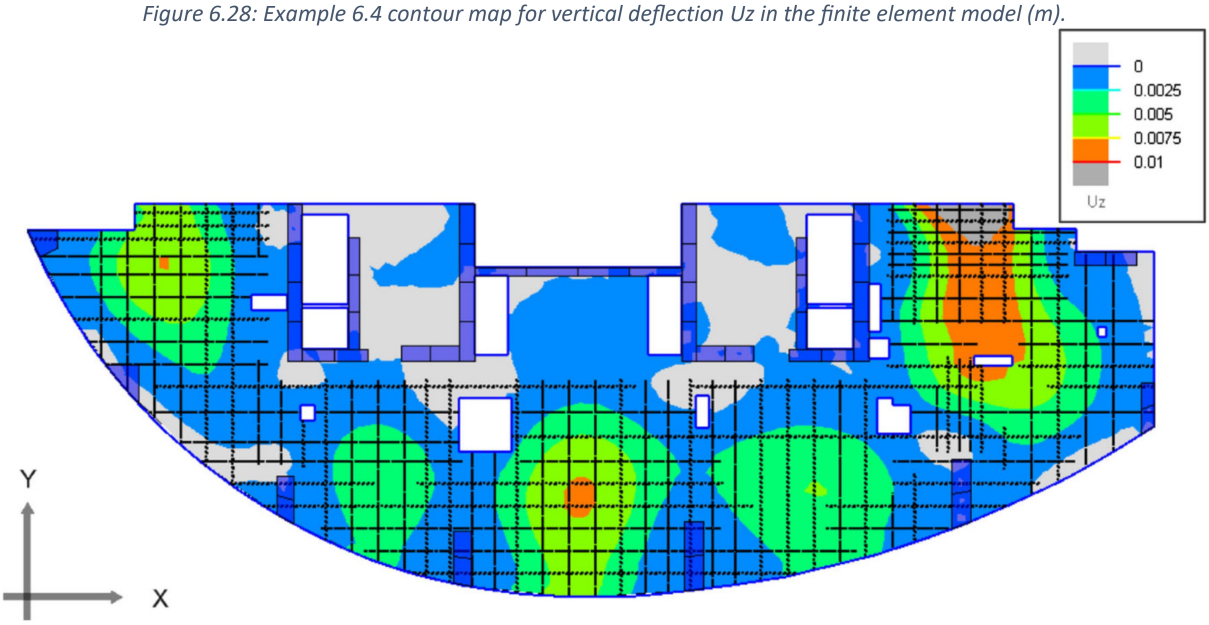

Figure 6.29: Example 6.4 contour map for vertical deflection Uz in the boundary element model (m).

Example 6.5

Purpose : Compare the results of PLPAK for a commercial building garage to those obtained from commonly used commercial finite element software.

Description : Figure 6.30 demonstrates a plain garage floor for a residential building with least column spacing of 7m. The garage dimensions are 35m in the long direction and 24m in the other. The material properties taken are Young's Modulus (E) = 2.1x10^6 t/m^2, Poisson's ratio (ν) = 0.16. The floor also contains structural elements such as cores, shear walls, beams, columns and openings. In this example, the structure is subjected to the pre-stressing loads only; all cables have a pre-stressing force of 1000kN (100t). A layout of post-tensioned cables was proposed as given in Figure 6.31.

The slab boundary is modeled using 87 boundary elements. The number of segments represented as internal cells are four hundred and fifty-six. Total number of extreme points is 783 for the model present BEM Model respectively. The generated model in the PLPAK pre-processor module (PLGen) is shown in Figure 6.32 while the numerical models are shown in Figure 6.34. The same slab is considered using FE auto-mesh of at least 0.25x0.25 m rectangular elements (6997 nodes and 6583 plate bending element (Figure 6.33)).

Results : The resulting deflection contour maps are shown in Figure 6.35 for both models. Moment results in the x-direction and y-direction are also demonstrated in Figure 6.36 and Figure 6.37 respectively. Contour spacing and color were adjusted manually to be able to relate the values. It is clearly noticeable that values produced by the BEM are verifiable by the FEM software.

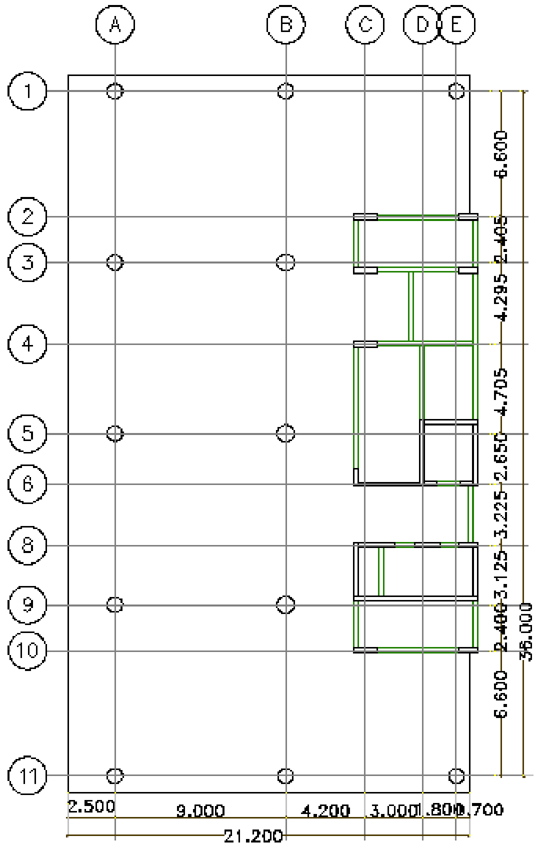

Figure 6.30: The structural system of post-tensioned garage floor in Example 6.5.

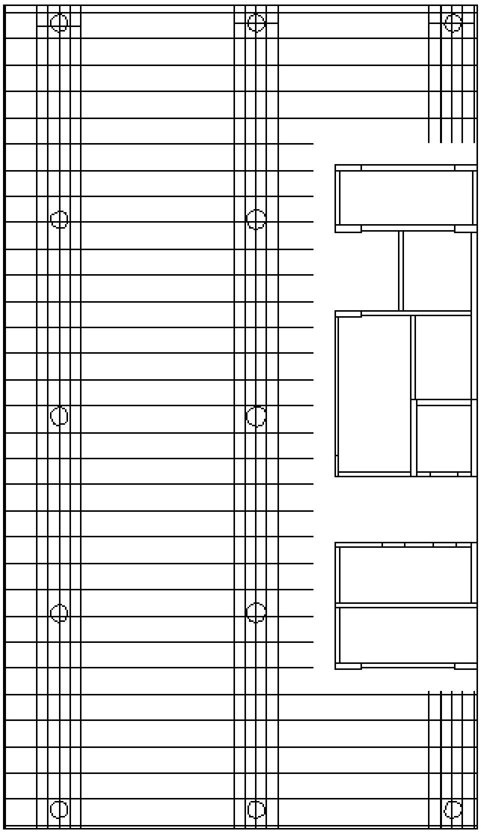

Figure 6.31: Layout of cables for the garage floor in Example 6.5.

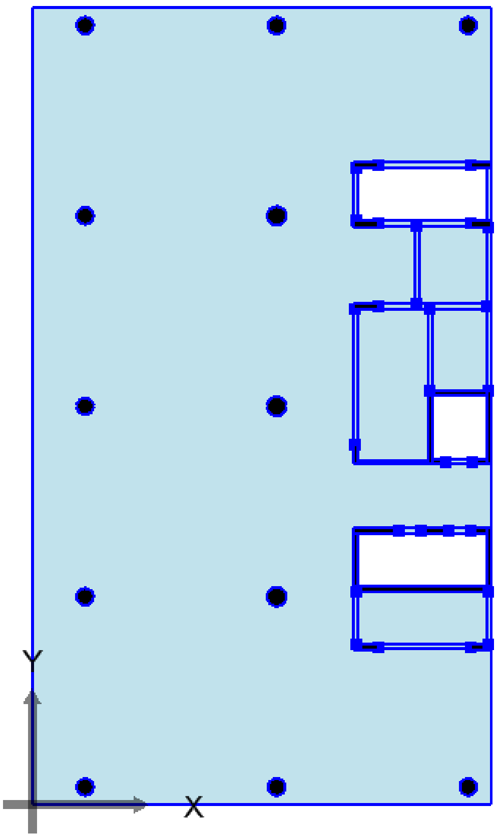

Figure 6.32: The PLGen model of the garage floor in Example 6.5.

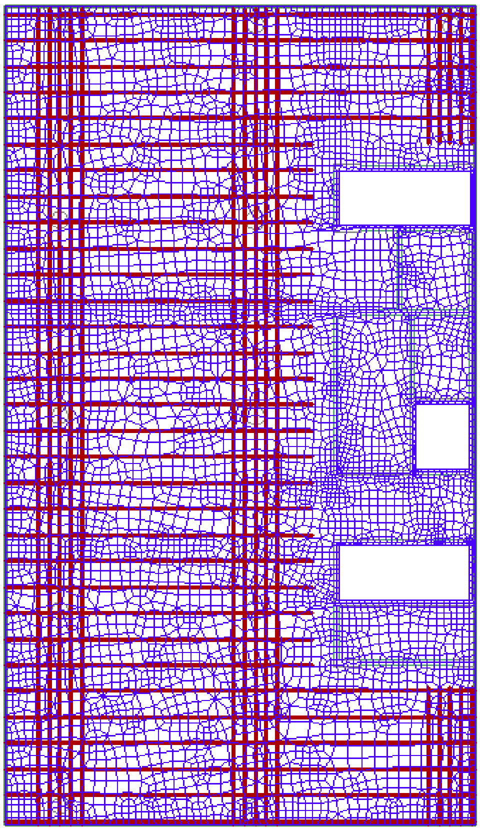

Figure 6.33: The used finite element mesh in the analysis in Example 6.5.

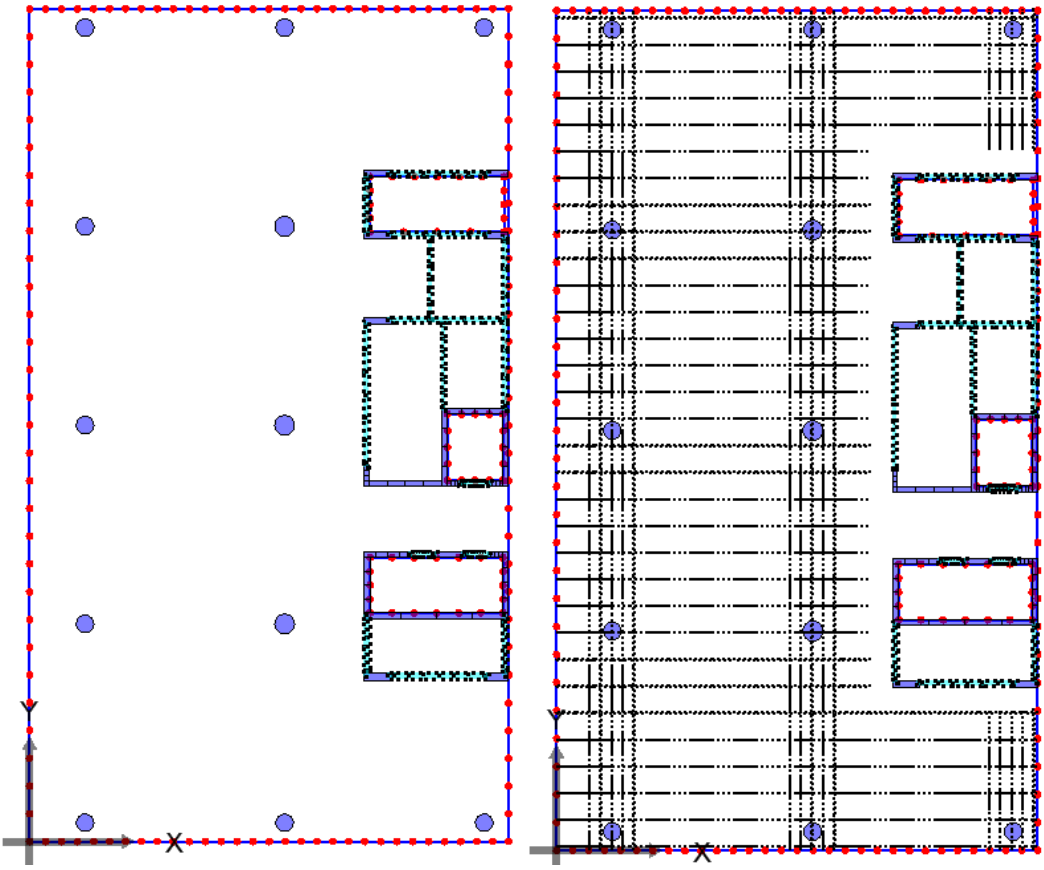

Figure 6.34: The PLView of the garage floor in Example 6.5 showing the numerical boundary element model before and after cable updating.

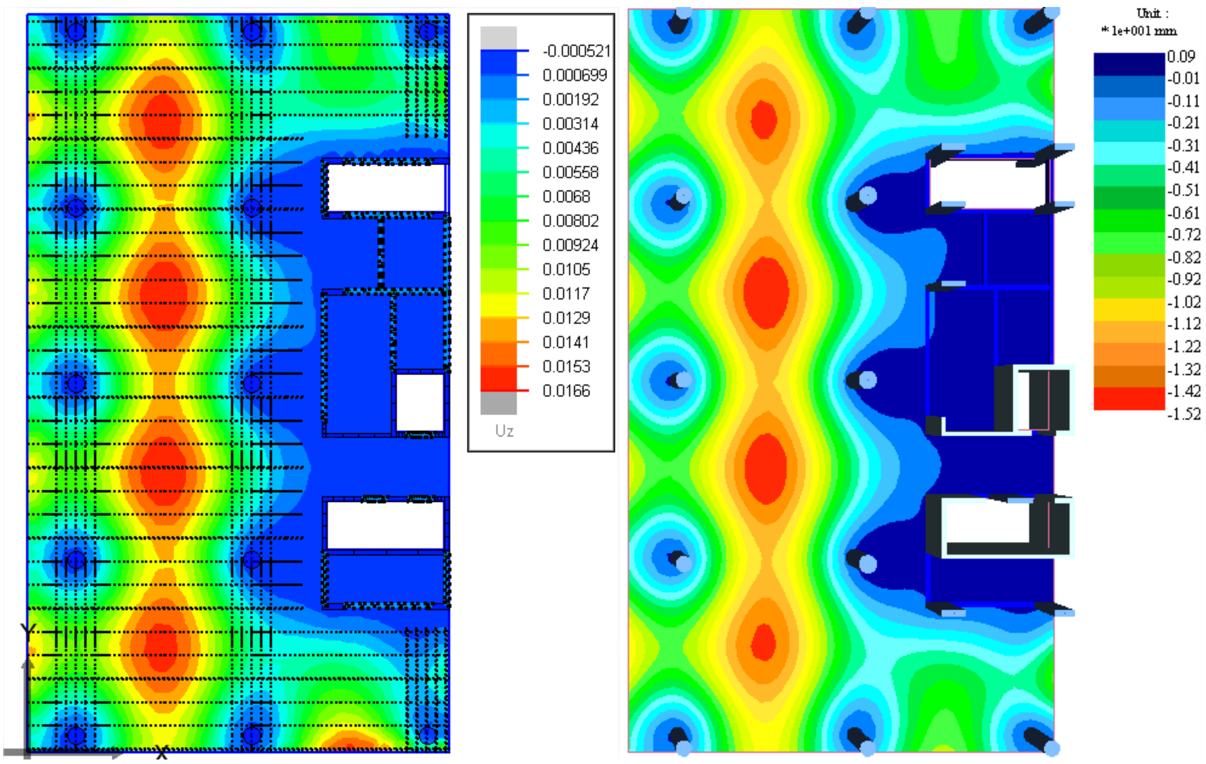

Figure 6.35: Results for deflections in Example 6.5 (Left: the proposed PLPAK-PTPAK, right: the finite element results).

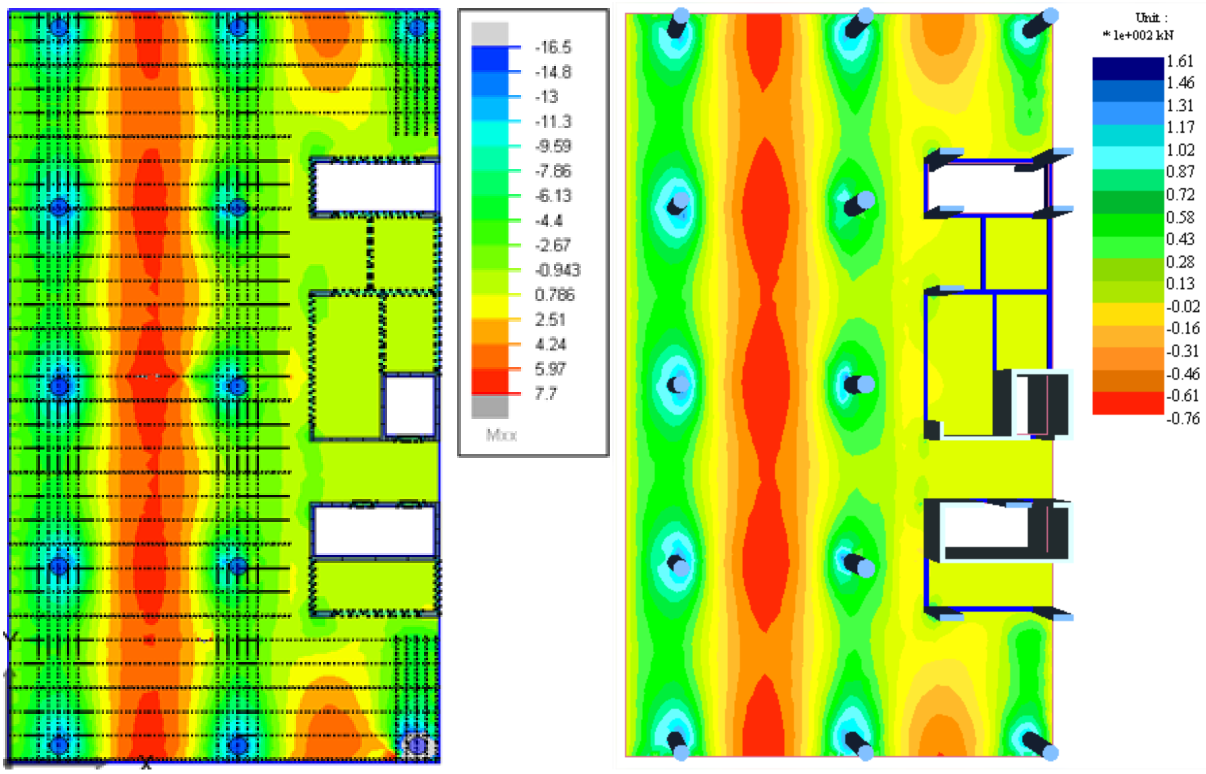

Figure 6.36: Results for moment in x-direction in Example 6.5 (Left: the proposed PLPAK-PTPAK, right: the finite element results).

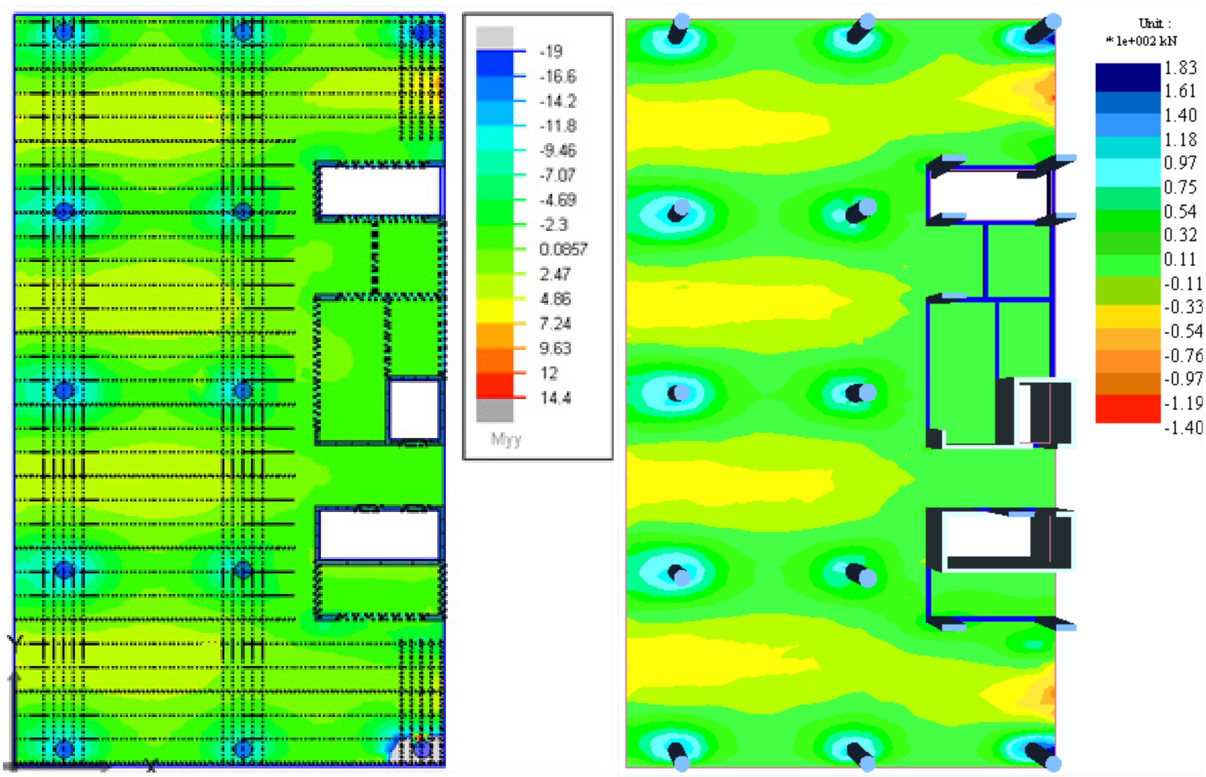

Figure 6.37: Results for moment in y-direction in Example 6.5 (Left: the proposed PLPAK-PTPAK, right: the finite element results).

Example 6.6

Purpose : Compare the results of PLPAK for an office building to those obtained from commonly used commercial finite element software.

Description : In this example the office building slab shown in Figure 6.38 is considered. The slab has maximum dimensions of 52x38 m and thickness of 0.22 m. Column spans vary from 5 to 9 m. The material properties used are E = 2.1×10^6 t/m^2, ν = 0.16. The slab is pre-stressed by cables in X & Y directions as shown in Figure 6.39 and Figure 6.40 respectively. Cable spacing varies from 0.65 m to 1.6 m in both directions. Cable force is equal to 16.5 t where cable groups are used. Each group contains from 3 to 6 cables. The slab is supported on group of columns of cross section 0.3 to 1.4 m^2 and central core of 3.0 m height. Figure 6.41 suggests the PLGen virtual model produced by the PLPAK.

The slab boundary is modeled using 245 boundary elements. Eleven thousand two hundred and eleven internal cells are used to represent the equivalent cable loads. Total number of extreme points is 23081. Wide columns or walls are modeled using the wall assembly option in the PLPAK, where each wall is divided into a series of connected supporting cells (shown in Figure 6.42). The results are demonstrated as contour maps and along section A-A using 310 internal points.

The same slab is considered using finite element mesh of 0.5x0.5 m rectangular elements, with internal meshing for shells 2x2. (7872 nodes and 7452 plate bending element (shown in Figure 6.43)).

Results : Figure 6.44 and Figure 6.45 demonstrate the distribution of deflection and bending moment contour maps in the considered slab, while Figure 6.46 and Figure 6.47 demonstrate bending moments and deflections results along section A-A. It can be seen that the PLPAK results are in good agreement when compared to results obtained from finite element analysis. A comparison is carried out to demonstrate the time and memory requirement for both the boundary and finite element. Table 6.4. provides the comparison in digits. The reduction in time of 33 % and in computer space reaches up to 99.4% as the gained when using BEM. It has to be noted that increase in meshing elements in finite element loads to drastically rise in analysis time.

Table 6.4: Capacity and elapsed time comparison in Example 6.6.

Commercial FE Software		PLPAK	
Space (MB)	Time (min.)	Space (MB)	Time (min.)
1500	15	9	5

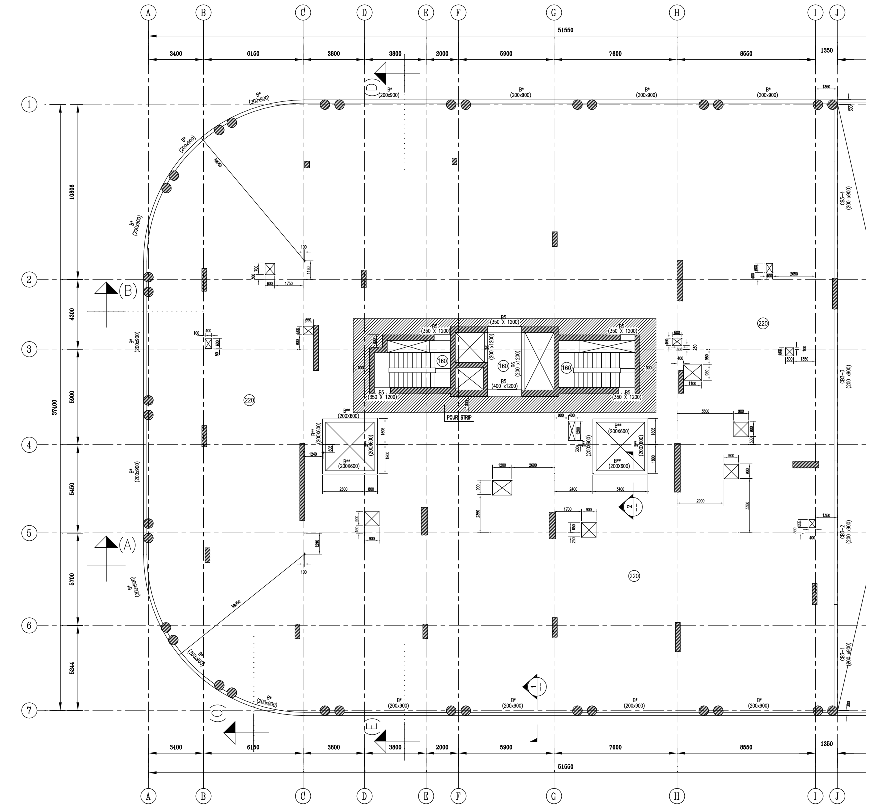

Figure 6.38: Structural System of the office building in Example 6.6.

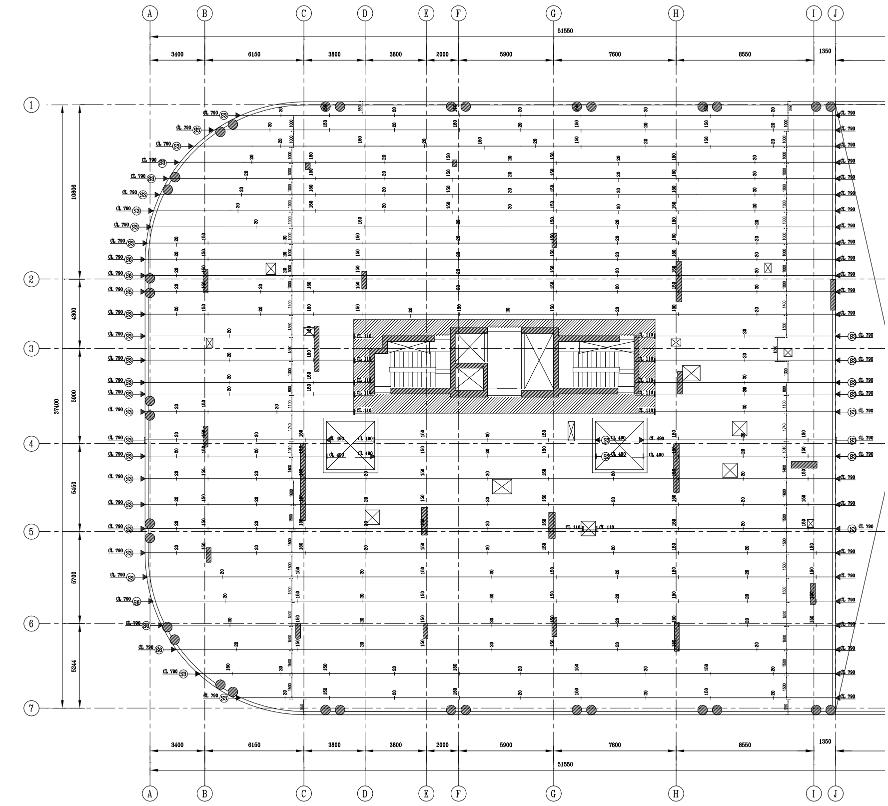

Figure 6.39: Cables in the X-direction for the office building in Example 6.6.

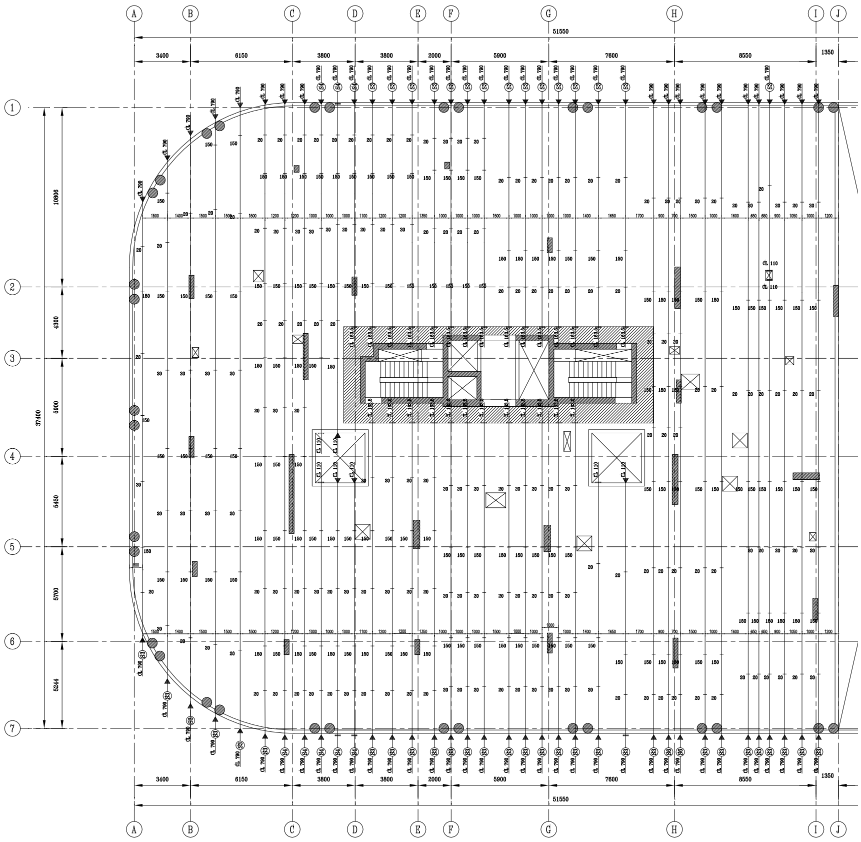

Figure 6.40: Cables in the Y-direction for the office building in Example 6.6.

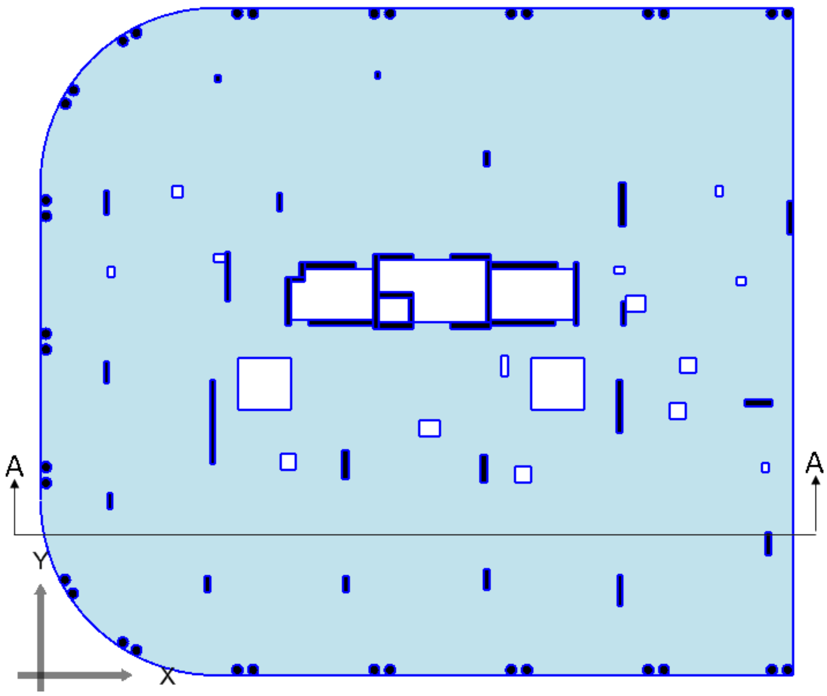

Figure 6.41: The PLGen model of the office building in Example 6.6.

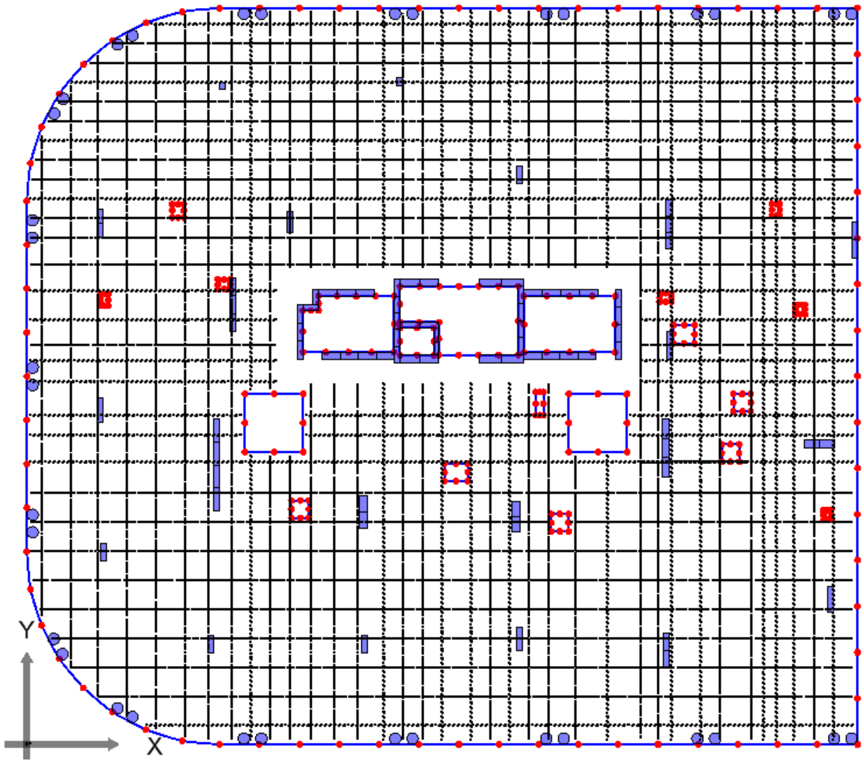

Figure 6.42: The PLView of the office building in Example 6.6 showing the boundary elements and the cable loading cells

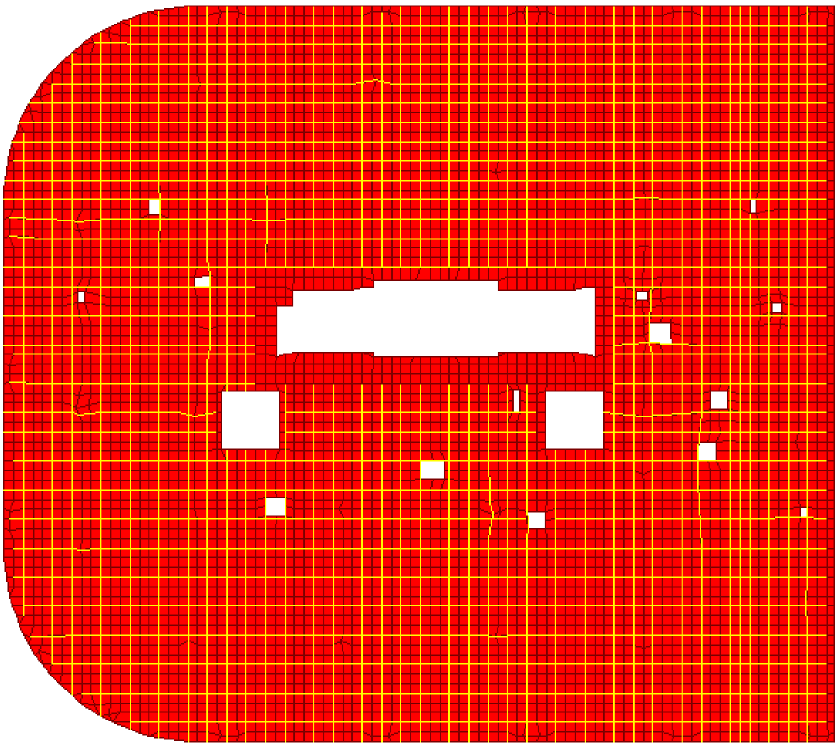

Figure 6.43: The used finite element divisions of the office building in Example 6.6 with cables

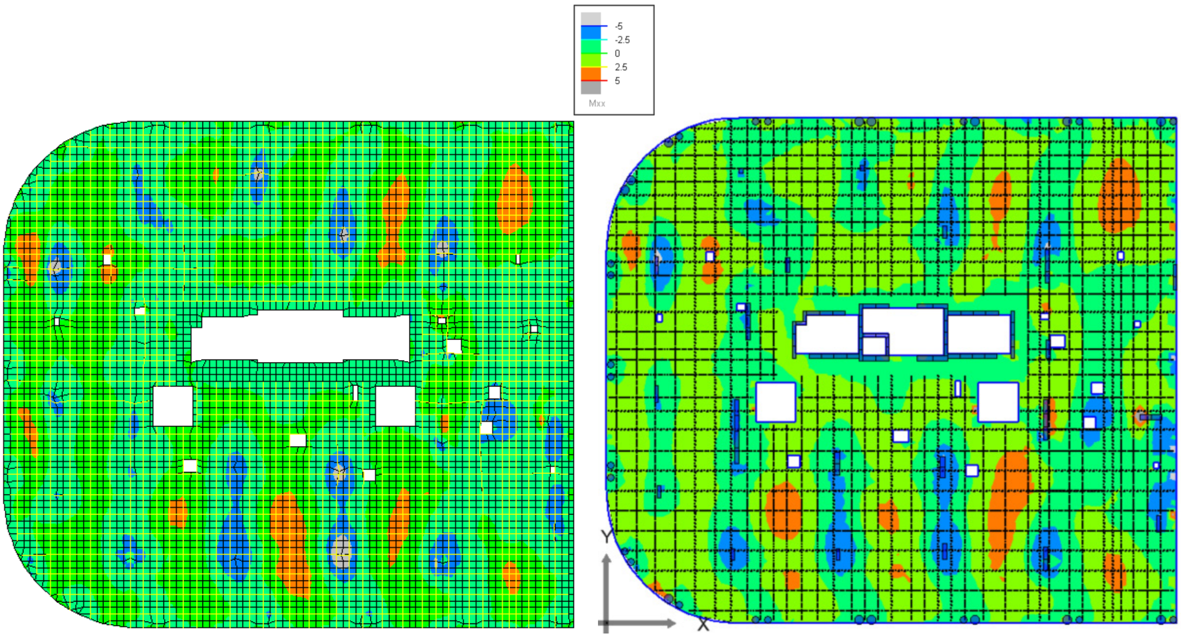

Figure 6.44: Results for moment in x-direction in Example 6.6 (Left: The finite element results, right: the proposed PLPAK-PTPAK).

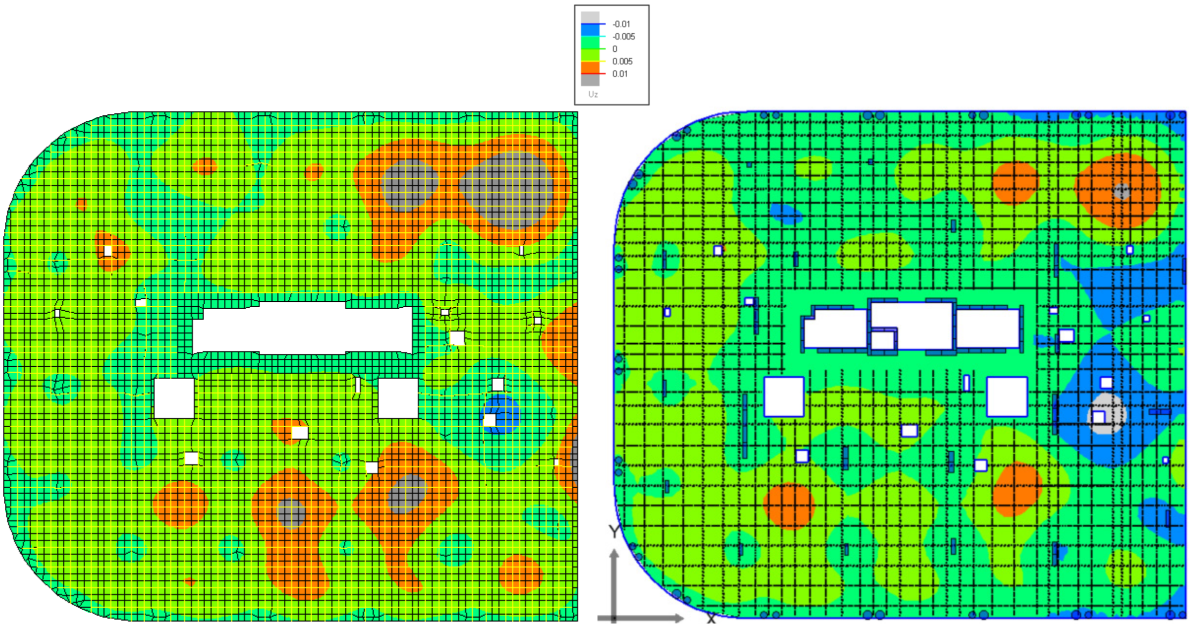

Figure 6.45: Results for deflection in Example 6.6 (Left: The finite element result, right: the proposed PLPAK-PTPAK).

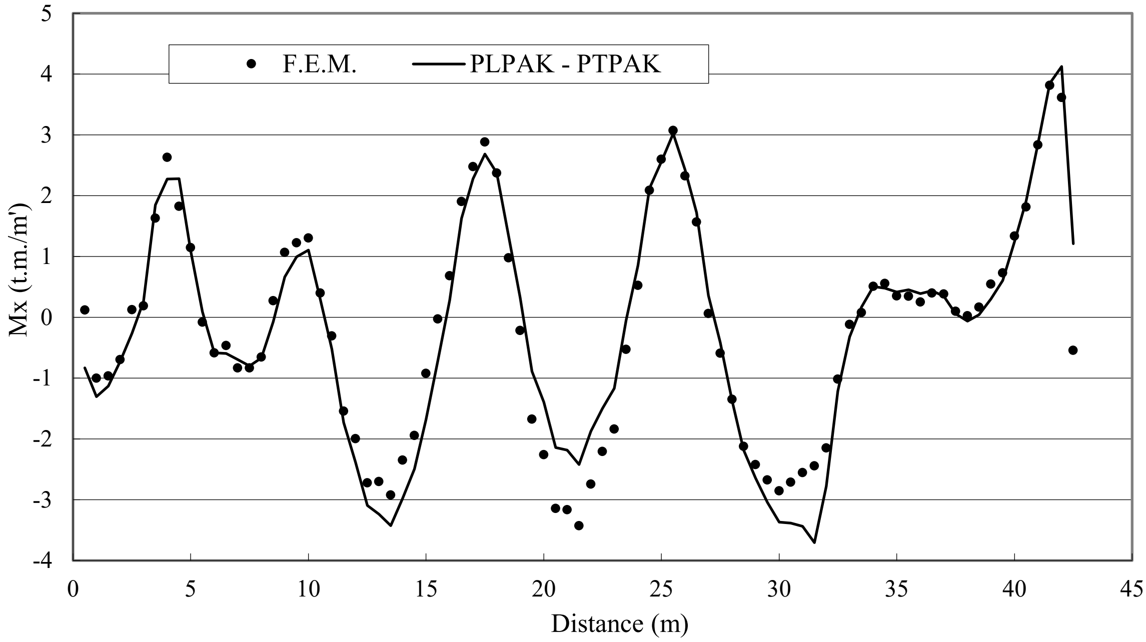

Figure 6.46: Example 6.6 moments in the x-direction along section A-A.

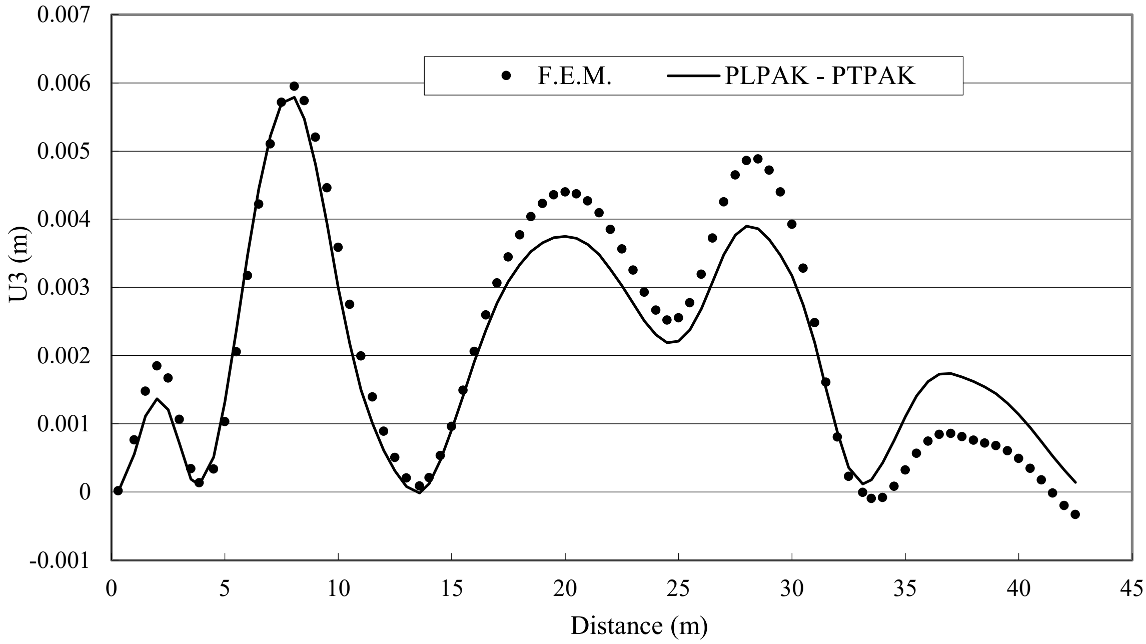

Figure 6.47: Example 6.6 deflections along for section A-A.

Example 6.7

Purpose : Compare the results of PLPAK to those obtained from commonly used commercial finite element software (ADAPT).

Description : In this example, a square slab 12 m ×12 m supported on four columns each 0.2 m × 0.2 m is considered as shown in Figure 6.48. Slab has material properties as follows ($E = 2.7828 \times 10^7\ kN/m^2$, $v = 0.2$). Slab thickness = 0.2 m. Slab is subjected to its own weight in addition to uniform load = $8\ kN/m^2$. The chosen design strips for the PLPAK and the FEM are shown in Figure 6.51 and Figure 6.52 respectively.

Results : Figure 6.49 and Figure 6.50 demonstrate the bending moment contour for the PLPAK and the FEM respectively. Table 6.5 shows the bending moment at the design strips. Figure 6.53, Figure 6.54 and Table 6.6 shows the stresses at the design strips.

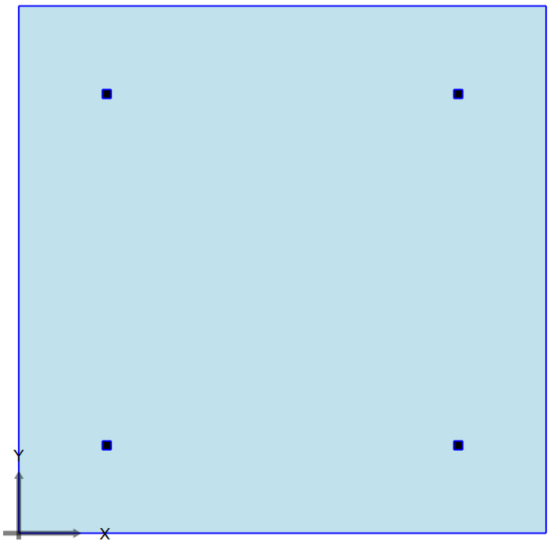

Figure 6.48: Example 6.7 slab model.

Table 6.5: PLPAK and FEM design strips bending moments in Example 6.7.

	PLPAK		ADAPT	
	+ve moment	-ve moment	+ve moment	-ve moment
Strip 1 (2m)	72.705	-138.3	156.5 (78.25*2)	-115.92
Strip 2 (4m)			309.9 (77.475*4)	-147.88
Strip 3 (6m)			445.76 (74.29*6)	-131.21

Table 6.6: PLPAK and FEM design strips stresses in Example 6.7.

	PLPAK		ADAPT	
	Top stress	Bottom stress	Top stress	Bottom stress
Strip 1 (2m)	8906.35	10726.41	8694	11740
Strip 2 (4m)	6750.01	10549.99	5609	11620
Strip 3 (6m)	3668.83	10082.55	3280	11140

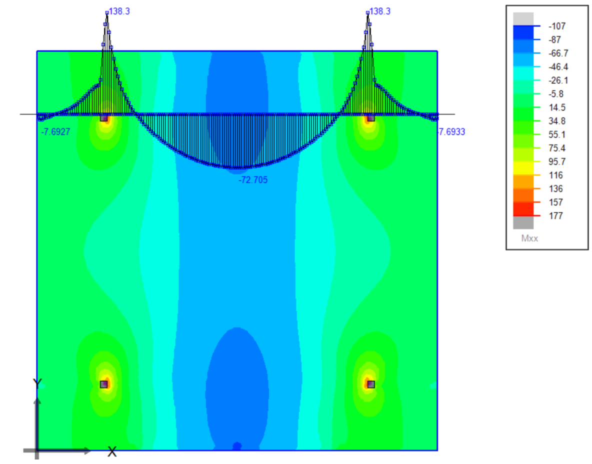

Figure 6.49: Example 6.7 PLPAK bending moment contour.

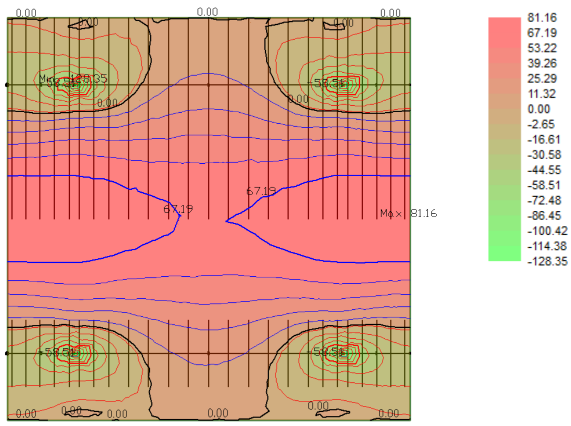

Figure 6.50: Example 6.7 FEM bending moment contour.

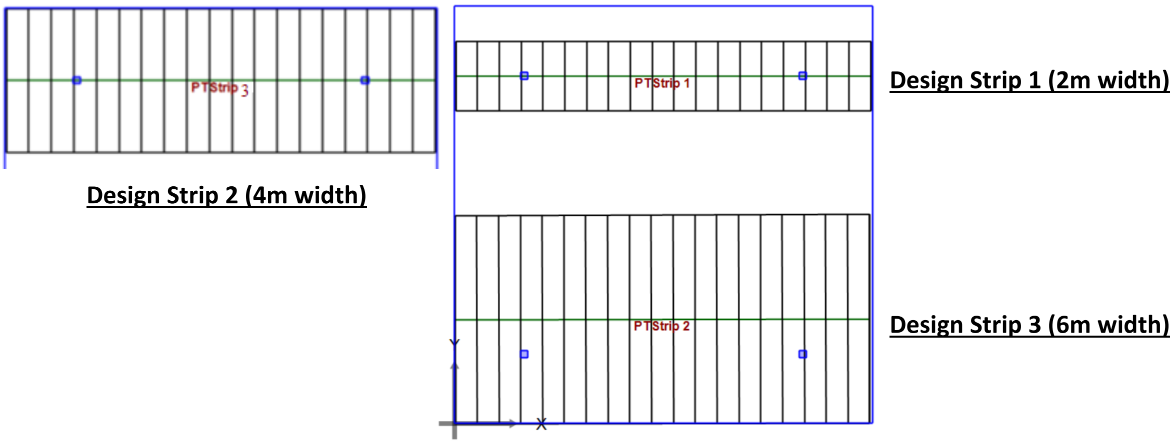

Figure 6.51: Example 6.7 PLPAK design strips.

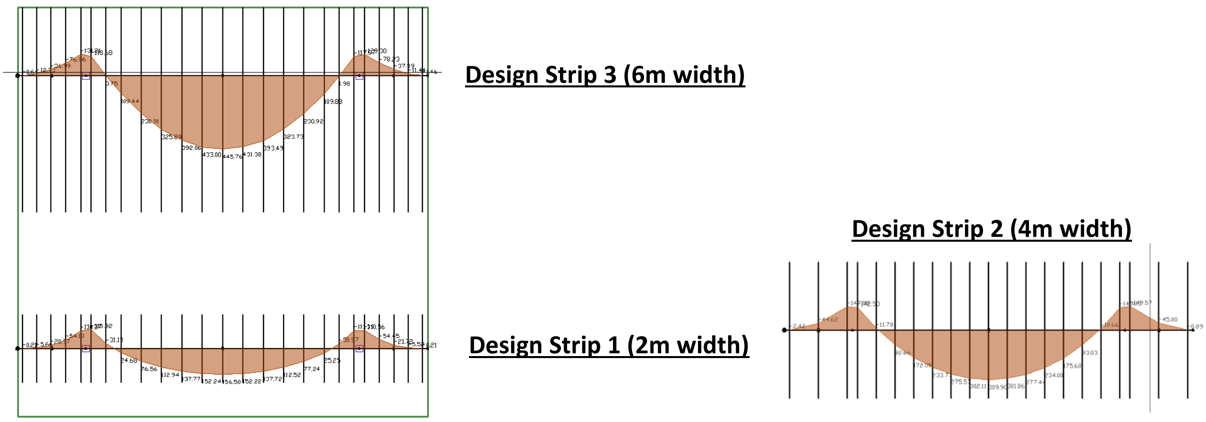

Figure 6.52: Example 6.7 FEM design strips.

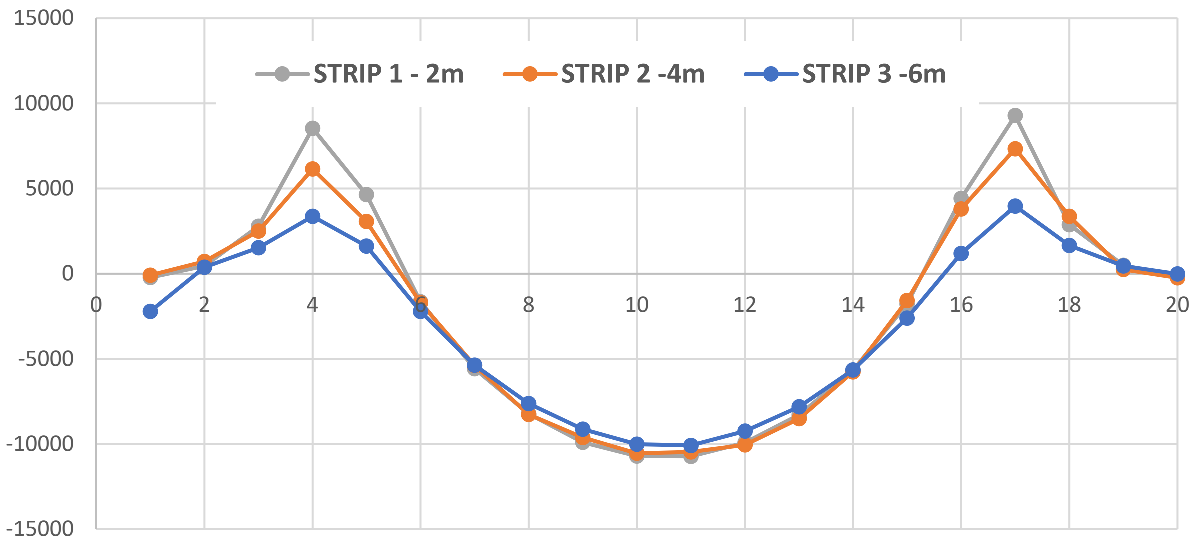

Figure 6.53: Example 6.7 PLPAK design strips stresses.

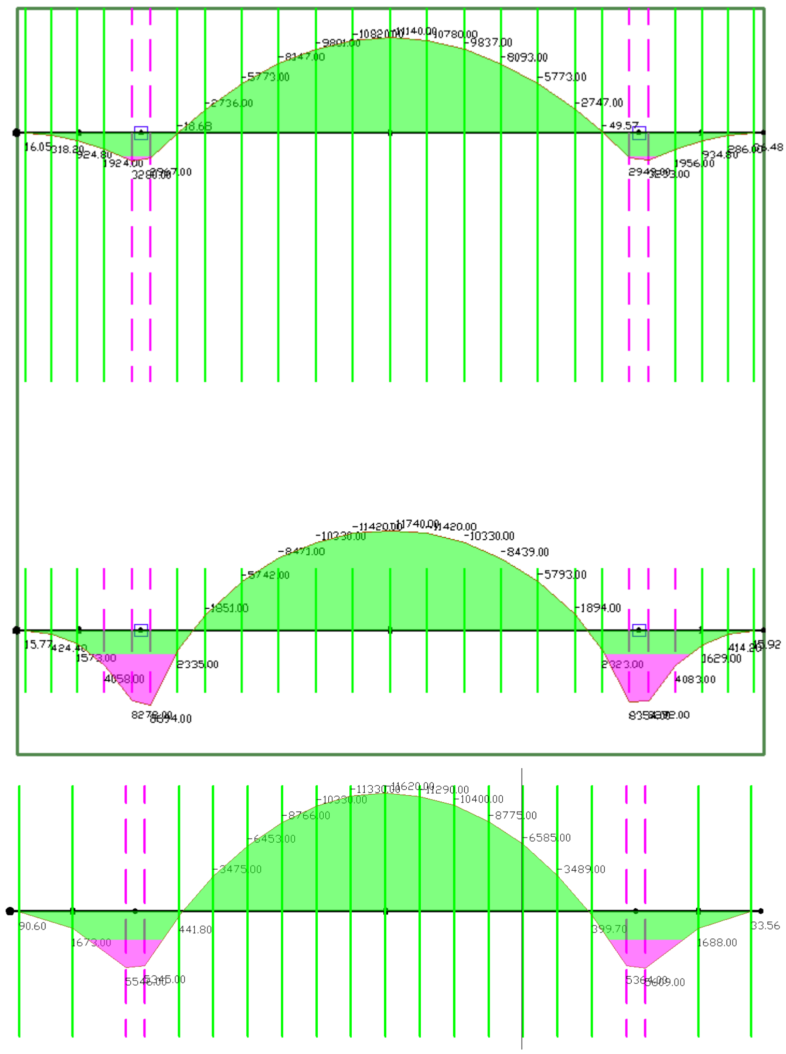

Figure 6.54: Example 6.7 FEM design strips stresses.

Example 6.8

Purpose : Compare the results of PLPAK to those obtained from commonly used commercial finite element software (ADAPT).

Description : In this example, a square slab 12 m ×12 m supported on four columns each 0.2 m × 0.2 m is considered with drops of thickness 0.1 m as shown in Figure 6.55 and Figure 6.56. Slab has material properties as follows ($E = 2.7828 \times 10^7\ kN/m^2$, $v = 0.2$). Slab thickness = 0.2 m. Slab is subjected to its own weight in addition to uniform load $= 8\ kN/m^2$. The design strips are shown at Figure 6.59.

Results : Figure 6.57 and Figure 6.58 demonstrate the bending moment contour for the PLPAK and the FEM respectively. Table 6.7 shows the bending moment at the design strips. Figure 6.60, Figure 6.62 and Table 6.8 shows the stresses at the design strips. Figure 6.61 shows the bending moment for a strip passing throw the drop in the PLPAK.

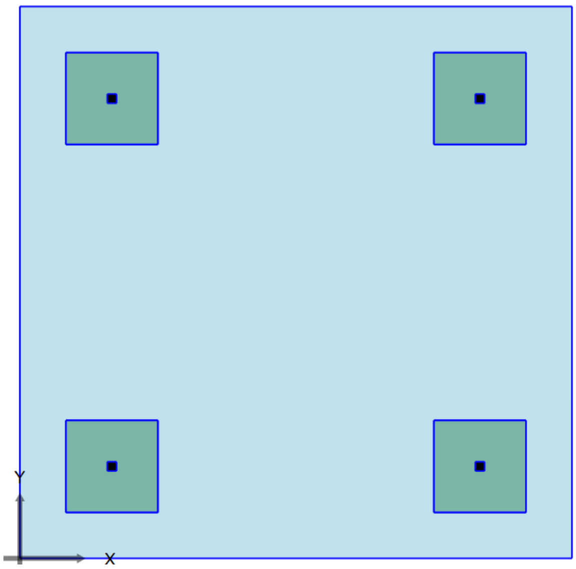

Figure 6.55: Example 6.8 PLPAK slab model.

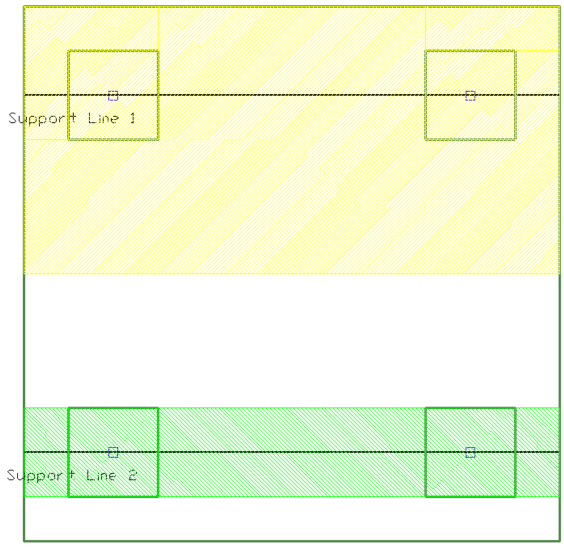

Figure 6.56: Example 6.8 FEM slab model.

Table 6.7: PLPAK and FEM design strips bending moments in Example 6.8.

	PLPAK		ADAPT	
	+ve moment	-ve moment	+ve moment	-ve moment
Strip 1 (2m)			147.57(73.785*2)	-114.25
-	71.04	-155	-	-
Strip 3 (6m)			428.83(71.47*6)	-112.88

Table 6.8: PLPAK and FEM design strips stresses in Example 6.8.

	PLPAK		ADAPT	
	Top stress	Bottom stress	Top stress	Bottom stress
Strip 1 (2m)	3312.96	10488.9	3372	11380
-	-	-	-	-
Strip 3 (6m)	1173.56	9989.69	1476	11010

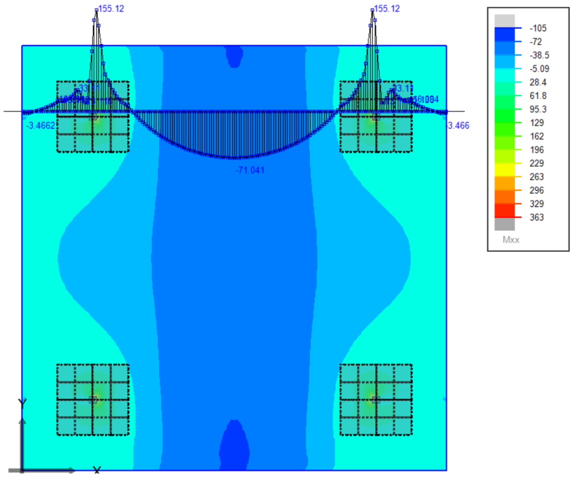

Figure 6.57: Example 6.8 PLPAK bending moment contour.

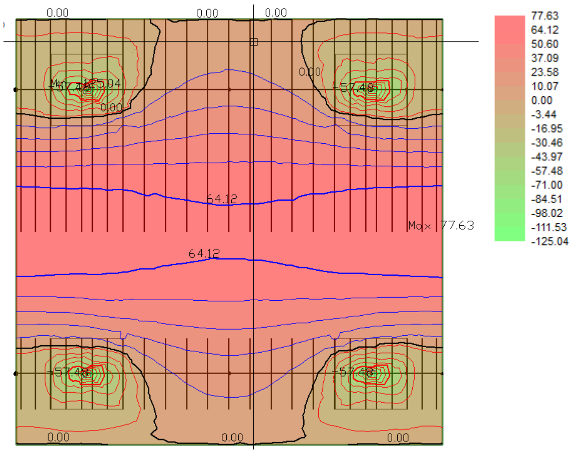

Figure 6.58: Example 6.8 FEM bending moment contour.

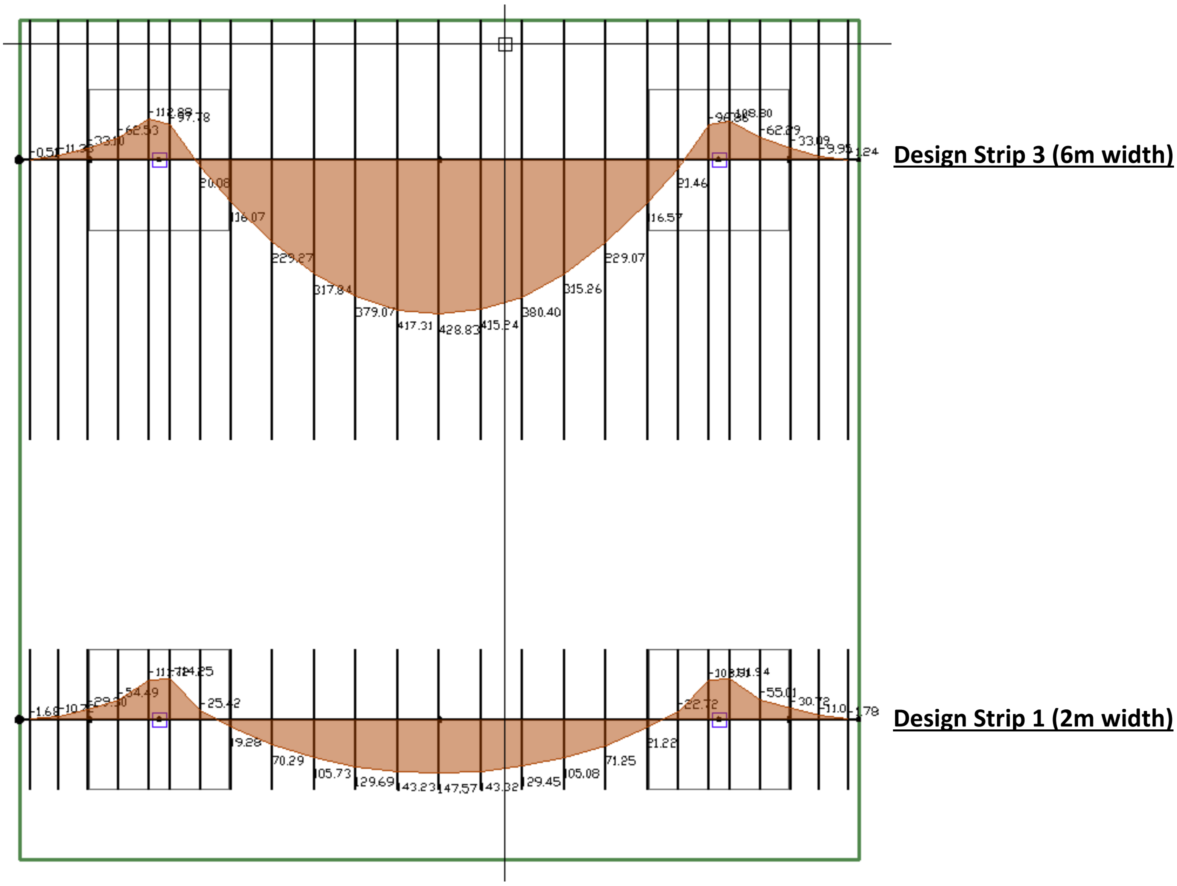

Figure 6.59: Example 6.8 design strips.

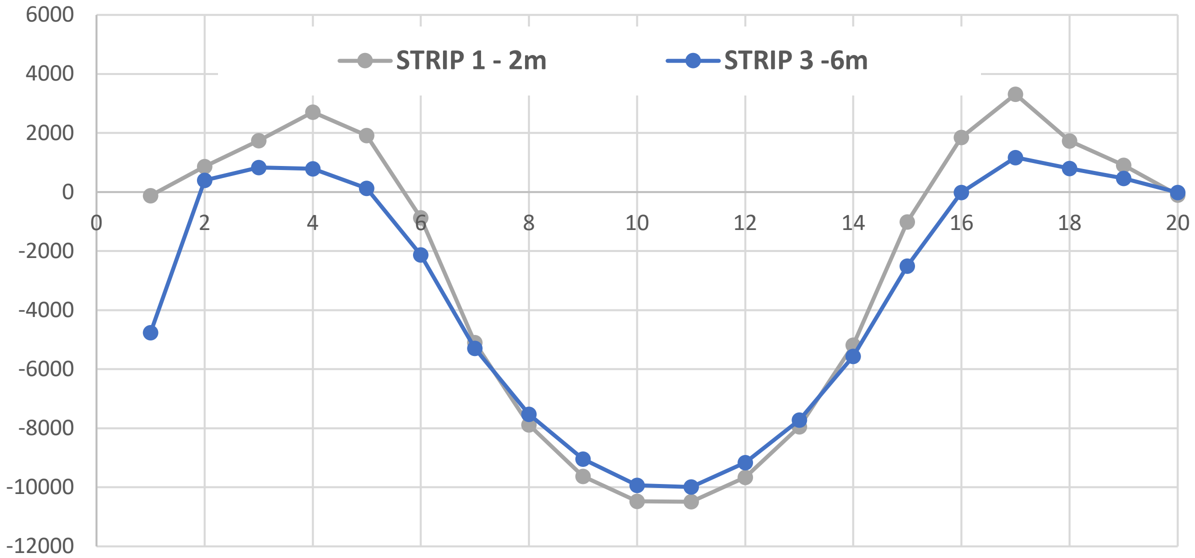

Figure 6.60: Example 6.8 PLPAK design strips stresses.

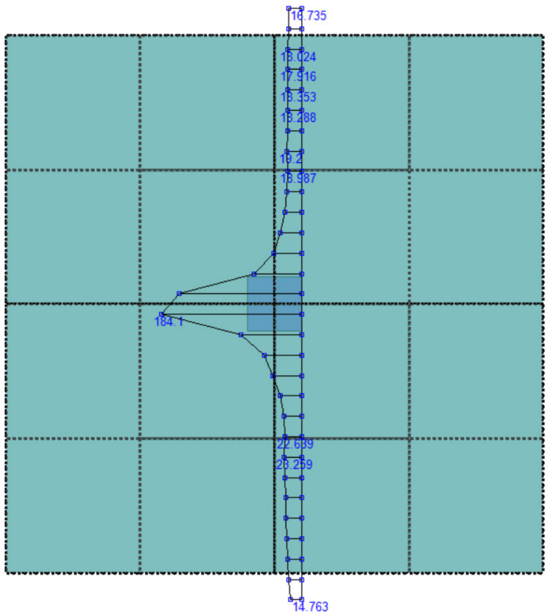

Figure 6.61: Example 6.8 PLPAK bending moment for strip passing throw the drop.

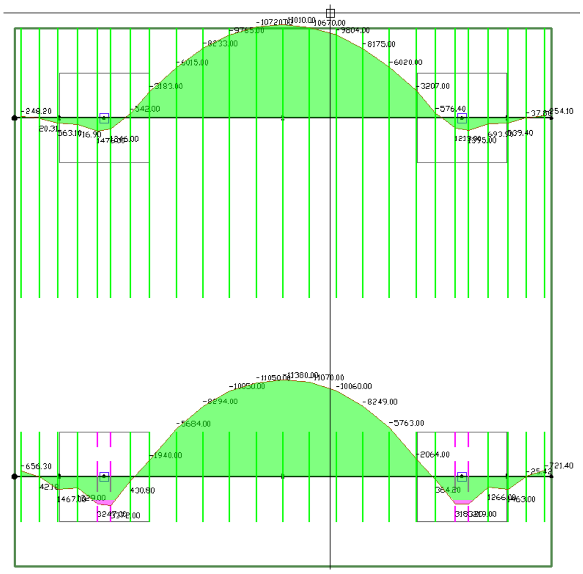

Figure 6.62: Example 6.8 FEM design strips stresses.

References

[1] Y. F. Rashed, “Boundary element modelling of flat plate floors under vertical loading,” *Int J Numer Methods Eng*, vol. 62, no. 12, pp. 1606–1635, Mar. 2005, doi: 10.1002/NME.1236.

[2] G. Hartley and A. Abdel-Akher, “Analysis of Building Frames,” *Journal of Structural Engineering*, vol. 119, no. 2, pp. 468–483, Feb. 1993, doi: 10.1061/(ASCE)0733-9445(1993)119:2(468).

[3] F. vander Weeën, “Application of the boundary integral equation method to Reissner’s plate model,” *Int J Numer Methods Eng*, vol. 18, no. 1, pp. 1–10, Jan. 1982, doi: 10.1002/NME.1620180102.

[4] J. C. F. Telles, “A self-adaptive co-ordinate transformation for efficient numerical evaluation of general boundary element integrals,” *Int J Numer Methods Eng*, vol. 24, no. 5, pp. 959–973, May 1987, doi: 10.1002/NME.1620240509.

[5] O. Enochsson and P. Dufvenberg, “Concrete slabs designed with finite element methods : modelling parameters, crack analyses and reinforcement design (MSc thesis),” Lulea University of Technology, Sweden, 2001. Accessed: Sep. 12, 2022. [Online]. Available: http://urn.kb.se/resolve?urn=urn:nbn:se:ltu:diva-47764

[6] SIMMONDS SH, “Flat Slabs Supported On Columns Elongated in Plan,” *Journal Proceedings*, vol. 67, no. 12, pp. 967–976, Dec. 1970, doi: 10.14359/7330.

[7] A. U. Abdelhady and Y. F. Rashed, “A practical boundary element analysis of slab-beam floor type,” *Eng Anal Bound Elem*, vol. 97, pp. 23–38, Dec. 2018, doi: 10.1016/J.ENGANABOUND.2018.09.006.

[8] G. R. Fernandes and D. H. Konda, “A BEM formulation based on Reissner’s theory to perform simple bending analysis of plates reinforced by rectangular beams,” *Computational Mechanics 2008 42:5*, vol. 42, no. 5, pp. 671–683, Apr. 2008, doi: 10.1007/S00466-008-0266-2.

[9] M. Wagdy and Y. F. Rashed, “Boundary element analysis of multi-thickness shear-deformable slabs without sub-regions,” *Eng Anal Bound Elem*, vol. 43, pp. 86–94, Jun. 2014, doi: 10.1016/J.ENGANABOUND.2014.03.011.

[10] Y. F. Rashed, “A boundary/domain element method for analysis of building raft foundations,” *Eng Anal Bound Elem*, vol. 29, no. 9, pp. 859–877, Sep. 2005, doi: 10.1016/J.ENGANABOUND.2005.04.007.

[11] M. El-Mohr, “Analysis of flat raft on non-homogenous soil by the boundary element method (MSc thesis),” Cairo University, 1992.

[12] Y. F. Rashed, M. H. Aliabadi, and C. A. Brebbia, “THE BOUNDARY ELEMENT METHOD FOR THICK PLATES ON A WINKLER FOUNDATION,” *INTERNATIONAL JOURNAL FOR NUMERICAL METHODS IN ENGINEERING Int. J. Numer. Meth. Engng*, vol. 41, pp. 1435–1462, 1998, doi: 10.1002/(SICI)1097-0207(19980430)41:8.

[13] M. A. Shaaban and Y. F. Rashed, “A coupled BEM-stiffness matrix approach for analysis of shear deformable plates on elastic half space,” *Eng Anal Bound Elem*, vol. 37, no. 4, pp. 699–707, Apr. 2013, doi: 10.1016/J.ENGANABOUND.2012.12.005.

[14] C. M. Wang, Y. K. Chow, and Y. C. How, “Analysis of rectangular thick rafts on an elastic half-space,” *Comput Geotech*, vol. 28, no. 3, pp. 161–184, Apr. 2001, doi: 10.1016/S0266-352X(00)00030-6.

[15] R. A. Fraser and L. J. Wardle, “Numerical Analysis of Rectangular Rafts on Layered Foundations,” *Geotechnique*, vol. 26, no. 4, pp. 613–630, Sep. 1976, doi: 10.1680/GEOT.1976.26.4.613.

[16] S. Syngellakis and C. X. Bai, “On the application of the boundary element method to plate—half-space interaction,” *Eng Anal Bound Elem*, vol. 12, no. 2, pp. 119–125, Jan. 1993, doi: 10.1016/0955-7997(93)90006-7.

[17] J. A. Hemsley, “ELASTIC SOLUTIONS FOR AXISYMMETRICAL LOADED CIRCULAR RAFT WITH FREE OR CLAMPED EDGES FOUNDED ON WINKLER SPRINGS OR A HALF-SPACE.,” *Proceedings of the Institution of Civil Engineers (London)*, vol. 83, no. pt 2, pp. 61–90, Mar. 1987, doi: 10.1680/iicep.1988.118.

[18] S. P. Timoshenko and J. N. Goddier, *Theory of elasticity*. Singapore: McGraw-Hill, 1982.

[19] L. D. Ta and J. C. Small, “An approximation for analysis of raft and piled raft foundations,” *Comput Geotech*, vol. 20, no. 2, pp. 105–123, Jan. 1997, doi: 10.1016/S0266-352X(96)00012-2.

[20] Y. H. Wang, L. G. Tham, Y. Tsui, and Z. Q. Yue, “Plate on layered foundation analyzed by a semi-analytical and semi-numerical method,” *Comput Geotech*, vol. 30, no. 5, pp. 409–418, Jul. 2003, doi: 10.1016/S0266-352X(03)00014-4.

[21] S. J. Chen and Y. C. Peng, “On spline finite element computation of plates on elastic foundations for various base-models,” *Journal of Sun Yat-Sen University (National Science Edition)*, no. 2, pp. 15–23, 1980, [Online]. Available: https://www.scopus.com/inward/record.uri?eid=2-s2.0-0002673669&partnerID=40&md5=a43509f62e563da455f3b3e080147876

[22] Y. H. Wang, X. M. Qiu, and Y. K. Cheung, “Bending plates on an elastic half-space analyzed by isoprametric elements,” *Chinese Journal of Geotechnical Engineering*, vol. 20, no. 4, pp. 7–11, 1998.

[23] L. Wardle and R. Fraser, “Finite element analysis of a plate on a layered cross-anisotropic foundation,” in *Proceedings of the first international conference of finite element methods in engineering. Australia: University of New South Wales*, 1974, pp. 565–578.

[24] J. E. Bowles, *Foundation Analysis and Design*, 5th ed. New York: McGraw-Hill, 1996.

[25] M. A. Shaaban, “Boundary element analysis of rafts on elastic half space (MSc thesis),” Cairo University, 2012.

[26] J. A. Hemsley, *Elastic Analysis of Raft Foundations*. London: Thomas Telford, 1998.

[27] O. E. Shehata, A. F. Farid, and Y. F. Rashed, “Practical boundary element method for piled rafts,” *Eng Anal Bound Elem*, vol. 97, pp. 67–81, Dec. 2018, doi: 10.1016/J.ENGANABOUND.2018.09.009.

[28] A. v. Mendonça and J. B. de Paiva, “A boundary element method for the static analysis of raft foundations on piles,” *Eng Anal Bound Elem*, vol. 24, no. 3, pp. 237–247, Mar. 2000, doi: 10.1016/S0955-7997(00)00002-3.

[29] R. Z. Moayed, E. Izadi, and M. Mirsepahi, “3D finite elements analysis of vertically loaded composite piled raft,” *J Cent South Univ*, vol. 20, no. 6, pp. 1713–1723, Jun. 2013, doi: 10.1007/S11771-013-1664-Y.

[30] *Code of Practice for Soil Mechanics – Part 4: Deep Foundations*. Egypt: National Housing and Construction Research Center, 2007.

[31] M. E. Mobasher, “A Coupled Stiffness BEM Pushover Lateral Analysis of Tall Buildings (MSc thesis),” Cairo University, 2013.

[32] R. W. Mohareb, Y. F. Rashed, M. Wagdy, and M. E. Mobasher, “Structural analysis of multistory building using coupled BEM-stiffness matrix,” *ECCOMAS Thematic Conference - COMPDYN 2013: 4th International Conference on Computational Methods in Structural Dynamics and Earthquake Engineering, Proceedings - An IACM Special Interest Conference*, pp. 3948–3974, 2013, doi: 10.7712/120113.4788.C1646.

[33] A. U. Abdelhady, “A Consistent BEM Based Modeling of Tall Buildings (MSc thesis),” Cairo University, 2016.

[34] B. S. Taranath, *Structural Analysis and Design of Tall Buildings*. New York: McGraw-Hill, 1988.

[35] B. S. Taranath, “Analysis of Interconnected Open Section Shear Wall Structures,” *Journal of the Structural Division*, vol. 101, no. 11, pp. 2367–2384, Nov. 1975, doi: 10.1061/JSDEAG.0004209.

[36] A. S. Gendy and T. I. El-Fayomy, “Accuracy enhancement of hybrid/mixed models for thin-walled beam assemblages,” *International Journal for Computational Methods in Engineering Science and Mechanics*, vol. 13, no. 4, pp. 227–238, Jul. 2012, doi: 10.1080/15502287.2012.682193.

[37] *Eurocode 8: Design Provisions for Earthquake Resistance of Structures*. London: British Standards Institution, 1996.

[38] M. E. Mobasher, Y. F. Rashed, and W. Elhaddad, “BIM Standards for Automated BEM Structural Analysis and Design of RC Plates,” *Journal of Computing in Civil Engineering*, vol. 30, no. 4, p. 04015054, Sep. 2015, doi: 10.1061/(ASCE)CP.1943-5487.0000531.

[39] M. A. Abdelwahab, Y. F. Rashed, and A. A. Mukhtar, “Dynamic boundary element analysis of multi story buildings,” *Journal of Engineering and Applied Science*, vol. 61, pp. 249–268, Jun. 2014.

[40] A. K. Chopra, *Dynamics of Structures*. Prentice Hall, 1995.

[41] M. A. Abdelwahab, Y. F. Rashed, and A. A. Mukhtar, “Time History Boundary Element Analysis of Multi Story Buildings,” *Journal of Engineering and Applied Science*, vol. 62, pp. 165–185, Apr. 2015.

[42] D. Negrut, R. Rampalli, G. Ottarsson, and A. Sajdak, “On an Implementation of the Hilber-Hughes-Taylor Method in the Context of Index 3 Differential-Algebraic Equations of Multibody Dynamics (DETC2005-85096),” *J Comput Nonlinear Dyn*, vol. 2, no. 1, pp. 73–85, Jan. 2007, doi: 10.1115/1.2389231.

[43] E. Nagy, M. A. Abdelwahab, and Y. F. Rashed, “Damped time history boundary element analysis of buildings,” *Journal of Engineering and Applied Science*, vol. 65, pp. 23–42, Feb. 2018.

[44] Y. F. Rashed, “Boundary element analysis of post-tensioned slabs,” *International Journal of Advanced Structural Engineering*, vol. 7, no. 2, pp. 143–158, Jun. 2015, doi: 10.1007/S40091-015-0088-3/TABLES/3.

[45] M. P. Collins and D. Mitchell, *Prestressed Concrete Structures*. Canada: Response Publications, 1997.